# CHARACTERISATION OF THE MECHANISMS OF RETINAL GANGLION CELL DEATH IN DIRECT AND INDIRECT TRAUMATIC OPTIC NEUROPATHY

By Chloe Naomi Thomas

A thesis submitted to the University of Birmingham for the degree of
DOCTOR OF PHILOSOPHY

Neuroscience and Ophthalmology group
Institute of Inflammation and Ageing
College of Medical and Dental Sciences
University of Birmingham

September 2018

## Abstract

Retinal ganglion cells (RGCs) exist in the retina and their axons form the optic nerve (ON), the main connection from the eye to the brain. RGCs are post-mitotic neurons, therefore, if these cells degenerate by injury or disease, they are not endogenously replaced, leading to irreversible blindness. Military and civilian populations can be injured by explosive blasts during conflict or terrorist attacks, which can cause traumatic ocular injuries. Primary blast injuries (PBI) are caused by the primary blast wave (a rapid increase in atmospheric pressure). In closed-space explosions the blast wave can propagate off surfaces and cause repeated impact. Secondary blast injuries occur from blunt force by debris carried in the blast wind. There are no effective treatments and an urgent need for therapeutic interventions to help preserve vision.

This thesis investigates cell death mechanisms in RGCs using *in vivo* rodent models of repeated PBI (rPBI) and blunt ocular injury. Apoptotic caspase-2-dependent and necroptotic RGC death is likely to occur after blunt ocular injury in a site-specific manner. Caspase-2 knockdown using a small interfering RNA (siRNA) provided some structural and functional protection at the periphery of the impact site, with pharmacological inhibition of necroptosis using Necrostatin-1s providing some RGC protection, likely at the impact site centre. Furthermore, performing intravitreal injections in close proximity to the time of rPBI caused exacerbated RGC death and vitreal inflammation, which was absent when treatment was given before the injury.

Collectively, this research provides novel insights into cell death signalling in traumatic ocular injuries caused by primary blast wave exposure and blunt impact, and into therapeutics which could preserve vision in victims injured during terrorist attacks or war.

## Acknowledgements

**Lt Col Richard Blanch** and **Dr Zubair Ahmed** for their endless support throughout my PhD. They have helped me to grow as a scientist, encouraged me to take up opportunities and have been supportive through difficult parts of the project. Thank you.

**Dr Tonia Rex** for welcoming me into her lab and her home.

**Neuroscience and Ophthalmology group**. I have enjoyed being part of a dedicated group of scientists who enjoy research and discussion. I started my PhD project knowing very few basic lab skills and little about the visual system and have ended it with a wide range of skills and a passion for eye research. I am very grateful to the Neuroscience and Ophthalmology group for the time and effort spent teaching me and I have gained some great friends.

**Alexandra Bernardo-Colon**, who helped me find my feet with the blast injury project and has become a great friend.

**Ella Courtie** and **Gareth Essex**, who were both dedicated to the research during undergraduate and summer projects and a joy to have around.

Additionally, I would like to thank the **Biomedical Services Unit** at University of Birmingham and the animal facilities at Vanderbilt University for their assistance in looking after my animals, and to the funding body **Fight for Sight** for funding the PhD research.

My partner **Dan** for his support throughout this experience. It has been a challenge being dedicated to our research. Over the past 3-years we have both had weekend and evening trips into the lab and have spent 4-months on opposite sides of the world. Thank you.

**Funding:** Fight for Sight PhD studentship (grant number: 1560/1561).

## Publications

Full formatted publications are included in Appendices.

**Appendix 1:** Caspases in retinal ganglion cell death and axon regeneration. Chloe N Thomas, Martin Berry, Ann Logan, Richard J Blanch, Zubair Ahmed. *Cell Death and Discovery* (2017) 3 17032.

**Appendix 2:** Caspase-2 mediates site-specific retinal ganglion cell death after blunt ocular injury. Chloe N Thomas, Adam M Thompson, Eleanor McCance, Martin Berry, Ann Logan, Richard J Blanch, Zubair Ahmed. *Investigative Ophthalmology & Visual Science* (2018) 59 4453-4462.

# Contents

## List of Figures

## List of Tables

## Abbreviations

βIIIT. Beta-III-tubulin

ABO. Acoustic blast overpressures

AGO2. Argonaute 2

AIF. Apoptosis inducing factor

ALS. Amyotrophic lateral sclerosis

Apaf-1. Apoptotic protease activating factor 1

APS. Ammonium persulfate

ASC. Apoptosis-associated speck-like protein containing a CARD

Bak. Bcl-2 antagonist or killer

Bax. Bcl-2 associated X protein

Bcl. B-cell lymphoma

BETTS. Birmingham Eye Trauma Terminology

Bid. BH3 interacting domain death agonist

BIR. Bacovirus IAP domain

BRN3A. Brain-specific homeobox / POU domain protein 3A

BSA. Bovine serum albumin

CARD. Caspase recruitment domain

CASP9 DN. Caspase-9 dominant negative

cDNA. Complementary DNA

cIAP. Cellular inhibitor of apoptosis

CNS. Central nervous system

CNTF. Ciliary neurotrophic factor

CPP. Cell penetrating peptides

CRASH. Corticosteroid randomization after significant head injury

CTE. Chronic traumatic encephalopathy

DAMP. Damage-associated molecular pattern

DAMPs. Damage-associated molecular pattern molecules

DAPI. 4',6-diamidino-2-phenylindole

DARC. Detection of apoptosing retinal cells

DD. Death domain

DED. Death effector domain

DISC. Death inducing signalling complex

DMSO. Dimethyl sulfoxide

dpi. Days post injury

dsRNA. Double-stranded RNA, Double stranded RNA

EBSS. Earle's Balanced Salt Solution

ECL. Enhanced chemiluminescence

EDTA. Ethylenediaminetetraacetic acid

EGTA. Ethylene glycol tetraacetic acid

ELISA. Enzyme linked immunosorbent assay

ELM. External limiting membrane

ERG. Electroretinogram, Electroretinogram

FADD. Fas-associated protein with death domain

ffERG. Full-field electroretinogram

GCC. Ganglion cell complex

GCL. Ganglion cell layer

GFP. Green fluorescent protein

H&E. Haematoxylin & Eosin

IAPs. Inhibitors of apoptosis

IDO. Indoleamine-2,3-dioxygenase

IL. Interleukin

ILM. Inner limiting membrane

INL. Inner nuclear layer

IONTS. The International Optic Nerve Trauma Study

IPL. Inner plexiform layer

kPa. Kilopascals

miRNA. Micro RNA

MLKL. Mixed lineage kinase domain-like

MOMP. Mitochondrial outer membrane permeabilisation

MRI. Magnetic resonance imaging

mTOR. Mammalian target of rapamycin

NAION. Non-arteritic ischaemic optic neuropathy

NASCIS 2. The National Acute Spinal Cord Injury Study 2

Nec-1. Necrostatin-1

Nec-1s. Necrostatin-1 stable

NFκβ. Nuclear factor κβ

NLR. Nod-like receptor

NLRP3. NOD like-receptor family pyrin domain containing 3

OCT. Optical coherence tomography

OCTc. optical cutting temperature compound

ON. optic nerve

ONL. Outer nuclear layer

ONT. Optic nerve transection

PAGE. Polyacrylamide gel electrophoresis

PAMP. Pathogen-associated molecular pattern

PAMPs. Pathogen-associated molecular pattern molecules

PBI. Primary blast injury

PCD. Programmed cell death

PEDF. Pigment epithelium derived factor, Pigment epithelium derived factor

PFA. Paraformaldehyde

PhNR. Photopic negative response

PIDD. p53 induced protein with a death domain

PN. Peripheral nerves

PNS. Peripheral nervous system

PPD. P-phenylenediamine

psi. Pounds per square inch

pTEN. Phosphatase and tensin homolog

PVC. Polyvinylchloride

PVDF. Polyvinylidene fluoride

PYD. Pyrin domain

qPCR. Quantitative polymerase chain reaction

RAIDD. RIP associated ICH-1 homologous protein with a death

RAPD. Relative afferent pupillary defect

RBPMS. RNA binding protein with multiple splicing

RCD. Regulated cell death

RGC. Retinal ganglion cells

RIHM. RIPK homotypic interaction motif

RIN. RNA integrity number

RIPK1. Receptor interacting protein kinase-1

RIPK3. Receptor interacting protein kinase-3

RISC. RNA-induced silencing complex

RLM-RACE. RNA ligase mediated rapid amplification of cDNA ends

RNAi. RNA interference

RNFL. Retinal nerve fibre layer

ROCK. Rho associated protein kinase

ROS. Reactive oxygen species

RPE. Retinal pigment epithelium

RT. Room temperature

SCI. Spinal cord injury

SDS. Sodium dodecyl sulphate

SEM. Standard error of the mean

siCASP2. siRNA against caspase-2

siEGFP. siRNA against enhanced green fluorescent protein

Smac/DIABLO. Second mitochondria-derived activator of caspase/direct inhibitor of apoptosis-binding protein with low pI

STR. Scotopic threshold response

TBI. Traumatic brain injury

tBid. Truncated bid

TBST. Tris buffered saline with Tween-20

TEMED. Tetramethylethylenediamine

TLR. Toll-like receptors, Toll-like receptors

TNF. Tumour necrosis factor

TNT. Trinitrotoluene

TON. Traumatic optic neuropathy

TRADD. TNF receptor-associated death domain

TRAF. TNF receptor associated factor

TUNEL. Terminal deoxynucleotidyl transferase dUTP nick end labelling

VEP. Visual evoked potential

XIAP. Mammalian IAP x-linked inhibitor of apoptosis protein

# Chapter 1 General Introduction

Parts of Chapter published in:

**Chloe N Thomas**, Martin Berry, Ann Logan, Richard J Blanch, Zubair Ahmed.

Caspases in Retinal Ganglion Cell Death and Axon Regeneration.

*Cell Death Discovery* (2017) 3 17032

Full text in Appendix I

## 1.1. The visual system

Vision is one of five senses that allow us to perceive our environment. Traumatic and degenerative ocular and optic nerve (ON) injury can result in permanent, debilitating blindness.

### 1.1.1. Gross anatomy of the eye

The eye (or globe) enables vision (Figure 1.1). The anterior portion of the eye consists of the pupil (a small aperture in the iris which allows light to enter the eye), the iris (controls pupil size and therefore amount of light entering the eye) and the cornea (the main refractive surface of the eye and protective covering). The cornea is continuous with the sclera, which provides outer protection to the globe and is continuous with the ON dura. The anterior segment is filled with aqueous humour and the posterior segment has a viscous gel called the vitreous humour. The neural retina populates the posterior ocular surface and contains sensory receptors and neurons, which collectively facilitate vision. Photoreceptors convert light into electrical signals, which are relayed to retinal ganglion cells (RGCs) and then conveyed through the visual pathways to the visual cortex for processing and interpretation.

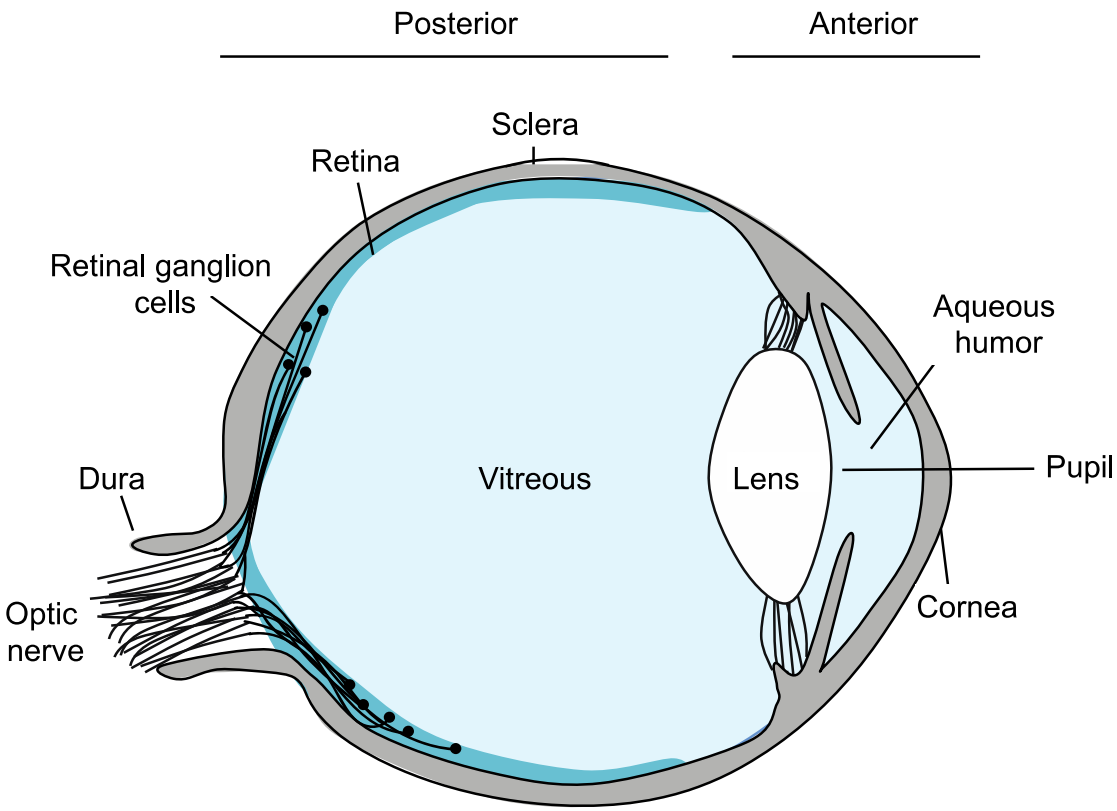


**Figure 1.1 Parasagittal section of the eye.** Light passes through the anterior portion of the eye, through the pupil, and is focused on the retina by the lens. The retina is located in the posterior segment of the eye and is connected to the brain by the RGCs, whose axons form the ON. The anterior segment of the eye is filled with aqueous humour, whereas the posterior segment contains the vitreous gel.

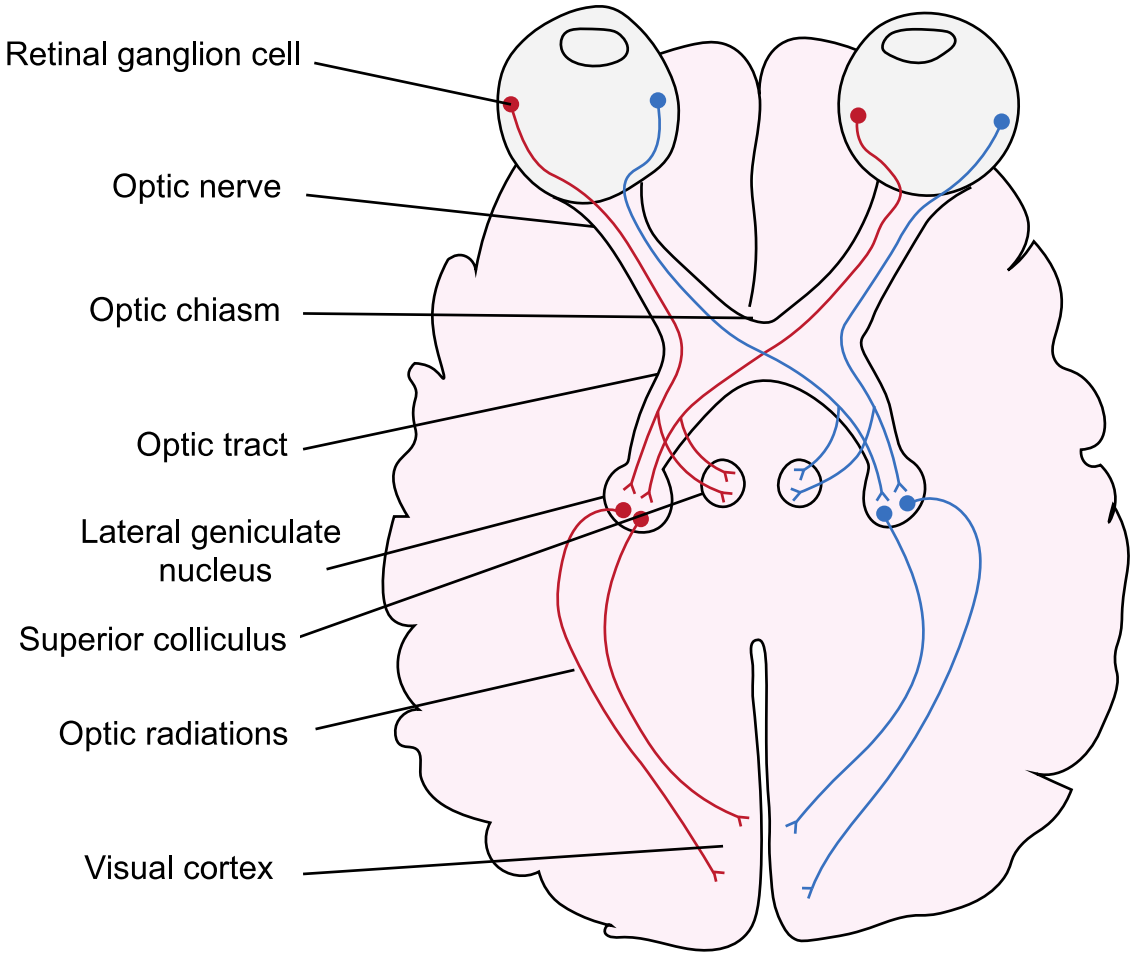


**Figure 1.2. Schematic of the visual pathway.** RGC axons form the ON and converge at the optic chiasm where in most animals, the nasal ~50% of axons decussate to join the remaining temporal axons from the contralateral eye, which project along contralateral optic tracts towards the lateral geniculate body (90% of axons in humans), superior colliculus (>90% of axons in rats) and other visual nuclei. The optic radiations project from the lateral geniculate nucleus to the primary visual cortex, where visual information is processed. Redrawn from (Haines and Mihailoff, 2018).

### 1.1.2. The retina and visual pathway

The retina comprises of three main nuclear neuronal layers (Figure 1.3): the outer nuclear layer (ONL), which is populated by rod and cone photoreceptors; the inner nuclear layer (INL) is composed of bipolar cells, amacrine cells, Müller glia and horizontal cell nuclei; and the ganglion cell layer (GCL), which consists of RGCs and displaced amacrine cells. The retina opposes the retinal pigment epithelium (RPE), whose basement membrane sits on the vascular choroid. RPE cells are supportive to photoreceptors, and the choroid supplies oxygen and nutrients to the outer half of the retina. Müller glia provide further structural and metabolic support and have processes extending throughout the retina forming the internal and external limiting membranes (ILM / ELM) (Berry et al., 2008).

Light is focused on the retina by the cornea and crystalline lens and is detected by rod and cones and converted into electrochemical signals, then transmitted to RGCs via bipolar cells. Unmyelinated RGC axons pass through the retinal nerve fibre layer (RNFL) and through the lamina cribrosa where RGC axons become myelinated by oligodendrocytes and form the ON. ON axons converge at the optic chiasm (Figure 1.2), where in most mammals ~ 50% of axons decussate to join the remaining temporal axons from the contralateral eye, which project along the contralateral optic tract towards the lateral geniculate body (90% of axons in humans), superior colliculus (>90% of axons in rats) and other visual nuclei. The optic radiations project from the lateral geniculate nucleus to the primary visual cortex, where visual information is processed (Berry et al., 2008).

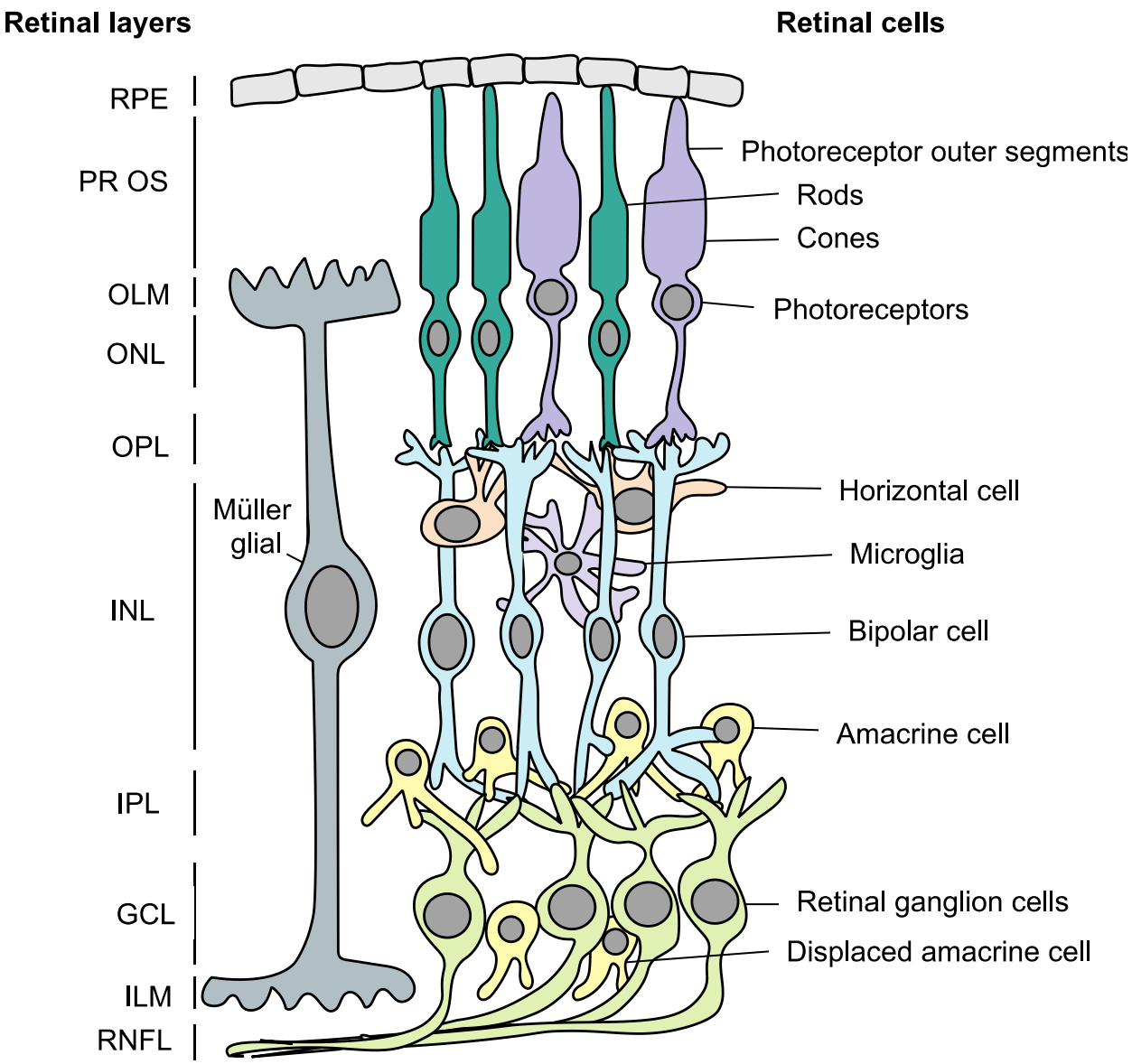


**Figure 1.3. Cell types in the retina and functional layers**. Light is detected and converted into an electrical signal by the photoreceptor outer segments, which is transmitted to the RGCs via the bipolar cells. Horizontal and amacrine cells influence this signal and microglia provide structural and metabolic support. Müller cells project across the retinal layers and form the inner and outer limiting membranes. Redrawn from (Berry et al., 2008). **Abbreviations:** RPE, retinal pigment epithelium; PR OS, photoreceptor outer segments; OLM, outer limiting membrane; ONL, outer nuclear layer; OPL, outer plexiform layer; INL, inner nuclear layer; IPL, inner plexiform layer; GCL, ganglion cell layer; ILM, inner limiting membrane; RNFL, retinal nerve fibre layer.

### 1.1.3. Methods for quantifying RGCs

RGCs can be marked using immunofluorescent stains, back-labelled with dyes or imaged using *in vivo* techniques (Mead and Tomarev, 2016). RGC markers include Brain-specific homeobox / POU domain protein 3A (BRN3A), RNA binding protein with multiple splicing (RBPMS) and β-III-tubulin (βIIIT) (Mead et al., 2014, Mead and Tomarev, 2016). BRN3A is an RGC specific transcription factor, but, it only stains certain RGC sub-populations and has been shown to be downregulated after certain injuries (Nadal-Nicolas et al., 2009). RBPMS is a more recently discovered RGC marker and is a protein involved in transcriptional modifications of mRNA. RBPMS expression is highly correlated with Fluorogold-labelled RGCs; 97% of $RBPMS^+$ cells are also $Fluorogold^+$ (Kwong et al., 2010), and RBPMS has good correlation with Fluorogold labelling following optic nerve crush (ONC), excitotoxic injury and glaucoma (Kwong et al., 2011, Kwong and Lam, 2000, Rodriguez et al., 2014a). βIIIT is a neuronal-specific microtubule protein found within RGC membranes and axons; therefore, βIIIT stains the RNFL and cell membranes, making accurate quantification subjective and difficult. The current gold standard RGC marker is Fluorogold dye injection into the ON or the superior colliculus. The fluorogold dye is retrogradely transported along surviving RGC axons to the RGC bodies in the retina. However, there are some limitations. Firstly, macrophages phagocytose dead RGCs taking up the dye, and themselves start to fluoresce. This means there could be over-estimation of the number of surviving RGCs. Secondly, injections into the ON or the brain are invasive and can cause further injury and RGC death. This means that fluorogold injections are suitable for ONC studies, where the ON is already injured, but not for non-invasive studies as this can lead to additional trauma.

RGCs can also be imaged *in vivo*. This means, RGCs can be imaged using a non-invasive method at multiple time points and has clinical translatability. One promising technique for measuring of retinal apoptosis is Detection of Apoptosing Retinal Cells (DARC) technology. This method uses a confocal scanning laser ophthalmoscope to image fluorescent cells expressing Annexin-5 on the outside of the phospholipid membrane, a prominent feature of apoptosis (Yap et al., 2018, Cordeiro et al., 2004, Maass et al., 2007). DARC has been used successfully in multiple animal studies of neuroprotection [summarised in review article (Yap et al., 2018)] and in glaucoma patients (Cordeiro et al., 2017). However, not all cells die by apoptotic mechanisms. Smith et al., have used an adeno-associated virus to labels RGCs with green fluorescent protein (GFP), and have shown long-lasting results and no adverse side effects in mouse studies (Smith and Chauhan, 2018). Adaptive optics scanning light ophthalmoscopy can also be used to image RGCs in human eyes, but without injections, and therefore, has good clinical translatability (Rossi et al., 2017).

### 1.1.4. Central nervous system regenerative properties

The neural retina is an extension of the central nervous system (CNS), thus after injury or disease, injured neurons (including RGCs) are not endogenously replaced and their loss can lead to irreversible blindness. Contributing factors to the lack of CNS regeneration include limited growth stimulatory factors (e.g. neurotrophic factors), which are normally retrogradely transported along RGC axons to the cell bodies and promote survival, elevated myelin and glial derived inhibitory factors [e.g. NoGo, oligodendrocyte myelin glycoprotein and myelin associated glycoprotein (MAG) (Sandvig et al., 2004)], and lesion site glial scar formation causing a chemical and

physical scar (Fischer and Leibinger, 2012). Current research aims to prevent RGC degeneration and promote axonal regeneration.

In contrast, the peripheral nervous system (PNS) does regenerate after injury. Peripheral nerves (PN) are myelinated by Schwann cells which endogenously produce neurotrophic factors. CNS neurons are myelinated by oligodendrocytes and receive neurotrophic factors from their target tissue. Surgical placement of a PN graft on the cut end of the ON or into the vitreous can stimulate RGC axonal regeneration (Berry et al., 1999, Berry et al., 1996).

Mature CNS neurons lose their endogenous regenerative ability (Fischer and Leibinger, 2012). During development, immature CNS neurons can re-form functional connections. However, in mature CNS neurons, some genes are down-regulated such as genes in the mammalian target of rapamycin (mTOR) pathway (Morgan-Warren et al., 2013), suggesting that mTOR may act as a molecular switch that can be switched on to promote neuronal regeneration. Phosphatase and tensin homolog (pTEN) protein inhibits mTOR, and virus-assisted conditional mTOR gene knockdown results in a ~45% increase in RGC neuroprotection and ~10% increase in axonal regeneration (Park et al., 2008). Therefore, combined RGC survival and axonal regeneration therapies need to be considered due to the multifactorial response in CNS injury.

## 1.2. Inflammatory responses

### 1.2.1. Innate and adaptive immunity

The immune response acts as a defence mechanism to prevent the invasion of pathogens and insults which may cause tissue damage. The immune system consists of innate and adaptive responses (Figure 1.4) (Dempsey et al., 2003). The first line of

defence is the innate immune system, which is activated within minutes of an insult. It consists of circulating and resident macrophages (e.g. microglia in the CNS), mast cells, dendritic cells, natural killer cells, neutrophils and complement protein, as well as both physical and chemical barriers. Innate immune system cells provide a rapid, non-specific response, but also secrete signals which activate the adaptive immune response. The adaptive immune response consists of B and T cells, and is slower than the innate response but mounts a more specific response to invading pathogens and insults.

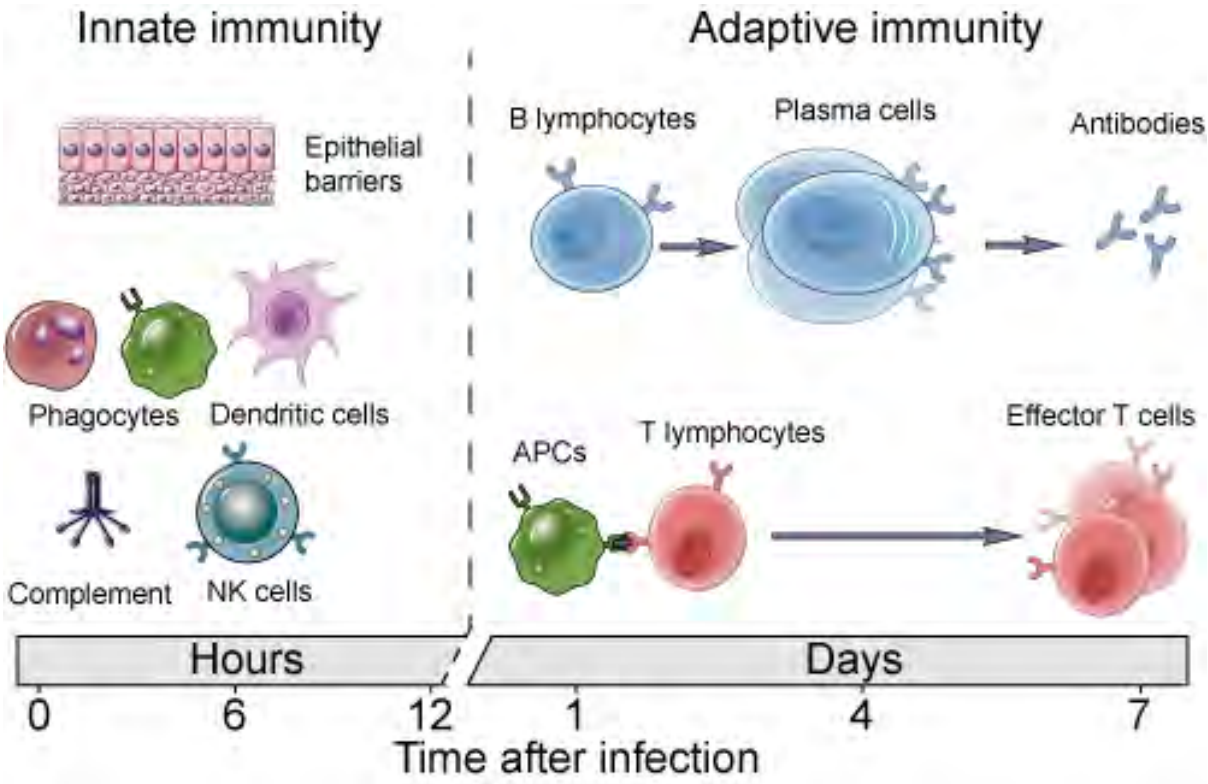


**Figure 1.4 Cells involved in the innate and adaptive immune systems**. The non-specific innate immune response occurs within 0-12 hours after exposure to the initial insult and involves phagocytic, dendritic and natural killer cells, as well as complement and epithelial barriers. The specific adaptive immune response is delayed due to the production of specific B and T cells against the insulting antigen. Figure reproduced from https://www.creative-diagnostics.com/innate-and-adaptive-immunity.html

### 1.2.2. Inflammatory cells

#### 1.2.2.1. Monocytes and macrophages

Monocytes are a multipotent population of circulating bone-marrow derived leukocytes, which can differentiate into macrophages or dendritic cells (Shi and Pamer, 2011, Mosser and Edwards, 2008, Chinnery et al., 2017). Monocytes have many functions, including phagocytosis, release of cytokines or chemokines, antigen presentation, immune modulation and tissue repair. Macrophages are typically defined as phagocytic cells; however, they also have a crucial role in the regulation of inflammation, wound healing and fibrosis (Mosser and Edwards, 2008, Mosser, 2003, Kou and Babensee, 2011). Macrophages can be separated into functional sub-populations. Firstly, M1 macrophages are 'classically activated' and have a role in host defense, including phagocytosis of pathogens, the production of oxygen and nitrogen radicals (MacMicking et al., 1997) and degrading extracellular matrix during inflammation through secreting collagenases, elastase and hyaluronidase enzymes (Kou and Babensee, 2011, Xia and Triffitt, 2006). Secondly, M2 macrophages are 'alternatively activated', and are further divided into three sub-populations. M2a macrophages produce extracellular matrix proteins and have a role in wound healing and tissue remodeling (Duffield, 2003, Mantovani et al., 2004), whereas, M2b macrophages regulate inflammatory responses and limit tissue damage through the synthesis and secretion of cytokines, growth factors and signaling molecules, but they do not produce extracellular matrix proteins and, therefore, do not actively promote wound healing (Fleming and Mosser, 2011). M2c macrophages are involved in immune suppression and the modification, reorganisation and degradation of the extracellular matrix. Collectively, M2 macrophages induce chemotaxis, proliferation and activation of fibroblasts into the tissue lesion (Song et al., 2000), and also promote

wound healing through production of extracellular matrix proteins, such as fibronectin (Gratchev et al., 2001).

Macrophages can be immunolabelled using antibodies against the CD68 protein. In rats, ED1 is a monoclonal antibody clone directed against the CD68 protein (Damoiseaux et al., 1994). CD68 is present on circulating macrophages, tissue macrophages (e.g. microglia in the CNS) and cells in monocyte lineage, such as osteoclasts, monocytic phagocytes (Damoiseaux et al., 1994).

#### 1.2.2.1.1. Microglia

Microglia are resident CNS macrophages and acquire a phagocytic phenotype during an inflammatory response (Nayak et al., 2014). Microglia sense a variety of exogenous and endogenous signals allowing a dynamic response to sterile injuries and infectious agents.

### 1.2.2.2. Neutrophils

Neutrophils are an abundant population of circulating leukocytes which are amongst the first responders to tissue injury. Neutrophils have an important role in wound healing, through phagocytosis, releasing metalloproteinases and producing growth factors. After CNS injury, inflammatory mediators are released which promote neutrophils to acquire a hyper activated state and release metalloproteinases, proteases, TNF-$\alpha$ and ROS, allowing neutrophils to breach the blood-brain-barrier and enter the CNS (Scholz et al., 2007). However, these soluble mediators also induce neuronal death, meaning neutrophil hyper activation can be detrimental and promote further tissue damage (Nguyen et al., 2007).

#### 1.2.2.3. B and T cells

B and T cells are part of the adaptive immune response and have the ability to recognise specific antigens. Although they have a delayed response to an initial insult, they can respond quickly to repeated exposure to the same antigen through developing memory cells (Ling et al., 2006).

### 1.2.3. Inflammatory response in the CNS

Following CNS injury, there is an immune response from resident and circulating inflammatory cells. Pathogen-associated molecular pattern molecules (PAMPs) are released by invading pathogens (e.g. LPS) or immune cells and dying cells can release damaged tissue releasing damage-associated molecular pattern molecules (DAMPs) (e.g. ATP, heparin sulfate, DNA and RNA), both activating an immune response (Matzinger, 1994, Bianchi, 2007). Astrocytes and microglia express ectoenzymes which convert extracellular ATP into adenosine, and allow the ATP-mediated neuroinflammation to dampen and the return of homeostasis.

Sterile inflammation (inflammation in the absence of pathogens) can be triggered by physical, chemical or metabolic insults (Chen and Nunez, 2010). This type of inflammation can be initially beneficial and promote the clearance of damaged tissue, restore tissue homeostasis and promote tissue repair, but when prolonged in uncontrolled circumstances, it can become detrimental and result in further damage.

The inflammatory response following CNS injury is dominated by the innate immune system, in particular, resident microglia and circulating macrophages (Cui et al., 2009). Once cell debris has been phagocytosed, these cells display the antigens to

lymphocytes and activate the adaptive immune response (Schroeter and Jander, 2005). The CNS is thought to be an immune privileged site; however, it is now known that T and B lymphocytes can cross the intact BBB.

### 1.2.4. Macrophages after CNS and ocular injury

In the CNS, one of the fundamental roles of macrophages is to remove myelin debris (Stoll et al., 1989), which facilitates axonal regrowth and remyelination. In models that promote vitreal inflammation, infiltrating macrophages promote RGC survival and axon regeneration (Leon et al., 2000, Lorber et al., 2005, Pernet and Di Polo, 2006, Yin et al., 2003). For example, injuring the lens increases the survival of axotomised RGCs by 8-fold and promotes ON axon regeneration beyond the injury site by 100-fold (Fischer et al., 2001). Further studies have shown increased RGC survival after intravitreal injection of vehicle (Mansour-Robaey et al., 1994) and implantation of pre-injured PN fragments into the vitreous (Berry et al., 1996, Berry et al., 1999). These effects are likely to be due to increased ocular inflammation and intravitreal macrophage activation.

Yin et al., claims that a small $Ca^{2+}$ binding protein called oncomodulin stimulates RGC axonal regeneration following vitreal inflammation (Yin et al., 2006). Macrophages which infiltrate into the vitreous within 24 hours of injury to the lens have elevated levels of oncomodulin mRNA and protein, but macrophages which infiltrate the vitreous at later time points do not show high levels of oncomodulin (Yin et al., 2006, Yin et al., 2009). However, not all research groups are in agreement that macrophages containing oncomodulin cause RGC axon regeneration (Müller et al., 2007; Hauk et al., 2008). Some studies have demonstrated that neutrophils also express

oncomodulin and these cells promote ON regeneration (Kurimoto et al., 2013). Furthermore, the cytokine CNTF has been widely studied in ON axonal regeneration and high concentrations or viral delivery of CNTF have been reported to cause considerable (Leaver et al., 2006, Muller et al., 2007) (Cui and Harvey, 2000, Cui et al., 1999), modest (Lingor et al., 2008) or no axon regeneration of the ON (Leon et al., 2000, Pernet and Di Polo, 2006).

### 1.3. Ocular injury

Ocular injury can be classified according to the Birmingham Eye Trauma Terminology System (BETTS) (Pieramici et al., 1997) and segmented into either closed or open globe injuries (Figure 1.5). Closed globe injuries can be classified into either contusion (blunt trauma) or lamellar laceration (partial thickness wound). Open globe injuries can be due to a laceration (either penetrating, perforating or an intraocular foreign body) or globe rupture.

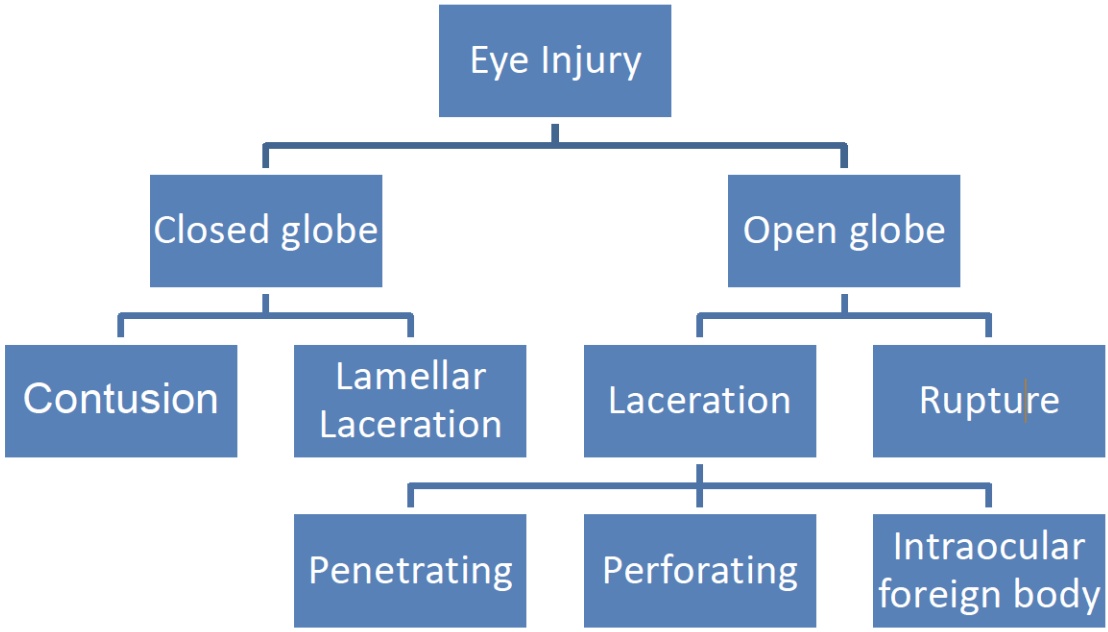


**Figure 1.5 Birmingham Eye Trauma Terminology System.** Closed globe injuries can be classified into either contusion or lamellar laceration. Open globe injuries are either laceration, which can be further separated into penetrating, perforating or intraocular foreign body, or a rupture of the globe. Figure reproduced from Pieramici et al., (Pieramici et al., 1997).

### 1.3.1. Traumatic optic neuropathy

Traumatic optic neuropathy (TON) describes a collection of diseases in which RGCs and the ON are damaged, causing visual loss (Sarkies, 2004). TON is a major cause of visual loss after brain and ocular injury and can be direct, where the ON is directly injured, for example, by penetrating injury from an object or projectile, avulsion from the globe following rotational injury or due to crush or cut injury from bone fragments after impact (Thanos et al., 2012, Steinsapir and Goldberg, 2011). Indirect TON is more common, with brain or ocular injury associated with secondary RGC injury. Common clinical characteristics of TON include reduced visual acuity, reduced colour perception and an ipsilateral relative afferent pupillary defect (RAPD) (Sarkies, 2004). Spontaneous recovery occurs in a minority of patients (Wu et al., 2008). However, the most common outcome is permanent visual loss. At present, there are no effective treatments for TON (Levin et al., 1999, Steinsapir et al., 2000, Edwards et al., 2005). Consequently, there is an unmet clinical need for TON treatments and the development of clinically viable therapeutics. ON atrophy is often delayed, developing 4-6 weeks after injury. The delayed nature of TON suggests that there is a therapeutic window for targeting and preventing RGC degeneration (Sarkies, 2004), although the time course of structural changes does not necessarily relate to the time course in which RGC death is preventable.

#### 1.3.1.1. Epidemiology and prevalence of TON

Civilians have a 19.8% lifetime prevalence of ocular injury, with greater prevalence in young males and occupations such as farming and military service (Wong et al., 2000). Primary causes of TON include falls, road traffic accidents and assaults, and are often associated with additional ocular and head injuries (Lee et al., 2010).

According to National Clinical Guidelines published in 2014, there are 1.4 million people in England and Wales attending emergency departments with a recent head injury each year, with 33-50% of these admittances being children under 15 years old (Davis et al., 2015). Traumatic brain injury (TBI) affects up to 160,000 people each year in the UK (headway.org), with severity ranging from minor to life-changing disability and death. TBI has variable manifestations and severity, diagnosis can be difficult and good prognostic markers are currently lacking. TON occurs in 0.5-5% of cases (Steinsapir and Goldberg, 1994, Nau et al., 1987). Moreover, 80% of mild TBI veterans injured during Operation Iraqi Freedom also exhibited symptoms of visual dysfunction (Cho et al., 2009a), suggesting that TBI and visual dysfunction are linked.

#### 1.3.1.2. Current treatments for TON

TON has historically been treated with high dose steroids (e.g. methylprednisolone) or ON decompression surgery (Levin et al., 1999). However, no studies have shown the efficacy of high-dose steroids or surgery in TON treatment. The National Acute Spinal Cord Injury Study (NASCIS) is a series of studies comparing corticosteroid (high-dose methylprednisolone) therapy with placebo after spinal cord injury (SCI) (Bracken et al., 1990). The NASCIS has failed to reach all their primary outcome

measures. However, the NASCIS did show increased infectious complications in the steroid-treated groups. The International Optic Nerve Trauma Study (IONTS) is a non-randomised interventional study which compared high-dose corticosteroid therapy to optic canal decompression surgery, measuring visual outcomes after TON (Levin et al., 1999). There were no clear benefits of either steroids or surgery on visual acuity, but there were improved outcomes in the observation only group.

The Corticosteroid Randomization After Significant Head Injury (CRASH) study enrolled 10,000 TBI patients internationally and demonstrated an increased mortality in patients treated with high-dose steroid therapy (48-hour infusion of methylprednisolone) compared to placebo (Edwards et al., 2005), suggesting high-dose steroid use has detrimental effects in TBI and TON patients. Several animal studies also indicate high-dose steroid toxicity to the injured ON (Steinsapir et al., 2000, Ben Simon et al., 2006, Diem et al., 2003).

There are currently no effective TON therapies and current treatment with high-dose steroids could cause more degeneration. A greater understanding of the intracellular mechanisms following ON trauma will aid the development of TON-specific treatments.

#### 1.3.1.3. Indirect TON

TON most commonly occurs due to indirect trauma leading to secondary optic neuropathy. Indirect TON results from forces transmitted from a distant site to the ON and tends to cause delayed pathology in comparison to direct ON injury and may differ

in severity depending on the injury site (Sarkies, 2004). TON can occur after an explosive blast, which can result in both primary and secondary blast injuries.

### 1.3.2. Explosive blast injuries

An explosive blast is created by the instantaneous conversion of a solid or liquid matter into its gaseous form, which produces energy in the form of light, sound, heat and pressure (Horrocks, 2001, Champion et al., 2009). Explosive blasts can cause explosive blast injuries, which can be characterised into four types: primary, secondary, tertiary and quaternary (Figure 1.6). Primary blast injury (PBI) is caused by the initial blast overpressure wave and can cause injury to the lungs (blast lung), tympanic membrane rupture, abdominal haemorrhage and perforation, eye rupture and injury, and concussion (Scott et al., 2015, Scott, 2011). Secondary blast injuries are due to blunt trauma or penetrating ballistic injuries caused by debris and shrapnel carried in the blast wind. Tertiary blast injuries result from the blast wind projecting individuals into a fixed object, such as a wall or building, or due to structural collapse and can cause fractures, amputations and TBI. Quaternary injuries are all explosion-related injuries which are not due to primary, secondary or tertiary mechanisms and can include thermal and chemical burns and inhalational injuries (Scott et al., 2015, Scott, 2011).

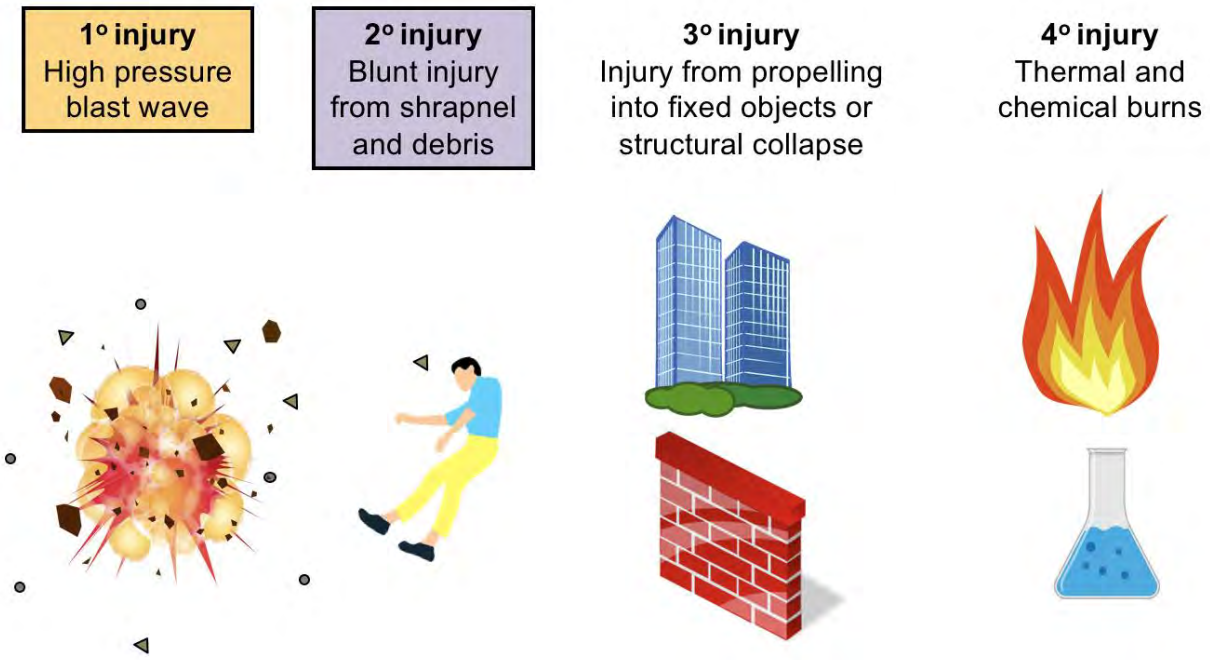


**Figure 1.6 Types of injuries caused by stages of an explosive blast.** PBI is due to the high overpressure blast wave. Secondary injury describes blunt injury from shrapnel and debris carried in the blast wind. Tertiary injury is due to either the subject being carried in the blast wind and impacting a fixed object (e.g. a building) or structural collapse. Quaternary injury is due to thermal or chemical burns.

#### 1.3.2.1. Prevalence of ocular injury after explosive blasts

The incidence of ocular trauma following an explosion is high, with an estimated 10% of surviving blast victims sustaining eye injuries (Goh, 2009), despite the relative surface of the eye being approximately 0.1% of the total body surface area (Bridges, 2006). In military personnel in the British Armed Forces deployed in Iraq and Afghanistan between July 2004 and May 2008, ocular injuries occurred in 10% of major trauma cases and between 78 - 86% of military personnel were injured by explosive devices (Murray et al., 2005, Blanch et al., 2011). In blast exposed individuals, closed eye injuries occurred in 43% of cases and ON atrophy occurred in 4% of cases (Cockerham et al., 2011). The prevalence of TON is approximately 20% of military ocular injuries (Weichel et al., 2008). There is a greater prevalence of retinal injury after ocular trauma in the military compared to the civilian population (60% vs. 2%) (Weichel et al., 2008, Jones et al., 1986).

Ocular PBIs occur in approximately 9% of US war related eye injuries (Ritenour and Baskin, 2008). Secondary blast ocular injuries are the most common type of blast injury and occur in ~42% of eye injury cases (Scott et al., 2015). The prevalence of tertiary and quaternary blast injuries are lower, representing 1% and 3% of eye injury cases, respectively (Scott et al., 2015).

Due to an increasing frequency of terrorist attacks, civilians are now exposed to blast injuries which were previously only occurring in war zones (Champion et al., 2009). A retrospective study of bombing events over a 20 year period identified >36,000 bombing incidents, ~ 6,000 bomb-related injuries and 700 bomb-related deaths in the US between 1983 and 2002 (Bridges, 2006, Kapur et al., 2005). It is estimated that

terrorist attacks have increased four-fold worldwide from 1999 to 2006, and injuries related to blast explosions have increased eight-fold (Wolf et al., 2009). Civilian victims are frequently exposed to multidimensional injuries involving PBIs, blunt and penetrating injuries and burns. Penetrating injuries are seen more frequently in civilian terrorist bombings compared to military explosions, largely due to the lack of body armour (Yeh and Schecter, 2012).

Penetrating and blunt eye injuries can be prevented by wearing eye protection; however, the primary blast wave can penetrate eye protection. Educational programmes highlighting the importance of wearing eye protection have promoted a 16% increase in compliance in combat Operations Iraqi and Enduring Freedom from 2003 - 2006 (Thomas et al., 2009). There were also fewer causalities experiencing eye injury when wearing eye protection; 17% of casualties with ocular injuries wore eye protection and 26% of casualties did not wear eye protection (Thomas et al., 2009). Ocular injuries still occur due to high energy blunt projectiles, refusal to wear eye protection, penetration of the primary blast overpressure wave or loss of eyewear during blast overpressure and wind (Lemke et al., 2013, Weinstein et al., 2018).

## 1.4. Primary blast injury

Explosive blast injury is a major cause of visual loss within the military (Cockerham et al., 2011, Warden, 2006, Rex, 2014). Military personnel can be exposed to repeated low-pressure blast waves throughout training and in combat. Military special operation officers attend breacher training, to learn how to breach rooms, doors and buildings, and part of the training is to deal with explosive blasts. Throughout breacher training, soldiers can be exposed to 12 sub-threshold blasts per day and an average of 13 blasts during deployment (Rex et al., 2015). In addition to understanding the pathology caused by a single high-pressure primary blast wave, it is important to understand the effects of repeated low-pressure blast waves.

### 1.4.1. Primary blast wave (Friedlander waveform)

Blast overpressure refers to the increase in pressure above atmospheric pressure after a blast, and the waveform consists of a positive phase followed by a sub-atmospheric negative pressure phase. Typically this has a Friedlander waveform (Ning and Zhou, 2015) (Figure 1.7). A Friedlander blast waveform reflects the large amount of pressure exploding from an explosive core, followed by a negative pressure wave which sucks objects back towards the explosive core. A blast wave can travel at a speed of 8000 m/s and can reach pressures up to 30,000 times normal atmospheric pressure (Housden, 2012, Cullis, 2001, Kocsis and Tessler, 2009). When travelling through tissue of different densities, the blast wave accelerates and decelerates, which causes PBIs (Housden, 2012). Fluid or gas-filled structures such as the eyes and lungs are particularly susceptible to PBI.

Pressure can be measured in kilopascals (kPa) or pounds per square inch (psi). Approximately, 1 psi is 6.9 kPa.

In an enclosed space, a blast wave reflects off different structures, slowing down the dissipations of the blast wave and causing it to remain at high pressure for longer and amplify its destructive capacity (Golan et al., 2014, Kluger, 2003). The waveform is a jagged wave with multiple positive and negative deflections (Figure 1.7C). Furthermore, it can lead to greater damage due to structural fragments carried in the blast wind and causing penetrating secondary blast injuries (Champion et al., 2009, Golan et al., 2014). A study by Leibovici et al., demonstrated a significantly higher

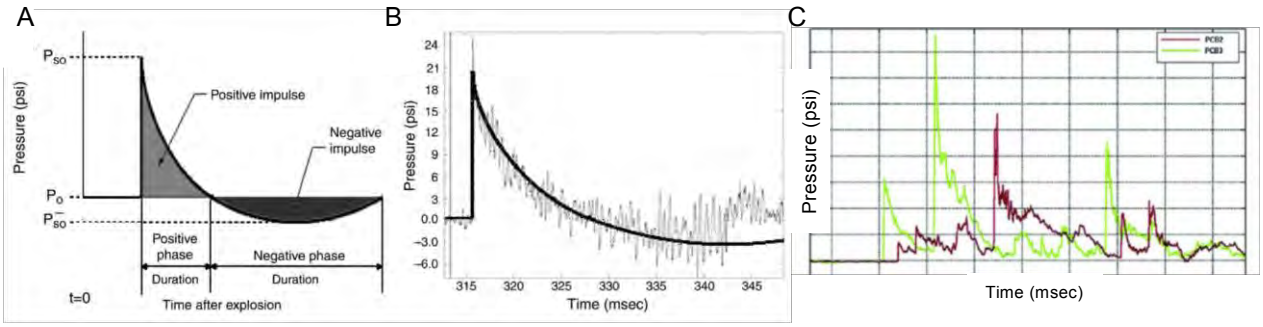

### 1.4.2. Animal models of PBI

Animal models can be used to study the effects of PBI and to test novel therapeutics, But, there are variations between models which makes comparisons difficult, for example, the method of blast-wave induction (e.g. using a modified paintball gun, blast tube, acoustic blast overpressure [ABO]), the location of the blast wave exposure on the body (e.g. head, eye, body), animal species, quantity and frequency of blast waves, and the pressure of the blast wave.

Animal models used to model PBI are summarised in Table 1.1.

### 1.4.3. Primary blast wave-induced brain injury

Head injury is a major reason for blast-induced mortality in victims of terrorist bombings (Yeh and Schecter, 2012). Doughtery et al., conducted a retrospective cohort study in 2011 of 2254 blast-injured American personnel in Iraq and concluded that 37% of individuals had sustained some degree of blast-induced neurotrauma (Dougherty et al., 2011). Blast injury can induce significant brain injuries including subarachnoid and subdural haemorrhage, as well as symptoms such as headache, tinnitus, amnesia, and post-traumatic stress disorder (Yeh and Schecter, 2012).

The mechanisms for how blast injury leads to TBI are not fully understood, but may be due to rupture of cortical vessels leading to diffuse axonal shearing and intracerebral, epidural and subdural haemorrhage formation (Bridges, 2006). It is further suggested that mild TBI could be caused by free radical release and neuronal cell death (Cernak et al., 2001). A recent study has shown that as the primary blast wave pressure increases, there is increased TBI and mortality in rats (Mishra et al.,

2016). Using a compressed gas shock-tube, Mishra et al., showed that a blast wave pressure of 145 kPa (approximately 12 psi) was the upper limit for mild TBI, 146-220 kPa (approximately 22-32 psi) caused moderate TBI and 221-290 kPa (approximately 33 – 42 psi) induced severe TBI and > 290 kPa (approximately 42 psi) was lethal to the rats (Mishra et al., 2016). In rats exposed to pressures in the mild TBI range, they showed increased oxidative and nitrosative markers (Mishra et al., 2016). A study by Pun et al., identified that low-level primary blast injury from a pressure of 7.1 psi in an open space by TNT explosives caused DNA-damage in oligodendrocytes and astrocytes in the white matter as early as 1 day post injury. Caspase-3 expression was low, suggesting that the cell death was non-apoptotic (Pun et al., 2011). They also showed there were darkening and shrunken cortical neurons in the cerebral cortex at 1 days after injury, but there were signs of recovery by day 4, and genetic analysis showed upregulation of repair genes by day 4 (Pun et al., 2011). This indicates that mild blast wave exposure may cause temporary neuronal injury, which is quickly resolved.

Most of the animal models of PBI are performed under anaesthesia, with mice restrained in a head holder to prevent head movement. Goldstein et al., performed the blast injury in a shock tube with a single blast of ~77 kPa and didn't restrain the mice so allowed for head rotation. This led to head acceleration and deceleration effects and demonstrated chronic traumatic encephalopathy (CTE) pathology, which includes phosphorylated tauopathy, myelinated axonopathy, neuroinflammation and neurodegeneration. This pathology is comparable to brains of military personnel exposed to explosive blasts (Tagge et al., 2018, Goldstein et al., 2012, Goldstein et al., 2014).

### 1.4.4. Visual system pathology

Ocular PBI can include sub conjunctival haemorrhages, traumatic uveitis and cataract, glaucoma, retina oedema, macular lesions and choroidal rupture. Military veterans with blast-related neurotrauma also report chronic photophobia and display visual tracking impairments due to damage to brain nuclei (Goodrich et al., 2013, Lemke et al., 2013).

Hines Beard et al., showed retinal, ON and corneal pathology after exposure to a 26 psi blast wave (Hines-Beard et al., 2012), and the damage was similar to veterans who had sustained closed-globe injuries (Cockerham et al., 2011) C57/Bl6 mice exposed to a blast overpressure wave of 26 psi directly to the eye displayed increased ON axons with degenerative profiles and collapsed myelin at 28 days post injury (dpi); however, the authors did not quantify the degree of RGC death (Bricker-Anthony et al., 2016). Other studies have shown progressive retinal degeneration after PBI; for example, Dutca et al., showed there was reduced ganglion cell complex (GCC) thickness at 4 months after exposure to a 20 psi blast wave (Dutca et al., 2014), and Mohan et al, demonstrated a reduced GCL cellularity at 10 months following a blast wave exposure of 20 psi (Mohan et al., 2013).

Repeated exposure to primary blast waves cause retinal injury and ON injury. For example, Vest et al., showed that repetitive blast exposure in quick succession causes significant ON axonal degeneration: 3 blasts separated by 0.5 seconds caused degeneration in 15% of RGC axons 2 weeks after injury, but no significant injury occurred if this interval was increased to 10 minutes (Vest et al., 2019). Furthermore, exposure to 15 psi once per day over 6 consecutive days only caused degeneration

in 3% of axons (Vest et al., 2019), suggesting that the impact of multiple blasts in quick succession causes more ocular pathology and may be representative of closed-space explosions where the blast overpressure wave will impact multiple times within seconds. Also using this model, Bernardo et al., showed increased oxidative stress and activation of the inflammasome pathway after exposure to 2 blasts exposures of 15 psi over 3 consecutive days (Bernardo-Colon et al., 2018). Another study which investigated repeated exposure of one blast of 43.5 psi on 3 consecutive days, demonstrated the activation of Müller glia, degeneration of photoreceptors and increased phosphorylated tau in neurons and glia, but a lack of biochemical changes in the brain (Mammadova et al., 2017). Taken together, these studies suggest that there is long-lasting neuronal inflammation, retinal and ON injury after repeated PBI exposure.

Human studies of individuals exposed to explosions and studying the effects of PBIs can be potentially confounded by secondary, tertiary and quaternary blast injuries. A recent study investigated the effect of ocular and visual system pathology in marine trainers at a breacher school (Capo-Aponte et al., 2015). The breacher school instructors are exposed to thousands of controlled isolated low-level primary blast waves of approximately 6 psi, without exposure to secondary or tertiary injuries, and could be exposed to approximately 15 blasts per day (Capo-Aponte et al., 2015). The study found that exposure to low-level blasts reduced corneal endothelial cell density counts and general visual field sensitivity, but did not affect oculomotor function, visual acuity, retinal and ON integrity and colour vision, highlighting that exposure to 6 psi can caused some visual pathology, but is likely to be within safe levels for training.

| *Blast orientation* | *Model* | *Pressure* | *Animal* | *Visual system pathology* | *Time points measured* | *Assessment* | *Reference* |
|---|---|---|---|---|---|---|---|
| Unilateral, right side | ABO by shock tube | 80 psi | Rats | Reduced ERG, reduced contrast sensitivity, increased retinal thickness | 2, 4, 6 and 8 months | ERG, optokinetic tracking, SD-OCT | (Allen et al., 2018) |
| Unilateral, left eye | Single and repeated blast with modified paintball gun | 15 – 26 psi | Mice | Increased cleaved caspase-1, IL-1α, IL-1β and IL-18. Degenerating ON axons and reduced VEP were prevented by high vitamin C and E and ketogenic diets. | 14 – 28 days | Western blotting, ELISA, PPD-stained ON resin semi-thin sections, VEP amplitudes | (Bernardo-Colon et al., 2018) |
| Unilateral | Modified paintball gun | 23-30 psi | Mice | Retinal detachment, cornea and lens damage, regional cell death, decreased ERG | 3-28 days | Gross examination, visual acuity, ERG, OCT, TUNEL, histology | (Bricker-Anthony et al., 2014b) |
| Unilateral; evaluation of contralateral eye | Modified paintball gun | 26 psi | Mice | Mild blunt injury, *commotio retinae*, decreased visual acuity, photoreceptor death, oxidative stress, microglial activation | 3-28 days | Gross examination, ERG, optokinetic tracking, OCT, histology | (Bricker-Anthony and Rex, 2015) |
| Unilateral | Modified paintball gun | 26 psi | Mice | ON degeneration, neuroinflammation, increase ROS, retinal cell death, transient increase in IOP, corneal injuries | 7-60 days | Gross examination, OCT, intraocular pathology, histology | (Bricker-Anthony et al., 2016) |
| Unilateral, right side | Single or repeated blast waves by shock tube | 10 psi | Rat | Apoptosis, gliosis | 5 days | Histology | (Choi et al., 2015) |
| Unilateral and bilateral, facing blast | Shock tube | 20 psi | Rat | Reduced ERG post blast, axonal degeneration | 1-14 days | ERG, histology | (DeMar et al., 2016) |
| Unilateral, left side facing | Air-blast inside open chamber | 20 psi | Mice | Decreased pERG, RGC loss and dendritic rearrangement, increase in spontaneous activity of RGCs | 1-16 weeks | pERG, multielectrode array, SD-OCT, dendritic field analysis, measures of IOP | (Dutca et al., 2014) |
| Unilateral side of head | Gas-driven shock tube | 11 psi | Mice | CTE-like pathology, phosphorylated tauopathy, myelinated axonopathy, | 14 days | Histological and behavioural tests | (Goldstein et al., 2012) |

| | | | | | | | |
|---|---|---|---|---|---|---|---|
| | | | | chronic neuroinflammation, learning and memory deficits | | | |
| Unilateral | Air-blast directly to skull's parietal-squamosal area | 0-70 psi | Mice | Neuronal loss in cortex, axonal degeneration, enlargement of forebrain, selective thinning of retinal layers, microglia activation | 24 hours-11 weeks | Histology, behavioural tests | (Guley et al., 2016) |
| Unilateral | Modified paintball gun | 26 psi | Mice | Corneal oedema, corneal abrasion, ON avulsion, poor visual acuity | 3-28 days | Gross examination, IOP, OCT, visual acuity | (Hines-Beard et al., 2012) |
| Bilateral | Air-blast directed to eye | 26 psi | Mice | Increased inflammation and apoptosis | 4-72 hours | Histology, TUNEL, western blot, ELISA | (Jiang et al., 2013, Jiang et al., 2014) |
| Facing blast | | 8-17 psi | Rabbits | Increased retinal thickness | 48 hours | IOP, direct ophthalmoscopy, OCT, histology | (Jones et al., 2016) |
| Supine face on | Single blast by shock tube | 25-45 psi | Mice | Degeneration, motor and memory deficits | 1-14 days | Behavioural tests, histology, TUNEL | (Koliatsos et al., 2011) |
| Unilateral, right side | Repeated exposure: 1 per day for 3 days with open-ended shock tube | 43.5 psi | Mice | Muller glial activation, photoreceptor death, increased phosphorylated tau. | 30 days | IF staining for GFAP, Iba1, CD68, phosphorylated tau, ONL thickness | (Mammadova et al., 2017) |
| Unilateral, left side of head | Air-blast inside open chamber | 20 psi | Mice | Decrease in RNFL, ON damage, decreased pupil light reflex, increase in oxidative stress proteins | 1 hour-10 months | pERG, ffERG, OCT, pupil light reflex, electron microscopy, histology | (Mohan et al., 2013) |
| Unilateral, right side | Single blast by shock tube | 12-22 psi | Rats | Fibre degeneration | 7-14 days | Histology | (Petras et al., 1997) |
| Unilateral | Air-blast directly to skull's parietal-squamosal area | 50-60 psi | Mice | Axonal injury, activation of microglia, impaired motor and visual performance, increased trail depression and contextual fear | 3 days-11 weeks | Behavioural tests, histology | (Reiner et al., 2014) |
| Unspecified | Explosive blast (case report) | Unspecified | Dog | Complete retinal detachment, vitreal haemorrhage, fibrin clots | 10 days | Ophthalmoscopic examination | (Shelah et al., 2007) |
| Isolated eye in gelatine | *Ex vivo* pig eye | 0-30 psi | Pig | Chorioretina and retinal detachment, disruption to | Unspecified | Histology, ultrasound bio microscopy | (Sherwood et al., 2014) |

| | | | | | | | |
|---|---|---|---|---|---|---|---|
| | | | | cornea, delamination of sclera | | | |
| Unilateral, right side | Single blast by shock tube | 17.5 psi | Rat | Apoptosis in retina and ON | 3-48 hours | TUNEL, histology | (Wang et al., 2014a) |
| Unilateral, left eye | Repeated blasts with modified paintball gun | 15 psi | Mice | Increased ON degeneration with blasts 0.5 sec apart, but no change from sham if interblast interval was 10 mins. Reduced VEP | 14 days | PPD stained ON semi-thin sections and VEP | (Vest et al., 2019) |
| Facing blast | Single blast wave by explosive charge detonations | 26-70 psi | Rat | Increase in inflammatory proteins, oedema and apoptosis | 1-14 days | Histology, western, TUNEL, ELISA | (Zou et al., 2013a) |

**Table 1.1. Visual system pathology in animal models of PBI .** Blast wave values are all converted to psi for direct comparison. This table has been modified and updated from DeWalt and Eldred 2017, De Mar et al., 2016 (DeWalt and Eldred, 2017, DeMar et al., 2016). **Abbreviations:** ELISA: enzyme linked immunosorbent assay; ERG: electroretinogram; ffERG: full-field electroretinogram; IF staining: immunofluorescent staining; IOP: intraocular pressure; kPa: kiloPascals; OCT: optical coherence tomography; pERG: pattern electroretinogram; psi: pounds per square inch; RGC: retinal ganglion cells; SD-OCT; spectral domain optical coherence tomography; TUNEL terminal deoxynucleotidyl transferase dUTP nick end labelling.

### 1.4.5. Retinal cell death in PBI

Multiple studies have demonstrated increased cleaved caspase-3 in the GCL and ON between 3 and 72 hours after whole animal (Wang et al., 2014b, Choi et al., 2015) and direct local ocular blast exposures (Jiang et al., 2013). Moreover, caspase-3 activation displays cumulative increases with multiple exposures (Choi et al., 2015), comparable to repeated exposure in combat, potentially leading to worse structural and functional visual outcomes (Weichel et al., 2008). Additionally, an alternative model using trinitrotoluene (TNT) explosives detected active caspase-3 exclusively in photoreceptors and not RGCs (Weichel et al., 2008). Other apoptotic markers, such as Bax, Bcl-xL and Cytochrome C are also elevated in the retina up to 24 hours after PBI (Jiang et al., 2013). DBA/2J mice lack the ocular regulatory mechanisms of immune privilege in the anterior chamber (Mo et al., 2003), and are thus used as a closed globe injury model to approximate features of open globe injury, without complications of infection (Bricker-Anthony and Rex, 2015). In this model, full length inflammatory caspase-1 is immunolocalised to the INL and GCL in control retinae, but immunostaining declines after PBI (Bricker-Anthony and Rex, 2015), suggesting caspase-1 cleavage. Bernardo et al., showed there was increased oxidative stress and activation of the inflammasome pathway after exposure to 2 blasts of 15 psi over 3 consecutive days (Bernardo-Colon et al., 2018). However, expression of necroptotic markers RIPK1 and RIPK3 were increased in the retina, with RIPK1 localised to the ONL, INL and Müller glia, and RIPK3 to the ONL, INL and GCL 3 and 28 days post-ocular PBI (Bricker-Anthony et al., 2014a). These findings suggest potential activation of necroptotic and/or pyroptotic death pathways. See section 1.6 for more details on cell death mechanisms.

Research into blast-induced RGC degeneration is in its infancy. However, roles for apoptotic and potentially inflammatory caspases in RGC death are apparent. There is currently no effective treatment for ocular PBI, highlighting the urgent need for an effective therapy.

## 1.5. Blunt ocular injury

Secondary blast injury can be caused by debris carried in the blast wind and impacting the eye or penetrating and causing an intraocular foreign body. Many improvised explosive devices are made by suicide bombers intent on maximising injury through adding nails and screws to their explosives (Stein, 2005). Blunt trauma can cause open globe injuries if the projectile force is sufficient to rupture the globe. Blunt ocular injuries can also be caused by sports injuries, for example, from the impact of a squash ball, or from a road traffic accident.

Blunt ocular trauma can also cause commotio retinae which is characterised by a closed globe injury with photoreceptor OS and RPE disruption and subsequent photoreceptor death (Blanch et al., 2013, Blanch et al., 2012b, Sipperley et al., 1978, Meyer et al., 2003). In commotio retinae, there is retinal opacification and reduced visual acuity which varies depending on the injury severity and lesion location. There are no current treatments for commotio retinae (Meyer et al., 2003, Sipperley et al., 1978, Kiel and Chen, 2001), although visual acuity can improve spontaneously.

### 1.5.1. Prevalence of blunt ocular injury

Blunt ocular trauma can be caused by road traffic accidents, sports injuries, and from explosive devices used in military combat or terrorist bombings. Secondary blast injury is the most common type of explosive blast injury, occurring in approximately 42% of

cases (Scott et al., 2015). In a study assessing closed globe combat ocular injuries, 16.3% of cases had commotio retinae, with ocular contusion being the most frequent closed-globe injury in 71.4% of eyes (Islam et al., 2016). After blunt ocular trauma, the ganglion cell complex (GCC) [RNFL, GCL and inner plexiform layer (IPL)] thickness is reduced in 40.9% of cases, and there is preserved visual acuity in 2/3$^{rd}$ of these cases (Cennamo et al., 2013). The GCC thickness is decreased at two weeks after injury and plateaus at 20 weeks, suggesting that there is delayed and progressive RGC degeneration. However, the cohort size was small (22 individuals) and therefore may not be representative (Cennamo et al., 2013).

### 1.5.2. Animal models of blunt ocular injury

Animals models used to study blunt ocular trauma are summarised in Table 1.2. Blunt impact to a rat inferior sclera can cause localised retinal injury with death of 18.4% photoreceptors and loss of photoreceptor function. Electroretinogram (ERG) amplitudes reduced to ~50% of intact values at 2 weeks after injury (Blanch et al., 2012b). In addition, RGCs die surrounding the injury site (Blanch et al., 2012b), although the mechanisms of cell death have not yet been characterised. In some animal models, the globe is ruptured, which causes complications from infection and inflammation.

#### 1.5.2.1. Cell death in blunt ocular injury

Caspase-9 promotes photoreceptor death in a rat blunt ocular injury model and intravitreal injection of a dominant negative mutant (inactive) caspase-9 promotes photoreceptor survival and recovers some photoreceptor function (Blanch et al., 2014). Caspase-1 immunostaining increased in the INL and GCL at 28 dpi in C57 Bl/6

mice, suggesting possible activation of the pyroptotic death pathway (Bricker-Anthony and Rex, 2015). See section 1.6 for more details on cell death mechanisms.

| *Species* | *Impact site* | *Energy, J* | *Velocity, m/s* | *Weight, g* | *Injuries reported* | *References* |
|---|---|---|---|---|---|---|
| Porcine | Nasal sclera over ora serrata | 0.49-1.8 | 50-64 | 0.38 | Retinal breaks, choroidal rupture, RPE disruption at low energy. Commotio retinae at >0.68J. Gross retinal disruption at 1.8J | (Blight and Hart, 1977, Hart and Blight, 1979) |
| Porcine | Lateral sclera over pars plana | 0.32 | 33 | 0.57 | Commotio retinae, vitreous haemorrhage, no breaks / dialyses | (Gregor and Ryan, 1982b) |
| Owl Monkey | Central cornea | 0.39-1.05 | 47 | 0.35-0.95 | Commotio retinae only | (Sipperley et al., 1978) |
| Cat | Central cornea | 0.44 | 50 | 0.35 | Commotio retinae, variable hyphema | (Bunt-Milam et al., 1986) |
| Rabbit | Lateral sclera over retina | 0.57-1.62 | 46.8-79 | 0.52 | Retinal tears and necrosis, choroidal and vitreous haemorrhage. Commotio retinae at lower energy, rupture at higher energy | (Cox, 1980) |
| Porcine | Central cornea | 0.49-1.9 | 50-100 | 0.38 | No injury at low energy. Dialysis in 50% at higher energy | (Hart and Blight, 1979) |
| Porcine | Paracentral cornea | 1.25 | 52.3 | 0.95 | Commotio retinae, RPE disruption, RPE and retinal detachment | (Gregor and Ryan, 1982a) |
| Rat | Inferior sclera | - | 20 | 0.095-0.91 | Globe rupture with higher weights, vitreous haemorrhage, retinal atrophy, commotio retinae. | (Blanch et al., 2012b) |
| Mouse | PBI to the left eye with contralateral blunt injury | 26 psi blast | N/A | N/A | Reduced visual acuity, retinal cell death, increased oxidative stress and microglial reactivity. No ON injury | (Bricker-Anthony and Rex, 2015) |

**Table 1.2 Animal models of blunt ocular trauma** . Modified and updated from Blanch et al., 2012 (Blanch et al., 2012a).

## 1.6. Cell death mechanisms

Cell death can occur through multiple mechanisms that can be characterised according to cellular morphology and cell signalling pathway members (Figure 1.8). I have focused on apoptosis and necroptosis which are summarised in Table 1.3. For further descriptions of cell death mechanisms, the reader is referred to a recent review: (Galluzzi et al., 2018).

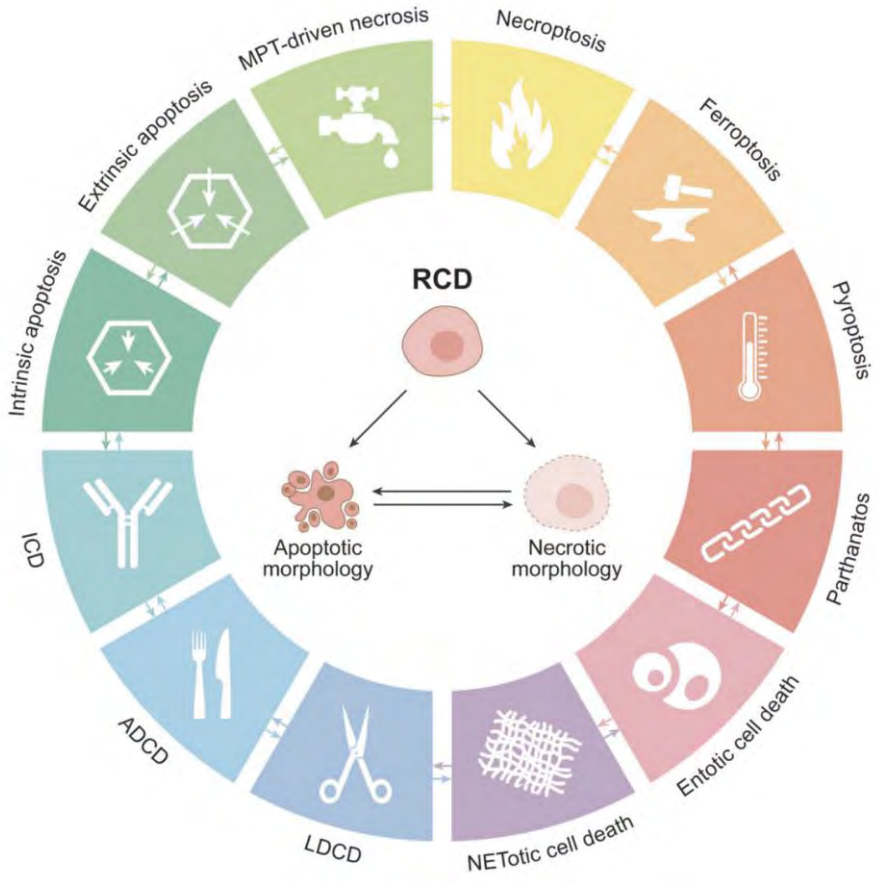


**Figure 1.8. Major cell death mechanisms .** Cells can die through regulated cell death (RCD) routes, or display apoptotic or necrotic morphology. **Abbreviations:** ADCD; autophagy-dependent cell death, ICD; immunogenic cell death, LDCD; lysosome-dependent cell death, MPT; mitochondrial permeability transition. Reproduced from Galluzzi et al., 2018 (Galluzzi et al., 2018).

| | *Apoptosis* | *Necrosis* | *Necroptosis* |
|---|---|---|---|
| **Type of cell death** | Controlled | Uncontrolled | Controlled |
| **Trigger** | Trauma, toxic stress, self-renew, aging, development | Trauma, toxic stress, infection | Trauma, toxic stress, infection |
| **Morphology** | Extensive membrane blebbing, condensation and fragmentation of the nucleus | Extensive organelle and cell swelling, loss of membrane integrity, release of extracellular contents | Cytoplasmic swelling, rupture of the plasma membrane and swelling of the intracellular content |
| **Signalling pathway** | Specific, intrinsic or extrinsic pathway | Non-specific | Specific e.g. TNFR1 pathway |
| **Executioner** | Caspases (-2, -3, -6, -7, -8 and -9) | - | RIPK1 and -3 |
| **Role of mitochondria** | Release of cytochrome c, interaction with Bcl-2 protein family. Mitochondrial dysfunction | Mitochondrial dysfunction, failure of ATP production | Mitochondrial dysfunction, production of ROS |
| **Complex formed** | Apoptosome | - | Necroptosome |
| **Inflammatory response** | Anti-- or pro- inflammatory | Pro-inflammatory | Pro-inflammatory |
| **DAMP release** | Yes | Yes | Yes |
| **Inhibitor** | z-VAD-fmk | - | Necrostatin-1 |
| **Human condition** | Physiological or pathological | Pathological | Pathological |

**Table 1.3. Mechanisms of apoptosis, necrosis and necroptosis .** Figure modified from Zhao et al., 2015 (Zhao et al., 2015)

### 1.6.1. Apoptosis

Apoptosis describes a regulated form of programmed cell death (PCD), which occurs during normal development, after injury and in other disease states (Bahr, 2000, Elmore, 2007). Apoptosis is caspase-dependent, with well described morphological changes, including the regulated formation of apoptotic bodies and removal of debris by phagocytosis, therefore eliciting minimal inflammatory responses. At the other end of the cell death spectrum, necrosis describes uncontrolled cell lysis associated with inflammation, and commonly follows trauma, ischaemia or excitoxicity (Elmore, 2007, Ryan and Salvesen, 2003).

#### 1.6.1.1. Extrinsic apoptotic pathway

The extrinsic apoptotic pathway is activated through ligand-activation of tumour necrosis factor (TNF) receptor members (Kischkel et al., 1995) including Fas/CD95 receptor, successive recruitment of adaptor proteins, such as Fas-associated protein with death domain (FADD) (Kischkel et al., 1995, Chinnaiyan et al., 1995) and subsequently pro-caspase-8 (Wajant, 2002). Interactions between Fas/CD95, FADD and caspase-8 form the death induced signalling complex (DISC) (Kischkel et al., 1995, Muzio, 1998) and initiate caspase-8 activation (Wajant, 2002, Muzio, 1998), which sequentially cleaves and activates executioner caspases-3, -6 and -7 (Fan et al., 2005). Additionally, caspase-8 can cleave the B-cell lymphoma (Bcl)-2 protein family member BH3 interacting domain death agonist (Bid) into truncated Bid (tBid), which stimulates mitochondrial outer membrane permeabilisation (MOMP), releasing apoptogenic factors (Kuwana et al., 1998) including cytochrome C, apoptotic protease activating factor 1 (Apaf-1), second mitochondria-derived activator of caspase/direct

inhibitor of apoptosis-binding protein with low pI (Smac/DIABLO), HtrA2/Omi, endonuclease-G and apoptosis inducing factor (AIF) (Kroemer et al., 2007, Nickells, 2010).

Caspase-8 also acts as a non-enzymatic scaffold in the assembly of a pro-inflammatory “FADDosome” (caspase-8-FADD-RIPK1) complex, inducing nuclear factor κβ (NFκβ)-dependent inflammation (Henry and Martin, 2017)

#### 1.6.1.2. Intrinsic apoptotic pathway

The intrinsic apoptotic pathway is mitochondria-dependent and activated by intracellular insults, such as DNA damage and loss of extracellular membrane integrity, leading to MOMP (Kuwana et al., 1998). Mitochondrial-derived cytochrome c complexes with Apaf-1, and successively recruits pro-caspase-9 to form a protein complex termed the apoptosome (Li et al., 1997, Adams and Cory, 2002), allowing activation of caspase-9 and sequentially downstream executioner caspases (Li et al., 1997).

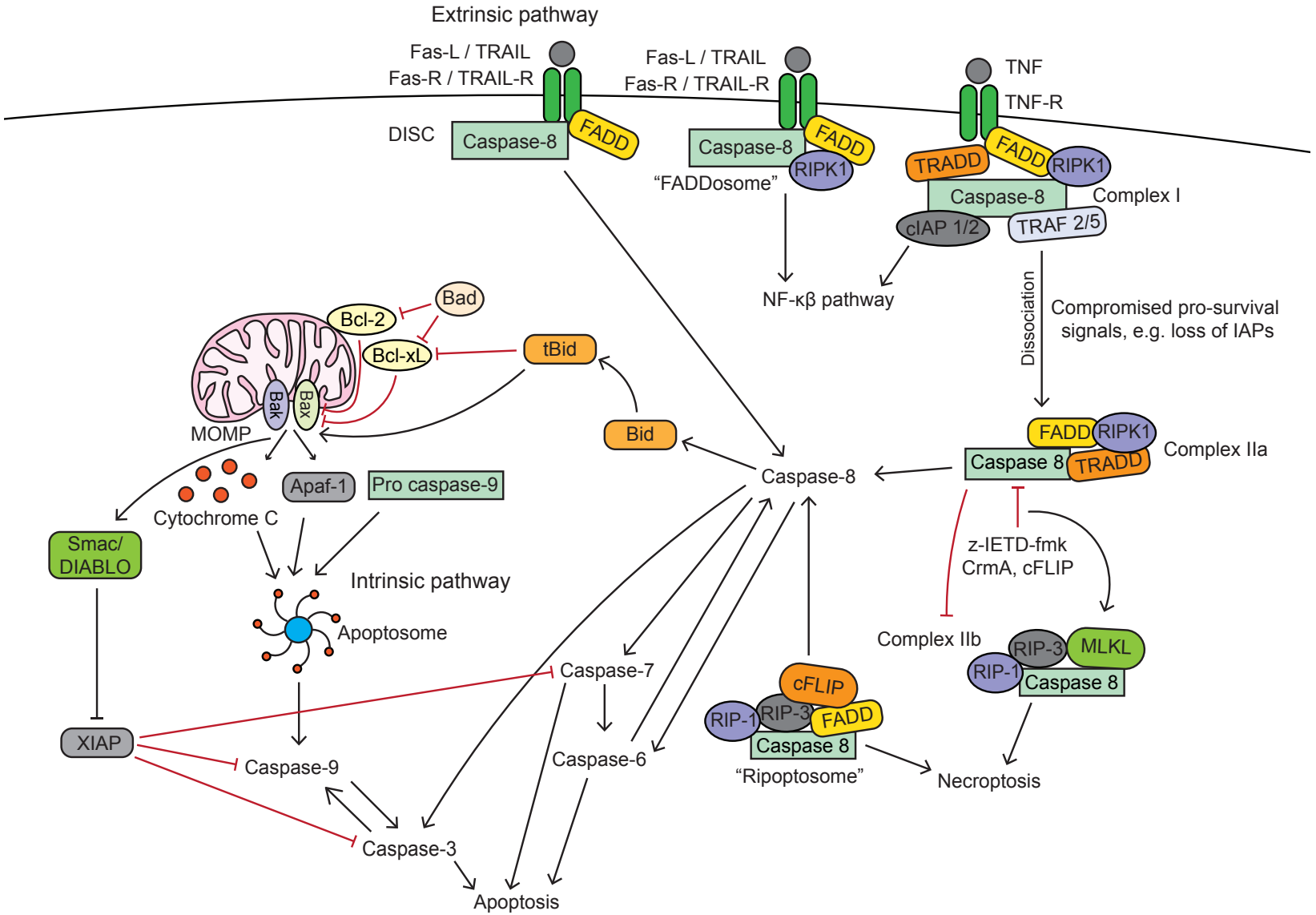
Extrinsic pathway
Fas-L / TRAIL
Fas-R / TRAIL-R
DISC
Caspase-8
FADD
Fas-L / TRAIL
Fas-R / TRAIL-R
Caspase-8
FADD
RIPK1
"FADDosome"
TNF
TNF-R
TRADD
FADD
RIPK1
Caspase-8
Complex I
cIAP 1/2
TRAF 2/5
NF-κβ pathway
Dissociation
Compromised pro-survival signals, e.g. loss of IAPs
Bad
Bcl-2
Bcl-xL
tBid
Bak
Bax
MOMP
Bid
Caspase-8
FADD
RIPK1
Caspase 8
TRADD
Complex IIa
Cytochrome C
Apaf-1
Pro caspase-9
Smac/
DIABLO
Intrinsic pathway
Apoptosome
z-IETD-fmk
CrmA, cFLIP
Complex IIb
RIP-3
MLKL
RIP-1
Caspase 8
Caspase-7
cFLIP
RIP-1
RIP-3
FADD
Caspase 8
"Ripoptosome"
XIAP
Caspase-9
Caspase-6
Necroptosis
Caspase-3
Apoptosis

**Figure 1.9 Apoptotic caspases in the canonical intrinsic and extrinsic apoptotic pathways and the necroptotic pathway .** Death receptor activation mediates the extrinsic pathway. Fas-R and TRAIL-R recruit FADD (Kischkel et al., 1995, Chinnaiyan et al., 1995) and pro-caspase-8 (Wajant, 2002), forming the DISC (Kischkel et al., 1995, Muzio, 1998), leading to proximity-induced caspase-8 activation (Muzio, 1998, Wajant, 2002) and downstream activation of executioner caspase-3, -6 and -7 (Fan et al., 2005). Caspase-8 can also activate the intrinsic pathway through truncating BH3-interacting domain death agonist (Bid) into tBid, which then promotes Bak and Bax mitochondrial membrane insertion, increasing MOMP and releasing apoptogenic factors (Kuwana et al., 1998), including Apaf-1, Cytochrome C and second mitochondria-derived activator of caspase/direct inhibitor of apoptosis-binding protein with low pI (Smac/DIABLO) (Kroemer and Blomgren, 2007, Nickells, 2010). Cytochrome C, Apaf-1 and pro-caspase-9 form the septameric apoptosome complex (Adams and Cory, 2002, Li et al., 1997), which activates caspase-9 and successively downstream executioner caspases. Smac/DIABLO indirectly promotes apoptosis by opposing XIAP inhibition of caspase-3, -7 and -9 (Scott et al., 2005). Caspase-8 can also form complex I at the TNF receptor, which upregulates the NF-κβ survival inflammatory pathway; however, if survival signals are compromised (for example, IAPs) then complex I dissociates from the receptor forming complex IIa, which initiates caspase-8-dependent apoptosis (Micheau and Tschopp, 2003). Caspase-8 inhibits complex IIb formation and necroptosis and caspase-8 inhibition (for example, through z-IETD-fmk) induces complex IIb formation, causing necroptosis (Feltham et al., 2017). The 'ripoptosome' complex forms after cellular IAPs (cIAPs) or XIAP inhibition, causing caspase-8-dependent apoptosis and necroptosis (Tenev et al., 2011, Feoktistova et al., 2012).

### 1.6.2. Necroptosis

For decades, apoptosis has been considered to be the standard mechanism of PCD, whereas necrosis was considered to cause uncontrolled explosive death. Recently, a regulated form of necrosis has been described, termed necroptosis (Vandenabeele et al., 2010). Necroptosis is defined as a controlled cell death process, which results in cellular leakage, and is morphologically characterised by organelle swelling and cytoplasmic granulation (Vanden Berghe et al., 2014). Necroptosis is a regulated form of necrosis and is dependent on receptor interacting protein kinase (RIPK) 1 and RIPK3 (Vandenabeele et al., 2010, Gizycka and Chorostowska-Wynimko, 2015).

#### 1.6.2.1. Necroptotic pathway

RIPK1 and RIPK3 are kinases involved in TNF-induced regulated necrosis (Zhang et al., 2010, Declercq et al., 2009, Festjens et al., 2007). RIPK1 signalling mechanisms can cause apoptosis, necroptosis or cell survival (via the NFκβ pathway), depending on RIPK1 post-translational modifications and complex formation (Figure 1.9).

In response to TNF stimulation at the TNFR-1, RIPK1 is recruited alongside TRADD, TNF receptor associated factor (TRAF) 2/5 and cellular inhibitor of apoptosis (cIAP) 1/2 to form a membrane associated complex called complex I (Vanden Berghe et al., 2014). In complex I, RIPK1 is poly ubiquitinated leading to activation of the pro-survival NFκβ pathway. Compromised pro-survival signals [e.g. loss of inhibitors of apoptosis (IAPs)] lead to the dissociation of complex I and the formation of complex IIa. Complex IIa comprises of FADD and results in caspase-8 cleavage, activation and downstream apoptosis. When caspase-8 is inhibited (e.g. pharmacologically using z-IETD-fmk or

endogenous inhibitors CrmA or cFLIP), RIPK1 associates with RIPK3 via the RIPK homotypic interaction motif (RHIM) (a 16 amino acid motif found on some RIPK family members) domain (Sun et al., 2012) and forms complex IIb (Vanden Berghe et al., 2014, Moquin et al., 2013, Zhang et al., 2009, Cho et al., 2009b). Complex IIb consists of RIPK1, RIPK3, MLKL and caspase-8 and is endogenously inhibited by caspase-8. Complex IIb formation initiates downstream necroptosis. RIPK3 phosphorylates pseudo kinase mixed lineage kinase domain-like (MLKL) (Vandenabeele et al., 2010), which induces MLKL translocation to the plasma membrane (Weinlich et al., 2016) and its interaction with membrane lipids triggers membrane permeabilisation and subsequent cell death.

Necroptotic cells release their intracellular contents, causing inflammation and promoting cell damage and death in the surrounding area (Zhou and Yuan, 2014). Phagocytes clear necroptotic cells, although bystander damage may occur, and persistent inflammation may prevail with a defective immune system or chronic injury (Vandenabeele et al., 2010). Necroptosis occurs during development and in pathological conditions.

#### 1.6.2.2. RIPK1

RIPK1 contains an N-terminal kinase domain, C-terminal death domain and a central intermediate domain (Zhang et al., 2010). The intermediate domain is important for RIPK1-dependent activation of NFκβ, whereas the kinase domain is involved in cell death induction (Ofengeim and Yuan, 2013, Zhang et al., 2010). Caspase-8 can cleave RIPK1 to inhibit NFκβ activation (Lin et al., 1999).

### 1.6.2.3. Necroptosis inhibitors

Necrostatin-1 (Nec-1) is a synthetic allosteric inhibitor of RIPK1 and inhibits necroptotic cell death by preventing the transition from complex IIa to complex IIb (Vanden Berghe et al., 2014, Degterev et al., 2008, Degterev et al., 2005). Nec-1 is an effective inhibitor of RIPK1 activity but also inhibits indoleamine-2,3-dioxygenase (IDO), which has a role in immunomodulatory function (Zhou and Yuan, 2014). This is an unfavourable side effect of Nec-1 and lead to the development of a more stable Nec-1 analogue, termed Nec-1 stable (Nec-1s) (Figure 1.10). Nec-1s is also called 7-Cl-O-Nec-1 and has a chlorine at position 7 on the indoleamine moiety and a substitution of a thiohydantoin with a hydantoin (Figure 1.10 ii) (Takahashi et al., 2012). Nec-1s has a higher affinity and specificity than Nec-1 (Linkermann and Green, 2014), is >1000 fold more selective for RIPK1 than for other human kinases and does not interfere with IDO (Takahashi *et al.*, 2012). Nec-1s could offer a potential therapeutic option for necroptosis-dependent disease, including neurodegeneration (Takahashi *et al.*, 2012).

Alternatively, necroptosis can be inhibited using MLKL inhibitors (Yan et al., 2017), or repurposed FDA-approved drugs. Ponatinib and pazopanib are currently FDA-approved as cancer treatments and are small molecule inhibitors of TNF-$\alpha$-induced necroptosis; ponatinib directly inhibits RIPK1 and RIPK3, whilst pazopanib targets RIPK1 (Fauster et al., 2015). Further, anti-convulsant membrane blocker phenytoin acts at an earlier stage of necrosome formation but is much less potent than the necrostatins (von Massenhausen et al., 2018). However, there have been multiple clinical trials testing pharmacological RIPK1 inhibitors (Li et al., 2017, Harris et al.,

2017, Harris et al., 2016, Najjar et al., 2015, Teng et al., 2005), with none of these compounds reaching phase III clinical trials to date.

**i)** Necrostatin-1

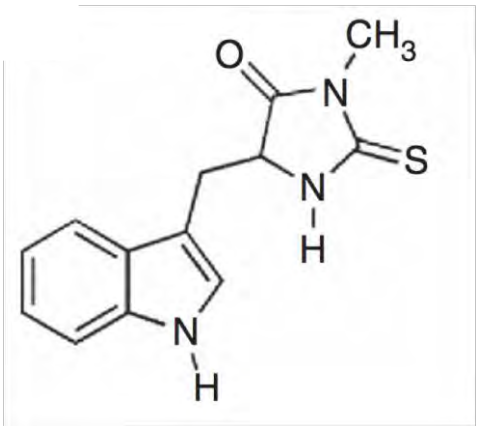


**ii)** Necrostatin-1s

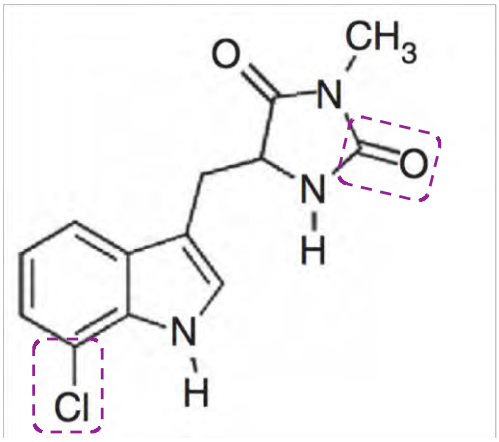

#### 1.6.2.4. Necroptosis in development

Necroptosis is mainly invoked by pathological circumstances, due to the activation of the pathway by pathological stimuli such as TNF-$\alpha$, but recent studies have suggested necroptosis also has a role during development (Shan et al., 2018, Weinlich et al., 2017). Apoptosis occurs during normal development, as evidenced by knockout mutant mice *casp3*$^{-/-}$, *casp9*$^{-/-}$ and *apaf-1*$^{-/-}$ displaying severe developmental defects and embryonic lethality (Kuida et al., 1996, Kuida et al., 1998, Cecconi et al., 1998, Yoshida et al., 1998). Mice which have mutations in necroptotic machinery (*ripk3*$^{-/-}$ and *mlkl*$^{-/-}$) have normal development and no abnormal phenotypes (Polykratis et al., 2014, Wu et al., 2013, Liu et al., 2017), suggesting that necroptosis may not be involved in the regulation of normal physiological development. However, a recent study found that some mammalian species (not rodents) which have an MLKL orthologue have smaller litter sizes and longer interbirth intervals (Stockley and Hobson, 2016). The authors suggest that necroptosis may eliminate unfit offspring early in pregnancy and eliminate the burden of rearing unhealthy offspring. Therefore, necroptosis may play a role in ensuring vitality of healthy offspring. Further research suggested that necroptosis may abort defective mutant embryos. RIPK3 and MLKL deficiency can prevent embryonic lethality induced by genetic mutations, suggesting that necroptotic machinery is required for embryonic abortion (Shan et al., 2018). However, these studies are recent and partly speculative, therefore further investigation is required.

#### 1.6.2.5. Necroptosis in neurodegeneration

Necroptosis occurs in many pathological conditions including ischemia-reperfusion injury, inflammation and pathogen infection amongst others (Zhou and Yuan, 2014).

Necroptosis promotes neuronal cell death in traumatic and neurodegenerative disease (Zhang et al., 2017). RIPK1 is elevated in a rat experimental model of intracerebral haemorrhage, and RIPK1 inhibition or genetic knockdown reduces the severity of brain injury (Shen et al., 2017). RIPK1, RIPK3 and MLKL expression is elevated in *post mortem* amyotrophic lateral sclerosis (ALS) spinal cord tissue and neuron viability is increased in an ALS mouse model (optineurin knockout; OPTN -/-) with mutations in RIPK1 and RIPK3 (Re et al., 2014, Ito et al., 2016, Politi and Przedborski, 2016). Necroptosis has an emerging role in Alzheimer's disease mice, Nec-1 reduces cognitive impairments and β-amyloid and tauopathy in an AD amyloid precursor protein/presenilin 1 (APP/PS1) mouse model and in mice treated with aluminium that have Alzheimer's disease-like pathology (Yang et al., 2017, Qinli et al., 2013). In Niemann-Pick disease, a progressive neurodegenerative autosomal recessive lysosomal storage disorder, there are elevated levels of RIPK1, RIPK3 and MLKL in *post mortem* human brain tissue and in a mouse model of Niemann-Pick disease, type C1 (NPC1 -/-), Nec-1 significantly prolonged lifespan (Cougnoux et al., 2016). In a controlled cortical impact TBI mouse model, Nec-1 reduced histopathology and improved function (You et al., 2008). Nec-1 also preserved tissue viability in weight-drop and laminectomy SCI models (Wang et al., 2014c). Together, these studies suggest that necroptosis has an evident role in traumatic neuronal death and neurodegeneration.

#### 1.6.2.6. Necroptosis in ocular disease

Necroptosis also occurs in eye disease. After ON transection (ONT), RIPK1-dependent mechanisms promote RGC death and intravitreal injections of either Nec-1 or RIPK1 siRNA leads to a 3-fold increase in RGC survival at 14 dpi (Lysko Meghan, 2012). In a retinal ischemia-reperfusion model, there is increased expression of RIPK1 and RIPK3 and inactive caspase-8 present in the GCL, and Nec-1 administration reduced retinal damage and provided RGC neuroprotection *in vivo* and *in vitro* (Dvoriantchikova et al., 2014, Kim et al., 2017). Moreover, in the rd10 mouse model of retinitis pigmentosa, RIPK1 and RIPK3 are elevated and RIPK1 inhibition (by Nec-1 subcutaneous implantation) or RIPK3 knockout preserves cone photoreceptors and their function (Murakami et al., 2012). In a mouse model of age-related macular degeneration, induced by double stranded RNA (dsRNA), RIPK1 and RIPK3 are elevated and induce degeneration and inflammation in RPE cells and photoreceptors (Murakami et al., 2014). Furthermore, photoreceptors die by RIPK-dependent mechanisms in a mouse model of retinal detachment (Murakami et al., 2011). Necroptosis occurs in photoreceptors in a P23H rhodopsin model of retinal degeneration, with subcutaneous injections of Nec-1s (15 mg/kg body weight) rescuing ONL thinning (Viringipurampeer et al., 2016).

## 1.7. Caspases

Caspases are a family of **c**ysteine **asp**artate prote**ases** that have a role in apoptosis, proliferation, DNA damage response, tumour suppression and inflammation, amongst other roles (Connolly et al., 2014). Caspases have roles in neuronal pruning during development, can induce RGC death after trauma and disease, and can promote RGC axonal regeneration (Thomas et al., 2017). Such processes are attenuated by endogenous and pharmacological inhibitors as well as gene knockdown using small interfering RNA (siRNA), to both understand signalling mechanisms and develop therapeutics to prevent cell death.

Caspases can be divided into two major phylogenic sub-families, either interleukin-1β-converting enzyme (ICE) inflammatory caspases or mammalian counterparts of CED-3 apoptotic caspases (Nicholson, 1999, Nicholson and Thornberry, 1997).

### 1.7.1. Caspase structure

Caspases consist of a pro-domain, and a large (p20) and small (p10) catalytic subunit (Figure 1.11) (Nicholson, 1999). Cleavage of the pro-caspase at the conserved Asp-X bond results in formation of the heterotetramer and release of the pro-domain leaving the mature caspase (Lavrik et al., 2005).

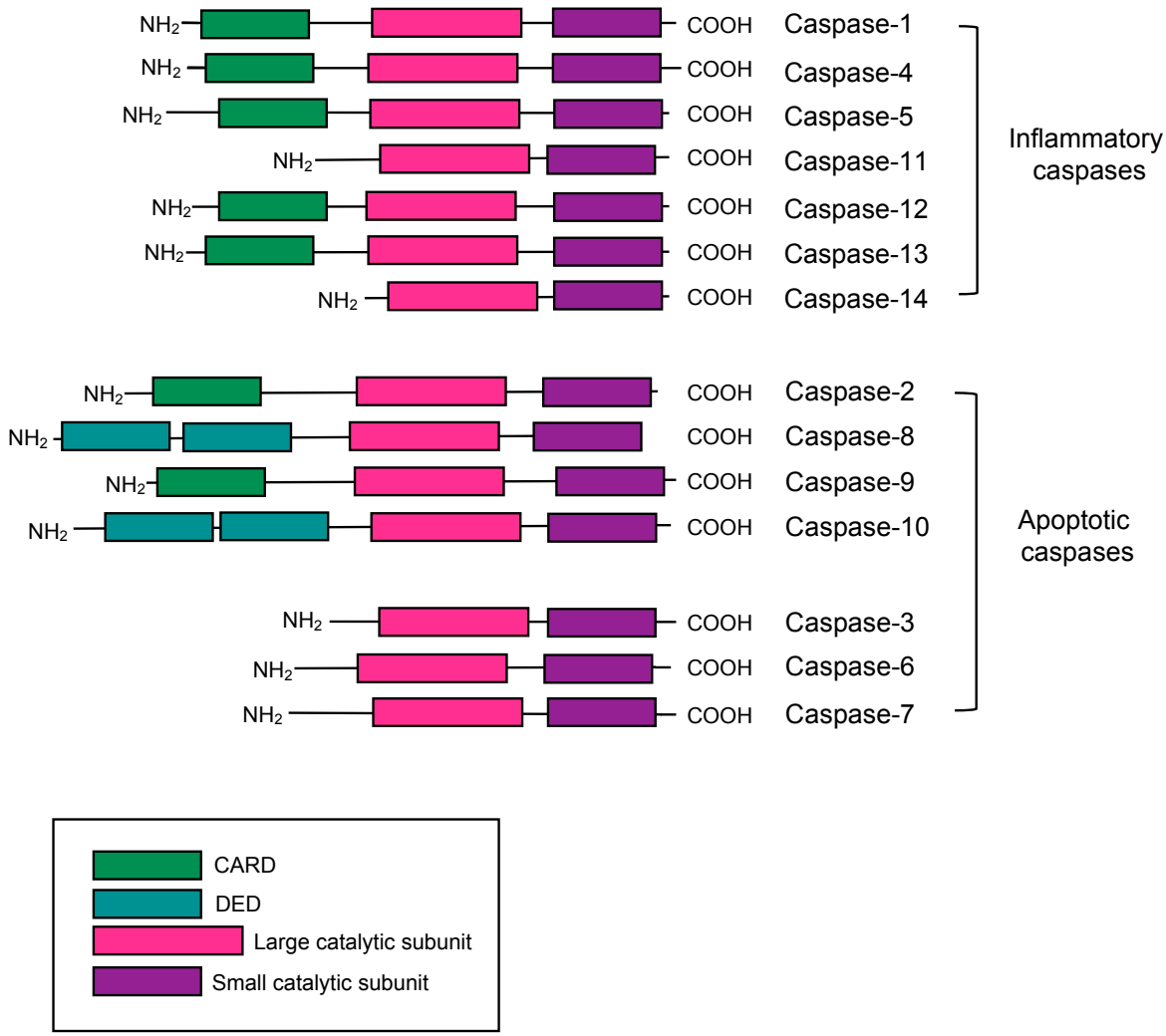
NH2
COOH
Caspase-1
Caspase-4
Caspase-5
Caspase-11
Caspase-12
Caspase-13
Caspase-14
Inflammatory caspases
Caspase-2
Caspase-8
Caspase-9
Caspase-10
Caspase-3
Caspase-6
Caspase-7
Apoptotic caspases
CARD
DED
Large catalytic subunit
Small catalytic subunit

#### 1.7.1.1. Death domains

The caspase pro-domain contains death domain (DD) superfamily members, which are important in the recruitment of pro-caspases and for interactions between receptors and adaptor proteins. DD members include the DD death effector domain (DED), caspase recruitment domain (CARD) and the pyrin domain (PYD) subfamilies (Figure 1.11) (Cullen and Martin, 2009, Fan et al., 2005). Caspase-8 and caspase-10 contain DEDs, whereas caspase-9 and caspase-2 contain CARDs (Fan et al., 2005, Kumar, 2007).

#### 1.7.1.2. Adaptor proteins

Adaptor proteins contain DDs and facilitate interactions with TNF family death receptors or form complexes with other adaptor proteins. Adaptor proteins include RIP associated ICH-1 homologous protein with a death domain (RAIDD), FADD, TNF receptor-associated death domain (TRADD) and Apaf-1, which are essential for pro-caspase recruitment and subsequent activation (Tinel and Tschopp, 2004, Lin et al., 2000, Bouchier-Hayes and Green, 2012).

### 1.7.2. Caspase activation

Caspases can be activated by proximity-induced dimerization, within protein complexes, feedback loops and through pro-enzyme cleavage (Parrish et al., 2013, Cullen and Martin, 2009). Initiator caspases are activated in complexes at extracellular receptors or within cytoplasmic protein complexes. Activated initiator caspases proteolytically cleave executioner caspases in the cytoplasm, initiating and amplifying the cascade.

### 1.7.3. Apoptotic caspases

Caspases are the main components of the apoptotic signalling cascade and induce apoptosis through initiator and executioner family members: initiator caspases (caspase-2, -8, -9 and -10) activate executioner caspases (caspase-3, -6 and -7) through catalytic cleavage of their activation domain (Fan et al., 2005, Kumar, 2007). Activated executioner caspases then hydrolyse or cleave proteins leading to cellular apoptosis (Nicholson, 1999). Caspases can be activated through the canonical intrinsic or extrinsic apoptotic pathways (Section 1.6.1) and (Figure 1.9).

### 1.7.4. Inflammatory caspases and pyroptosis

Inflammatory caspases (-1 or -11 in mice and -1, -4 and -5 in humans) can be activated in the inflammasome protein signalling complex (Figure 1.12) (Jimenez Fernandez and Lamkanfi, 2015, Vanaja et al., 2015, Broz and Dixit, 2016).

Inflammasomes are large multimeric protein complexes that sense pathogen- and host-derived danger signals, and typically comprise of a Nod-like receptor (NLR), adaptor protein apoptosis-associated speck-like protein containing a CARD (ASC) and caspase-1 (Franchi et al., 2009, Vanaja et al., 2015, Broz and Dixit, 2016). The main function of the inflammasome is to activate caspase-1 to cleave precursor cytokines interleukin (IL) -1β and IL-18 into their mature active forms, induce pyroptosis (a lytic form of cell death) and cleave gasdermin-D into its cytotoxic N-terminal fragment, which forms a plasma membrane pore, releasing pro-inflammatory cytokines (Shi et al., 2015, He et al., 2015, Kayagaki et al., 2015). Inflammasome activation is a two-step process; initial inflammasome priming is required for transcriptional upregulation of machinery, including NOD-like-receptor family pyrin domain

containing 3 (NLRP3) and pro IL-1β (Broz and Dixit, 2016, Vanaja et al., 2015), followed by the trigger, such as a pathogen-associated molecular pattern (PAMP) or damage-associated molecular pattern (DAMP), which induces inflammasome assembly and activation.

The canonical NLRP3 inflammasome can be activated by PAMPs (for example, *Staphylococcus aureus*) and host-derived DAMPs [e.g. ATP, phagolysomal rupture, cathepsin release, ion flux, calcium influx, mitochondrial reactive oxygen species (ROS) and oxidised mitochondrial DNA] (Broz and Dixit, 2016, Menu and Vince, 2011). Potassium efflux has been proposed as a universal trigger for NLRP3 activation (Munoz-Planillo et al., 2013) including P2X7 receptor-mediated potassium pore opening, pannexin-1 and pore-forming toxins (Munoz-Planillo et al., 2013). However, potassium efflux is not a common mechanism for all activation pathways (Wolf et al., 2016, Gaidt et al., 2016)

Caspase-11, -4 and -5 can be activated by bacterial lipopolysaccharide-induced oligomerisation (Kayagaki et al., 2015), cleaving gasdermin-D and indirectly activating the NLRP3 inflammasome via pannexin-1 and potassium efflux (Yang et al., 2015). NLRP3 inflammasome can also be activated by caspase-8 which also directly cleaves IL-1β (Lawlor et al., 2015, Allam et al., 2014). MLKL translocates to the cell membrane and disrupts it, triggering potassium efflux and assembly of the NLRP3 inflammasome (Gutierrez et al., 2017). MLKL activation also provides a mechanism for processing and release of IL-1β independently of gasdermin-D (Gutierrez et al., 2017).

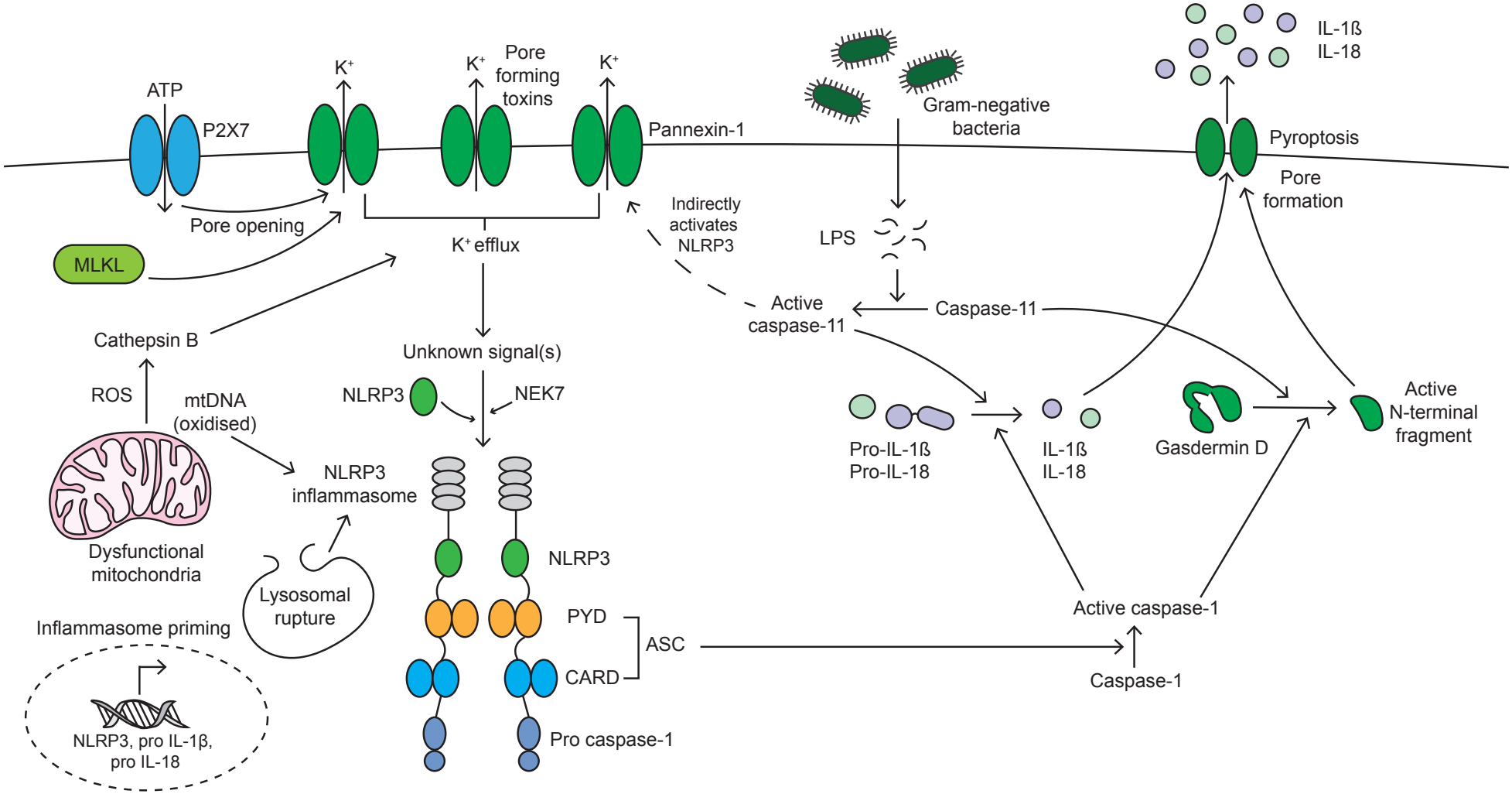
ATP
P2X7
K+
K+
Pore forming toxins
K+
Pannexin-1
Gram-negative bacteria
IL-1ß
IL-18
Pyroptosis
Pore formation
Pore opening
MLKL
K+ efflux
Indirectly activates NLRP3
LPS
Active caspase-11
Caspase-11
Cathepsin B
Unknown signal(s)
ROS
mtDNA (oxidised)
NLRP3
NEK7
Pro-IL-1ß
Pro-IL-18
IL-1ß
IL-18
Gasdermin D
Active N-terminal fragment
NLRP3 inflammasome
Dysfunctional mitochondria
Lysosomal rupture
NLRP3
PYD
ASC
CARD
Pro caspase-1
Active caspase-1
Caspase-1
Inflammasome priming
NLRP3, pro IL-1β, pro IL-18

**Figure 1.12. Inflammatory caspases.** Inflammatory caspase-1 is activated within the inflammasome protein complex (Jimenez Fernandez and Lamkanfi, 2015, Vanaja et al., 2015, Broz and Dixit, 2016), which typically consists of a Nod-like receptor (NLR; such as Nod-like-receptor pyrin domain containing 3 (NLRP3)), adaptor protein apoptosis-associated speck-like protein containing a CARD (ASC) and caspase-1 (Franchi et al., 2009, Vanaja et al., 2015, Broz and Dixit, 2016). Initial inflammasome priming is required for transcriptional upregulation of inflammasome machinery, such as NLRP3, pro-IL-1β and pro-IL-18 (Broz and Dixit, 2016, Vanaja et al., 2015). A second signal then induces inflammasome assembly and activation. The NLRP3 inflammasome is activated by lysosomal rupture, reactive oxygen species (ROS), oxidised mitochondrial DNA (mtDNA) and cathepsin B (Broz and Dixit, 2016, Menu and Vince, 2011). Potassium ($K^+$) efflux is a common NLRP3-activation mechanism, induced by P2X7-mediated pore opening, pore-forming toxins, pannexin-1 or MLKL-mediated pore opening (Munoz-Planillo et al., 2013). The NLRP3 inflammasome activates caspase-1, which cleaves precursor cytokines IL-1β and IL-18 into their active forms and gasdermin-D into its N-terminal fragment. The N-terminal fragment of gasdermin-D forms a plasma membrane pore facilitating pro-inflammatory cytokine release and inducing pyroptosis (Kayagaki et al., 2015, Shi et al., 2015, He et al., 2015). Gram-negative bacterial lipopolysaccharide (LPS) can activate caspase-11 (Kayagaki et al., 2015), which also cleaves gasdermin-D and indirectly activates the NLRP3 inflammasome via pannexin-1 (Yang et al., 2015).

### 1.7.5. Caspase-2

Caspase-2 is the most evolutionary conserved caspase (Bouchier-Hayes and Green, 2012) and has a prominent role in apoptosis induced by various stimuli, including DNA damage, heat shock, endoplasmic reticulum stress and oxidative stress (Ho et al., 2008, Tu et al., 2006, Tinel and Tschopp, 2004, Sidi et al., 2008, Upton et al., 2008). Caspase-2 is unique compared to other caspases, as it can act as both an initiator and an executioner caspase and does not fit into either the classically described intrinsic or extrinsic apoptotic pathways (Guo et al., 2002, Lassus et al., 2002). The structure of caspase-2 resembles that of an initiator caspase, due to a CARD and it can induce MOMP (Guo et al., 2002, Lassus et al., 2002). But, caspase-2 can also act as an executioner caspase, as it has substrate specificity similar to caspase-3 and -7 (Talanian et al., 1997). *Caspase-2* knockout mice have no strong phenotype and only display a few minor apoptotic defects in some cell populations (Bergeron et al., 1998, O'Reilly et al., 2002, Marsden et al., 2004). Caspase-2 localises to the cytosol and is the only caspase which also localises within the nucleus (Colussi et al., 1998, Baliga et al., 2003).

#### 1.7.5.1. Non-apoptotic roles of caspase-2

Caspase-2 also has crucial non-apoptotic roles, in cell division and genomic stability, oxidative stress and tumour suppression (Ho et al., 2009, Dorstyn et al., 2012, Bouchier-Hayes and Green, 2012, Olsson et al., 2015, Forsberg et al., 2017). In *caspase-2* knockout mouse embryonic fibroblasts, there was dysregulation of cell-cycle checkpoints and defective apoptosis following DNA damage. Disruption of cell-cycle checkpoints can often lead to genomic instability, a common phenotype of

cancerous cells (Dorstyn et al., 2012). Caspase-2 is also associated with tumour suppression, since there is enhanced cell proliferation and defective cell-cycle arrest in *caspase-2* knockouts after irradiation (Ho et al., 2009).

#### 1.7.5.2. Caspase-2 in neurodegeneration

Recent publications have indicated a pivotal role of caspase-2 in neuronal injury, including after ON injury and in SCI (Ahmed et al., 2011, Vigneswara et al., 2014, Vigneswara et al., 2012, Vigneswara et al., 2013, Vigneswara and Ahmed, 2016). Following ON axotomy and crush, active caspase-2 is localised to RGCs (Vigneswara et al., 2012, Ahmed et al., 2011, Vigneswara et al., 2014). Intravitreal injections of siCASP2 (Ahmed et al., 2011) or pharmacological inhibitor z-VDVAD-fmk (Vigneswara et al., 2012) protected >95% and ~60% of RGC for up to 30 days respectively. Intravitreal injections of siCASP2 has been shown to protect RGCs for up to 18 weeks if administered every 8 days (Vigneswara and Ahmed, 2016). Additional studies demonstrated that simultaneous caspase-2 and -6 suppression promoted RGC survival and supported RGC regeneration by promoting retinal-glial CNTF secretion (Vigneswara et al., 2014).

Caspase-2 has an evolving role in Alzheimer's disease. Caspase-2 is required for dendritic spine alterations and promotes cognitive decline in an Alzheimer's disease transgenic mouse model (J20 APP) (Pozueta et al., 2013) and is also involved in β-amyloid-induced neuronal death *in vitro* (Troy et al., 2000). Caspase-2 cleavage of tau at Asp314 impairs cognitive and synaptic function *in vivo* in tauopathy mouse models (Zhao et al., 2016). The expression of a mutant tau which is resistant to

caspase-2 cleavage prevented memory deficits and neurodegeneration in mice. Likewise, mutant tau is prevented from entering dendritic spines and impairing synaptic function in neuronal cell cultures *in vitro*. By reducing caspase-2 protein levels, long-term memory deficits were restored in a mouse model of Alzheimer's disease, suggesting a prominent role for caspase-2 in this disease and possible therapeutic opportunities (Zhao et al., 2016).

#### 1.7.5.3. Caspase-2 pathway

DNA damage-induces PIDDosome formation from RAIDD (Duan and Dixit, 1997) and p53 induced protein with a death domain (PIDD) (Tinel and Tschopp, 2004, Lin et al., 2000, Bouchier-Hayes and Green, 2012) which recruit and activate pro-caspase-2. RAIDD and PIDD interact via DDs, and RAIDD and caspase-2 interact through CARD domains. However, PIDD and RAIDD are not essential for caspase-2 activation *in vivo* (Manzl et al., 2009, Kim et al., 2009), with an alternative caspase-2 activation mechanism involving caspase-8 and the DISC (Manzl et al., 2009, Wagner et al., 2004, Droin et al., 2001, Lavrik et al., 2006, Olsson et al., 2015, Olsson et al., 2009) or in association with TRAF1 and RIPK1 (Lamkanfi et al., 2005). Endoplasmic reticulum stress also leads to caspase-2 activation (Krumschnabel et al., 2009). Mitochondrial caspase-2 can also mediate apoptosis directly from the mitochondrial compartment (Lopez-Cruzan et al., 2016).

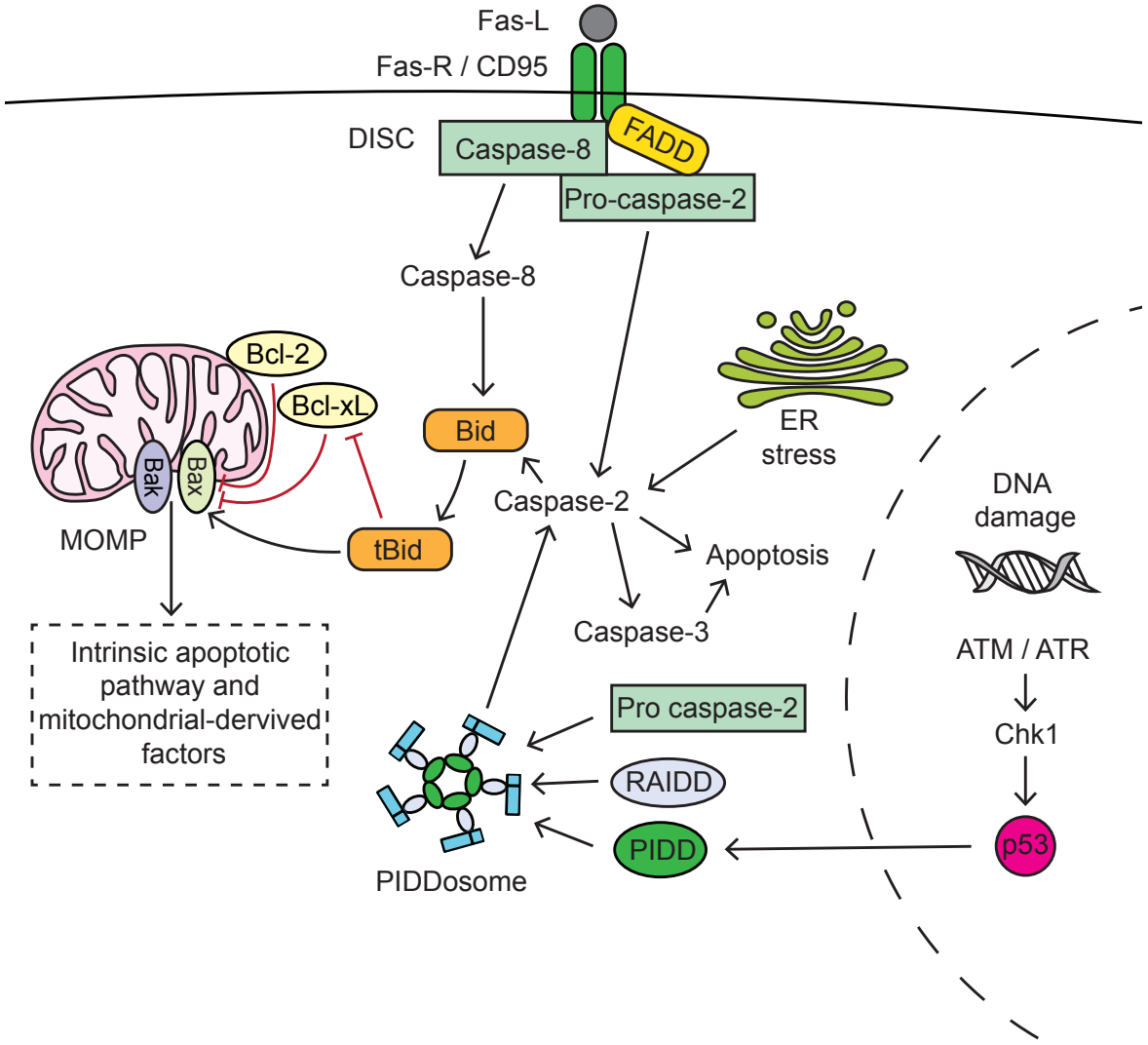


**Figure 1.13. Caspase-2 activation mechanisms.** Caspase 2 is activated by DNA damage; upregulation of p53 and the formation of a protein complex termed the PIDDosome, which includes p53 induced protein with death domain (PIDD), RIP associated ICH 1 homologous protein with death domain (RAIDD) and pro caspase 2 (Tinel and Tschopp, 2004, Duan and Dixit, 1997, Lin et al., 2000, Bouchier-Hayes and Green, 2012). Caspase 2 is also activated by endoplasmic reticulum (ER) stress and by the Fas R within the death inducing signalling complex (DISC), alongside Fas associated protein with death domain (FADD) and caspase 8 (Ho et al., 2008, Tu et al., 2006, Tinel and Tschopp, 2004, Sidi et al., 2008, Upton et al., 2008). Active caspase 2 cleaves and activates caspase 3, cleaves BH3 interacting domain death agonist (Bid), which initiates mitochondrial outer membrane permeabilisation (MOMP) and activates the intrinsic apoptotic pathway, or initiates apoptosis directly.

### 1.7.6. Caspase inhibitors

Caspases can be inhibited by endogenous inhibitors or manipulated through pharmacological mechanisms. Caspase activity can also be modulated by siRNA-mediated gene knockdown, dominant-negative proteins and conditional and global gene knockout.

#### 1.7.6.1. Endogenous inhibitors

There exists a complex network of apoptotic and anti-apoptotic regulators, which both directly or indirectly effect caspases, and determines cell fate, as well as providing regulation to prevent inappropriate caspase activation and cell death. In trauma or disease, pro- and anti- apoptotic molecules are modified, for example, through post-translational modifications (e.g. cleavage) or through altered expression.

The Bcl-2 family includes pro-apoptotic [Bcl-2 antagonist or killer (Bak), Bcl-2 associated X protein (Bax) and Bid] and anti-apoptotic (Bcl-2 and Bcl-xL) members (Zong et al., 2001, Adams and Cory, 1998, Youle and Strasser, 2008, Czabotar et al., 2014), which regulate apoptosis by balanced mechanisms. Furthermore, IAP are cytosolic and directly bind to inhibit active caspases through targeting their bacovirus IAP domain (BIR) (Gyrd-Hansen and Meier, 2010). Mammalian IAP x-linked inhibitor of apoptosis protein (XIAP) directly inhibits caspase-3, -6 and -9 (Deveraux et al., 1997). Mitochondrial-derived apoptogenic factors Smac/DIABLO and HtrA2/Omi are IAP inhibitors and inhibit IAP by binding to the caspase BIR domain, preventing IAP binding and thus promoting caspase activity (van Loo et al., 2002). IAP can eliminate inhibitors by promoting their ubiquitination and downstream proteasomal degradation (MacFarlane et al., 2002, Hu and Yang, 2003).

### 1.7.6.2. Pharmacological inhibitors

A number of specific and broad-spectrum caspase inhibitors are designed based upon the amino-acid sequence of caspase substrate cleavage sites, acting as pseudo enzymes for active caspases, and therefore, act as competitive inhibitors with caspase substrates. Broad-spectrum inhibitors include Boc-D-fmk, Q-VD-Oph (inhibits caspase-1, -2, -3, -6, -8 and -9), z-VAD-fmk (inhibits all caspases but caspase-2 very weakly) (Rozman-Pungercar et al., 2003, Caserta et al., 2003, Callus and Vaux, 2007, Ekert et al., 1999). Specific caspase substrate amino acid sequence cleavage sites include WEHD (caspase-1), YVAD (caspase-1), VDVAD (caspase-2), DEVD (caspase-3), LEVD (caspase-4), VEID (caspase-6), LETD (caspase-6), IETD (caspase-8 and -10) and LEHD (caspase-9) (Callus and Vaux, 2007, McStay et al., 2008, Chauvier et al., 2007, Nicholson, 1999, Nicholson and Thornberry, 1997). Caspase peptide inhibitors are linked to chemical groups that improve their permeability, efficacy and stability. Peptides linked to aldehydes (or nitriles or ketones) are reversible inhibitors (e.g., Ac-DEVD-CHO) and bind to the catalytic site but do not irreversibly chemically alter the enzyme, whereas peptides linked to halmethylketones (chloro or fluoro) (e.g. z-VAD-fmk) bind irreversibly. The chemical group -fmk is non-specific (Schotte et al., 1999, Chauvier et al., 2007).

Cross-reactivity with 'off-target' caspases limits interpretation of many studies using these inhibitors (Table 1.4). For example, the sequences DEVD which is the caspase substrate cleavage site from caspase-3, also binds to caspase-6, -7, -8, -9 and -10. Similarly, VDVAD, which should be specific for caspase-2, also binds caspase-3 and -7 substrates, and LETD, which should be specific for caspase-6, also binds to caspase-3, -8 and -9 substrates (McStay et al., 2008, Berger et al.,

2006, Pereira and Song, 2008). Some caspases sequences are more specific for other caspases than their target caspase. For example, the VEID sequence is the target for caspase-6, but it has a stronger affinity for caspase-3; IETD has a stronger affinity for caspases -3 and -6 than its target caspases -8 and -10 (McStay et al., 2008, Berger et al., 2006, Pereira and Song, 2008). In addition, z-VAD-fmk also binds other cysteine proteases, such as calpains and cathepsins (Rozman-Pungercar et al., 2003).

| *Cleavage site sequence* | *Caspase* | *Off-target* |
|---|---|---|
| Boc-D-fmk, Q-VD-Oph | 1, 2, 3, 6, 8, 9 | - |
| z-VAD-fmk | 1, 2, 3, 7, 6, 8 9 | Other cysteine proteases such as calpains and cathepsins |
| YVAD | 1 | - |
| WEHD | 1 | - |
| VDVAD | 2 | 3, 7 |
| DEVD | 3 | 6, 7, 8, 9, 10 |
| LEVD | 4 | - |
| VEID | 6 | - |
| LETD | 6 | 3, 8, 9 |
| IETD | 8, 10 | 3, 6 |
| LEHD | 9 | 8, 10 |

**Table 1.4. Caspase cleavage sites, their intended caspase target and off-target effects.** (McStay et al., 2008, Pereira and Song, 2008, Berger et al., 2006)

### 1.7.7. RNA interference

RNA interference (RNAi) occurs through post-transcriptional gene silencing by preventing mRNA translation into proteins. RNAi is sequence specific and can occur through microRNA (miRNA), modulation through endogenous non-coding double-stranded RNA (dsRNA) or through exogenous synthesised siRNA (Guzman-Aranguez et al., 2013). siRNAs are dsRNA with sense (passenger) and antisense (guide) strands. However, RNAi technology may cause alternative signalling induced by short RNA species and off-target effects; thus, appropriate controls are still critical (Jackson and Linsley, 2010).

#### 1.7.7.1. siRNA mechanism

dsRNA molecules are processed by ribonuclease Dicer into shorter siRNA fragments (Figure 1.14). siRNAs are subsequently incorporated into a multi-protein complex termed the RNA-induced silencing complex (RISC), where an ATP-helicase unwinds and dissociates the sense strand, leaving the endonuclease argonaute 2 (AGO2) associated with the antisense strand. The AGO2-siRNA complex then binds to complementary nucleotides in target mRNA coding region and induces its cleavage and degradation, therefore preventing its translation into protein and knockdown of the target gene expression (Guzman-Aranguez et al., 2013).

#### 1.7.7.2. siRNA off-target effects

RNAi targets specific mRNA sequences to induce gene silencing, but, some off-target effects do occur (Jackson and Linsley, 2010). For example, siRNA can induce

unintended knockdown through binding to sequences with similar homology (Thakur et al., 2012). Furthermore, long dsRNA (>30 nucleotides) can induce immune response activation through Toll-like Receptor activation (TLR), cytokine production, interferon release and subsequent non-specific gene expression alterations (Kleinman et al., 2008, Forsbach et al., 2008). The siRNAs (siCASP2 and siEGFP) that I chose to use in my studies are not known to have off-target effects and do not activate the immune response (Ahmed et al., 2011).

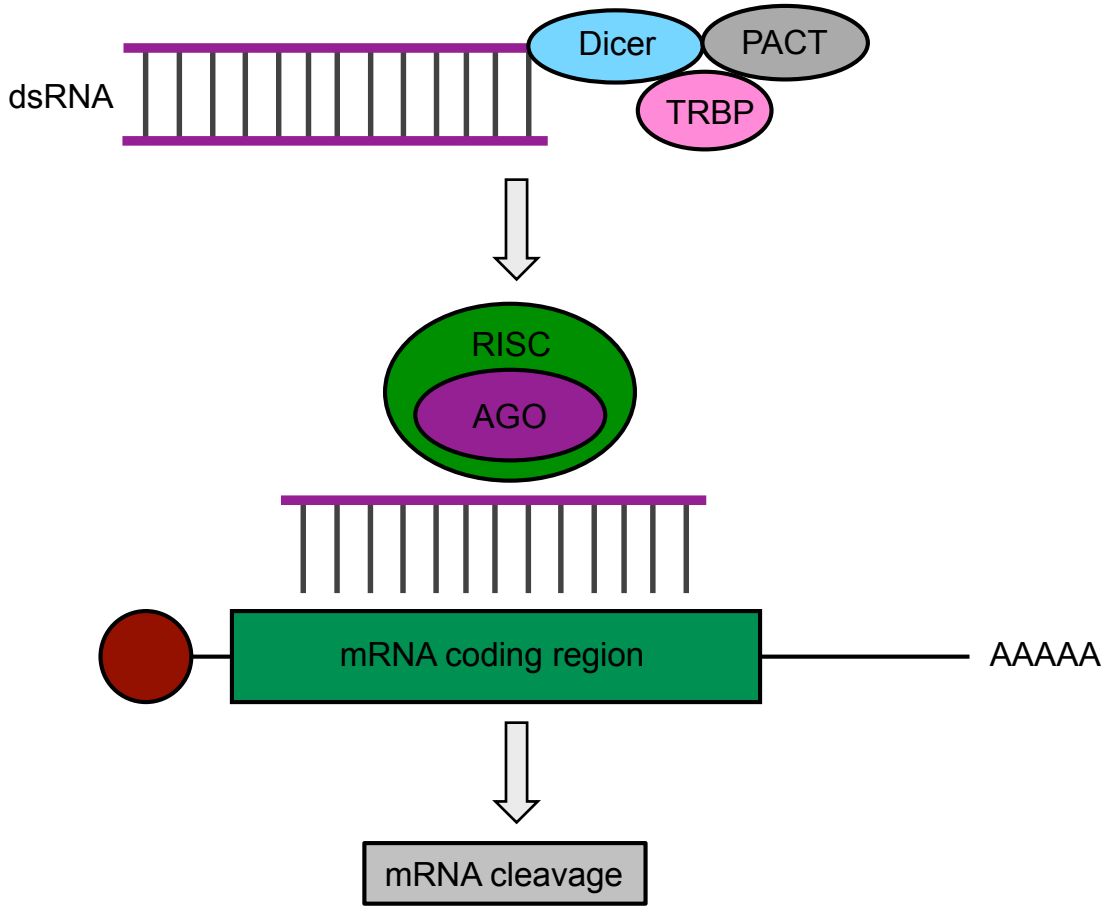


promote cleavage of specific mRNA by the active RISC complex and AGO endonuclease. Redrawn from Titze-de-Almeida et al., (Titze-de-Almeida et al., 2017).

#### 1.7.7.3. siCASP2

siRNA against caspase-2 (siCASP2 also known as QPI-1007) is a naked chemically synthesised modified RNA duplex with 19 nucleotides and chemical modifications including 2'-O-methylation (antisense strand) and L-DNA and 5' inverse base cap (sense strand) which prevent its degradation by vitreal and serum nucleases (Figure 1.15) (Titze-de-Almeida et al., 2017, Ahmed et al., 2011). siCASP2 antisense strand has sequence homology for human, rat and mouse caspase-2 mRNA (Figure 1.15), allowing the same siCASP2 sequence to be used across species. siCASP2 leads to significant caspase-2 knockdown *in vitro*, with >80% reduction in *Casp2* mRNA in human HeLa cells and ~65% knockdown in rat PC12 cells (Ahmed et al., 2011). There was a ~50% reduction in *Casp2* mRNA in siCASP2-treated intact rat retinae compared to siEGFP injected controls, although these differences did not reach statistical significance (Ahmed et al., 2011). Further, siCASP2 does not activate the innate immune system, shown through a lack of *in vivo* interferon responses and *in vitro* cytokine production (Ahmed et al., 2011) and low-risk systemic toxicity (Solano et al., 2014). siCASP2 also causes specific RNAi-mediated caspase-2 mRNA cleavage, as shown through RNA ligase-mediated rapid amplification of cDNA ends (RLM-RACE) experiments, which detected caspase-2 mRNA specific cleavage products (Ahmed et al., 2011). Together, this data suggests that siCASP2 knocks down caspase-2 *in vitro* and *in vivo*, does not induce an inflammatory response and causes specific RNAi-mediated cleavage of caspase-2.

siCASP2 is being tested in clinical trials with Quark Pharmaceuticals Inc. Phase I/IIa trials have been completed for non-arthritic ischaemic optic neuropathy (NAION), with

phase II/III currently on going, and phase II trials for acute primary angle closure glaucoma are also ongoing.

**A.** siCASP2 (QPI-1007) structure

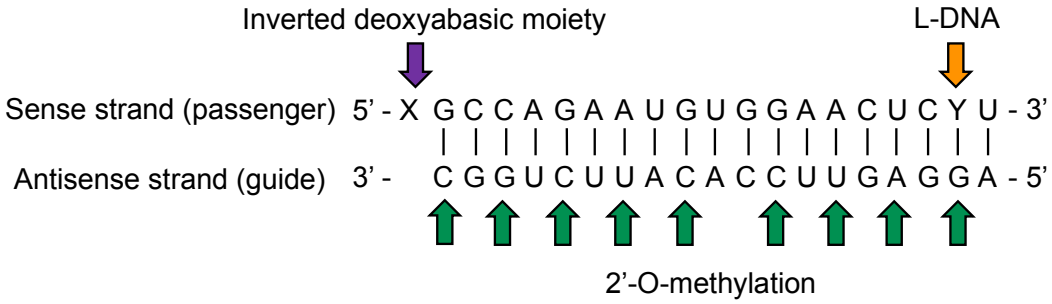


**B** siCASP2 caspase-2 mRNA sequence homology

**i)** Human

**3'- C GGUCUUACAC**
201 …AAAUGAGGGA GCUCAUCCAG GCCAAAGUGG GCAGUUUCAG CCAGAAUGUG

**CUUGAGGA -5'**
GAACUCCUCA ACUUGCUGCC UAAGAGGGGU CCCAAGCUU UUGAUGCCUT…

**ii)** Rat

201 …UAUCACUUUG GAAAUGAGGG AGCAAUCCA GGCCAAGGG GGCAGUUUCA

**3'- CGGUCUUACA CCUUGAGGA-5'**
GCCAGAAUGU GGAACUCCUC AACCUGCUGC CAAAGAGAGG ACCCCAGGCU…

**iii)** Mouse

321…TAGAGAAGGA CATTATCACT TTGGAAATGA GGGAGCTCAT CCAGGCCAAA

**3'- CGGUCUU ACACCUUGAG GA -5'**
GGGGGCAGTT TCAGCCAGAA TGTGGAACTC CTCAACCTGC TGCCAAAGAG…

## 1.8. Caspases and RGCs

### 1.8.1. RGC degeneration

Caspase-dependent RGC death occurs after eye and brain injuries, in retinal and ON degenerative disorders (Monnier et al., 2011, Patil and Sharma, 2004) and during development (Bahr, 2000, Cellerino et al., 2000). Common mechanisms of RGC death between different conditions could lead to broadly translatable therapeutics. Caspase involvement in RGC death in animal models, primary cell culture and human *post mortem* specimens are highlighted in this section. Table 1.5A provides a summary of previous studies investigating the efficacy of pharmacological inhibitors, gene knock out and gene knock down of different caspases and their impact on the number of surviving RGCs. As evident from the table, the most promising is treatment with siCASP2 to knock down *caspase-2* mRNA, since 95% of RGCs were protected from cell death up to 12 weeks after ONC injury (Vigneswara and Ahmed, 2016, Ahmed et al., 2011). However, the functional effects of this treatment was not assessed in this study, nor ON axon morphology; therefore further investigation is required to assess this treatment's efficacy and whether it is translatable to clinic. siCASP2 is currently in Phase II clinical trials with Quark Pharmaceuticals, but the results have yet to be released.

Furthermore, there are multiple inhibitors which inhibit molecules downstream of caspase-2, in particular caspase-3, -8 and -9 (summarised in Table 1.6). Many studies have investigated the effects of these classical caspases as they are part of the canonical apoptotic pathway; therefore, it is not known whether these therapeutics affect caspase-2 and this would be interesting to investigate in the future.

| *Caspase* | *Model* | *Inhibitor* | *Time at end of study (days)* | *RGC survival (% of RGCs in untreated eyes)* | *RGC survival (% of RGCs in treated eyes)* | *References* |
|---|---|---|---|---|---|---|
| Broad spectrum | ONT | z-VAD | 14 | 16.8 * | 34.5 * | (Monnier et al., 2011) |
| | 75 mins raised IOP | Q-VD-OPH | 7-21 | 39-64 | 63-71 | (Patil and Sharma, 2004) |
| Caspase-1 | ONC | NLRP3 -/- | 3-28 | 78-13 | 89-25 | (Puyang et al., 2016) |
| | NMDA-RGC explants | YVAD-fmk | 2 | 18 | 12 | (Schuettauf et al., 2011) |
| Caspase-2 | ONC | z-VDAD-fmk | 15 | 12.3 | 60 | (Vigneswara et al., 2012, Vigneswara et al., 2014) |
| | ONC | siCASP2 | 21-84 | 10-7 | 95-96 | (Ahmed et al., 2011, Vigneswara and Ahmed, 2016) |
| | Optic neuritis | siCASP2 | 21 | 65.5 | 79.3 | (Lidster et al., 2013) |
| Caspase-3 | ONT | z-DEVD-cmk | 7-28 | 10-34.3 | 24.3-47.4 | (Kermer et al., 1999a, Sanchez-Migallon et al., 2016, Monnier et al., 2011) |
| | NMDA-RGC explants | DEVD-fmk | 2 | 18 | 26 | (Schuettauf et al., 2011) |
| Caspase-3 and -6 | NMDA-RGC explants | DQMD-fmk | 2 | 18 | 41.6 | (Schuettauf et al., 2011) |
| Caspase-6 | ONT | SIMA 13a | 13 | 16.8 * | 37 * | (Monnier et al., 2011) |
| | ONC | CASP6 DN | 21 | 14.2 | 39.4 | (Vigneswara et al., 2014) |
| | ONT | z-VEID | 14 | 16.8 * | 48.2 * | (Monnier et al., 2011) |
| | NMDA-RGC explants | VEID-fmk | 2 | 18 | 41.6 | (Schuettauf et al., 2011) |
| | 30 mins artery ligation | z-VEID-fmk | 14 | 33.9 | 46.2 | (Shabanzadeh et al., 2015) |
| | 30 mins artery ligation | siCASP6 | 14 | 30* | 48* | (Shabanzadeh et al., 2015) |
| Caspase-7 | ONT | CASP7 -/- | 28 | 38 | 76 | (Choudhury et al., 2015) |
| Caspase-8 | ONT | z-IETD (+/-) -fmk | 14 | 16.8 * | 31.5-60.7 * | (Weishaupt et al., 2003, Monnier et al., 2011) |
| | ONT | IETD-CHO | 14 | NA | 33.1 | (Weishaupt et al., 2003) |
| | NMDA-RGC explants | IETD-fmk | 2 | 18 | 27 | (Schuettauf et al., 2011) |
| | 30 mins artery ligation | z-IETD-fmk | 14 | 33.9 | 42.2 | (Shabanzadeh et al., 2015) |
| | 30 mins artery ligation | siCASP8 | 14 | 30.0* | 48.4* | (Shabanzadeh et al., 2015) |
| Caspase-8 and -9 | ONT | z-IETD-fmk and z-LEHD-fmk | 14 | NA | 38.7 | (Weishaupt et al., 2003) |
| Caspase-9 | ONT | z-LEHD- (+/-) -fmk | 14 | 16.8 * | 29.1-34.9 * | (Weishaupt et al., 2003, Monnier et al., 2011) |
| | NMDA-RGC explants | LEHD-fmk | 2 | 18 | 39 | (Schuettauf et al., 2011) |

**Table 1.5. Pharmacological inhibitors, knockdown and knockouts of the caspases and their effect on surviving RGCs in disease models .** The percentage of surviving RGCs in treated and untreated retinae in models of RGC injury. Animals are treated with specific pharmacological inhibitors, gene knock-down (e.g. siRNA) or are gene knock-out animals (-/-). * The values for uninjured Fluorogold and $RBPMS^+$ RGCs were not stated in Shabanzadeh et al., 2015 (Shabanzadeh et al., 2015), but values from Weishaupt et al., 2003 (Weishaupt et al., 2003), who also used female Sprague Dawley adult rats and identical counting techniques, were used to calculate percentages. This table is published in Thomas et al., 2017 (Thomas et al., 2017). **Abbreviations:** ONT; Optic nerve transection, ONC; Optic nerve crush, NMDA; N-methyl-D-aspartate, RGC; Retinal ganglion cells, IOP; intraocular pressure, NLRP3; NOD-like receptor protein 3, siCASP2; Small interfering RNA against caspase-2, CASP6 DN; caspase-6 dominant negative.

| *Disease* | *Injury* | *Treatment* | *Effect on caspase by treatment* | *End of the study (days)* | *Effect on RGCs* | *References* |
|---|---|---|---|---|---|---|
| Direct ON injury | ONC | ROCK inhibition | Reduced cleaved caspase-3 immunostaining in GCL and primary RGC culture lysate | 14 | ROCK shRNA increases RGC survival to 143% of EGFP shRNA control. | (Tura et al., 2009, Koch et al., 2014) |
| | ONC | Calcineurin inhibition | Reduced cleaved caspase-9 protein | - | N/D | (Grosskreutz et al., 2005) |
| | ONC | Deletion of CHOP | Reduced full-length caspase-3 immunostaining | 14 | CHOP KO mice had 52% surviving RGC compared to 24% in sham | (Hu et al., 2012) |
| | ONT | Kv1.3 siRNA | Reduced caspase-3 and -9 mRNA expression | 14 | KV 1.3-1169 siRNA increases RGC survival 3.5-fold compared to control | (Koeberle et al., 2010) |
| | ONC | Valproic acid (VPA) | Reduced cleaved caspase-3 RGC immunostaining | 14 | VPA treatment leads to 44% surviving RGC compared to 27% with vehicle | (Zhang et al., 2012a, Zhang et al., 2012b) |
| Glaucoma | Hypertonic saline injections into limbal vein | Morphine | Reduced cleaved caspase-3 and -8 protein | 56 | Morphine treatment causes 65.9% surviving RGCs compared to 17.3% in control | (Husain et al., 2012) |
| | Laser photocoagulation | Cobra venom factor (CVF; complement depletion) | Reduced cleaved caspase-8 and -9 protein | 42 | CVF treatment causes 41.5% surviving RGCs compared to 28.4% in control | (Jha et al., 2011) |
| | Suture pulley compression | C-Jun N-terminal kinase (C-JNK) inhibitor | Reduced cleaved caspase-3 immunostaining | 0.5 | C-JNK inhibition causes 23.6% $TUNEL^+$ RGCs compared to 52.4% in vehicle control and 1.49% in uninjured | (Liu et al., 2011) |
| | Saline injection into anterior chamber | Cyclosporine A (CSA; inhibits cyclophilin D and MPTP) | Reduced cleaved caspase-3 protein, immunolocalised to RGCs | 14 | CSA treatment causes 93% surviving RGCs compared to 77% in ischaemic | (Kim et al., 2014) |
| | Translimbal photocoagulation laser model | Minocycline, tetracycline antibiotic | Reduced caspase-1 and -4 but not caspase-8 and -12 gene expression | 8 | N/D | (Levkovitch-Verbin et al., 2014b, Levkovitch-Verbin et al., 2014a) |

| | | | | | | |
|---|---|---|---|---|---|---|
| Glutamate excitotoxicity | Glutamate - primary rat RGC culture | Pilocarpine (M1 muscarinic receptor agonist) | Reduced caspase-3 gene expression and full-length protein | 1 | Cell viability is 42% after 1mM of glutamate, increased by 32% with pilocarpine treatment | (Zhou et al., 2008, Kurokawa et al., 1999b) |
| | NMDA administration | Thioredoxin (TRX) | Reduced cleaved caspase-3 and -9 protein | 7 | TRX treatment causes 56.6% surviving RGCs compared to 13.4% in control | (Inomata et al., 2006) |
| Ischaemic injury | Ischaemic reperfusion injury | Brain derived neurotrophic factor (BDNF) | Reduced full-length caspase-2 GCL immunostaining | 7 | BDNF treatment causes 69.6% surviving RGCs compared to 44.1% in sham | (Kurokawa et al., 1999b, Kurokawa et al., 1999a) |
| | Ischaemic reperfusion injury | Valproic acid (VPA) | Reduced cleaved caspase-12 protein | 7 | VPA treatment causes 83.5% surviving GCL cells compared to 57.5% in sham | (Zhang et al., 2011) |
| Branch retinal vein occlusion (BRVO) | Laser photocoagulation | Minocycline, tetracycline antibiotic | Reduced cleaved caspase-3 immunostaining in GCL | 7 | *In vivo* OCT imaging shows increased RNFL + GCL thickness 3 days after minocycline. Minocycline protects 55.2% of RGCs compared to 46.8% in saline control. | (Sun et al., 2013) |
| Diabetic retinopathy | STZ | Somatostatin (SST) | Reduced cleaved caspase-8 and -3 protein | 14 | Reduced $TUNEL^+$ cells in GCL, 36.8% in STZ compared to 13.7% in treated. | (Hernandez et al., 2013) |
| | STZ | Edaravone (free radical scavenger) | Reduced cleaved caspase-3 protein | 28 | Reduced $TUNEL^+$ cells in GCL, 42% in vehicle compared to 9.5% in treated. | (Yuan et al., 2014) |
| | High glucose primary RGC culture | Erythropoietin (EPO; antioxidant) | Reduced full-length caspase-3 and -9 protein | - | Reduced apoptotic Hoechst 33358 stained cells, 49.1% in high glucose cells compared to 25.7% in EPO treated. | (Wang et al., 2015) |
| | High glucose primary RGC culture | L-Carnitine (endogenous mitochondrial membrane compound) | Reduced full-length caspase-3 and -9 protein | - | Reduced apoptotic Hoechst 33358 stained cells, 49.1% in high glucose cells compared to 15.7% in L-Carntine treated. | (Cao et al., 2014) |
| Optic neuritis | EAE model | EPO | Reduced cleaved caspase-3 immunostaining | 8 | EPO treatment causes 55% RGCs to survive compared to 30% in vehicle control. | (Sattler et al., 2004) |

| | | | | | | |
|---|---|---|---|---|---|---|
| PBI | Blast wave | Compound 49b (beta-adrenergic receptor agonist) | Reduced cleaved caspase-3 | 3 | N/D | (Jiang et al., 2013) |

**Table 1.6. Treatments that affect targets upstream of caspases and prevent RGC death** . This table is reproduced from Thomas et al., 2017 (Thomas et al., 2017). **Abbreviations:** ROCK Rho-associated protein kinase; CHOP CCAAT/enhancer binding homologous protein; PBI primary blast injury; JNK Jun N-terminal kinase; MPTP mitochondrial permeability transition pore; BDNF Brain derived neurotrophic factor; STZ streptozotocin; SST somatostatin; TUNEL Terminal deoxynucleotidyl transferase dUTP nick end labelling; EPO erythropoietin; EAE experimental autoimmune encephalomyelitis; NMDA N-methyl-D-aspartate.

### 1.8.2. RGC axon regeneration

In addition to promoting RGC survival, caspase inhibition promotes RGC axon regeneration after ON injury. Pharmacological inhibition of caspase-6 and -8, using z-VEID-fmk and z-IETD-fmk, provide RGC neuroprotection and promote limited RGC axon regeneration (Monnier et al., 2011), with few axons extending >1000 μm beyond the lesion site. Similarly, few RGC axons regenerated through the lesion site with inhibition by a dominant negative form of caspase-6 (Vigneswara et al., 2014); however, combined suppression of caspase-2 and -6 using siCASP2 and a dominant negative form of caspase-6 promoted significant regeneration, with an average of 195 ± 9 axons growing beyond 1000 μm (Vigneswara et al., 2014). Caspase-6 is localised to RGCs and some microglia, the neuroprotective and pro-regenerative effects of caspase-6 inhibition are mediated indirectly by CNTF upregulation in retinal glia and are blocked by suppression of gp130 and the JAK/STAT pathway (Vigneswara et al., 2014). These studies reveal a novel non-apoptotic role for caspases and warrant further investigation.

## 1.9. Direct TON

Clinically, direct TON can be caused by penetrating injuries or direct compression from orbital haemorrhage or craniofacial fractures (Sarkies, 2004). ONT and ONC can be used to study degenerative mechanisms and evaluate neuroprotective and regenerative therapies (Berry et al., 1996, Berry et al., 1999). Following direct TON, RGCs begin to degenerate after 5 to 6 days (Cheung et al., 2004a), with 25%-30% of neurons surviving to 7 days (Berry et al., 1996, Berry et al., 1999, Ahmed et al., 2011, Vigneswara et al., 2012) and fewer than 10% remaining after 14 days (Berkelaar et al., 1994). RGC death occurs rapidly, with greater degeneration after ONT compared to ONC, and with injuries more proximal (closer to the eye) compared to more distal injuries (Berkelaar et al., 1994).

#### 1.9.1.1. Caspases in direct TON

RGC death after ON injury is progressive and the severity is dependent upon the type of lesion and distance from the eye (Villegas-Perez et al., 1993, Berkelaar et al., 1994). After direct TON, RGCs begin to degenerate 5 days after axotomy (Cheung et al., 2004b), and 90% die between 7 and 14 days (Berkelaar et al., 1994, Agudo et al., 2008, Berry et al., 1996, Ahmed et al., 2011) through caspase-dependent apoptosis (Garcia-Valenzuela et al., 1994, Rabacchi et al., 1994). Cleaved caspase-2 (Ahmed et al., 2011, Vigneswara et al., 2014, Vigneswara et al., 2012), -8 (Monnier et al., 2011, Weishaupt et al., 2003), -9 (Cheung et al., 2004b, Grosskreutz et al., 2005, Kermer et al., 2000a), -3 (Sanchez-Migallon et al., 2016, Chaudhary et al., 1999a, Cheung et al., 2004b, Kermer et al., 1999a, Kermer et al., 1999c, He et al., 2004, Levkovitch-Verbin et al., 2010), -6 (Monnier et al., 2011) and -7 (Chaudhary et al., 1999a, Choudhury et al., 2015), as well as inflammatory caspases-11 (Agudo et al., 2009) and -1 (Puyang

et al., 2016), have all been detected in RGCs after crush or axotomy, highlighting the crucial role played by caspases in axotomy-induced RGC death.

Caspase-3 is activated after RGC axotomy (Sanchez-Migallon et al., 2016, Chaudhary et al., 1999a, Cheung et al., 2004b, Kermer et al., 1999a, Kermer et al., 1999c, He et al., 2004, Levkovitch-Verbin et al., 2010), and z-DEVD-fmk inhibition reduces RGC death (Chaudhary et al., 1999b, Kermer et al., 2000b, Kermer et al., 1999c, Kermer et al., 1999b, Sanchez-Migallon et al., 2016, Liu et al., 2015a). However, z-DEVD-fmk also inhibits caspase-6, -7, -8 and -9 (McStay et al., 2008, Pereira and Song, 2008) and neither delayed nor multiple treatments of z-DEVD-fmk improves RGC survival further than treatment at time of injury (Sanchez-Migallon et al., 2016). Caspase-3 is also indirectly reduced by RGC neuroprotective therapies, such as either Rho-associated protein kinase (ROCK) inhibition (Tura et al., 2009, Koch et al., 2014) or treatment with the broad-spectrum histone deacetylase inhibitor, valproic acid (Zhang et al., 2012a, Zhang et al., 2012b). Moreover, in a rabbit model of indirect TON from a fluid percussion injury, increased levels of cleaved caspase-3 protein are found in retinal lysates from injured animals compared to control animals, and full-length caspase-3 localises to RGCs. Pharmacological inhibition of caspase-3 with z-DEVD-fmk is neuroprotective of RGCs (Liu et al., 2015b), although z-DEVD-fmk is non-specific also inhibits caspase-6, -7, -8 and -9 (McStay et al., 2008, Pereira and Song, 2008). Therefore, it can only be concluded that RGCs die by apoptotic mechanisms and via caspase-3 specifically.

Caspase-7 gene knockout also protects a limited proportion of RGCs after axotomy (Choudhury et al., 2015) and pharmacological inhibition of caspase-6 and -8, using

z-VEID-fmk and z-IETD-fmk, or a CASP6 DN provides some RGC neuroprotection and promotes regeneration (Monnier et al., 2011). Caspase-6 is localised to RGCs and some microglia, regeneration is an indirect effect of CNTF production by retinal glia (Vigneswara et al., 2014). In addition, combined caspase-8 and -9 inhibition provides additive survival benefits compared to inhibition of a single caspase (Weishaupt et al., 2003, Chaudhary et al., 1999a, Cheung et al., 2004b), which may suggest either that both intrinsic and extrinsic apoptotic pathways are activated following direct ON injury or that there are increased off-target effects. Inhibition of caspase-8 can also promote caspase-independent RGC death, such as necroptosis (Feltham et al., 2017).

Recent studies have indicated a pivotal role of caspase-2 in apoptotic RGC injury (Ahmed et al., 2011, Vigneswara et al., 2014, Vigneswara et al., 2012, Vigneswara et al., 2013, Vigneswara and Ahmed, 2016). After ON axotomy and crush, active caspase-2 is exclusively localised to RGCs, and its inhibition using siRNA provides significant neuroprotection (Vigneswara et al., 2012, Ahmed et al., 2011, Vigneswara et al., 2014). For example, intravitreal administration of either siCASP2 (Ahmed et al., 2011) or the pharmacological inhibitor z-VDVAD-fmk (Vigneswara et al., 2012) protect 98% and 60% of RGCs, respectively, for up to 30 days and >95% of RGCs are protected from death for 12 weeks if siCASP2 is injected every 8 days (Vigneswara and Ahmed, 2016). Pharmacological inhibition with z-VDVAD-fmk can also inhibit caspase-3 and -7 (Pereira and Song, 2008), but activity of these caspases was not affected in this study, suggesting that the effect of z-VDVAD-fmk was mediated by inhibition of caspase-2 (Vigneswara and Ahmed, 2016). The siCASP2 is being developed as a therapeutic by Quark Pharmaceuticals Inc. and is currently in Phase

III clinical trials for ischemic optic neuropathy and glaucoma (Vigneswara and Ahmed, 2016).

NLRP3-induced neuro-inflammation promotes RGC death after partial ONC (Puyang et al., 2016). NLRP3 expression is up-regulated in retinal microglia and NLRP3 inflammasome activation upregulates retinal cleaved caspase-1 and IL-1β, which is prevented in NLRP3 knockout mice, in which RGCs are protected against axotomy-induced RGC death (Puyang et al., 2016). The P2X7 ionotropic ATP-gated receptors are implicated in RGC degeneration; P2X7-mediated potassium efflux induces NLRP3 inflammasome formation and caspase-1 activation (Munoz-Planillo et al., 2013). P2X7 receptor-deficient mice displayed delayed RGC loss and fewer phagocytic microglia at early time points after RGC axotomy (Nadal-Nicolas et al., 2016). Intravitreal administration of a selective PX27 receptor antagonist A438079 delayed RGC death, suggesting P2X7 receptor antagonism as a potential therapeutic strategy. Caspase-11 expression is also upregulated in RGCs after ONC and ONT (Agudo et al., 2009).

## 1.10. Hypothesis and aims

**Hypothesis:**

My hypothesis is that RGC death in TON is driven by caspase-2 in the apoptotic pathway.

**Aims:**

To test this hypothesis, my aims were to:

I. Characterise changes in the expression of members of the apoptotic and non-apoptotic cell death pathways in the rat retina after blunt ocular injury using immunofluorescent staining, western blotting and RT-qPCR.

II. Characterise changes in the expression of members of the apoptotic and non-apoptotic cell death pathways in the mouse retina after repeated ocular blast injuries using by similar methods to aim 1.

III. To test whether the knockdown of caspase-2, a key member of the apoptosis pathway, promotes the survival and function of RGCs after blunt ocular injury and repetitive ocular blast injury.

IV. To test whether the inhibition of other non-apoptotic death pathways promotes the survival and function of RGCs after blunt ocular injury and repetitive ocular blast injury.

# Chapter 2 Materials and Methods

## 2.1. *In vivo* procedures

Animals for blunt injury experiments were female Lister-hooded rats weighing 180-220 g purchased from Charles River Laboratories (Margate, UK), kept on a 12-hour light-dark cycle with a daytime luminance of 80 lux and fed and watered *ad libitum*. Animal procedures were licensed by the UK Home Office and approved by the University of Birmingham's Animal Welfare and Ethical Review Committees

Animals for blast injury experiments were 12-week-old male C57/Bl6 mice purchased from Jackson Laboratory (Bar Harbor, Maine USA). All animal experiments were performed under regulation of the Institutional Animal Care and Use Committee of Vanderbilt University according to the Association for Assessment and Accreditation of Laboratory Animal Care guidelines. Blast injury *in vivo* procedures were performed in Dr Tonia Rex's laboratory at Vanderbilt University in Nashville, TN, USA.

All animal procedures were conducted in accordance with the ARVO Statement for the Use of Animals in Ophthalmic and Vision Research.

### 2.1.1. Blunt ocular injury model

Adult female Lister Hooded rats weighing 180-220 g from Charles River (Margate, UK) were used for blunt ocular injury experiments. Blunt ocular injury surgeries were performed by Lt Col Richard Blanch or myself. Surgery was performed under inhalational anaesthesia with 3% isoflurane in oxygen, and analgesia (buprenorphine) injected subcutaneously before and after surgery. The ocular surface and surrounding skin were prepared with 5% povidone iodine in water. The animal was placed in a head holder and a lateral canthotomy performed allowing easier access to the lower eyelid and conjunctiva (Figure 2.1 and Figure 2.2). A temporary traction suture was placed in the lower eyelid and pulled downwards. Next, the lower conjunctiva was released, and a temporary traction suture placed through the inferior limbal conjunctiva, the globe was rotated upwards exposing the inferior sclera. A focal blunt injury was induced by propelling a 0.095 g spherical plastic pellet using compressed air at a pressure of 0.1 bar (~14.5 psi) to directly impact the inferior scleral surface at a speed of 20 m/s (Blanch et al., 2012b). The lateral canthus was closed using a horizontal subcuticular mattress suture and animals allowed to recover.

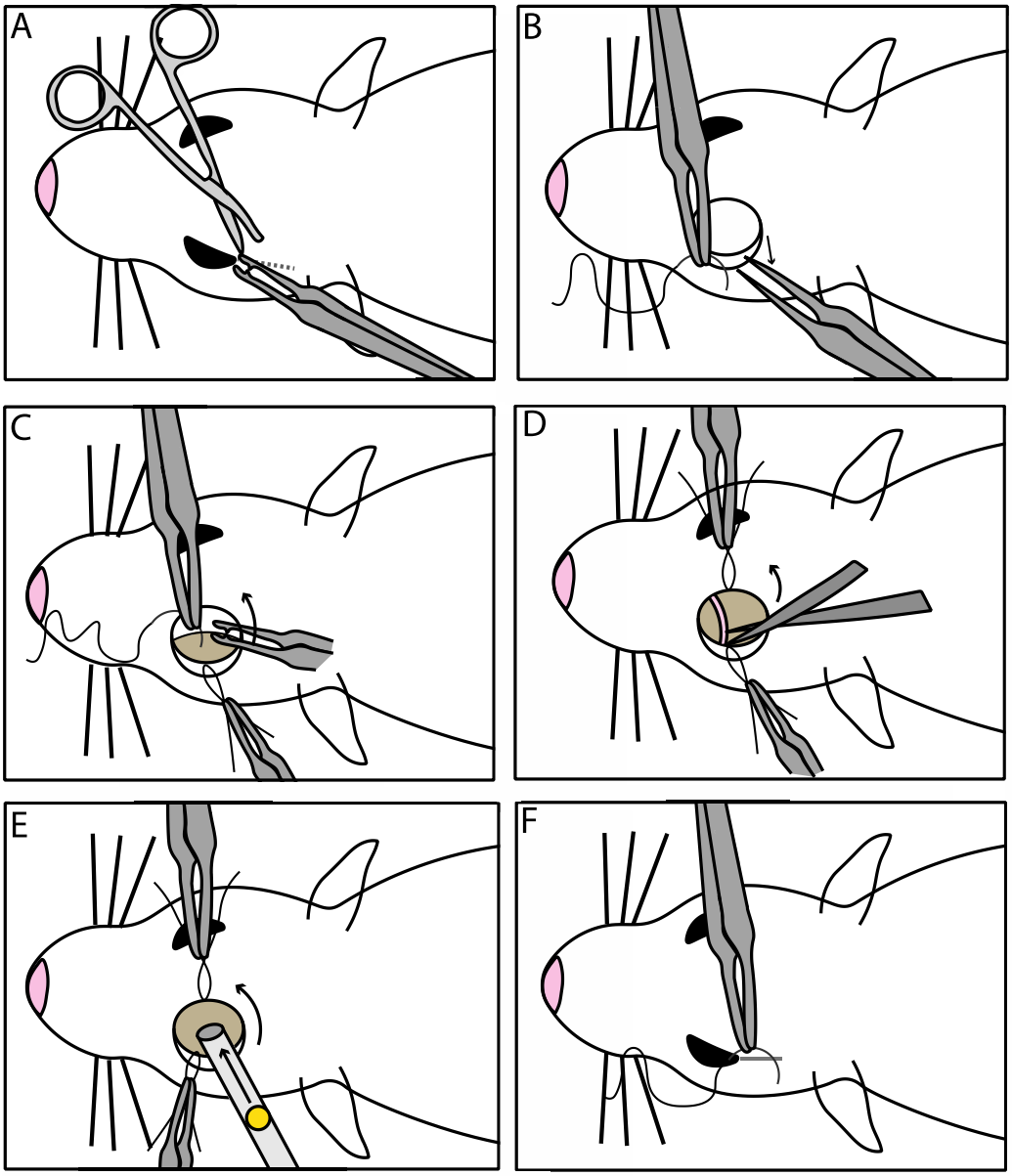


**Figure 2.1 Schematic diagram of blunt ocular injury model. A)** A blunt incision exposes the sclera and conjunctiva. **B)** Temporary suture of the lower eyelid to expose the conjunctiva. **C)** A limbal traction suture is performed. **D)** The eye is rotated superiorly to expose the inferior sclera and Tenon's capsule is bluntly detached. **E)** A 0.095 g plastic pellet is propelled down the barrel to impact the inferior sclera. **F)** Temporary sutures are removed, and a horizontal subcuticular mattress suture performed.

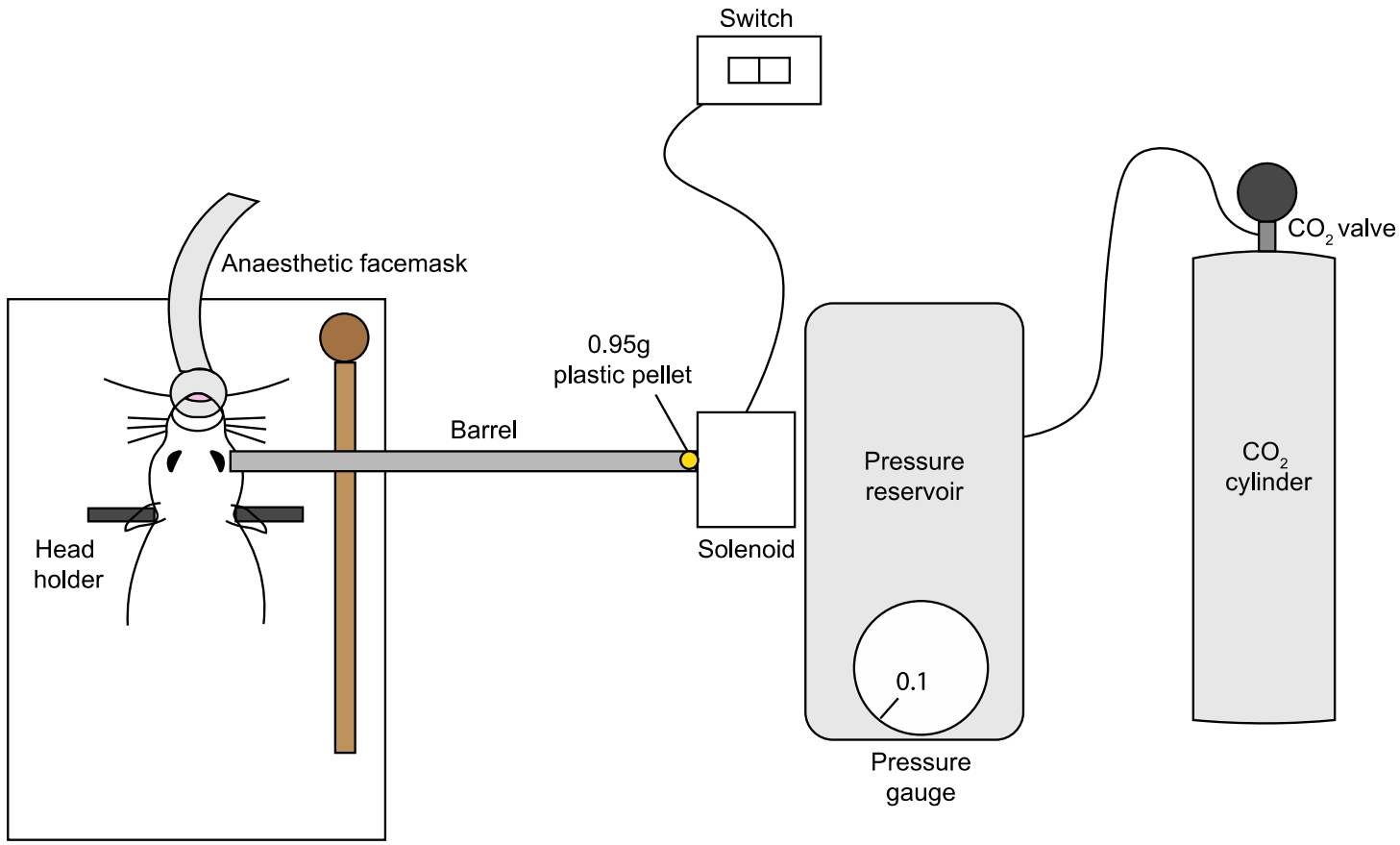


**Figure 2.2. Blunt ocular injury model experimental set up.** The rat is placed in a head holder and a low weight / high velocity plastic pellet (0.095 g at 20 m/s) is projected at the inferior sclera using compressed air of controlled pressure (from the $CO_2$ cylinder). The $CO_2$ valve is opened, and the pressure reservoir increased to 0.1 bar. The electrical switch opens the solenoid actuated valve, allowing projection of the pellet down the barrel to impact the globe. Model previously described in Blanch et al., 2012 (Blanch et al., 2012b).

### 2.1.2. Repeated primary blast injury model

The primary blast injury model was previously described and updated by Dr Rex's lab (Figure 2.3) (Hines-Beard et al., 2012, Bricker-Anthony et al., 2014a, Bricker-Anthony et al., 2014b, Bricker-Anthony and Rex, 2015, Bernardo-Colon et al., 2018, Vest et al., 2019). Anaesthetised male 12-week old C57/Bl6 mice were exposed to 2-3% isoflurane in oxygen and placed in custom-built polyvinylchloride (PVC) tubing. Eyes were inspected under a bright field microscope for scratches and abnormalities before injury. Mice were placed into the PVC barrel with a foam peanut and playdough moulded onto the right side to soften the blunt injury to the right eye. Surgical tape was placed across the shoulders to prevent movement during the blast-wave exposure. A modified paintball gun (Empire Paintball, Sewell, New Jersey, USA) was set to a pressure of ~15 psi (between 14-18 psi). A pressure transducer recorded the blast overpressure wave before and after the blast and viewed using LabVIEW software (National Instruments ™). The left eye was positioned in line with a mouse eye sized hole in the outer PVC barrel tube. The PVC barrel tube was positioned at 162 mm (4 full turns of the wheel) from the paintball gun barrel. Sham mice were exposed to all procedures excluding the blast wave which was blocked using reinforced cardboard and recorded with a pressure of ~2 psi. GenTeal ® Tears (Alcon, Novartis, Fortworth, Texas, USA) eye drops were applied after blast to prevent corneal dehydration after anaesthetic exposure. Mice were allowed to recover. An rPBI was performed; two blasts of 15 psi in quick succession (~1 sec apart) was performed over three consecutive days, 24 hours apart (Figure 2.3B). Mice received unilateral rPBI to the left eye or were sham-treated. Intravitreal treatments were injected bilaterally. In some experiments, indirect injury to the right eyes were analysed. This will be highlighted in each section.

**A)** Primary blast ocular trauma model set up

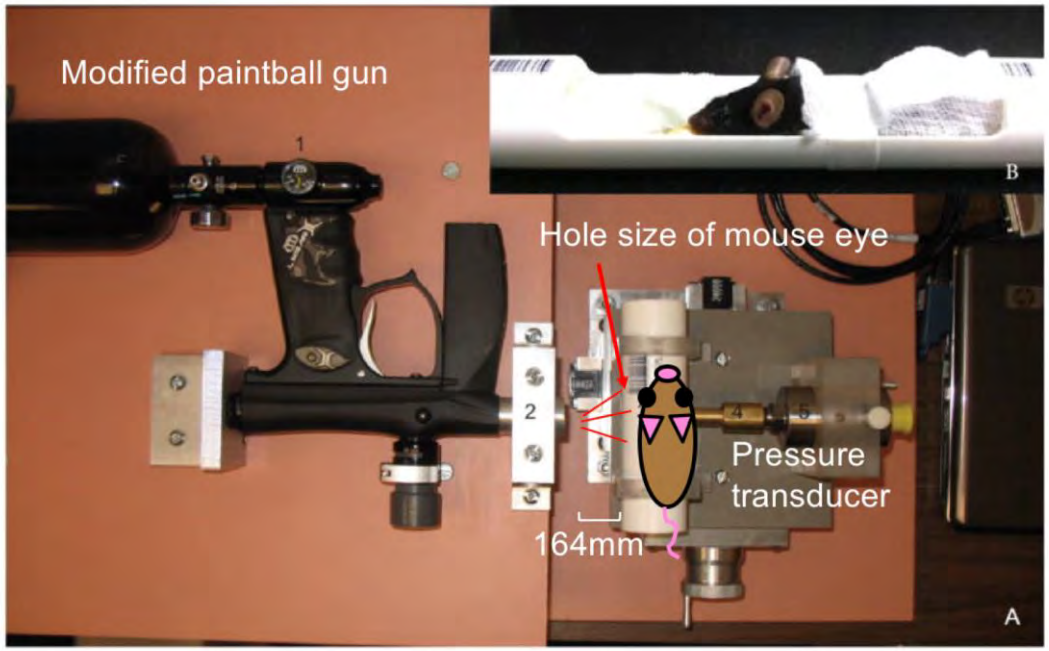


**B)** Time frame of repeated PBI model

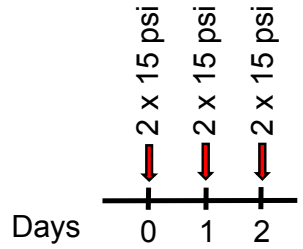


**C)** Blast overpressure measurements

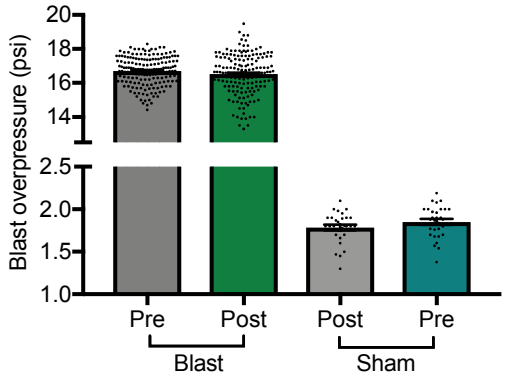


**F**

F

V

C

Overpressure waves in blast and sham groups.

### 2.1.3. Intravitreal injections

Intravitreal injections were performed either using a pulled glass micropipette (produced using a flaming glass micropipette puller from Intracel, Sutter Instruments Co. USA) (Chapters 3 and 4) or a 31-gauge needle with bevelled tip attached to a 10 µl Gastight Syringe (Hamilton) (Chapters 5 and 6). Intravitreal injections were performed under inhalational anaesthetic with 2-3% isoflurane at a 45$^{o}$ angle 1 mm peripheral to the limbus and avoiding the lens.

#### 2.1.3.1. siCASP2

siCASP2 was supplied under Material Transfer Agreement with Quark Pharmaceuticals Inc. (Ness Ziona, Israel) and was reconstituted in sterile PBS. 5 µl of a 4 mg/ml solution was intravitreally injected in rat blunt injury experiments (Chapters 3 and 4) and 2 µl of a 1 mg/ml solution in mouse blast injury experiments (Chapters 5 and 6). An siRNA against enhanced green fluorescent protein (siEGFP) was used as an siRNA control. The siCASP2 sequence for the sense strand was 5'-GGCUACGUCCAGGAGCGCACC-3' and for the antisense strand was 5'-UGCGCUCCUGGACGUAGCCUU-3'. The siEGFP sequence has been previously described (Hamar et al., 2004); the sense strand was 5'-GCCAGAAUGUGGAACUCYU-3' and antisense strand was 3'-CGGUCUUACACCUUGAGGA-5'.

#### 2.1.3.2. Necrostatin-1s

Nec-1s (BioVision Incorporated, CA, USA) was reconstituted at 3.6 mM in 10% dimethyl sulfoxide (DMSO; Sigma) and 0.9% β-methyl-cyclodextrin (Sigma) in sterile PBS. 5 µl was injected in rat experiments (Chapters 3 and 4) and 2 µl in mouse experiments (Chapters 5 and 6).

### 2.2. *In vivo* analysis

#### 2.2.1. Optical coherence tomography

Optical coherence tomography (OCT) uses near infra-red light to construct a high-resolution cross-sectional retinal image. For mouse experiments (Chapters 5 and 6), OCT imaging was conducted using a Bioptigen ultra-high-resolution SD-OCT system with a mouse retinal bore (Bioptigen, North Carolina, USA). Pupils were dilated using 1% tropicamide and GenTeal $^{TM}$ lubricant gel was used to maintain corneal clarity.

#### 2.2.1.1. Measurement of retinal layer thickness

Whole retinal and GCC thickness (RNFL, GCL and IPL) were measured in OCT images in line with the ONH. Image J was used to manually dissect the layers and measure the area, which was divided by the length of the retinal segment measured to calculate the thickness.

#### 2.2.1.2. Quantification of hyper-reflective dots in the vitreous

Hyper-reflective dots in the vitreous can indicate vitreal inflammation or debris in the vitreous (e.g. injected compound). The number of eyes in which hyper reflective dots

were observed was quantified and displayed as a percentage of total number of eyes that were imaged in that experimental group.

### 2.2.2. Electroretinography and visual evoked potential

#### 2.2.2.1. Principles

The scotopic (dark-adapted) and photopic (light-adapted) electroretinogram (ERG) reflect retinal cell electrical activity (Figure 2.4). The a-wave is the initial negative deflection from baseline which occurs due to photoreceptor hyperpolarisation and reflects rod function in scotopic conditions and cone function in photopic conditions (John R. Heckenlively, 2006). The b-wave is measured from the a-wave trough to the maximum positive deflection and represents the electrical activity of second order neurons including ON bipolar cells and Müller glia. In the photopic ERG, there is the photopic negative response (PhNR) which is a negative deflection after the b-wave and is a downstream measure of inner retinal function including RGCs. As a downstream measure, it is dependent on activity of first and second order neurons (photoreceptors and bipolar cells) (John R. Heckenlively, 2006). Thus, a change in PhNR may be due to changes in either RGC function or upstream cells such as photoreceptors. The PhNR is commonly used to assess RGC function: it is reduced in experimental and human glaucoma (Viswanathan et al., 1999) and is correlated with RGC loss in ONT (Li et al., 2005) .

The visual evoked potential (VEP) measures the electrical responses of the visual pathway between the optic nerve and the occipital cortex to visual stimuli. In a rat model of optic neuritis, VEP amplitudes correlate with RGC axonal loss at 6 dpi (You

et al., 2011). VEPs are clinically used to assess ON function (Holder, 2004). The N1 peak represents a negative deflection at ~75 ms, and P1 represents a positive deflection at ~100 ms (Figure 2.4).

**A)** Photopic ERG

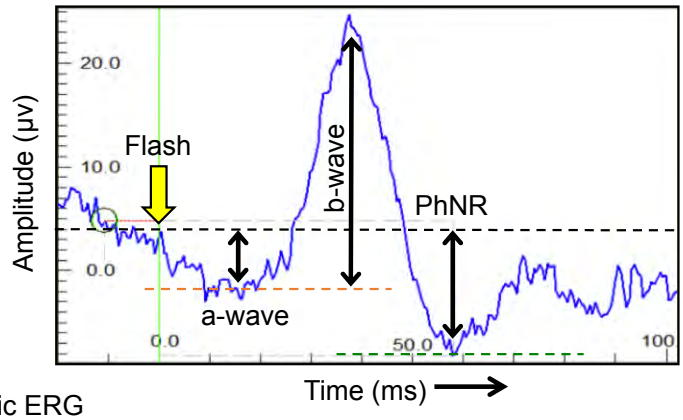


**B)** Scotopic ERG

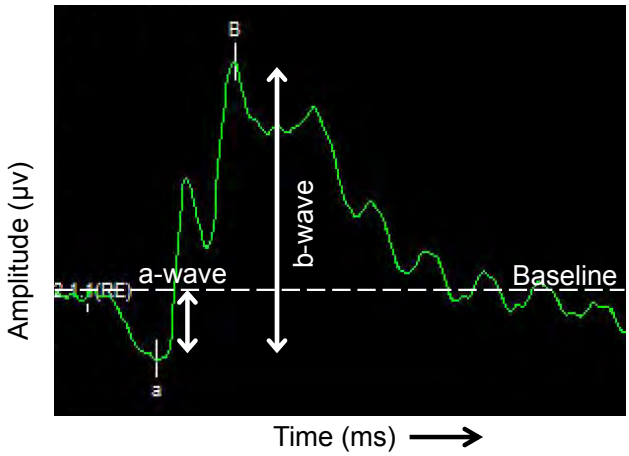


**C)** VEP

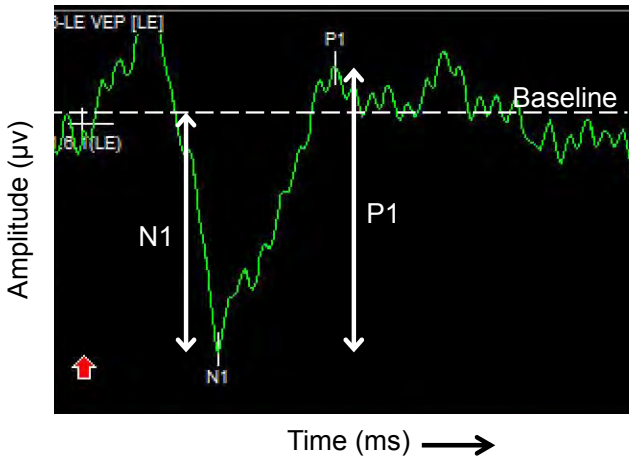

#### 2.2.2.2. Recordings and analysis

In Chapters 3 and 4, ERG recordings were performed by Lt Col Richard Blanch on a HMsERG machine (Ocuscience, Kansas City, MO USA) and analysed by a blinded observer (Chloe Thomas) using the manufacture's semi-automated software, ERG view (Ocuscience, Kansas City, MO, USA), with the marker position manually verified. Animals were dark-adapted overnight, and all preparations performed under dim red light (>630 nm). Scotopic (dark-adapted) flash ERGs were recorded from -2.5 to +1 log units with respect to standard flash in half log unit steps, and photopic (light-adapted) flash ERGs were recorded with a flash intensity of 30,000 mcd/$m^2$ white light over the same range. DTL fibre corneal electrodes (Unimed Electrode Supplies, Farnham, UK) with pressure-moulded contact lenses (Agar Scientific, Stansted, UK) were used with needle skin electrodes (Unimed).

In Chapters 5 and 6, mice were dark-adapted overnight and scotopic ERG and VEPs recorded using the Celeris system with a heated mouse platform to maintain body temperature (Diagnosys LLC, Lowell, MA). Mouse eyes were dilated with 1% tropicamide and anaesthetised with 20 mg/kg ketamine and 8 mg/kg xylazine and 8 mg/kg urethane cocktail. For VEP recordings, mice were exposed to 50 flashes of white light at 1Hz, 0.5 cd.s/$m^2$ and for scotopic ERG recordings, 50 flashes of 1.0 cd.s/$m^2$ of white light. After recordings, mice received subcutaneous injections of 1ml saline and were allowed to recover on heated mats.

## 2.3. Tissue preparation and cryosectioning

### 2.3.1. Tissue preparation

All animals were sacrificed by terminal anaesthetic. Tissue was prepared for immunofluorescent staining and immunohistochemistry.

In blunt ocular injury rat experiments (Chapters 3 and 4), animals were perfused intracardially under terminal anaesthetic (pentobarbital sodium) with 4% paraformaldehyde (PFA; TAAB Laboratories Equipment Ltd, Aldermaston, Berkshire, UK) in PBS. Eyes were enucleated, penetrated through the cornea using a needle and post-fixed for 24 hours in 4% PFA. The anterior portion of the eye (cornea, iris, and lens) and vitreous were removed forming eye cups. For orientation purposes, cuts were made through the retinal scleral cup (Figure 2.5): before enucleation, the inferior limbus was marked using a temporary suture through the conjunctiva and the injury site identified under a light microscope (identified by haemorrhage or retinal opacification) and cuts made perpendicular to the injury site. Sagittal 15 µm sections were cut in a plane parallel to the centre of the injury site and the ONH and every section was collected and labelled in order. For immunostaining, slides containing the centre of the impact site and ONH were identified and then slides counted either side to find sections corresponding to a distance of 600, 1200 and 1800 µm from the impact site.

In blast mouse experiments (Chapters 5 and 6), animals were perfused intracardially under terminal anaesthetic (Avertin) with 4% electron microscopy grade PFA (Electron Microscopy Sciences, Hatfield, Pennsylvania, USA) in PBS. Tissue was fixed for 24 hours in 4% PFA in PBS and then eyes enucleated and ONs dissected. ONs were

dissected to be used for resin-embedding and optical cutting temperature compound (OCTc) embedding.

Eye cups, whole eyes and ONs were cryoprotected by immersion in 10%, 20% and 30% sucrose in PBS for >12 hours each. Tissue was placed in OCTc embedding media (Tissue-Tek, Sakura, USA or Thermo Fischer Scientific, Cheshire, UK) in a plastic embedding mould and frozen in dry ice then stored at -80$^{o}$C until cryosectioning. Embedded eyes and ONs in OCTc blocks were cut into 15 µm sections using a cryostat (Bright Instruments, Huntington, UK) and mounted onto charged SuperFrost ® Plus coated glass microscope slides (Thermo Fisher Scientific). Slides were dried for ~2 hours on a heated plate and stored at -20$^{o}$C or -80$^{o}$C until use.

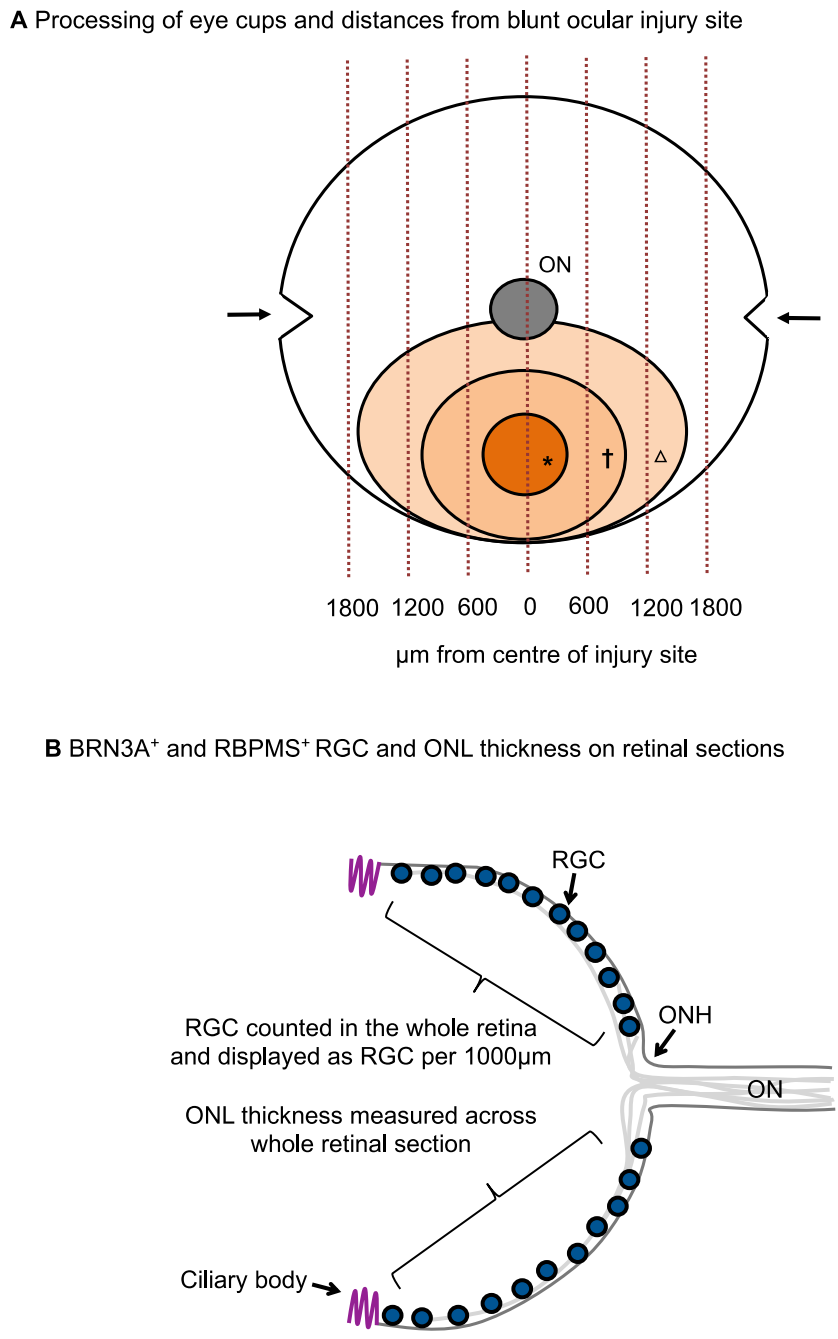


**Figure 2.5 Processing of eye cups and measurements on retinal sections in blunt ocular injury.** **A)** Blunt injured retinal cups were examined under a light microscope to find the impact site; this was lined up with the ON and small cuts perpendicular performed. Eye cups were cryosectioned parallel to the ON and impact site and slides stained at 0, 600, 1200 and 1800 µm either side of the centre of the impact site. **B)** RGC counts and ONL thickness measurements were performed across the whole retinal section.

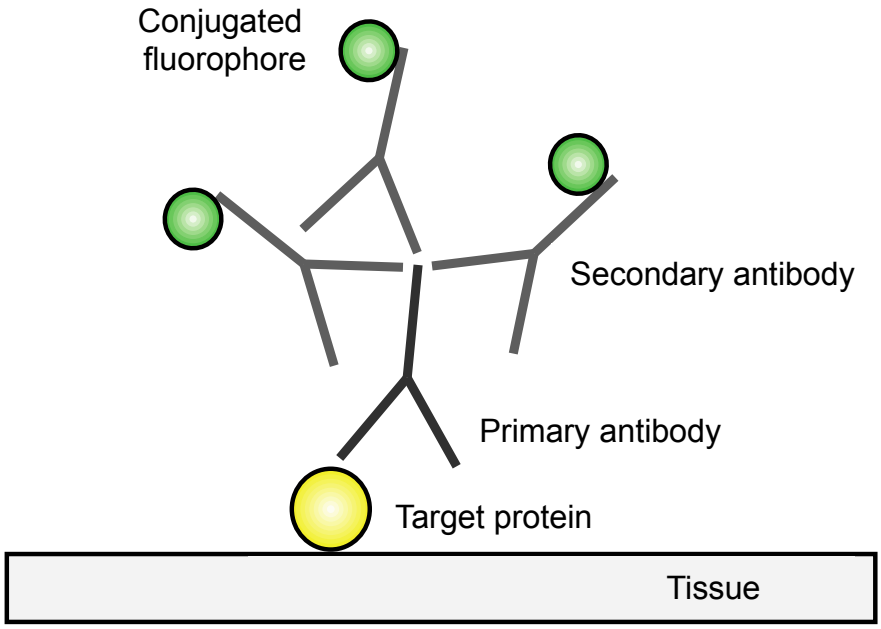
Conjugated
fluorophore
Secondary antibody
Primary antibody
Target protein
Tissue

### 2.4.2. Methods

Frozen cryosections were left to thaw for 20 mins and washed 3 x 5 mins in PBS, followed by 20 mins permeabilisation and blocking in 1% Triton-X-100 (Sigma) and 3% bovine serum albumin (BSA; Sigma). Tissue sections were incubated overnight at 4$^{o}$C with primary antibody (Table 2.1) in 0.5% Tween-20 and 3% BSA before washing 3 x 5 mins in PBS and incubating with secondary antibodies (Table 2.1) at room temperature (RT). Tissue sections were washed 3 x 5 mins in PBS then mounted in Vectashield mounting medium containing nuclear stain 4',6-diamidino-2-phenylindole (DAPI) (Vector Laboratories, Peterborough, UK). Controls with omitted primary antibody were included in each run and these were used to set the background threshold levels for image capture. Sections were viewed under an epi-fluorescent microscope equipped with an AxioCam HRc, controlled using Axiovision Software (All from Zeiss, Hertfordshire, UK).

| *Antibody* | *Detects* | *Host* | *Dilution* | *Source* | *Catalogue number* |
|---|---|---|---|---|---|
| BRN3A (C-20) | RGC-specific transcription factor | Goat | 1:200 (IF) | Santa Cruz | sc-31984 |
| BRN3A (14A6) | RGC-specific transcription factor | Mouse | 1:200 (IF) | Santa Cruz | sc-8429 |
| RBPMS | RGC marker | Rabbit | 1:400 (IF) | Millipore | ABN1362 |
| β actin | Loading control | Mouse | 1:10,000 (WB) | Sigma | A5441 |
| β III tubulin | Neuronal marker | Mouse | 1:200 (ICC) | Sigma | T8660 |
| Caspase-2 (H19) | Apoptotic protein | Rabbit | 1:500 (WB), 1:200 (IF) | Santa Cruz | sc-623 |
| Caspase-2 L | Apoptotic protein | Rabbit | 1:200 (IF), 1:400 (WB) | Abcam | AB2251 |
| RIPK1 | Necroptotic protein | Mouse | 1:200 (IF and WB) | BD Pharmigen | 551041 |
| RIPK3 | Necroptotic protein | Rabbit | 1:1000 (WB) | Abcam | AB56164 |
| RIPK3 (B2) | Necroptotic protein | Mouse | 1:200 (WB) | Santa Cruz | sc-374639 |
| MLKL-P | Phosphorylated MLKL at Ser 345 | Rabbit | 1:500 (IF), 1:2000 (WB) | Cell Signaling | #62233S |
| MLKL (clone 3H1) | Necroptotic protein | Rat | 1:500 (IF), 1:2000 (WB) | Millipore | MABC604 |
| GFAP | Activated glia | Mouse | 1:200 (IF) | Sigma | G3893 |
| ED1/CD68 | Macrophages | Rabbit | 1:200 (IF) | Abcam | AB125212 |
| Alexa Fluor 488 | Mouse IgG | Donkey | 1:400 | Invitrogen, Molecular Probes | A21202 |
| Alexa Fluor 594 | Mouse IgG | Donkey | 1:400 (IF) | Invitrogen, Molecular Probes | A21203 |
| Alexa Fluor 488 | Rabbit IgG | Donkey | 1:400 (IF) | Invitrogen, Molecular Probes | A21206 |
| Alexa Fluor 594 | Rabbit IgG | Donkey | 1:400 (IF) | Invitrogen, Molecular Probes | A21207 |
| Alexa Fluor 488 | Rat IgG | Goat | 1:1000 (IF), 1:1000 (WB) | Invitrogen, Molecular Probes | A11006 |
| HRP-linked | Mouse IgG | Horse | 1:1,000 (WB) | Cell Signaling Technologies | #7076S |
| HRP-linked | Rabbit IgG | Goat | 1:1,000 (WB) | Cell Signaling Technologies | #7074S |
| HRP-linked | Rat IgG | Goat | 1:5,000 (WB) | Cell Signaling Technologies | #7077S |

**Table 2.1 Antibody table.** Abbreviations: Immunofluorescent staining (IF), western blotting (WB), immunocytochemistry (ICC).

### 2.4.3. RGC quantification

RGCs can be counted in retinal sections or in retinal whole mounts and there are a variety of RGC markers which each have advantages and disadvantages (Mead et al., 2014, Mead and Tomarev, 2016) and have been described in Section 1.1.3.

#### 2.4.3.1. RGC quantification on retinal cryosections

In Chapters 3 and 4, RGCs were counted in retinal cryosections and at multiple sites with respect to the impact site to account for variability in cell death with respect to distance from the impact site. Seven retinal sections per eye were analysed from each eye: one through the optic disc and centre of the impact site (0 μm) and in two sections at 600, 1200 and 1800 μm either side of this plane (Figure 2.5). RGC survival was measured by counting $BRN3A^+$ or $RBPMS^+$ cells across the entire retinal section. Only the central section through the impact site is a radial section through the injury site. Sections cut tangentially through the circular zones of injury at the periphery of the injury site will over-represent cells in these peripheral zones, whilst the single section through the disc and the centre of the injury site passes perpendicularly through these zones and so they are proportionally less represented in the overall count for that section.

In Chapters 5 and 6, RGCs were also counted on retinal cryosections but only $RBPMS^+$ cells were counted on cryosections in line with the ONH. The retina was measured and images were taken in the central, middle and peripheral portion of the retinal section (Figure 2.7A).

#### 2.4.3.2. RGC quantification on retinal whole mounts

Retinal whole mounts are created by removing the cornea, iris, lens, vitreous and sclera from PFA-fixed eyes and creating a clover shape (Figure 2.7B). I used a modified method which was more time efficient but had the same outcome. The eye was protruded using curved forceps and an incision performed across the cornea. The retina was carefully squeezed out of the incision using curved forceps and dissected from any remaining lens or iris using forceps in sterile PBS. Some of the photoreceptor outer segments are sloughed using this technique, but the RGCs remain intact. The retina was bluntly dissected to form four clover shaped petals.

Retinal whole mounts were permeabilised in 500 µl 0.5% Triton-X 100 in PBS at -80$^{o}$C for 15 mins, followed by thawing in 500 µl 0.5% Triton-X 100 in PBS for 15 mins at RT. Whole mounts were incubated overnight in primary antibody (BRN3A and RBPMS; Table 2.1) diluted in antibody buffer (2% Triton-X 100, 2% BSA in PBS) at 4$^{o}$C. The following day, whole mounts were washed 3 x 10 mins in PBS at RT then incubated with secondary antibody (Table 2.1) in antibody buffer for 2 hours at RT followed by 3 x 10 mins washes in PBS at RT and mounting with Vectashield aqueous mounting media counting DAPI (Vector Laboratories Ltd.).

Retinal whole mounts were imaged using a Zeiss LSM 710 confocal microscope (Carl Zeiss) in the CISR imaging centre at Vanderbilt University and imaged and analysed using ZEN black software (Carl Zeiss). Z-stacks and automated stitching was performed. Images were also taken on an AxioPlan epifluorescent microscope (Carl Zeiss, Herefordshire, UK) in the far, mid and central portion of the retina (Figure 2.7). The size of the petal was measured from the ONH to the edge and divided into 3 segments. Images were taken of all three segments.

**A)** Counting RGC in retinal sections

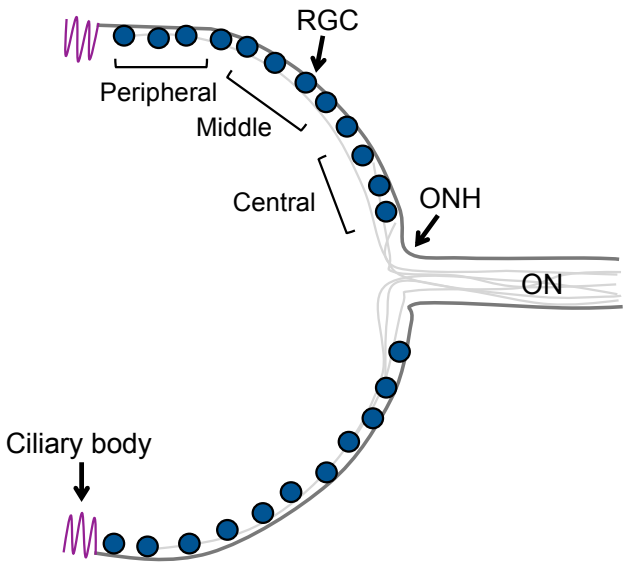


**B)** Counting RGC in retinal wholemounts

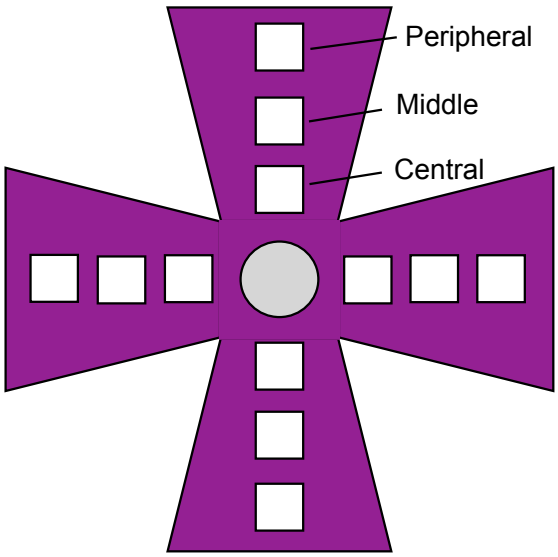


calculated as number of RGCs per mm of retina. **B)** RBPMS$^+$ RGCs were quantified in the central, middle and peripheral boxes on retinal whole mounts on each leaf and quantified as RGC density per mm$^2$.

## 2.5. Haematoxylin and Eosin staining to measure ONL thickness

Haematoxylin and eosin (H&E) are histological stains used to study morphology and tissue structure. Haematoxylin stains nucleic acids a deep blue-purple and eosin stains non-specific proteins such as cytoplasm and extracellular matrix.

### 2.5.1. Method

Tissue sections were rehydrated in PBS for 5 mins followed by 6 mins in Harris haematoxylin (Sigma) then washed 3 x 5 mins in $dH_2O$. Slides were submerged in 1% acid alcohol (70% ethanol, 1% HCl in $dH_2O$) for 90 secs followed by 3 x 5 mins washes in $dH_2O$. Slides were incubated in eosin (Sigma) for 3 mins followed by 3 x 5 mins washes in $dH_2O$. Tissue was dehydrated in ascending concentrations of ethanol (50%, 70%, 90%, 3 x 100%) for 5 mins each time followed by 3 x 5 mins in HistoClear™ (National Diagnostics, Hull, UK). Slides were mounted using VectaMount™ permanent mounting media (Vector Laboratories Ltd.) and left to set overnight.

### 2.5.2. ONL thickness measurements

In H&E stained tissue sections, the ONL was manually segmented using Photoshop (Adobe). The ONL area was measured using Image J and ONL thickness calculated by dividing the ONL area by the length of the retinal section, as described previously by Blanch et al., 2014 (Blanch et al., 2014). The ONL exclusively contains photoreceptor nuclei, therefore this method can be used as a measure of photoreceptor cell survival, with systematic sampling across the whole retina. To account for variability with respect to distance from the impact site, seven retinal sections per eye were analysed: one through the optic disc and centre of the impact site (0 μm) and at 600, 1200 and 1800 μm either side of this plane (Figure 2.5).

## 2.6. ON semi-thin resin sections

Resin-embedded cross sectional ON semi thin sections were used to study axonal myelin morphology, the quantity of intact and degenerating axons and glial reactivity after blast injury. The far proximal section of the ON (closest to the eye) was dissected and resin embedded and the remaining ON processed for cryosectioning and immunofluorescent staining.

### 2.6.1. Fixation and sonication

ONs were fixed in 4% electron microscopy grade PFA (Electron Microscopy Science, Hatfield, Pennsylvania, USA) in PBS, placed in 2% glutaraldehyde in 0.1 M cacaodylate buffer (16% w/v in dd$H_2O$, pH 7.4) for 1.5-2 hours on ice. Tissue was washed 3 x 5 mins in PBS. Next, the ONs were placed in 0.1 M cacaodylate buffer in a 48 well culture plate on ice, then transferred to 2% osmium (osmium tetroxide (Electron Microscopy Sciences) in cacaodylate buffer) and incubated for 45 mins on ice. ONs were then moved to a fresh plate with cacaodylate buffer and washed 3 x 5 mins in cacaodylate buffer. ON tissue was dehydrated in ascending concentrations of 200-proof ethanol (50%, 70%, 95%, and 100%) for 30 mins each at RT in a fume hood and then 100% ethanol for 15 mins. The ONs were placed in a glass scintillation vial containing a 1:1 mixture of propylene oxide and ethanol and incubated for 30 mins at RT. The propylene oxide and ethanol mixture was removed and rapidly replaced with 100% propylene oxide and incubated for 1 hour at RT.

### 2.6.2. Tissue embedding

Propylene oxide was aspirated and replaced with a 1:1 mixture of propylene oxide and Epon epoxy resin (all solutions from Electron Microscopy Sciences, Hatfield,

Pennsylvania, USA) (Table 2.2) and incubated overnight at 4°C. The following day, the solution was replaced with fresh 1:1 propylene oxide and Epon resin and incubated for > 4 hours at RT. ON tissue was moved to a culture plate containing 100% Epon and incubated overnight at RT in a vacuum containing drierite dessicant. All stages with Epon were performed at RT in a vacuum. ON tissue was moved to fresh 100% Epon and incubated for > 6 hours, then moved to fresh 100% Epon and incubated overnight. The following day, fresh 100% Epon was replaced and incubated > 6 hours. ON tissue was placed in a mould containing 100% Epon and incubated overnight in a vacuum. Air bubbles were removed, and the mould placed in a 60°C oven for 3 days to harden the resin.

| *Chemical* | *Amount* |
|---|---|
| Dodecenylsuccinic anhydride (DDSA) | 5.5 ml |
| Araldite 502 | 1.5 ml |
| Embed 812 | 2.5 ml |
| DMP30 | 0.19 µl |
| **Total:** | 9.69 ml |

**Table 2.2 Chemicals in Epon epoxy resin .** All solutions from Electron Microscopy Sciences.

### 2.6.3. Sectioning

The resin moulds were trimmed using a dissecting microscope and razor blade into a double pyramid with the ON in the centre. Semi-thin sections of ~1-2 µm thick were cut using a Reichert-Jung Ultracut E microtome (Leica Microsystems, Vienna, Austria) and a diamond knife. The sections were collected on a slide using $dH_2O$ and dried in a 60$^oC$ oven until the water evaporated, then the sections were cooled to RT.

### 2.6.4. PPD and toluidine blue staining

Slides were stained with 1% w/v p-phenylenediamine (PPD) (Sigma-Aldrich, St Louis, Missouri, USA) in 1:1 mixture of methanol and 2-propanol, for 3 mins and then rinsed 3 x 1 min in a 1:1 mixture of methanol and 2-propanol. Slides were rinsed in 100% ethanol for 1 min and allowed to air dry. Slides were placed at 60$^oC$ on a hot plate and covered with 1% w/v toluidine blue in $dH_2O$ (Fisher, Waltham, Massachusetts, USA) for ~1 min. Slides were washed in $dH_2O$, air dried and mounted with Permount $^{TM}$ mounting media (Thermofisher Scientific) and allowed to set overnight.

### 2.6.5. Imaging and ON axon quantification

ON semi-thin sections were imaged using an x100 oil immersion objective on AxioPlan microscope (Carl Zeiss). Images were stitched together using Photoshop software (Adobe). ON area was measured using Image J and divided by 5 to show the area of 1/5$^{th}$ of the total ON area. This was further divided into 9 counting squares and a 9-grid counting grid superimposed onto the image (Counting Grid Plugin in Image J) (Figure 2.8). Intact and degenerating axons were counted using the Cell Counter Image J Plugin and the total number of intact and degenerating axons in the whole ON were calculated. “Intact axons” have an intact myelin sheath that has uniform thickness,

whilst “degenerating axons” have a degenerative profile with unravelling myelin sheath or axonal compaction, but it is unknown if the axon itself is degenerating or whether it just displays myelin pathology. Throughout this thesis these axons are described as “degenerating axons”. Axonal density was also quantified, which is the total number of intact and degenerating axons per $mm^2$.

**A)** Optic nerve counting grid

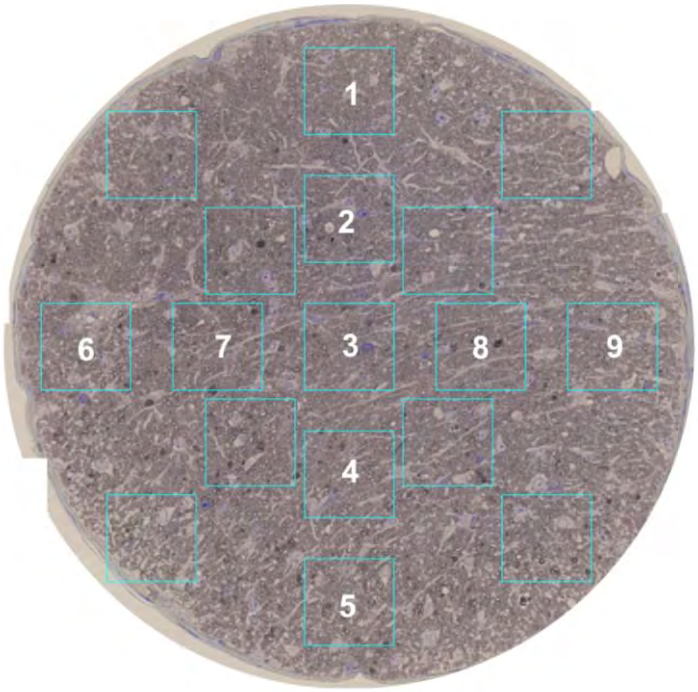


**B)** Intact optic nerve axons

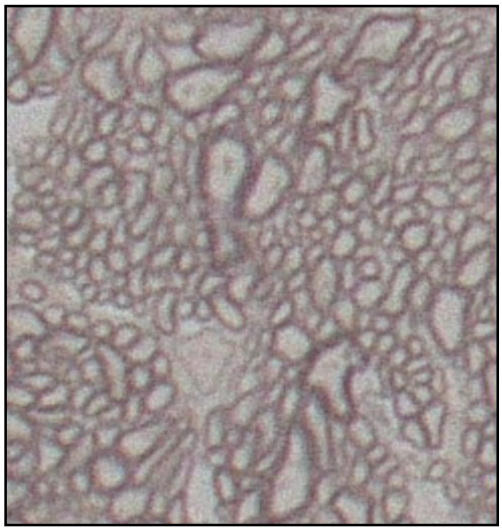

**C)** Degenerating optic nerve axons

'Onioning'

Collapsed

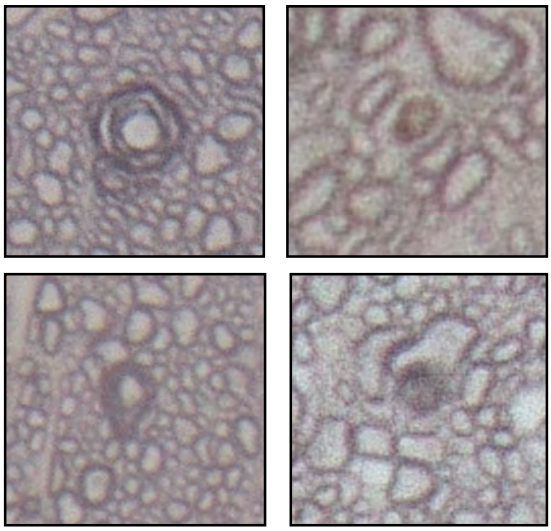

## 2.7. Western blotting

Western blotting is a semi-quantitative technique that identifies proteins through specific antibodies and separates them based on their molecular weight, allowing the visualisation of protein subunits and post translational modifications (Figure 2.9).

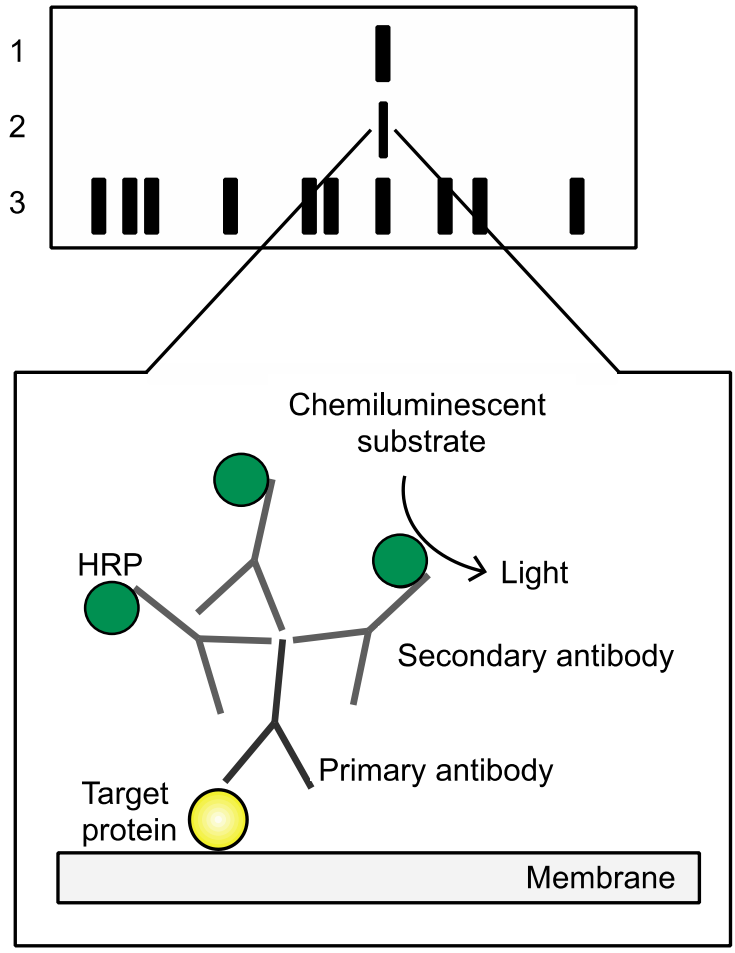


**Figure 2.9 Principles of western blotting**. Lysed proteins are loaded into lanes in an SDS-gel and separated according to molecular weight. Primary antibodies detect a specific protein antigen on the membrane, then HRP-conjugated secondary antibodies bind to their corresponding IgG on primary antibodies, allowing for signal amplification and detection.

### 2.7.1. Tissue preparation

Animals were euthanised by anaesthetic overdose and retinae dissected and snap frozen in liquid nitrogen and stored at -80$^{o}$C.

For blunt injury experiments (Chapter 3 and 4), 6 retinae from each experimental group were pooled and homogenised (using Ika ® basic ultra-turrax homogeniser, Ika, Germany) on ice at 1000 rpm rising to 3000 rpm over 2 mins in a solution of 200 µl RIPA lysis buffer (20 nM Tris HCl, 150 mM NaCl, 1 mM ethylenediaminetetraacetic acid (EDTA), 0.5 mM ethylene glycol tetraacetic acid (EGTA), 1% NP-40) supplemented with 5 µl/ml protease inhibitor cocktail (Cat no. P8340, Sigma). The homogenate was incubated on ice for 30 mins and then centrifuged at 13,000 g at 4$^{o}$C for 10 mins. Supernatant was collected, aliquoted and stored at -80$^{o}$C.

For rPBI experiments (Chapter 5 and 6), mice were culled by anaesthetic overdose and retinae removed and snap frozen in dry ice and stored at -80$^{o}$C. Retinae were processed individually: 80 µl of lysis buffer (2% v/v Triton-X-100 in PBS) supplemented with 100X Halt $^{TM}$ protease inhibitor cocktail (Thermo Fisher Scientific) and phosphatase inhibitor cocktail (Sigma) which inhibits serine/threonine phosphatases, was added to each retina and probe sonicated at 10 microns for 10 secs submerged in ice cold water. Retinal lysate was centrifuged at 13,000 rpm for 10 mins at 4$^{o}$C, then supernatant removed and stored at -80$^{o}$C.

### 2.7.2. Polyacrylamide gel electrophoresis

Tris-glycine sodium dodecyl sulphate (SDS) -polyacrylamide gel electrophoresis (PAGE) 12% Tris-glycine gels were made compromising of stacking and resolving

gels (Table 2.3). Briefly, all solutions for the resolving gel were combined, with tetramethylethylenediamine (TEMED) added last to instigate the gelling process. The resolving gel solution was pipetted into a 1mm cassette (Novex, Life Technologies) and topped with ethanol to remove air bubbles and set for ~20 mins at RT. The ethanol was removed and stacking gel solution added to the cassette and either a 10 or 12 well comb inserted and left to set at RT.

Retinal lysate samples were defrosted on ice and a DC ™ protein assay (Bio-Rad Laboratories, Inc.) used to determine protein concentration. Dilutions of BSA (2, 1.5, 1 and 0.5 mg/ml) diluted in protein lysis buffer were used to create a standard curve. 5 µl of each sample was pipetted into a 96 well plate with 20 µl of reagent A* and 160 µl of reagent B. Plates were incubated for 15 mins at RT in the dark to prevent signal degradation and read on a Victor X3 Spectrophotometer (Perkin, Elmer, Waltham, MA, USA) at 750 nm.

Equal concentrations of retinal lysate were added to 2X laemmli sample buffer (Sigma) and proteins denatured through heating samples to 90$^{o}$C for 4 mins. The gel was loaded into an XCell SureLock™ system (Invitrogen, Life Technologies) and tris glycine running buffer added (15 mM Tris, 192 mM glycine, 0.1% SDS in dd$H_2O$). Samples were loaded into wells with an equal total protein concentration per lane. Proteins were separated by electrophoresis at default settings on the PowerEase® 500 power supply (Invitrogen; 125 V, 35 mA) for 2 hours.

### 2.7.3. Protein transfer and detection

Proteins were transferred from the gel to a more stable membrane. A polyvinylidene fluoride (PVDF) membrane (Immoblion, Millipore, Watford, UK) was activated in 100% methanol (Fisher Scientific, Leicestershire, UK). The proteins were transferred to the PVDF membrane in transfer buffer (25 mM Tris, 192 mM glycine, 20% (v/v) methanol, 0.01% v/v SDS in dd$H_2O$), using an XCell II™ blot module (Life Technologies) for 2 hours at 25 V and 125 mA. Membranes were washed in Tris buffered saline with Tween-20 (TBST) (10 mM Tris, 150 mM NaCl, 0.05% Tween-20) then incubated in blocking buffer [5% w/v dried skimmed milk powder (Marvel, Lincolnshire, UK) in TBST] for 1 hour at RT. The membrane was incubated in primary antibody solution (5% w/v Marvel in TBST) in a 50ml falcon tube on a roller overnight at 4$^oC$, then washed 3 x 10 mins in TBST and incubated with HRP-conjugated secondary antibodies (5% Marvel in TBST) for 1 hour at RT. The membrane was washed 3 x 10 mins in TBST.

To develop the signal, the membrane was incubated in enhanced chemiluminescence (ECL) solutions (GE Healthcare, Buckinghamshire, UK); at a 1:1 ratio of reagent 1 and 2 for 1 min, then either blotted dry in filter paper and placed in clear plastic inside a cassette and exposed to Amersham Hyperfilm ™ ECL (GE Healthcare Limited, Buckinghamshire, UK) in a dark room or developed using the digital imaging system: ChemiDoc ™ MP System (Bio-Rad, Hemel Hempstead, UK) or G Box chemiluminescence and fluorescence gel doc (Syngene, Cambridge, UK). Antibodies were then stripped using stripping buffer (25 mM glycine-HCl, 1% w/v SDS, pH 2) for 1 hour at RT and the membrane re-probed to detect other proteins. Membranes were stored short-term in TBST at 4$^oC$.

| *Component* | *Stacking gel* | *Resolving gel* |
|---|---|---|
| Protogel ™ (40% Acrylamide, 0.8% Bisacrylamide Stabilised Solution; National Diagnostics) | 0.4 ml | 1.83 ml |
| 0.5 M Tris/Cl pH 6.8 | 1.85 ml | - |
| 1.5 M Tris/Cl pH 8.8 | - | 1.65 ml |
| $dH_2O$ | 0.75 ml | 3.12 ml |
| 10% sodium dodecyl sulfate-polyacrylamide (SDS) (Fisher Bioreagents) | 30 µl | 66 µl |
| 10% ammonium persulfate (APS) | 15 µl | 23.1 µl |
| Tetramethylethylenediamine (TEMED) (Thermo Scientific) | 7.5 µl | 9.9 µl |

**Table 2.3. Components of the SDS-PAGE gel.**

## 2.8. Primary retinal cultures

Primary retinal *in vitro* cultures were used to assess the effects of neuroprotective compounds on RGC death, in Chapter 4.

### 2.8.1. Retinal dissection and cell culture

Adult male Sprague Dawley rats (200-300 g) were culled by $CO_2$ inhalation and death confirmed by cessation of heartbeat. Eyes were enucleated and placed in ice-cold PBS. Retinae were dissected then minced with surgical scissors to increase surface area and dissociated in 1.25 ml of papain (Worthington Biochem, NJ, USA) with 62.5 µl of DNase I added (Papain Dissociation System kit; Worthington Biolabs, New Jersey, USA) in Earle's Balanced Salt Solution (EBSS) for 90 mins at 37$^{o}$C. After 90 mins, retinae were triturated with a 10 ml serological pipette to dissociate any remaining fragments and centrifuged at 300 g for 5 mins at RT. The supernatant was discarded, and pellet resuspended in 1.35 ml EBSS (Worthington Biochem), 150 µl reconstituted albumin ovomucoid inhibitor (Worthington Biochem) and 75 µl DNase I. This cell suspension was added on top of 2.5 ml of albumin ovomucoid inhibitor to form a discontinuous density gradient and centrifuged at 70 g for 6 mins at RT, forcing the retinal cells through the viscous layer whilst capturing the debris. The supernatant was discarded, and cell pellet re-suspended in 1ml of supplemented Neurobasal A medium [Neurobasal A (Gibco) supplemented with 2% v/v B27 supplement (Life Technologies, Invitrogen, UK), 0.5 mM of L-Glutamine (Invitrogen) and 0.5% v/v Gentamycin (50 mg/ml Invitrogen)]. Cells were counted using a haemocytometer and plated at 125,000 cells per 300 µl in 8-well chamber slides (BD Biosciences). Wells were coated for 60 mins with 150 µl of 100 µg/ml poly-D-lysine, washed 2 x 5 mins in PBS then 30 mins with 150 µl of 10 µg/ml laminin. Cultures were incubated at 37$^{o}$C in

95% $O_2$ and 5% $CO_2$. Specific time courses of drug treatment are discussed in more detail in Chapter 4.

### 2.8.2. Immunofluorescent staining

Media were removed and cells fixed in 4% PFA in PBS for 10 mins, followed by 3 x 10 mins washes in PBS. Cells were permeabilised in 0.1% Triton-X 100 in PBS for 10 mins, washed 3 x 10 mins in PBS and then incubated in βIIIT primary antibody diluted in antibody diluting buffer (0.5% Tween-20 and 3% BSA in PBS) for 1 hour at RT. Cells were washed 3 x 10 mins in PBS and incubated in secondary antibody diluted in antibody diluting buffer for 1 hour at RT. Excess antibody was removed by washing 3 x 10 mins in PBS then removing the chamber slide and mounting with Vectashield aqueous mounting media containing DAPI (Vector Laboratories Ltd.).

### 2.8.3. *In vitro* RGC quantification

Fluorescent images were captured on an AxioPlan microscope (Carl Zeiss, Hertfordshire, England). Each well was divided into 9 sections and 4 images were taken per section, providing a non-biased sampling of RGCs per treatment. RGCs were distinguished from other retinal cells by their expression of βIIIT and the morphology of their cell bodies which were large and round. RGCs were counted per imaged and averaged per treatment group. Primary retinal cultures were performed on three independent occasions with each treatment in duplicate. Number of RGCs was normalised as a percentage of intact values per repeat.

## 2.9. Quantitative polymerase chain reaction

Quantitative PCR (qPCR) is a technique to quantify gene expression and can detect differences in mRNA expression between experimental groups.

Primer sequences can be designed to recognise specific DNA and placed in a qPCR reaction mix with SYBR green ®, which emits fluorescence after intercalating between DNA bases in dsDNA (Figure 2.10). This fluorescent signal is detected and measured following each qPCR amplification cycle, and a measure of how much DNA has been amplified can be calculated.

### 2.9.1. Primer design

Primers sequences were found on Primer Bank (Spandidos et al., 2010) (https://pga.mgh.harvard.edu/primerbank/index.html) using the NCBI Gene ID. Primers were chosen which were approximately 15 nucleotides in length with sequences that crossed exon-exon boundaries and had predicted specificity for the DNA of interest on the NCBI primer BLAST database (Ye et al., 2012) (https://www.ncbi.nlm.nih.gov/tools/primer-blast/). Primer Bank has primer sequences for human and mouse genes, but because I needed rat primers, I searched for mouse primers and then placed these sequences into Primer Bank against rat homology and replaced some bases so that the specificity was to rat mRNA. Primers were diluted to 100 µM in RNAse and DNase free water and diluted to a final reaction concentration of 100 nM. Primer sequences are displayed in Table 2.4.

**A)** SYBR green intercalates into dsDNA

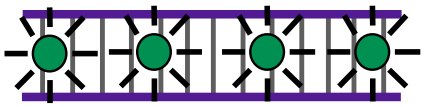

**B)** Single stranded cDNA releases SYBR green

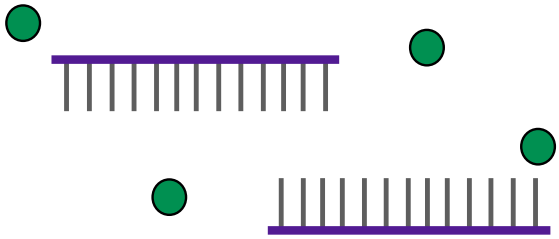

**C)** Forward and reverse primers anneal and elongate cDNA

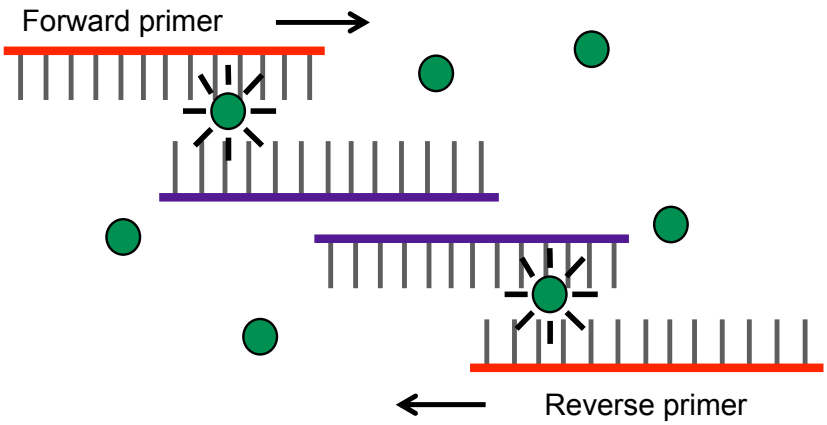


**D)** SYBR green binds to dsDNA product

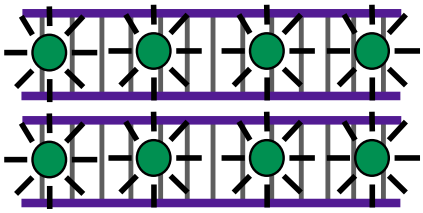

**F**

fl

d

a

cl

products, leading to an increase in fluorescent signal.

### 2.9.2. Primer specificity and efficiency

At the end of each qPCR reaction, a melt curve was performed to test for primer sequence specificity. One distinctive peak on the melt curve suggests that primer has bound to a single sequence on the cDNA transcript. Multiple peaks suggest either non-specific primer binding, binding to multiple cDNA sequences (and, therefore, the detection of multiple genes) or primer dimer formation where there is excess primer resulting in self binding. Primer efficiency tests were also performed with serial dilutions of RNA (2-fold dilutions from 1.56 ng-50 ng) to determine if the primers efficiently detected a 2-fold increase in cDNA with each qPCR cycle. Primers with an efficiency of 80-110% were acceptable and used in the study. RNA extracted from rat PC12 cells (pheochromocytoma adrenal medulla cell-line) was used to test primer efficiency (Figure 2.11).

| Gene | Forward primer | Reverse primer | Source |
|---|---|---|---|
| Rat *casp2* | 5'-CTGACAGGAGGAGCAGGATT-3' | 5'-CTAACAGTTCGCTCAGCAGC-3' | (Ahmed et al., 2011) |
| Mouse *ripk1* | 5'- GAAGACAGACCTAGACAGCGG-3' | 5'-CCAGTAGCTTCACCACTCGAC-3' | Primer Bank ID 34328467a1 |
| Rat *ripk1* | 5'-GAAAGACCTGGACAGCGGAG-3' | 5'-CCAGTAGCTTCACCACTCGAT-3' | |
| Mouse *ripk3* | 5'-CAGTGGGACTTCGTGTCCG-3' | 5'-CAAGCTGTGTAGGTAGCACATC-3' | Primer Bank ID 256017156c1 |
| Rat *Ripk3* | 5'-GAGTGGGACTACGTGTACG-3' | 5'-CAAGCTGTGTAGGTAGCACATC-3' | |
| Mouse *mlkl* | 5'- AATTGTACTCTGGGAAATTGCCA-3' | 5'-TCTCCAAGATTCCGTCCACAG-3' | Primer Bank ID 23274129a1 |
| Rat *mlkl* | 5'-AATTGTACTCTGGGAAATTGCCA-3' | 5'-TCTCCAAGATTCCGTCCACAG-3' | |
| Rat 18s | Unspecified sequence. | | QuantiTect ® primer assay Rn_18s Cat. No: QT02589300 (Qiagen) |

**Table 2.4 qPCR primer sequences.** The forward and reverse primer sequences of mouse primers from Primer Bank are displayed and their corresponding rat primer sequences.

**A)** Primer efficiency graphs

**i)** *casp2*

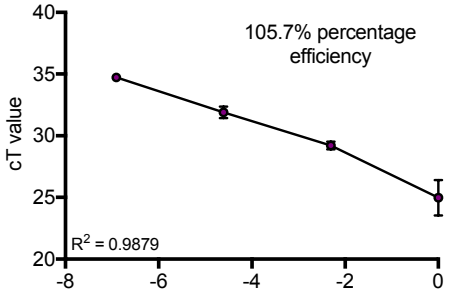


**ii)** *ripk1*

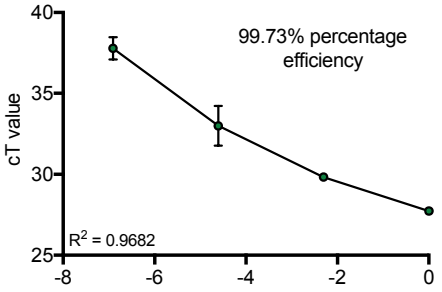


**iii)** *ripk3*

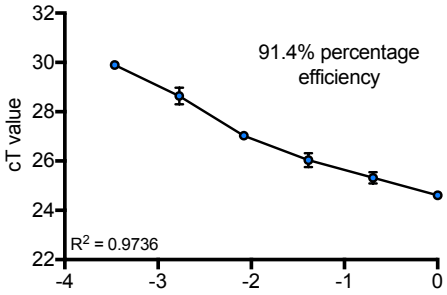


**iv)** *mlkl*

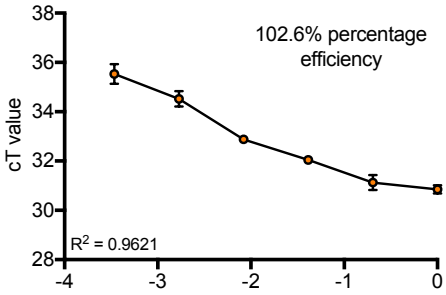


**B)** Melt curves

**i)** Specific

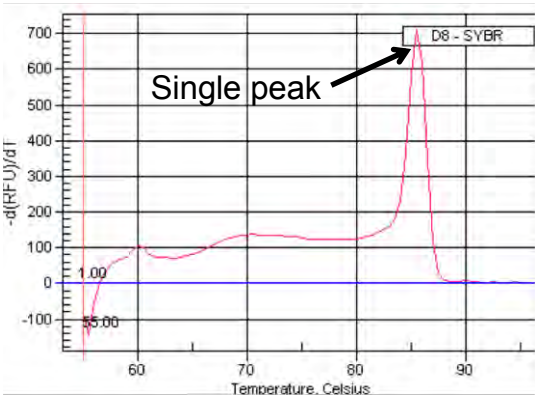


**ii)** Non-specific

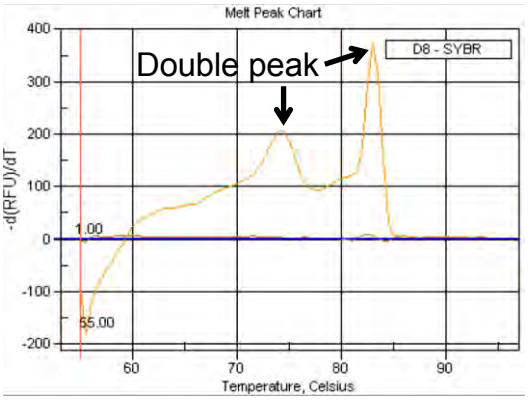

### 2.9.3. RNA extraction

RNA was extracted using the RNeasy Mini Kit (Qiagen) with a modified protocol. Retinae were dissected and snap frozen in liquid nitrogen and stored at -80$^{o}$C. Frozen retinae were defrosted on ice and tissue disrupted using a homogeniser (Ika ® basic ultra-turrax homogeniser, Ika, Germany) on ice in 500 µl TRIzol $^{TM}$ reagent (Invitrogen, Fisher Scientific, Thermo Fisher Scientific) for 30 secs at increasing speeds (1000, 2000 then 3000 rpm). Retinal lysates were incubated for 5 mins at RT to allow complete dissociation of nucleoprotein complexes. A volume of 200 µl of chloroform was added, vortexed and incubated for 5 mins at RT. Samples were centrifuged for 15 mins at 4$^{o}$C at 12,000 rpm, then ~200 µl of the aqueous phase was transferred to a 1.5 ml Eppendorf tube. RNA was solubilised in 700 µl of 100% ethanol and vortexed to mix. 600 µl of lysate was pipetted onto a RNeasy column and centrifuged at 1000 rpm for 30 secs at RT. RNA was captured on the column and the flow through discarded at each of the following purification steps. A volume of 500 µl of RW1 buffer was added and centrifuged at 10,000 rpm for 15 secs, followed by an additional DNase degradation step using the RNase-free DNase kit (Qiagen). Next, 80 µl of solution was added onto the spin column and incubated for 15 mins at RT. 500 µl of RW1 buffer was added to the spin column and centrifuged at 10,000 rpm for 15 secs, followed by 500 µl of RPE buffer and centrifuged at 13,000 rpm for 15 secs. The last step was repeated with prolonged centrifugation for 2 mins to ensure full ethanol removal. The spin column was centrifuged for 2 mins at 13,000 rpm in a fresh collection tube to ensure no carryover and potential contamination. To elute the purified RNA, the column was placed in a RNase free 1.5 ml collection tube and 30 µl of nuclease free water pipetted into the centre of the column, incubated for 2 mins at RT, then centrifuged at 13,000 rpm for 1 min at RT. RNA was stored at -80$^{o}$C.

### 2.9.4. RNA quantification

RNA concentration was measured by loading 1 µl of eluted RNA onto a Nanodrop ® spectrophotometer (Wilmington, DE, USA) or NanoPhotometer ® (Implen). The 260 nm / 280 nm absorbance ratio provides an estimate of nucleic acid purity, with values >1.8 acceptable but ~2 were considered more favourable. RNA integrity was assessed in a subset of samples using a Bioanalyser (Agilent Technologies Inc.) and a RNA

**A)** RNA integrity run with 28s and 18 bands **B)** Sample measurement

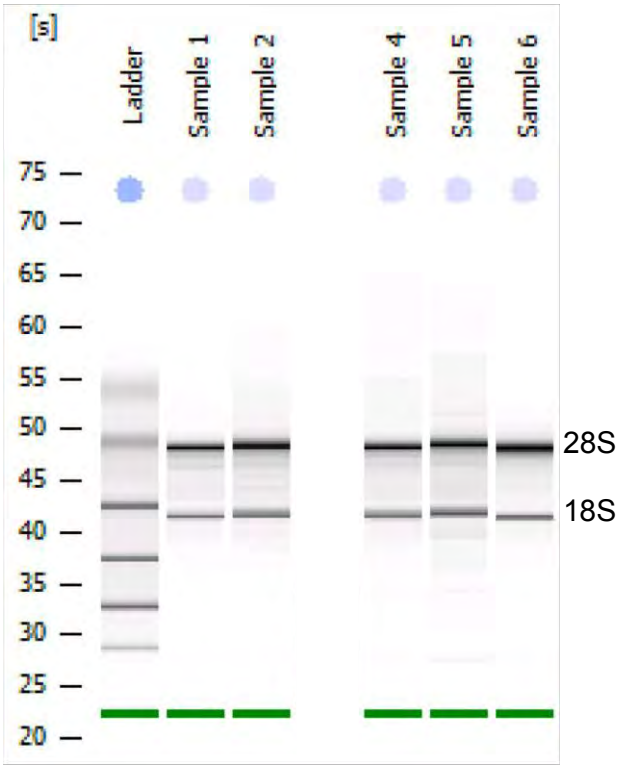


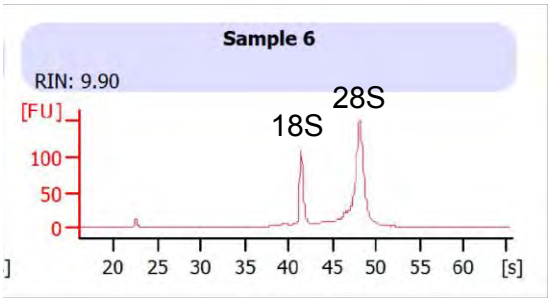

### 2.9.5. cDNA conversion

RNA was reverse transcribed into single-stranded complementary DNA (cDNA) using the Tetro cDNA synthesis kit (Bioline reagents Ltd. London, UK) or SensiFAST ™ cDNA synthesis kit (Bioline reagents Ltd.). Equal concentrations of RNA were converted per sample and a maximum of 1 µg of RNA was converted per 20 µl reaction. In the Tetro cDNA synthesis kit, the reaction mixture consisted of 4 µl 10x reverse transcription buffer, 1 µl 25x dNTPs, 1 µl 10x random primers, 1 µl multiscribe reverse transcriptase, with nuclease-free water and RNA (to reach 13 µl depending on RNA concentrations), in a sterile nuclease free 0.2ml Eppendorf. The cDNA reaction was run in a Bio-Rad T100™ thermal cycler (Bio-Rad) with the reaction conditions in Table 2.5A. cDNA was stored at -20ºC or -80ºC.

**A)** Thermal cycler reaction conditions

| *Step* | *1* | *2* | *3* | *4* |
|---|---|---|---|---|
| **Temperature (ºC)** | 25 | 37 | 85 | 4 |
| **Time (mins)** | 10 | 120 | 5 | ∞ |

**B)** qPCR reaction conditions

| *Step* | *1* | *2* | *3 (40 cycles)* | | *4 (melting curve)* |
|---|---|---|---|---|---|
| **Temperature (ºC)** | 50 | 96 | 95 | 58 | 55 |
| **Time** | 2 mins | 10 mins | 15 secs | 1 min | 30 secs |

**Table 2.5 cDNA conversion and qPCR reaction conditions. A)** Thermal cycler reaction conditions. **B)** qPCR reaction conditions.

### 2.9.6. RT-qPCR reaction

The cDNA volume per reaction was calculated from the starting amount of RNA converted to cDNA, assuming that there was ~100% reaction efficiency. Housekeeping genes that are not affected by injury or treatment were used as controls. Each qPCR reaction contained SYBR green master mix (Thermo Fisher Scientific), 1 µl primer (final concentration 200 nM), 5 µl nuclease free water and 4 µl cDNA at 2.5 ng/µl (10 ng 'converted cDNA' per reaction). The qPCR was performed in a QuantStudio 5 machine (Applied Biosystems by Thermofisher Scientific) and reaction conditions are displayed in Table 2.5.

### 2.9.7. Gene expression analysis

Gene expression was analysed using the ΔΔCT method. The housekeeping gene cT value (e.g. *18S*) was subtracted from the gene of interest (e.g. *Casp2*) cT value for each sample, to give a normalised cT value (ΔCT). The mean normalised cT value for the control experimental group (e.g. intact animals) was subtracted from all values (ΔΔCT). The ΔΔCT values for each experimental group were averaged and converted to fold-change using the equation 2^-ΔΔCT.

## 2.10. Statistical Analysis

Statistical analysis was carried out using SPSS (IBM Corp., Armonk, NY, USA) and GraphPad Prism GraphPad Prism version 7.00 (GraphPad Software, La Jolla California USA). The data were tested for normality using the Shapiro-Wilk test. Normally distributed data were analysed using one-way ANOVA and post-hoc Tukey tests with p values corrected for multiple comparisons. In experiments where multiple comparisons were made, the p values were corrected with Bonferroni correction and the correction factor is stated.

Generalised linear models (GLM) were used to determine if there was a statistically significant difference between treatment and vehicle eyes in RGC counts and ONL thickness at multiple points across the retina, as well as ERG amplitudes at different stimulus intensities. There were three main options to specify in the GLMs; 1) the correlation matrix; 2) the probability distribution; 3) and link function. In all of my experiments, the correlation matrix was set autoregressive (AR1), which assumes that values which are next to each other are related. For example, the cell counts or ONL thickness at positions in the eye or the ERG amplitudes at stimulus intensities that are closer to one another are more related. The probability distribution is either normal or gamma for numeric data. The variables that I used were either ERG amplitude or number of $RBPMS^+$ or $BRN3A^+$ RGCs or ONL thickness. The factors for ERG analysis were flash intensity and treatment, and for RGC quantification / ONL thickness were position in the retina and treatment. To determine if there were statistically significant differences between treatment and control values at individual positions of the retina in $BRN3A^+$ and $RBPMS^+$ cell counts and ONL thickness, an unpaired t-test was performed, with Holms Bonferroni correction applied to account for multiple comparisons.

Analysis of variance (ANOVA) statistical testing is used to determine differences in protein expression in western blots with post hoc Tukey testing to determine differences between individual time points.

Data is reported as mean ± standard error of the mean (SEM).

# Chapter 3 Caspase-2 mediates site-specific retinal ganglion cell death after blunt ocular injury

Parts of chapter are published in IOVS

**Chloe N Thomas**, Adam M Thompson, Eleanor McCance, Martin Berry, Ann Logan, Richard J Blanch, Zubair Ahmed.

Caspase-2 mediates site-specific retinal ganglion cell death after blunt ocular injury

*Investigate Ophthalmology & Visual Science (IOVS)* (2018)

Full paper is found in Appendix II

.

### 3.1. Rationale

Ocular trauma is common in civilian and military populations. Among other injuries, closed globe blunt ocular trauma causes acute disruption of photoreceptor outer segments (commotio retinae) and RGC death, both of which permanently impair vision. Caspase-2 dependent cell death is important and evidenced in models of RGC degeneration. It has previously been shown that RGC death after ONC is caspase-2-mediated. For example, axotomised RGCs activate caspase-2, whilst pharmacological inhibition of caspase-2 protects ~60% of RGCs for up to 21 days after ONC and siCASP2 protects >95% of RGCs for up to 12 weeks (Ahmed et al., 2011, Vigneswara and Ahmed, 2016, Vigneswara et al., 2014, Vigneswara et al., 2012). siCASP2 also protects RGCs in a mouse optic neuritis model (Lidster et al., 2013). siCASP2 (also known as QPI-1007) is currently in clinical trials for NAION (protocol: QRK007 NCT01064505) and acute primary angle-closure glaucoma (protocol: QRK208 NCT01965106) with Quark Pharmaceuticals Inc. (Ness Ziona, Israel). Caspase-2 is also activated and induces neuronal degeneration after SCI (Vigneswara et al., 2013) and in Alzheimer's disease (Troy et al., 2000, Zhao et al., 2016).

In this study, I assessed the role of caspase-2 as a mediator of RGC and photoreceptor death in a rat blunt ocular injury model.

### 3.2. Experimental design

To determine the role of caspase-2 in RGC and photoreceptor death after blunt ocular injury, groups of female Lister Hooded rats were subjected to unilateral or bilateral blunt eye injury under anaesthesia as a recovery procedure, as previously described in Section 2.1.1. Western blotting and immunofluorescent staining were performed at 5, 24 and 48 hours after injury to determine caspase-2 cleavage and protein localisation (Figure 3.1A) (see Section 2.7 Section 2.3 and Section 2.4.2). GFAP and ED1 immunofluorescent staining were also performed on cryosections at 5, 24 and 48 hours post injury (see Section 2.3 and Section 2.4.2). Bilateral blunt ocular injury was performed and knockdown of caspase-2 unilaterally through an intravitreal injection of 5 µl of 4 mg/ml siCASP2 in PBS and control contralateral intravitreal injection of 5 µl of 4 mg/ml siEGFP in PBS. Intravitreal injections were performed immediately after and at 7 days after injury (n=8 per group). Uninjured rats which were not given intravitreal injections were culled and acted as intact controls (n=8 animals). At the 14 day endpoint, RGC and photoreceptor functional and structural assessments were performed by recording scotopic and photopic ERGs (Section 2.2.2.2), and quantifying RGCs (Section 2.4.3) and ONL thickness in retinal cryosections (Figure 3.1B).

**A** *In vivo* protein and immunofluorescent studies

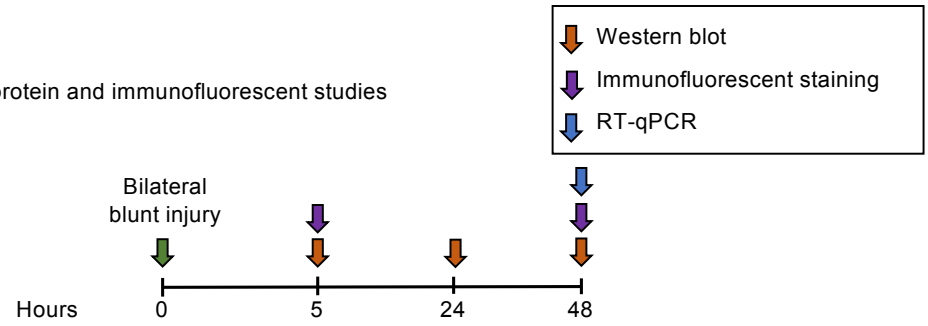


| *Experiment* | *Injury performed* | *N (retinae)* | *Timepoints* | *Measured endpoints* |
|---|---|---|---|---|
| Western blot | Bilateral blunt injury and eyes pooled | 18 retinae total (6 pooled retinae from 3 animals, repeated on 3 independent occasions) | Intact, 5, 24, 48 hours after injury | Caspase-2 protein expression and cleavage |
| Immunofluorescent staining | Unilateral blunt injury | 4 animals per timepoint | Intact, 5, 48 hours after injury | Caspase-2 retinal localisation |
| RT-qPCR | Bilateral blunt injury | 6 retinae from 3 animals | Intact and 48 hours after injury | *Casp2* mRNA expression |

**B** *In vivo* siCASP2 studies

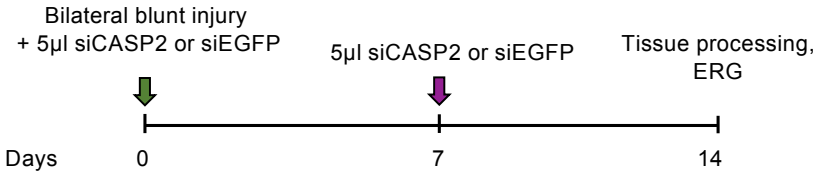


| *Treatment* | *Injury performed* | *Treatment* | *n (eyes)* |
|---|---|---|---|
| Intact | - | - | 8 |
| Blunt injury + siCASP2 | Bilateral blunt ocular injury | Unilateral 5µl intravitreal injection of 4mg/ml siCASP2 in PBS | 8 |
| Blunt injury + siEGFP | | Contralateral 5µl intravitreal injection of 4mg/ml siEGFP in PBS | 8 |

**Measured endpoints:** BRN3A$^+$ and RBPMS$^+$ RGC counts, ONL thickness on H&E cryosections, scotopic and photopic ERG.

**Figure 3.1. Experimental design** . **A)** *In vivo* protein and immunofluorescent staining studies and **B)** *in vivo* siCASP2 studies.

## 3.3. Results

### 3.3.1. Blunt ocular injury induced ED1$^+$ cell infiltration but no changes in GFAP expression at 2 dpi

Immunofluorescent staining was performed for GFAP and ED1 on retinal sections after blunt ocular injury at 5, 24 and 48 hours (images representative of n=4 animals per group). There were a few GFAP$^+$ glial processes in the RNFL of intact retinae, which was also the case up to 48 hours after blunt ocular injury (Figure 3.2). There were few ED1$^+$ cells (monocyte derived cells) in intact retinae and in the retina 5 and 24 hours after blunt ocular injury. The number of ED1$^+$ cells was higher in the retina 48 hours after blunt ocular injury (Figure 3.2), which suggests there was inflammatory cell infiltration at this time point.

### 3.3.2. *Casp2* mRNA rises 48 hours after blunt ocular injury

*Caspase-2* gene expression was analysed by qPCR at 48 hours after blunt ocular injury (n=3 animals received bilateral blunt ocular injury or were intact controls, 6 eyes per group). Results are presented as mean fold change compared to intact retinae. *Caspase-2* mRNA expression was significantly higher in injured retinae compared to intact retinae, with a 1.6-fold increase in expression compared to intact retina at 48 hours after blunt ocular injury (Figure 3.3A) (unpaired student's t-test $p<0.05$).

### 3.3.3. Caspase-2 is cleaved in RGCs after blunt ocular injury

Western blotting for caspase-2 and its cleaved fragments was performed on pooled retinae after bilateral blunt ocular trauma (n=3 animals per experimental group, 6 pooled retinae, repeated on 3 independent occasions; total 9 animals per group, 18 retinae). Western blotting of whole retinal lysates demonstrated that retinal levels of

the cleaved 12 kDa fragment of caspase-2 increased up to 48 hours after injury compared to intact animals (ANOVA $p<0.01$; Figure 3.3 Ci), though full-length 55 kDa caspase-2 levels remained unchanged (ANOVA $p>0.05$; Figure 3.3 Cii). Post hoc Tukey with multiple comparisons demonstrated that the 12 kDa cleaved caspase-2 fragment significantly increased at 48 hours after blunt ocular trauma compared to intact retinae (post hoc Tukey $p<0.05$). There was also a significant increase in the 12 kDa caspase-2 fragment between the 5 and 48-hour time points (post hoc Tukey $p<0.001$) and between 24 and 48 hours (post hoc Tukey $p<0.05$).

Caspase-2 immunofluorescence was performed to demonstrate retinal localisation (images representative of n=4 animals per time point). At 5 and 48 hours after blunt ocular injury, caspase-2 was localised to $BRN3A^+$ RGCs adjacent to the centre of the injury site with increased nuclear and cytoplasmic caspase-2 expression compared to intact retinae (Figure 3.4A). Caspase-2 was also detected in the INL; however, levels were not altered by injury, suggesting that caspase-2 is endogenously expressed in the INL. Caspase-2 was not detected by immunofluorescent staining in the ONL, where photoreceptor cell bodies are present (Figure 3.4B).

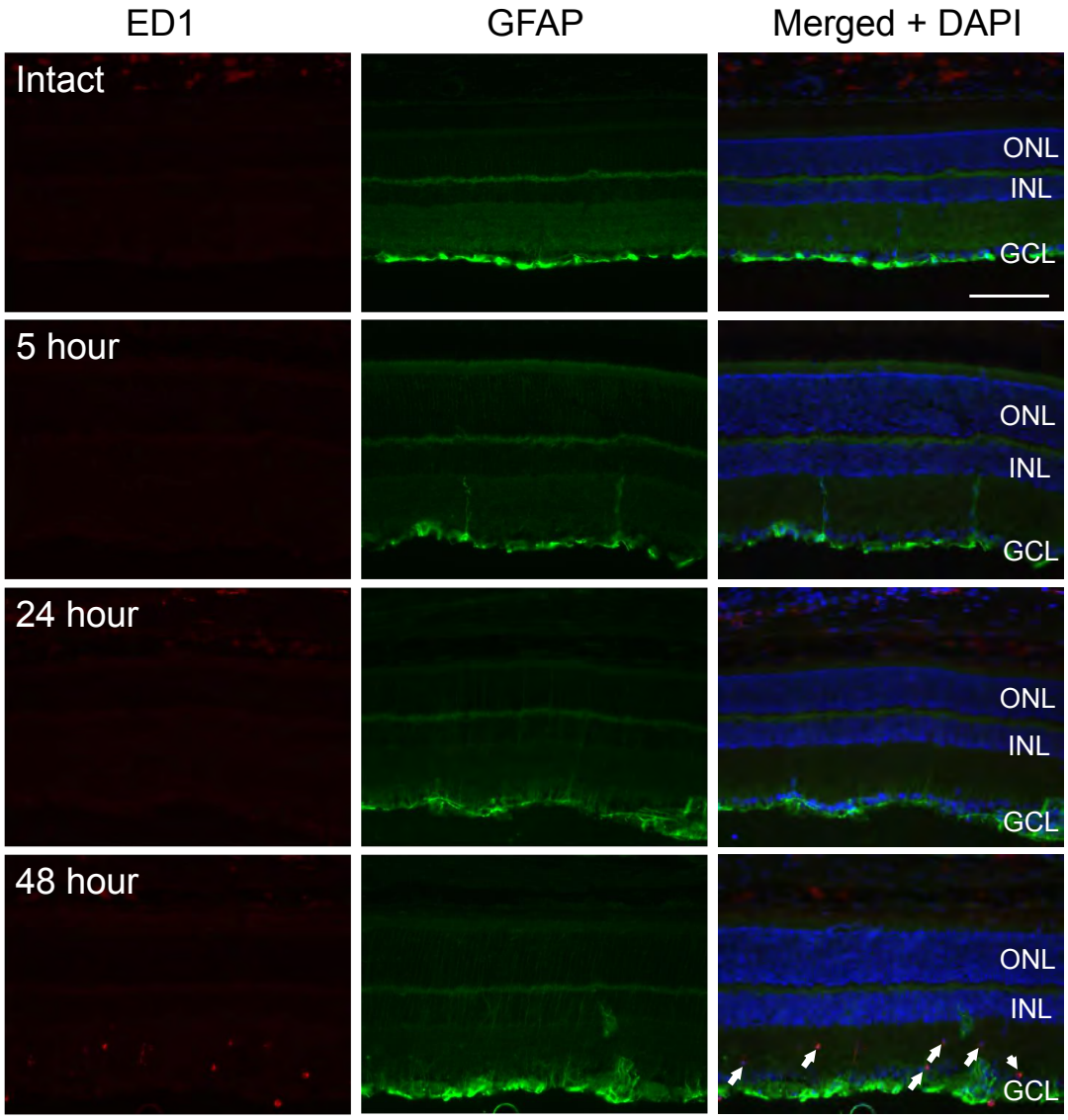


**Figure X Insert.** ED1⁺ cells and GFAP immunostaining after blunt ocular injury. ED1⁺ cells are not present in intact retinae or at 5 or 24 hours after blunt ocular injury, but there are ED1⁺ cells in the retina (arrows) at 48 hours after injury, suggesting macrophage infiltration. GFAP processes are present throughout the retina at 5, 24 and 48 hours after blunt ocular injury, suggesting glial activation. Nuclei were counterstained with DAPI (blue). Scale bar represents 100μm.

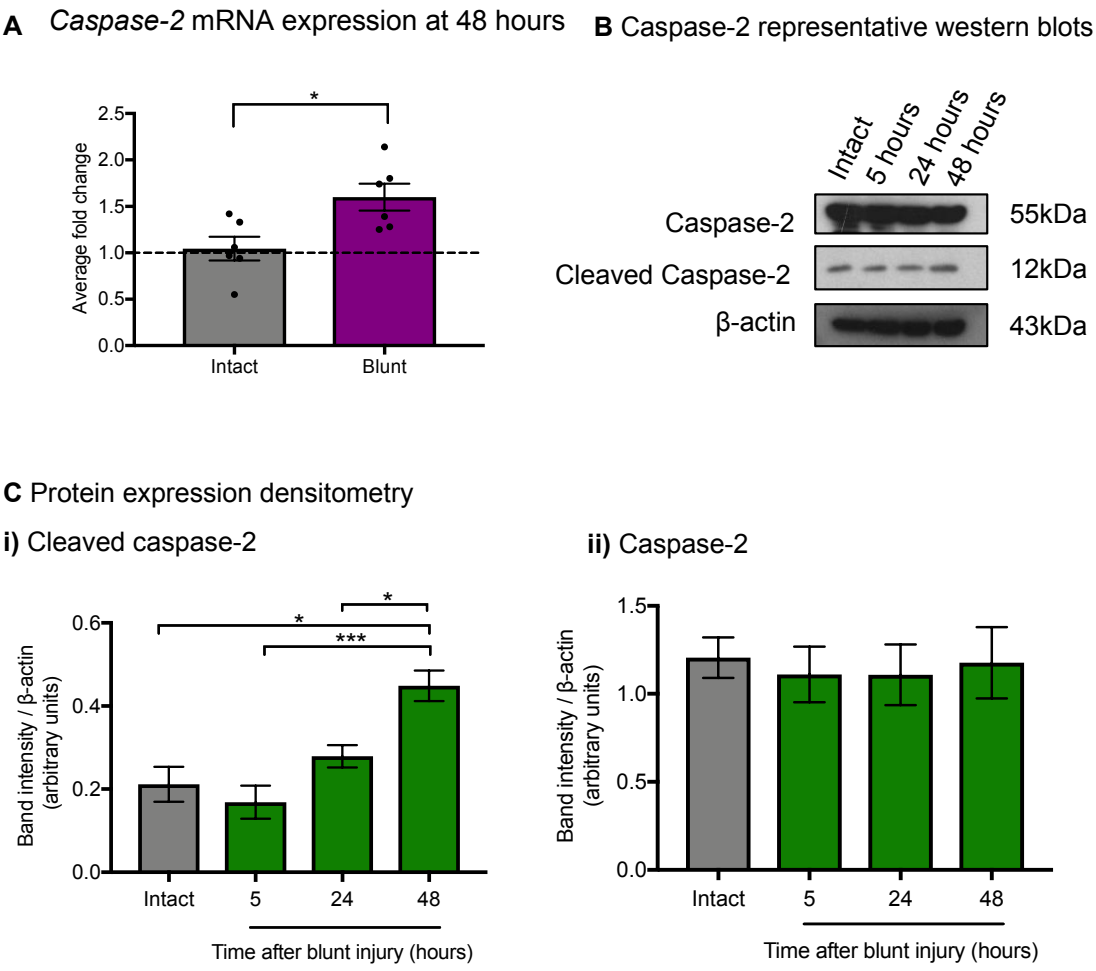


animals per group with bilateral blunt ocular injury, 6 pooled retinae, repeated on 3 independent occasions; total 9 animals per group, 18 retinae. Error bars represent mean ± SEM * $p < 0.05$, *** $p < 0.001$

**A)** Caspase-2 and BRN3A immunofluorescent staining in the GCL

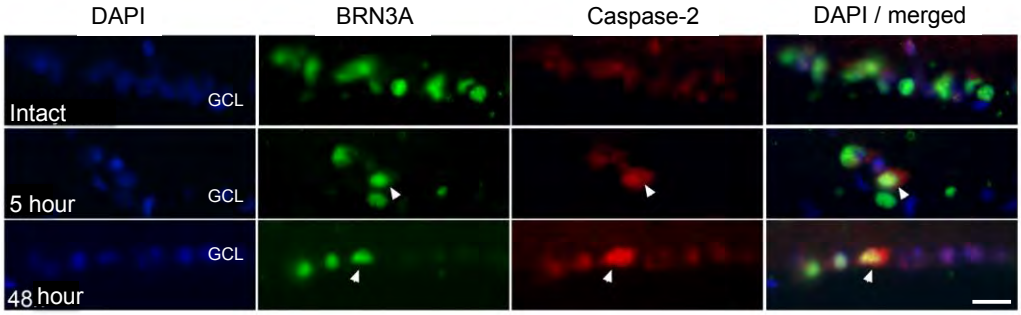


**B)** Retinal caspase-2 and BRN3A immunofluorescent staining

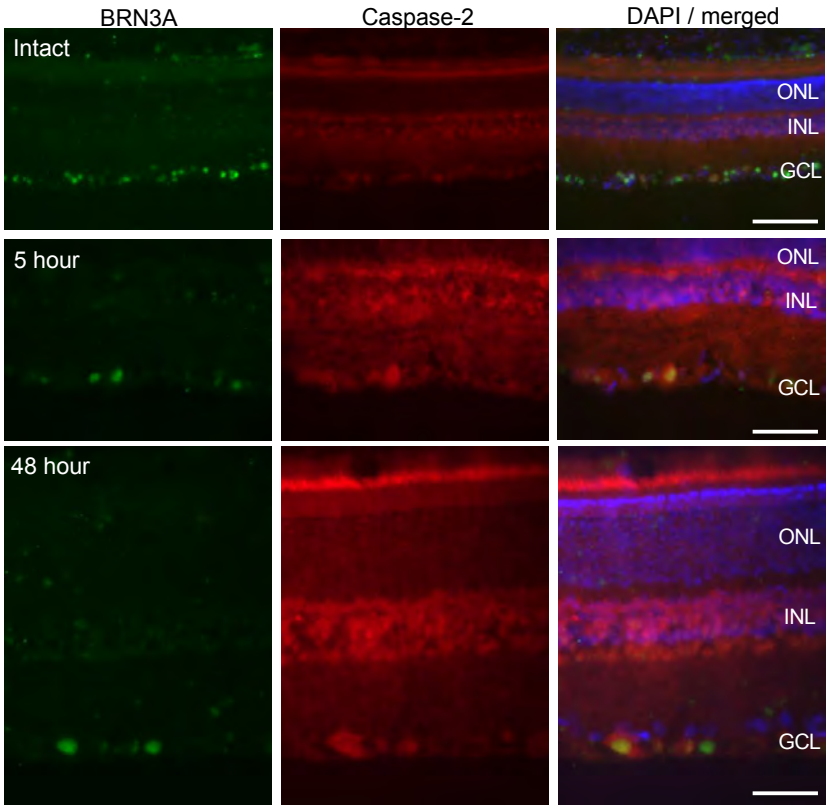


**Fig not to photoreceptors. A)** Caspase-2 (*red*) was immunolocalised to the nucleus and cytoplasm of BRN3A$^+$ cells (*green*) in the GCL, which are likely RGCs. Caspase-2 was present at 5 and 48 hours after injury but was less present in intact retinae. **B)** Caspase-2 immunofluorescent staining was not localised to photoreceptor cell bodies in the ONL. Caspase-2 immunostaining was present in the INL, but this was constant in intact retinae and 5 and 48 hours after blunt ocular injury. Nuclei were counterstained with DAPI (blue). **A)** Scale bar = 20 μm **B)** Intact; scale bar = 100 μm, 5 hour and 48 hours scale bar = 50 μm. Images are representative of n=4 animals per group.

### 3.3.4. siCASP2 treated eyes had more surviving BRN3A$^+$ RGCs adjacent to the centre of the injury site compared to siEGFP treated eyes, but there was no effect on ONL thickness

To assess the effects of siCASP2 treatment, bilateral blunt ocular injury was performed with unilateral intravitreal injection of siCASP2 and contralateral injection of siEGFP (n=8 eyes per condition, 8 animals). Animals were culled at 2 weeks after injury and eyes processed for immunofluorescent staining. Intact animals receiving no injections were also analysed (n=8 separate animals). Intravitreal injections of siCASP2 treatment increased the number of BRN3A$^+$ RGCs compared to siEGFP treated eyes, with an effect that varied with distance from the impact site (GLM $p<0.01$) (Figure 3.5A), suggesting that siCASP2 treatment might provide some neuroprotection to RGCs after blunt ocular injury . For example, the number of BRN3A$^+$ RGCs in treatment groups as a percentage of BRN3A$^+$ RGCs in the intact retina at 0, 600, 1200 and 1800μm from the impact site were 73.94% ± 4.51, 77.73% ± 2.61, 84.70% ± 3.87 and 84.64% ± 7.02 in siCASP2 treated eyes compared to 67.39% ± 4.06, 66.73% ± 2.57, 82.66% ± 4.59 and 85.26% ± 4.17 in siEGFP treated control eyes. The mean counts of BRN3A$^+$ RGCs per mm of retina in experimental groups are displayed in Figure 3.5C. There was a significantly greater number of BRN3A$^+$ RGCs immediately peripheral to the impact site (600 μm; $p<0.05$ student's t-test with Holms-Bonferroni correction) in siCASP2 treated eyes compared to siEGFP treated control eyes, indicating a likely pro-survival effect of caspase-2 knockdown on BRN3A$^+$ RGCs in that zone of injury. There was little effect of siCASP2 treatment on BRN3A$^+$ RGC survival central to the impact site (0 μm) and distant to the injury site (1200 and 1800 μm), indicating that the effect might be region specific.

To assess the effect of siCASP2 treatment on photoreceptor death after blunt ocular injury, I measured the ONL thickness on retinal sections at 600, 1200 and 1800 μm either side of the impact site as previously described (Blanch et al., 2014) and found there was no significant effect of siCASP2 treatment compared to siEGFP treated control retinae (Figure 3.5B; GLM p=0.372 for an effect of siCASP2, with no significant variation by distance from impact site [p=0.942]). For example, the normalised percentages of intact ONL thickness at 0, 600, 1200 and 1800 μm from the impact site were 76.89% ± 9.40, 74.60 ± 7.02, 71.75% ± 7.86 and 70.39% ± 8.16 in siCASP2 treated eyes compared to 73.81% ± 5.54, 71.98% ± 6.39, 65.41% ± 5.49 and 70.5% ± 6.88 in siEGFP treated control eyes. The mean ONL thickness values at different distances from the centre of the impact site in intact eyes, and after bilateral blunt injury treated with siCASP2 or siEGFP intravitreal injections are displayed in Figure 3.5D. These results suggest that the pro-survival effect of caspase-2 knockdown might be specific to RGCs and have minimal effect on photoreceptors.

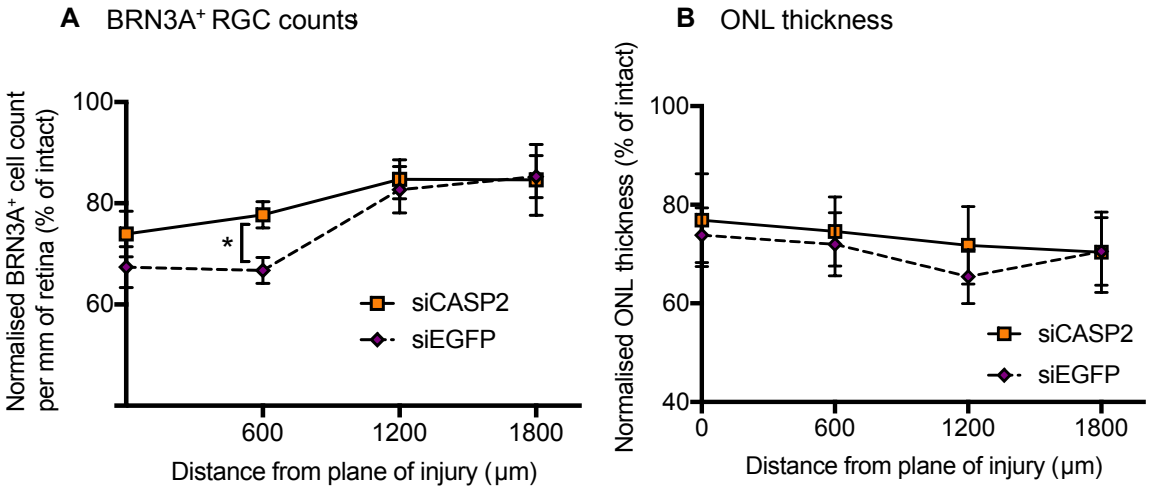


**C** Mean number of BRN3A$^+$ RGC per mm of retina

| | Mean number of BRN3A$^+$ RGC per mm of retina (± SEM) | | | |
|---|---|---|---|---|
| Treatment | 0µm | 600µm | 1200µm | 1800µm |
| Intact | 56.9 ± 2.19 | 59.9 ± 1.85 | 57.5 ± 2.97 | 63.1 ± 5.55 |
| Blunt + siCASP2 | 42.1 ± 2.57 | 46.5 ± 1.56 | 48.7 ± 2.22 | 53.4 ± 4.43 |
| Blunt + siEGFP | 38.4 ± 2.31 | 39.9 ± 1.54 | 47.5 ± 2.64 | 53.8 ± 2.63 |
| Student's t-test (with Holms Bonferroni correction) | p=0.9072 | p=0.0372 | p=1.4662 | p=0.9392 |

**D** Mean ONL thickness

| | Mean number of pixels of ONL thickness (± SEM) | | | |
|---|---|---|---|---|
| Treatment | 0µm | 600µm | 1200µm | 1800µm |
| Intact | 44.6 ± 0.86 | 46.2 ± 1.77 | 54.8 ± 3.65 | 65.6 ± 4.34 |
| Blunt + siCASP2 | 34.3 ± 4.21 | 34.5 ± 3.24 | 39.4 ± 4.31 | 46.2 ± 5.35 |
| Blunt + siEGFP | 32.9 ± 2.47 | 33.3 ± 2.96 | 35.9 ± 3.01 | 46.3 ± 5.52 |
| Student's t-test (with Holms Bonferroni correction) | p=3.1100 | p=2.3655 | p=1.0328 | p=0.9898 |

Figure legend on next page…

**Figure 3.5. There was an increase in the number of BRN3A$^+$ RGCs in siCASP2 treated eyes compared to siEGFP treated eyes in the immediate the periphery of the impact site, but there was no difference in ONL thickness**. **A)** The number of BRN3A$^+$ RGCs were counted across the entire retina and reported as a percentage of the number of BRN3A$^+$ RGCs per mm of intact retina. Animals received bilateral blunt injury, with unilateral intravitreal injections of siCASP2 and contralateral siEGFP control. siCASP2 treated eyes had a greater number of BRN3A$^+$ RGCs compared to siEGFP treated eyes (GLM $p<0.05$), with an effect at 600 µm peripheral to the centre of the injury site ($p<0.05$, student's t-test with Holms Bonferroni correction for multiple comparison). At the centre of the injury site (0 µm), there was no change in the number of BRN3A$^+$ RGCs after siCASP2 treatment compared to siEGFP. In the distant periphery (1200 µm, 1800 µm), there was less of a reduction in the number of BRN3A$^+$ RGCs after blunt ocular injury compared to changes at the centre, and there was no significant effect of siCASP2 treatment compared to siEGFP treatment (t-test with Bonferroni correction $p>0.05$). **B)** ONL thickness was not preserved by siCASP2 treatment compared to siEGFP treatment, suggesting no photoreceptor protection (GLM $p>0.05$). **(C-D)** The table shows the mean values in intact animals and after blunt ocular injury with siCASP2 or siEGFP treatment for **C)** the mean number of BRN3A$^+$ RGCs per mm of retina and **D)** the mean ONL thickness (pixel count). Experiments represent n=8 animals per group; 8 animals received bilateral blunt ocular injury with unilateral siCASP2 intravitreal injections and contralateral siEGFP control injections. n=8 intact animals were used. Error bars represent mean ± SEM

### 3.3.5. Caspase-2 knockdown significantly preserved PhNR amplitudes compared to control eyes after blunt ocular injury

Bilateral blunt ocular injury was performed with unilateral intravitreal injection of siCASP2 and contralateral injection of siEGFP control (n=8 eyes per condition, 8 animals). Scotopic and photopic electroretinography was performed at 2 weeks after blunt ocular injury to assess retinal function. Intact animals receiving no injections were also analysed (n=8 animals). PhNR amplitudes were lower in blunt ocular injured rats receiving siEGFP or siCASP2 intravitreal injections compared to intact animals (Figure 3.6A), suggesting that RGC function is reduced after blunt ocular injury. PhNR amplitudes were higher in siCASP2-treated animals compared to siEGFP treated animals after blunt ocular injury, suggesting that RGC function is preserved by siCASP2 treatment (Figure 3.6A; GLM p=0.042). This effect did not significantly vary with stimulus intensity across the range tested. The scotopic a-wave and b-wave and phototopic b-wave amplitudes were also decreased after blunt ocular injury compared to intact rats (Figure 3.6 B-D), but there was no significant effect of siCASP2 treatment compared to siEGFP on these waveforms (Figure 3.6 B-D; scotopic a wave amplitudes, p=0.145; scotopic b wave amplitudes, p=0.503; photopic b wave amplitudes, p=0.889). Together, these results suggest that siCASP2 treatment may protect RGC function.

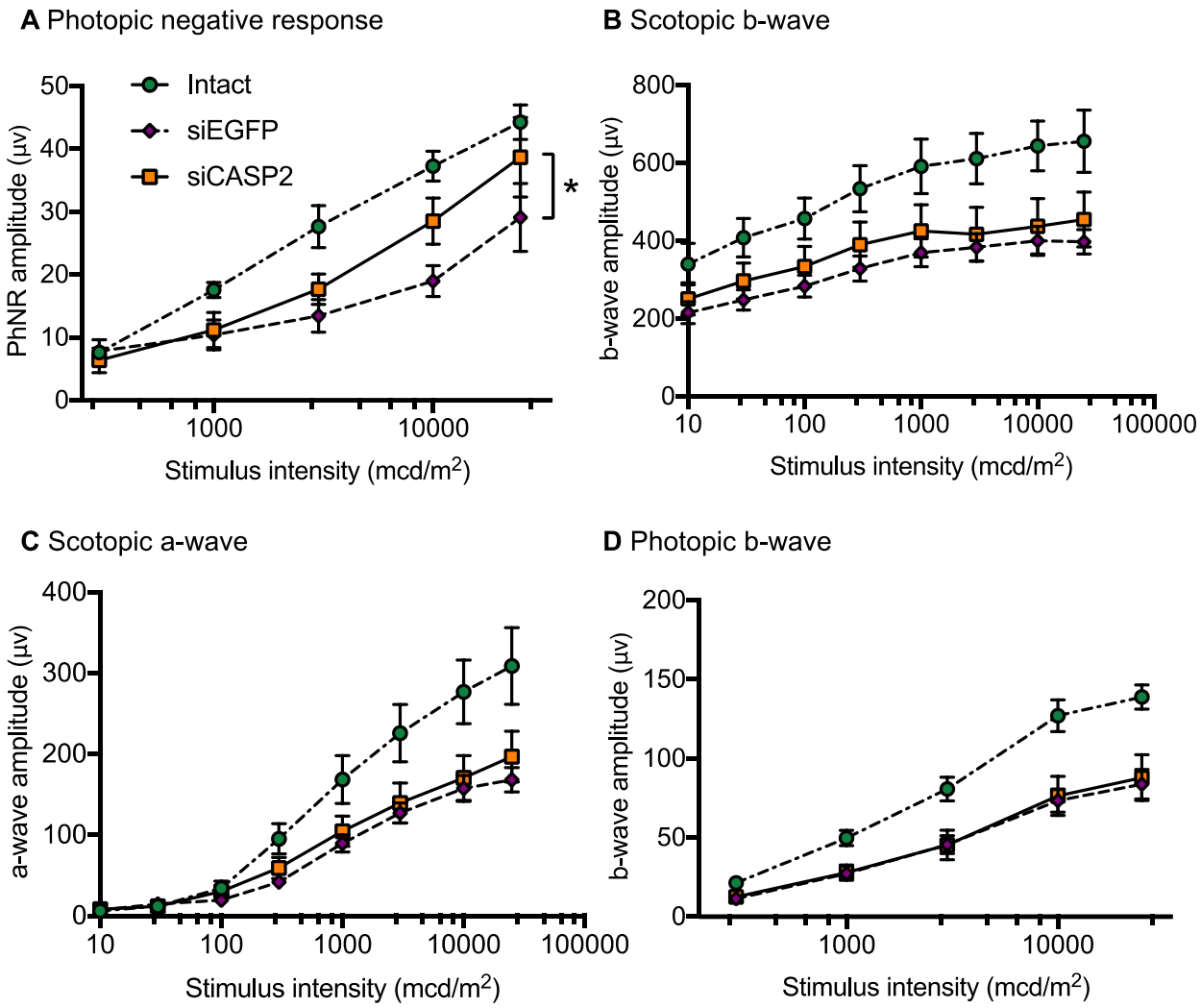


**Figure 3.6. ERGs show that a, b and PhNR wave amplitudes are reduced 14 dpi but that siCASP2 treatment has a protective effect on PhNR amplitudes compared to siEGFP treatment.** **A)** PhNR amplitudes were reduced after blunt ocular injury. PhNR amplitude was partly rescued by siCASP2 treatment compared to siEGFP control (GLM p=0.042). **(B-D)** The amplitudes of scotopic b-waves, scotopic a-waves and photopic b-waves were reduced after blunt ocular injury, but were not rescued by siCASP2 treatment compared to siEGFP control. n=8 animals; 8 animals received bilateral blunt ocular injury with unilateral siCASP2 intravitreal injection and contralateral siEGFP control injection. 8 intact animals were also analysed. Error bars represent mean ± SEM.

## 3.4. Discussion

Our model of blunt ocular injury caused commotio retinae and TON, with pathologies comparable to human conditions (Blanch et al., 2012b). It was previously established that photoreceptors structurally and functionally degenerate in this model, and that there was the greatest reduction in the number of GCL cells at the centre of the impact site and less towards the periphery (Blanch et al., 2012b). However, the GCL consists of RGCs and displaced amacrine cells in an approximate 1:1 ratio; therefore, previous studies from Blanch et al., have indicated a likely reduction in RGCs, but have not confirmed this with specific RGC markers (Blanch et al., 2012b). Moreover, Blanch et al., showed that photoreceptor death was mediated by caspase-9 (Blanch et al., 2014), but the signalling pathways which drive RGC death have not been investigated.

### 3.4.1. *Caspase-2* mRNA expression increased 1.6-fold after blunt ocular injury

I have demonstrated a 1.6-fold elevation in *caspase-2* mRNA expression 48 hours after blunt ocular injury compared to intact animals. Ahmed et al., previously showed that following ONC, *caspase-2* mRNA was localised to Thy1.1 expressing cells and that there was an approximate 7-fold increase in *caspase-2* mRNA expression (Ahmed et al., 2011). Due to the focal localisation of a blunt ocular injury compared to the generalised RGC death seen after ONC, I would expect a smaller increase in *caspase-2* gene expression proportional to the injury size. In the rat ONC model, <10% of RGCs survive 14 dpi (Berkelaar et al., 1994). In my experiments, I have shown approximately 75% of RGCs survive 14 dpi in the blunt ocular injury model, which may be why the change in *caspase-2* expression is smaller. One limitation of my study is that I used separate animals as controls and for blunt injured retinal tissue, which could introduce

differences in *caspase-2* mRNA expression due to inter-animal genetic variation rather than changes specific to the injury. To account for this, in future experiments, I could perform unilateral injury and use the contralateral eye as the control.

### 3.4.2. Caspase-2 was cleaved up to 48 hours after blunt ocular injury and was localised to BRN3A$^+$ RGCs

Caspase-2 was localised to injured BRN3A$^+$ RGCs and levels of the active form, cleaved 12 kDa caspase-2, increased over 48 hours after blunt ocular injury. Activated caspase-2 induces RGC death in diverse models of RGC degeneration, including ONC (Vigneswara and Ahmed, 2016, Vigneswara et al., 2014, Ahmed et al., 2011), glaucoma and optic neuritis (Lidster et al., 2013). Knockdown of caspase-2, using siCASP2, protects >95% of Fluorogold$^+$ back labelled RGCs from death after ONC (Vigneswara et al., 2014, Ahmed et al., 2011). In contrast, caspase-2 did not localise to the ONL, where photoreceptor cell bodies exist, after blunt ocular injury and caspase-2 knockdown using siCASP2 did not affect the ONL thickness, a measure of photoreceptor survival. This suggests that photoreceptor death may be independent of caspase-2 and that other cell death signalling mechanisms might responsible for photoreceptor death, for example, apoptotic caspase-9-dependent mechanisms (Blanch et al., 2014). Caspase-9 inhibition only improved ONL thickness in the peripheral retina, and only partly improved photoreceptor function, suggesting that perhaps an alternative cell death signalling pathway drives photoreceptor death in addition, or that multiple pathways are occurring in parallel.

The expression of *caspase-2* mRNA increased at 48 hours, but full-length retinal caspase-2 protein did not change up to 48 hours after blunt ocular injury. Protein and mRNA levels do not always correlate (Greenbaum et al., 2003), which could be due to a short protein half-life or delayed translation. I have shown caspase-2 localises to the nucleus and cytoplasm of $BRN3A^+$ RGCs. In apoptosis, caspase-2 translocates to the mitochondria and induces apoptosis through activation of the intrinsic pathway, but also constitutively exists in the mitochondria and is essential for mitochondrial oxidative stress induced apoptosis (Lopez-Cruzan et al., 2016). Caspase-2 has different cellular consequences depending on the stimulus. For example, DNA-damage agents lead to predominantly nuclear localisation and activation of caspase-2, whereas microtubule inhibitor, vincristine, leads to cytoplasmic caspase-2 activation (Ando et al., 2017, O'Byrne and Richard, 2017). In this current study and previous studies from our group (Vigneswara and Ahmed, 2016, Lidster et al., 2013, Ahmed et al., 2011, Vigneswara et al., 2012), we have discovered the mechanisms which initiate caspase-2 signalling in RGCs and this needs further investigation. Vigneswara et al., have recently suggested that pigment epithelium derived factor (PEDF) suppresses caspase-2 expression and prevents RGC death in a rat ONC model (Vigneswara and Ahmed, 2019); however, it is not known whether PEDF acts upstream of caspase-2 in other paradigms.

In alternative models of ocular trauma other cell death signalling pathways can be activated in the retina. This suggests that not all retinal cells die by apoptotic mechanisms. For example, in a mouse model of ocular blast injury caspase-1-dependent pyroptosis (Bernardo-Colon et al., 2018, Bricker-Anthony et al., 2014b),

necroptotic RIPK1 and RIPK3 localised to Müller cells and cells of the INL and IPL (Bricker-Anthony et al., 2014a), suggesting that different cell death signalling pathways can occur in an ocular blast injury model. Caspase-2 is consistently implicated in driving RGC death after various types of insults (Vigneswara et al., 2012, Vigneswara et al., 2014, Lidster et al., 2013, Ahmed et al., 2011), and is also implicated in the drive towards neuronal death in models of neurodegenerative diseases, including Alzheimer's disease (Zhao et al., 2016, Troy et al., 2000).

Immunofluorescent staining is often used to demonstrate caspase activation using antibodies against full-length protein, despite these antibodies not identifying caspase cleavage or activation. Caspase cleavage can be shown by western blotting, but another way to show caspase activity is through the use of pharmacologic caspase inhibitors, such as z-VAD-fmk. However, despite being widely used, the active sites of these pharmacological inhibitors are non-specific and have cross reactivity with other caspases and non-caspase targets such as calpains (McStay et al., 2008, Berger et al., 2006, Pereira and Song, 2008, Rozman-Pungercar et al., 2003). The pharmacological inhibition of caspase-2 is not as efficient at attenuating RGC loss as RNAi using siCASP2: pharmacological inhibitor z-VDVAD-fmk protected 60% of RGCs from death 21 days after ONC (Vigneswara et al., 2012), compared to >95% RGCs protected by siCASP2 treatment (Vigneswara et al., 2014, Ahmed et al., 2011). The use of siRNA knockdown is highly specific to caspase-2, without activating non-specific innate immunity (Ahmed et al., 2011) and the quantification of caspase-2 cleavage products using RLM-RACE ensures that cleaved caspase-2 is present (Ahmed et al., 2011).

### 3.4.3. siCASP2 treatment may provide region-specific BRN3A$^+$ RGC protection

siCASP2 knocks down caspase-2 *in vitro* and i*n vivo* and does not induce an immune response or off-target effects (see Section 1.7.7.3 for more details). siCASP2 protected a larger number of BRN3A$^+$ RGCs compared to siEGFP across the whole retina, which was likely driven by the significant difference in the number of BRN3A$^+$ RGCs 600 µm from the centre of the impact site. Treatment with siCASP2 might provide RGC neuroprotection in a region that surrounds the centre of the impact site where the highest proportion of RGCs undergoing caspase-2-dependent cell death exist. In contrast, RGCs central to the impact site, were less susceptible to modulation by altered caspase-2 activity. It is likely that more severe blunt force impact at the centre of the impact site predisposes the cells to necrototic 'explosive' cell death which cannot be prevented. Moreover, only a proportion of degenerating BRN3A$^+$ RGCs in the immediate periphery of the lesion site were protected by siCASP2 treatment, suggesting that the death of the remaining proportion of RGCs might be driven by alternative cell death mechanisms (e.g. necroptosis or pyroptosis) or by unregulated necrosis, and requires further investigation. At greater distances from the impact site, there was less BRN3A$^+$ RGC degeneration, meaning either there was no effect from siCASP2 or that caspase-2-dependent RGC death was not occurring in this injury zone.

### 3.4.4. siCASP2 may provide some functional restitution to RGCs but not to photoreceptors

The differential protection of RGCs by siCASP2 treatment was also reflected by some preservation of their function. The scotopic a-wave is the first negative deflection of the

flash ERG and is predominantly caused by photoreceptor hyperpolarisation, and represents rod function. siCASP2 treatment did not improve scotopic a-wave amplitudes, which suggests that rod photoreceptor function was not protected by caspase-2 knockdown. Under photopic conditions, rod photoreceptors are bleached, meaning the photopic a-wave is cone-mediated. In rats, photopic a-wave amplitudes are small, therefore variations in b-wave amplitudes were used instead as a downstream measure of photoreceptor function, even though the b wave is also dependent on bipolar cell function. Under both scotopic and photopic conditions, a-wave and b-wave amplitudes were reduced 2 weeks after blunt ocular injury, which agrees with previous studies from Blanch et al., (Blanch et al., 2014, Blanch et al., 2012b), but there was no protection from siCASP2 treatment. These results are consistent with the lack of effect of siCASP2 on ONL thickness, suggesting that siCASP2 treatment may not have a protective effect on photoreceptor structure or function.

The PhNR is a downstream measure of retinal function, dependent on activity in first and second order neurons (photoreceptors and bipolar cells) (John R. Heckenlively, 2006). A change in PhNR amplitude may be caused by changes in either RGC function or upstream cells such as photoreceptors. The PhNR amplitude is a common measure of RGC function and is reduced in experimental and human glaucoma (Viswanathan et al., 1999) and correlates with reduced RGC numbers in ON injury models (Li et al., 2005). Despite the rat photopic responses being heavily amacrine cell-dependent (Bui and Fortune, 2004), a significant proportion of the response is also RGC-dependent (Li et al., 2005). Since siCASP2 treatment did not affect photopic b-wave amplitudes,

any change in PhNR amplitude must be derived from effects downstream of ON-bipolar cells. siCASP2 treatment protected PhNR amplitudes 14 dpi compared to siEGFP treated controls, suggesting that surviving RGCs, in which caspase-2-dependent cell death was prevented, remain potentially viable and functional. This difference in PhNR amplitudes could also reflect increased electrical activity in RGCs that were dysfunctional but not yet dead. After blunt ocular injury, there is a >50% reduction in ERG amplitudes (Blanch et al., 2012b), despite only <20% of photoreceptors degenerating. Nonetheless, the preserved PhNR amplitudes observed in treated eyes in my study raises the possibility that siCASP2 induces a degree of functional RGC neuroprotection after blunt ocular injury and may be a potential therapeutic for RGC degeneration induced by blunt ocular injury.

### 3.4.5. Conclusion

In blunt ocular injury caspase-2 mediates the degeneration of a proportion of compromised RGCs and siCASP2 treatment might provide some functional and structural neuroprotection to BRN3A$^+$ RGCs, in particular, immediately peripheral to the impact site. Caspase-2 was not localised to photoreceptors and siCASP2-mediated caspase-2 knockdown did not structurally or functionally protect photoreceptors after retinal injury, suggesting that caspase-2 was activated exclusively in RGCs. Caspase-2 appears to drive RGC degeneration in a specific region relative to the blunt force impact site; however, the cell death signalling pathways which drive RGC degeneration at the centre of the impact site were not discovered in this study, and these RGCs may degenerate by alternative signalling mechanisms which could potentially be inhibited as well as caspase-2. The results of my study investigating the effects of siCASP2

suggest that caspase-2 signalling pathways drives RGC death in TON induced by blunt ocular injury, likely in a specific impact site region, and that caspase-2 knockdown using siCASP2 could be a potential new treatment for this condition.

# Chapter 4 Retinal ganglion cells die by necroptotic mechanisms in a site-specific manner in a rat blunt ocular injury model

## 4.1. Rationale

In Chapter 3, I showed that RGCs degenerate through caspase-2-dependent mechanisms in the peripheral portion of the impact site but did not identify the mechanisms of RGC death at the centre of the impact site (Thomas CN, 2018). In this chapter, I investigated necroptotic death mechanisms in the retina using a blunt ocular injury rat model. I demonstrated that necroptotic death occurs in the retina after blunt ocular injury and the inhibition of necroptosis using Nec-1s increased the number of $BRN3A^+$ and $RBPMS^+$ RGCs compared to vehicle at the centre of the impact site, suggesting that RGCs in this area can be protected.

## 4.2. Experimental design

To determine the role of necroptosis in RGC and photoreceptor death after blunt ocular injury, groups of female Lister Hooded rats were subjected to unilateral or bilateral blunt eye injury under anaesthesia as a recovery procedure, as previously described in Section 2.1.1. Western blotting and immunofluorescent staining were performed at 5, 24 and 48 hours after injury to determine RIPK1, RIPK3 and MLKL protein expression and localisation (Figure 4.1) (see Section 2.7 Section 2.3 and Section 2.4.2). Retinae were also collected at 48 hours and processed for qPCR analysis to assess *ripk1*, *ripk3* and *mlkl* mRNA expression (see Section 2.9). For western blotting bilateral blunt ocular injury was performed (n=3) and 6 eyes pooled at each time point. This was repeated on 3 independent occasions. For immunofluorescent staining, unilateral blunt injury was performed and eyes from separate intact animals used as controls. For qPCR experiments bilateral blunt injury was performed and eyes pooled and independent intact animals used as controls (n=6 retinae from 3 animals).

A selective necroptosis inhibitor, Nec-1s (BioVision Incorporated, CA, USA), was used to manipulate RGC survival in primary retinal cultures *in vitro* (see Section 2.8) and in a rat blunt ocular injury model *in vivo* (see Section 2.1.1). Immediately after bilateral blunt ocular injury, 5 µl of Nec-1s (3.6 mM in 10% DMSO, 0.9% methyl-β-cyclodextrin in PBS) was administered by unilateral intravitreal injection and 5 µl of vehicle (10% DMSO, 0.9% methyl-β-cyclodextrin in PBS) was injected into the contralateral eye. Injections were performed immediately after injury and again at 7 dpi and animals culled and tissue collected at 14 dpi (n=8 eyes/treatment, 8 animals total). Intact animals receiving no intravitreal injections were also analysed (n=8 animals). RGC and photoreceptor functional and structural assessments were performed using scotopic and photopic ERG recordings (see Section 2.2.2.2), RGC counting (see Section 2.4.3) and ONL thickness measurements in retinal sections. To account for variability with respect to distance from the impact site, 7 retinal sagittal sections per eye were analysed for RGC and ONL thickness, through the ONH and impact site centre (0 µm) and at 600, 1200 and 1800 µm either side of this plane (Figure 2.5).

**A** *In vivo* protein and immunofluorescent studies

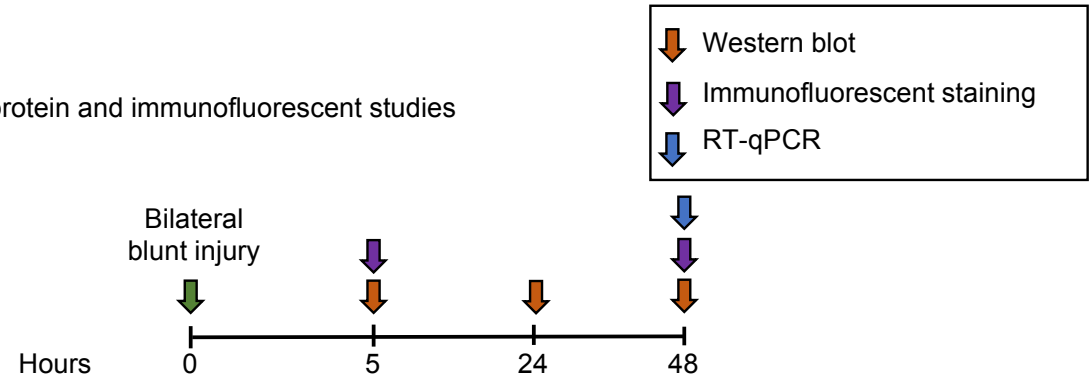


| *Experiment* | *Injury performed* | *N (retinae)* | *Timepoints* | *Measured endpoints* |
|---|---|---|---|---|
| Western blot | Bilateral blunt injury and eyes pooled | 18 retinae total (6 pooled retinae from 3 animals, repeated on 3 independent occasions) | Intact, 5, 24, 48 hours after injury | RIPK1, RIPK3, MLKL, MLKL-P (Ser 345) protein expression |
| Immunofluorescent staining | Unilateral blunt injury | 4 animals per timepoint | Intact, 5, 48 hours after injury | RIPK3 and MLKL retinal localisation |
| RT-qPCR | Bilateral blunt injury | 6 retinae from 3 animals | Intact and 48 hours after injury | *Ripk1*, *ripk3*, *mlkl* mRNA expression |

**B** *In vivo* Nec-1s studies

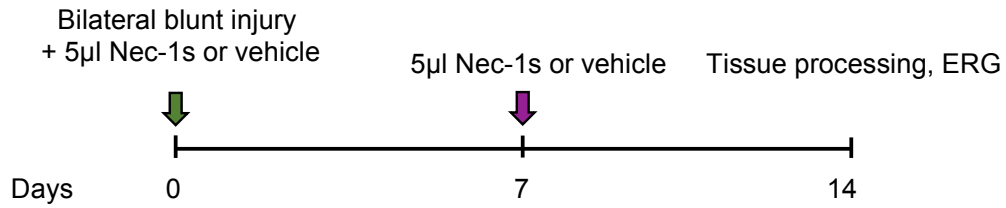


| *Treatment* | *Injury performed* | *Treatment* | *n (eyes)* |
|---|---|---|---|
| Intact | - | - | 8 |
| Blunt injury + Nec-1s | Bilateral blunt ocular injury | Unilateral 5µl intravitreal injection of 3.6mM Nec-1s in 10% DMSO, 0.9% methyl-β-cyclodextrin in PBS | 8 |
| Blunt injury + vehicle | | Contralateral 5µl intravitreal injection of 10% DMSO, 0.9% methyl-β-cyclodextrin in PBS | 8 |

**Measured endpoints:** BRN3A$^+$ and RBPMS$^+$ RGC counts, ONL thickness on H&E cryosections, scotopic and photopic ERG.

## 4.3. Results

### 4.3.1. There were no changes in *ripk1* and *mlkl* mRNA expression, but there was a decrease in *ripk3* expression, 48 hours after blunt ocular injury

*Ripk1*, *ripk3* and *mlkl* gene expression were analysed by RT-qPCR 48 hours after injury Figure 4.2C) (n=6 retinae per group from 3 animals receiving bilateral blunt ocular injury or intact controls). Results are presented as mean fold change compared to intact retinae. There was a trend towards higher *Ripk1* gene expression by 1.46 fold 48 hours after blunt injury compared to intact eyes, but this did not reach statistical significance (unpaired student's t-test p=0.098). *Ripk3* gene expression was 3.66-fold lower 48 hours after blunt injury compared to intact eyes (unpaired students t-test $p<0.05$). Similarly, *mlkl* mRNA expression was 2.10-fold lower 48 hours after blunt injury compared to intact eyes, but this did not reach statistical significance (t-test p=0.19).

### 4.3.2. MLKL protein expression was higher 5 hours after blunt ocular injury compared with intact eyes, but RIPK1, RIPK3 and MLKL-P (Ser345) expression was no different.

Bilateral blunt ocular injury was performed, and tissue collected for immunofluorescent staining or western blot at 5, 24 and 48 hours after injury, as well as from separate intact controls. Protein expression of RIPK1, RIPK3, MLKL and phosphorylated MLKL at Ser 345 were investigated using western blot (n=3 animals per experimental group, 6 pooled retinae, repeated on 2 independent occasions). Representative blots are shown in Figure 4.2A and densitometry of band intensities in Figure 4.2B.

Retinal RIPK1 expression tended to be higher in blunt injured eyes compared with controls, but the difference in band intensity measurements did not reach statistical significance (ANOVA p=0.494) (Figure 4.2Bi) Retinal RIPK3 expression was not significantly different 48 hours after blunt ocular injury compared with controls (ANOVA p=0.677) (Figure 4.2Bii). Retinal MLKL expression was significantly higher 5, 24 and 48 hours after blunt ocular injury (ANOVA p<0.0001) (Figure 4.2Biii). Band densitometry measurements for MLKL were higher in sham treated retinae compared with blunt injured eyes at all time points. The difference was 7.7-fold higher at 5 hours, 13.8-fold higher at 24 hours, and 10.7-fold higher 48 hours after blunt ocular injury (Tukey's post hoc test p<0.001 – p<0.0001). Phosphorylated MLKL (Ser 345) tended to be lower 48 hours after blunt ocular injury , but this difference did not reach statistical significance (ANOVA p=0.180) (Figure 4.2 Biv).

### 4.3.3. RIPK3 was localised to BRN3A$^+$ RGCs and MLKL expression was localised to OPL, ONL, INL cells and RBPMS$^+$ RGCs

Immunofluorescent staining was used to assess retinal localisation and images taken from the same region of the injury site (images are representative of n=4). RIPK3 showed co-localisation with cells expressing RGC-specific marker BRN3A and RIPK3 immunostaining intensity was consistent between intact eyes and after blunt ocular injury (Figure 4.3A). MLKL immunofluorescence was elevated in cells at the focal impact site at 48 hours post injury, as shown in a stitched image (Figure 4.3C), with elevated expression mainly in the OPL as well as some ONL cells, INL cells and RBPMS$^+$ RGCs (Figure 4.3B).

**A** Protein expression

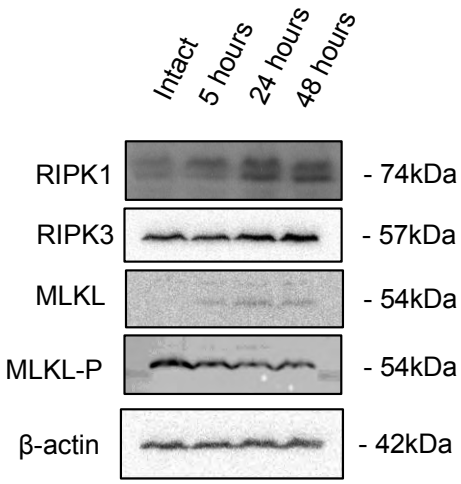


**B** Densitometry of western blots

**i)** RIPK1

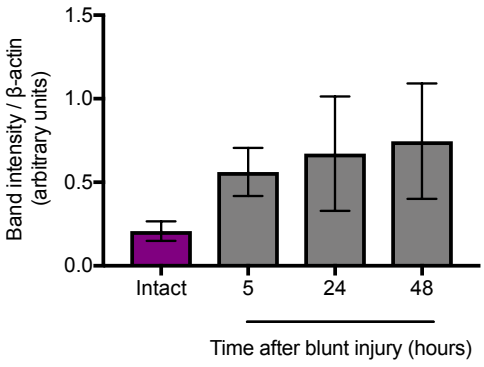


**ii)** RIPK3

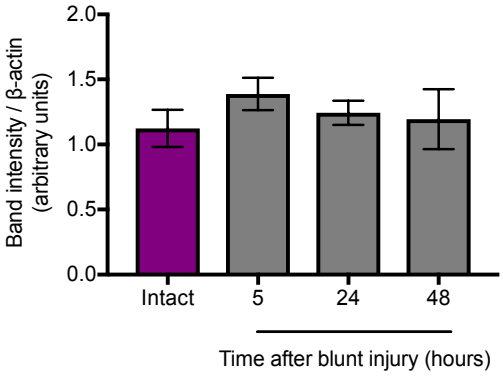


**iii)** MLKL

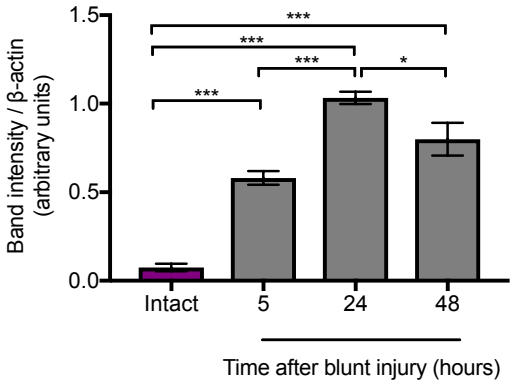


**iv)** MLKL-P (Ser 345)

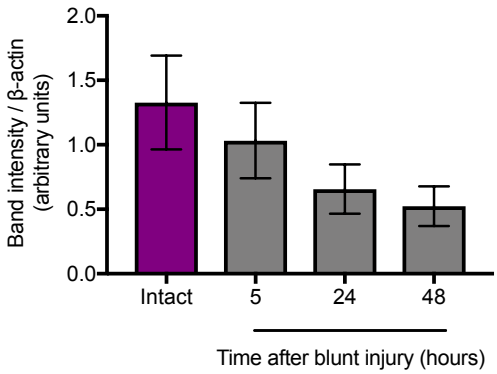


Figure continued on next page…

**C** Mean band intensities of western blots

| | Mean band intensity compared to β-actin ± SEM | | | |
|---|---|---|---|---|
| | *RIPK1* | *RIPK3* | *MLKL* | *MLKL-P (Ser 345)* |
| *Intact* | 0.208 ± 0.059 | 1.123 ± 0.143 | 0.075 ± 0.021 | 1.328 ± 0.364 |
| *5 hours* | 0.562 ± 0.144 | 1.388 ± 0.124 | 0.581 ± 0.039 | 1.033 ± 0.293 |
| *24 hours* | 0.672 ± 0.342 | 1.244 ± 0.093 | 1.033 ± 0.035 | 0.656 ± 0.191 |
| *48 hours* | 0.746 ± 0.345 | 1.194 ± 0.229 | 0.799 ± 0.093 | 0.524 ± 0.154 |

**D**

**F**
**r**
F
c
c
a
p
F
r
r
i
r

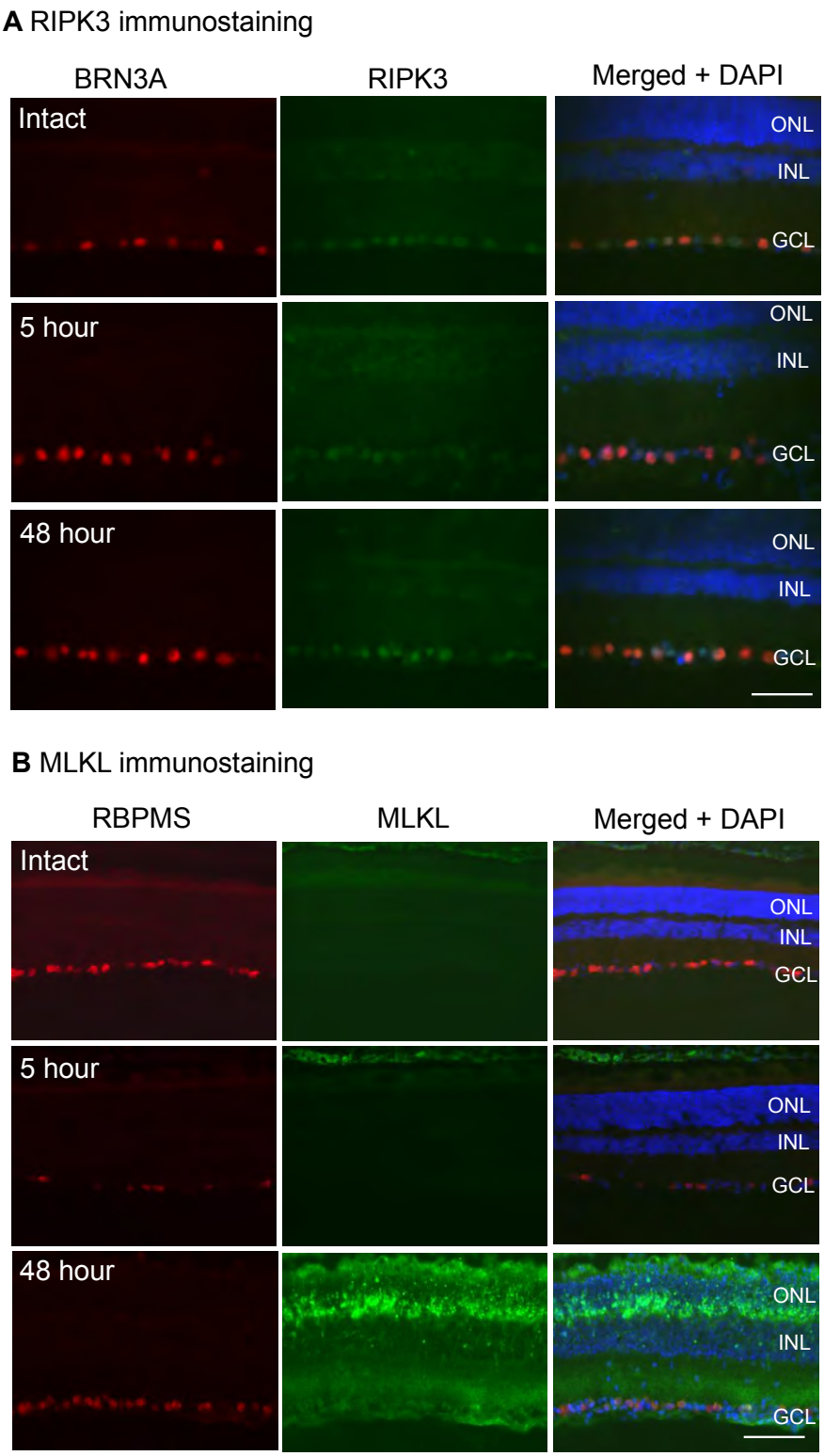


**Figure 3.** RIPK3 and MLKL immunostaining increases after blunt ocular injury and are immunolocalised to RGC. **A)** RIPK3 immunostaining increases in BRN3A-positive RGC at 5 and 48 hours after blunt ocular trauma. **B)** MLKL increases at 48 hour after blunt ocular trauma and is immunolocalised specifically to the focal injury site. MLKL is increased in the ONL cells, INL cells and also RBPMS-positive RGC. Nuclei were counterstained with DAPI (blue). **A.** Scale bar = 20μm **B.** Scale bar = 50μm

**C** MLKL immunostaining at 48 hours

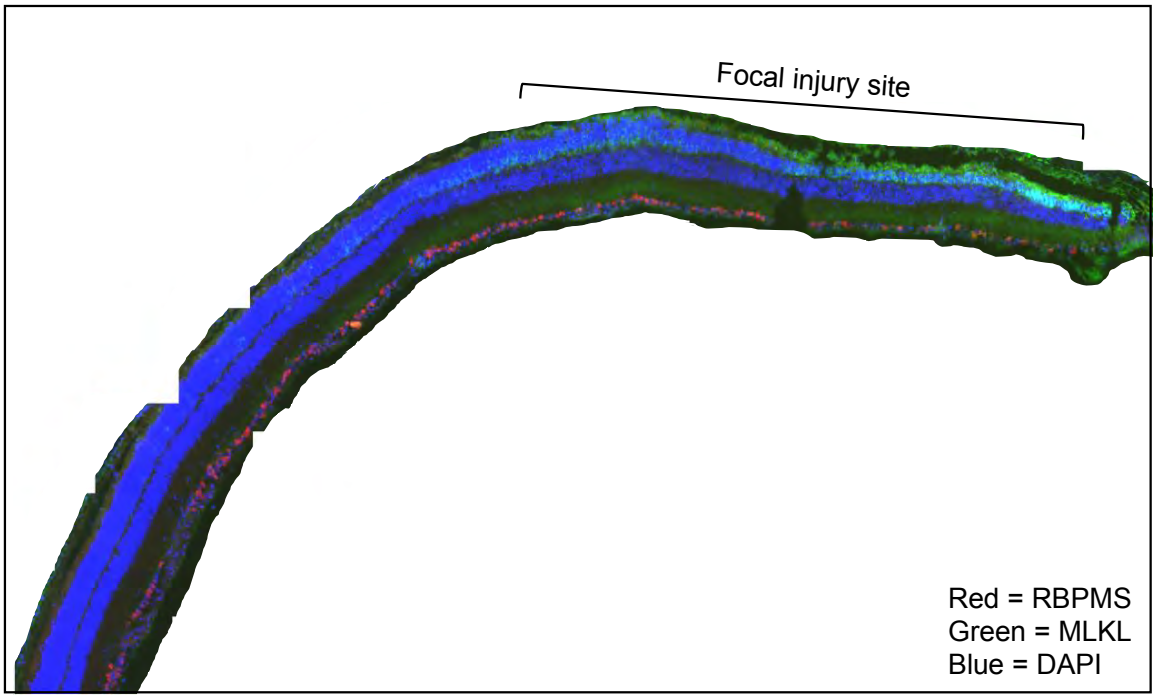


**Fig**
**diff**
**cor**
diff
exp
inju
RG
ML
cou
are

### 4.3.4. Nec-1s may be neuroprotective *in vitro*

Primary mixed retinal cultures were used to assess RGC survival after necroptosis inhibition using the potent inhibitor, Nec-1s, as shown in the experimental design (Figure 4.4A). Primary *in vitro* retinal cultures were treated with a concentration of $1x10^{-4}$ to $1x10^{-8}$ µg/µl of Nec-1s and showed significant βIIIT$^{+}$ RGC neuroprotection with treatment (ANOVA $p<0.05$) (Figure 4.4B). The greatest RGC neuroprotection was provided by a solution of $1x10^{-8}$ µg/µl Nec1-s which caused a ~1.5-fold increase in βIIIT$^{+}$ RGCs (post-hoc Tukey with multiple comparisons $p=0.03$). At high doses of Nec-1s, RGCs were not protected, and at concentrations between $1x10^{-5}$ and $1x10^{-4}$ µg/µl of Nec1-s, the number of βIIIT$^{+}$ RGCs were similar to vehicle-treated cultures, suggesting that higher Nec-1s concentrations do not further protect RGCs. Representative βIIIT immunostained retinal cultures are shown in Figure 4.4C, with RGCs highlighted with a white arrow.

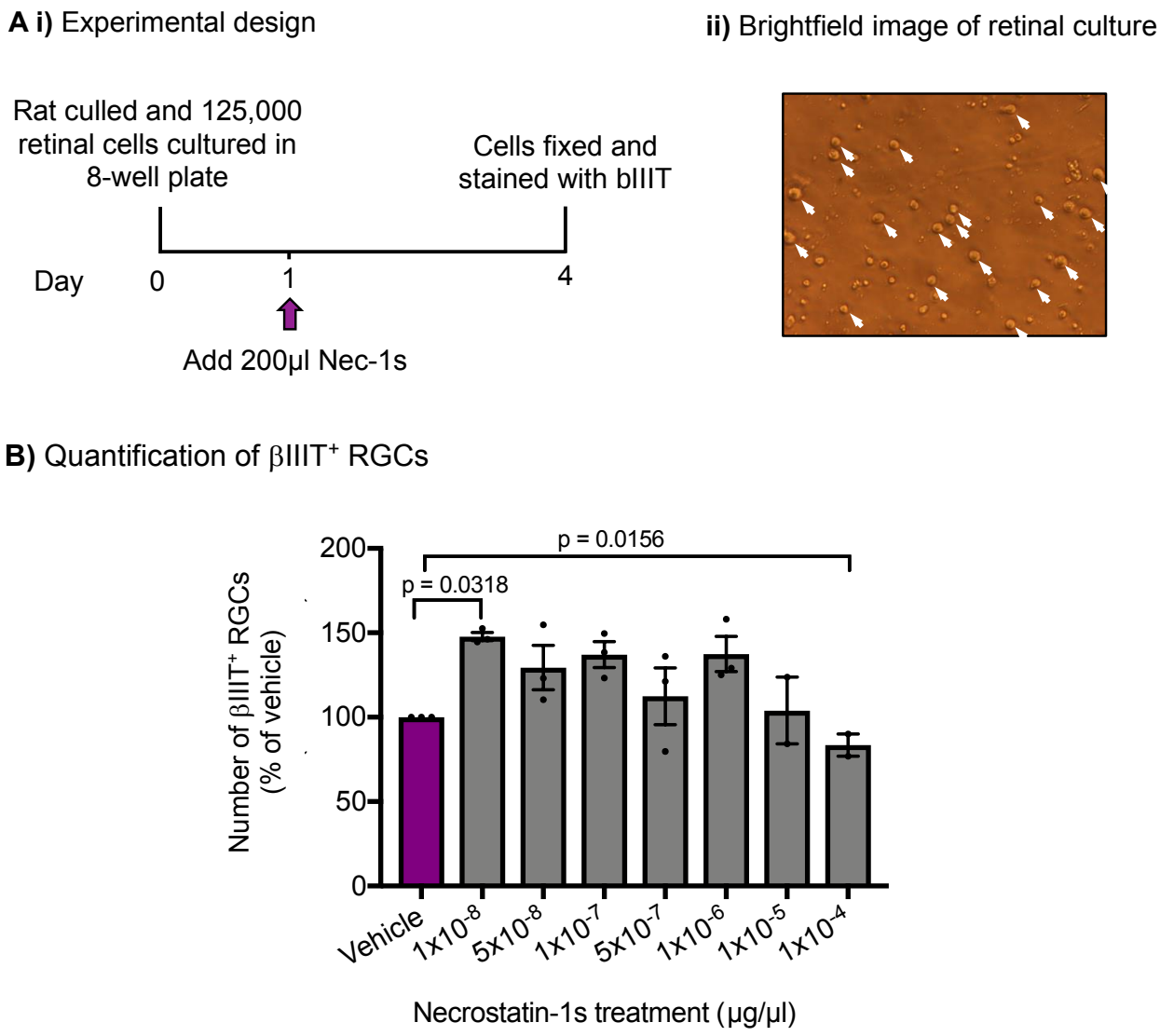


**Figure 4.** Primary retinal cultures were treated with Nec-1s compound or vehicle control. Dose responses were performed in duplicate and performed on 3 independent occasions. **A)** Experimental design of retinal cultures and Nec-1s treatment. bIIIT-positive RGC were quantified in through imaging 45 images per well. **B)** bIIIT-positive RGC were quantified and displayed as mean value as a percentage of vehicle control. Nec-1s provided a significant protection of bIIIT-positive RGC compared to vehicle control treated (PBS, 10% DMSO, 0.9% b-methyl cyclo-dextrin). **C)** Representative images of bIIIT-positive RGC from $1x10^{-4}$ to $1x10^{-8}$ µg/µl. Scale bar represents 100µm  Values are mean ± SEM.

**C)** βIIIT$^{+}$ RGCs in primary retinal cultures

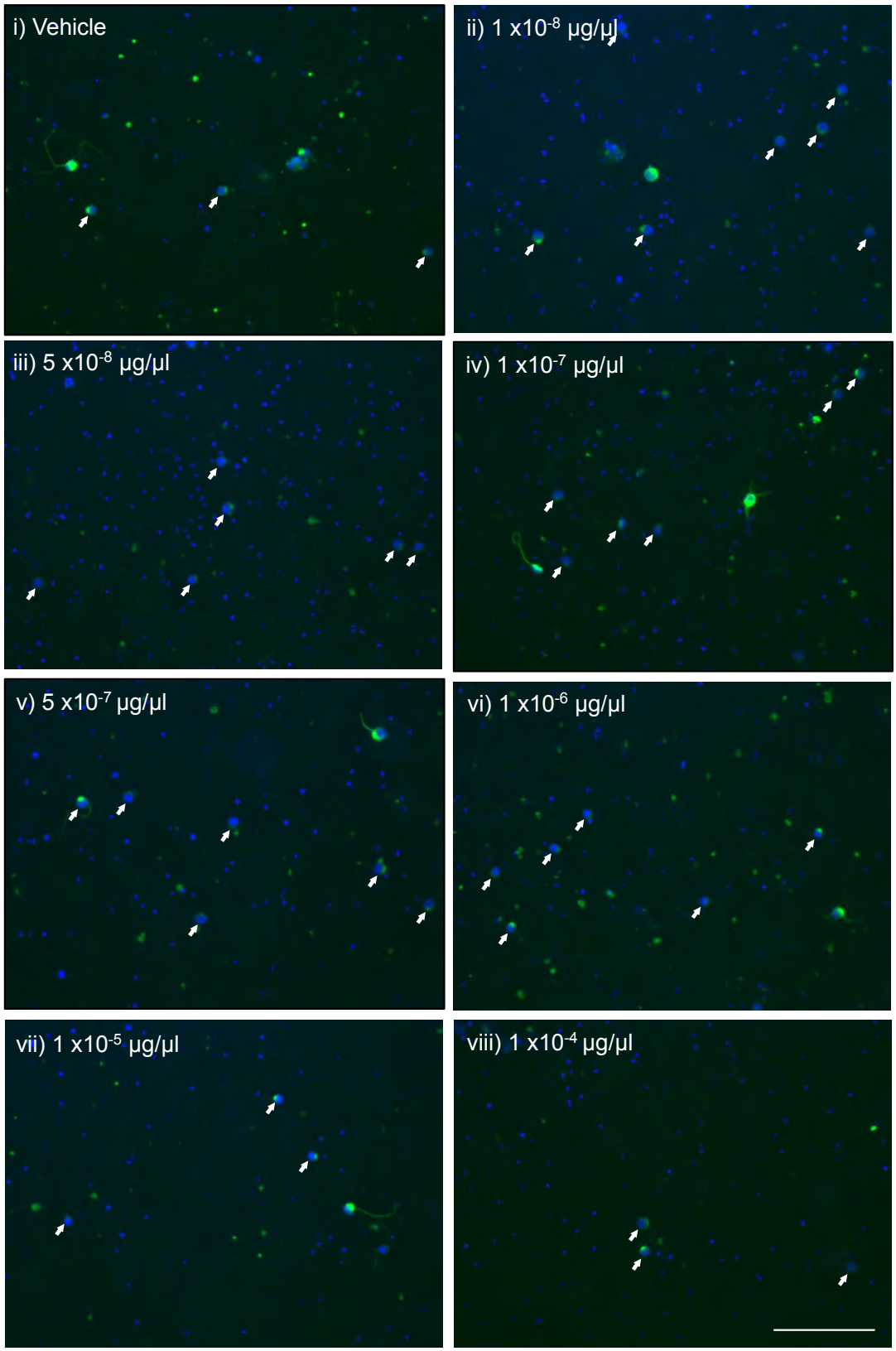


Scale bar = 100 µm

### 4.3.5. Nec-1s treated eyes had a higher number of BRN3A$^+$ and RBPMS$^+$ RGC at the centre of the blunt injury impact site compared to vehicle treated eyes, but there was no difference in ONL thickness

Bilateral blunt ocular injury was performed with unilateral intravitreal injection of Nec-1s and contralateral vehicle injection (n=8 eyes per condition, 8 animals). The number of BRN3A$^+$ and RBPMS$^+$ RGCs were quantified at varying distances from the centre of the impact site (0, 600, 1200 and 1800 μm). Nec-1s treated eyes had a greater number of BRN3A$^+$ and RBPMS$^+$ RGCs compared to vehicle controls, with an effect that varied by distance from the impact site (GLM, BRN3A$^+$ RGCs $p<0.01$, RBPMS$^+$ RGCs $p<0.05$). T-testing with Holms-Bonferroni correction for multiple comparisons was performed at each distance, but showed no significant differences after the multiple comparison corrections in the number of BRN3A$^+$ and RBPMS$^+$ RGCs, although it is likely that an increase at the centre of the impact site in Nec-1s treated compared to vehicle treated retinae is driving the significance in the GLM (0 μm; BRN3A$^+$ RGCs $p=0.1892$ and RBPMS$^+$ RGCs $p=0.2852$ with Holms Bonferroni correction) (Table 4.1 A-B). However, there was little effect of Nec-1s on the number of BRN3A$^+$ and RBPMS$^+$ RGCs at distances more peripheral from the impact site (600, 1200 and 1800 μm). The mean values for BRN3A$^+$ and RBPMS$^+$ RGC counts in intact retinae and blunt injured retinae treated with Nec-1s or vehicle intravitreal injections are displayed in Table 4.1 A-B. At the centre of the impact site, there were 72.05% of RBPMS$^+$ RGCs in Nec-1s treated eyes compared with 60.56% in vehicle treated retinae, as a percentage of the number of RBPMS$^+$ RGCs in intact eyes, and 77.64% of BRN3A$^+$ RGCs in Nec-1s treated retinae compared to 63.27% in vehicle treated control retinae. There were no

changes at more peripheral retinal sites, suggesting that Nec-1s treatment provides some region-specific protection of RGCs.

Photoreceptor survival was assessed by ONL thickness measurements on H&E stained retinal sections at 600, 1200 and 1800 μm either side of the impact site, as previously described (Blanch et al., 2014, Thomas CN, 2018). There was no significant effect on ONL thickness in Nec-1s injected eyes compared to vehicle control, with no significant variation by distance from impact site (GLM p=0.313). For example, the normalised ONL thickness at 0, 600, 1200 and 1800 μm from impact site were 53.92%, 53.45%, 45.19% and 57.02% of intact retinae in Nec-1s treated eyes compared to 47.36%, 47.09%, 43.4% and 53.30% in vehicle treated control eyes. The mean ONL thickness values at different distances from the centre of the impact site are displayed in Table 4.1C. Collectively, these results suggest that inhibition of the necroptotic pathway may be specific to RGCs and not photoreceptors.

### 4.3.6. Nec-1s treatment did not preserve ERG amplitudes after blunt ocular injury

Bilateral blunt ocular injury was performed with unilateral intravitreal injection of Nec-1s treatment and contralateral injection of vehicle control (n=8 eyes per condition, 8 animals). Scotopic and photopic electroretinography was performed at 2 weeks after injury to assess retinal function. Intact animals receiving no injections were also analysed (n=8 animals). There were reductions in the scotopic a-wave, scotopic b-wave, photopic b-wave and PhNR amplitudes after blunt ocular injury compared to intact animals, but, there was no improvement in amplitudes in Nec-1s treatment eyes

compared to vehicle treated eyes. Although more RGCs were present after treatment with Nec-1s, their function was still impaired.

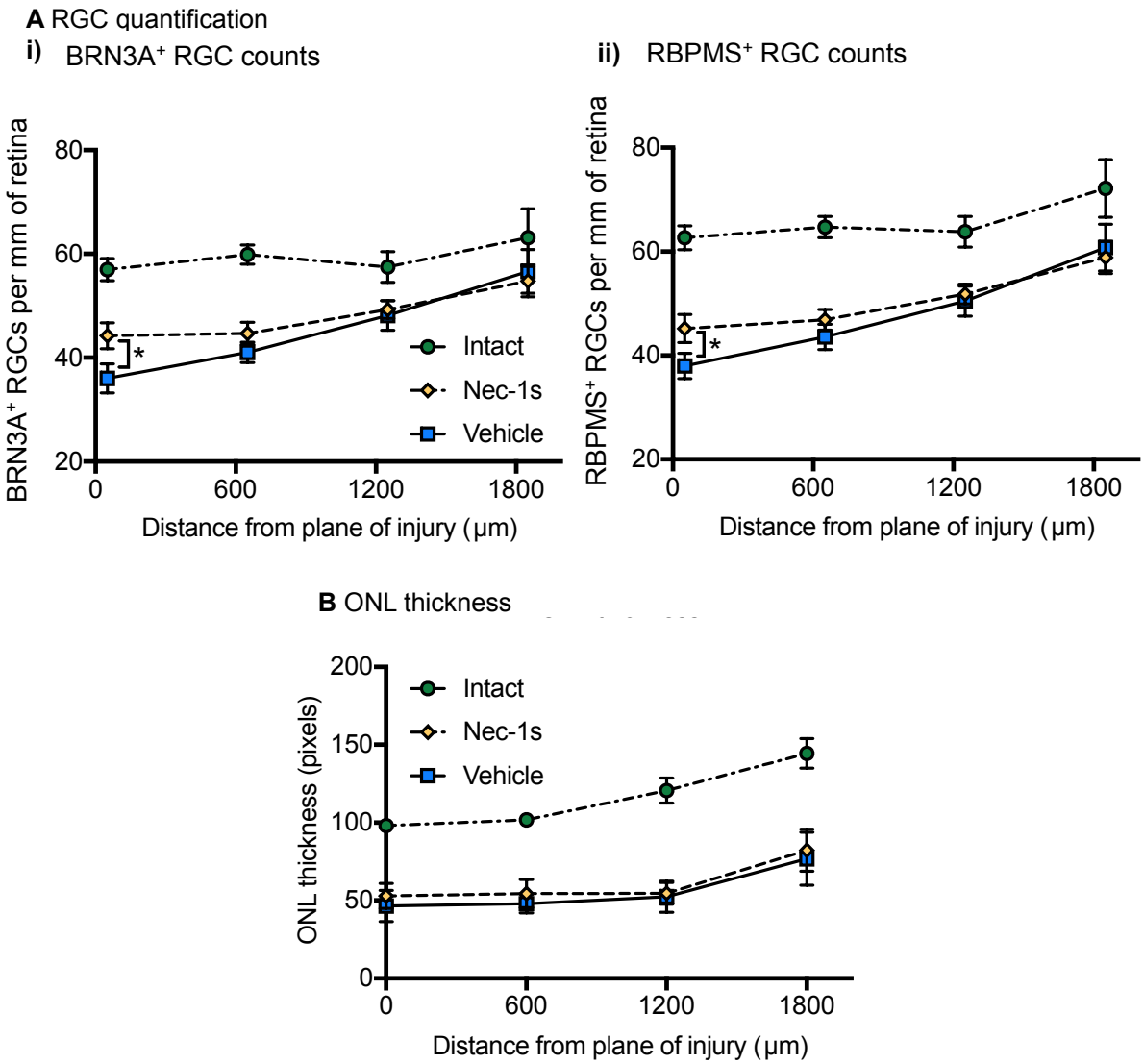


**Figure 4.** Nec-1s prevents RGC death but does not protect photoreceptors. **A)** BRN3A (a RGC specific transcription factor) positive RGC were counted across the entire retinae and reported as BRN3A positive cells per 1000µm of retinae, then normalised as a percentage of intact BRN3A counts. Unilateral intravitreal injection of Nec-1s promoted RGC survival at 600µm peripheral to the centre of the injury site (optic nerve head; 0 µm). At the centre of the injury site (0µm) RGC death is not prevented by Nec-1s. In the distant periphery (1200µm, 1800µm), there is less degeneration and therefore no significant effect of Nec-1s. **B.** Photoreceptors are not protected by Nec-1s. Outer nuclear layer (ONL) thickness is reduced after blunt ocular injury and Nec-1s does not improve ONL thickness compared to vehicle control. Error bars represent ± standard error of the mean (SEM).

**Figure 4.5. Nec-1s treatment is protective of BRN3A$^+$ and RBPMS$^+$ RGCs at the centre of the impact site, but does not preserve ONL thickness**. **(A-B)** The number of BRN3A$^+$ and RBPMS$^+$ RGCs were counted across entire retinal sections and reported as the number of BRN3A$^+$ RGCs per mm of retina. Animals received bilateral blunt ocular injury with unilateral Nec1-s treatment and contralateral vehicle control. After unilateral intravitreal injection of Nec-1s, the number of BRN3A$^+$ and RBPMS$^+$ RGCs was higher compared to vehicle control-treated eyes, across the retina with respect to retinal position (GLM; BRN3A $p<0.01$, RBPMS $p<0.05$), likely driven by larger numbers of RGCs detected at the centre of the injury site, although these differences did not reach statistical significance after correction for multiple comparisons (ONH; 0 μm; t-test with Bonferroni correction BRN3A$^+$ RGCs $p=0.1892$ and RBPMS$^+$ RGCs $p=0.2852$). In the distant periphery (1200 μm, 1800 μm), there was less retinal degeneration overall and no significant effect of Nec-1s treatment on the number of BRN3A$^+$ or RBPMS$^+$ RGCs compared to vehicle. **C)** ONL thickness was reduced after blunt ocular injury and Nec-1s treatment did not preserve ONL thickness compared to vehicle control (GLM $p=0.313$). Error bars represent mean ± SEM. n=8 per group (intact = 8 animals, n=8 bilateral blunt injured with unilateral Nec-1s intravitreal injection and contralateral vehicle intravitreal injection)

**A**

| Treatment | Mean number of BRN3A+ RGCs per mm of retina (± SEM) 0μm | 600μm | 1200μm | 1800μm |
|---|---|---|---|---|
| Intact | 56.95 ± 2.19 | 59.87 ± 1.85 | 57.48 ± 2.97 | 63.10 ± 5.55 |
| Blunt + Nec-1s | 44.21 ± 2.50 | 44.66 ± 2.16 | 49.29 ± 1.72 | 54.76 ± 3.05 |
| Blunt + vehicle | 36.03 ± 2.81 | 41.01 ± 1.95 | 48.13 ± 2.88 | 56.60 ± 4.23 |
| Unpaired t-test (with Holms Bonferroni correction) | p=0.1892 | p=0.6909 | p=0.7346 | p=1.4590 |

**B**

| Treatment | Mean number of RBPMS+ RGCs per mm of retina (± SEM) 0μm | 600μm | 1200μm | 1800μm |
|---|---|---|---|---|
| Intact | 62.68 ± 2.29 | 64.70 ± 2.05 | 63.84 ± 2.98 | 72.16 ± 5.56 |
| Blunt + Nec-1s | 45.16 ± 2.74 | 46.86 ± 2.04 | 51.84 ± 1.91 | 58.87 ± 3.12 |
| Blunt + vehicle | 37.96 ± 2.47 | 43.57 ± 2.44 | 50.47 ± 2.88 | 60.76 ± 4.51 |
| Unpaired t-test (with Holms Bonferroni correction) | p=0.2852 | p=0.9555 | p=1.3956 | p=0.7355 |

**C**

| Treatment | Mean number of pixels of ONL thickness (± SEM) 0μm | 600μm | 1200μm | 1800μm |
|---|---|---|---|---|
| Intact | 98.12 ± 1.91 | 101.72 ± 3.90 | 120.66 ± 8.03 | 144.34 ± 9.55 |
| Blunt + Nec-1s | 52.91 ± 7.99 | 54.36 ± 9.13 | 54.53 ± 7.06 | 82.31 ± 13.62 |
| Blunt + vehicle | 46.47 ± 10.01 | 47.90 ± 5.98 | 52.38 ± 10.11 | 76.79 ± 17.06 |
| Unpaired t-test (with Holms Bonferroni correction) | p=1.0014 | p=1.0240 | p=0.7330 | p=1.2418 |

**Table 2. Average BRN3A+ and BRPMS+ RGC and ONL thickness after blunt ocular injury with Nec-1s injections . (A-B)** BRN3A and RBPMS counts in intact animals and after blunt ocular injury with vehicle or Nec-1s intravitreal injections. Values are mean number of BRN3A cells per 1000μm of retinae ± SEM. **C)** ONL thickness in intact animals and after blunt ocular injury with vehicle or Nec-1s intravitreal injections. Values are mean pixels of ONL ± SEM.

mean pixels of ONL ± SEM.

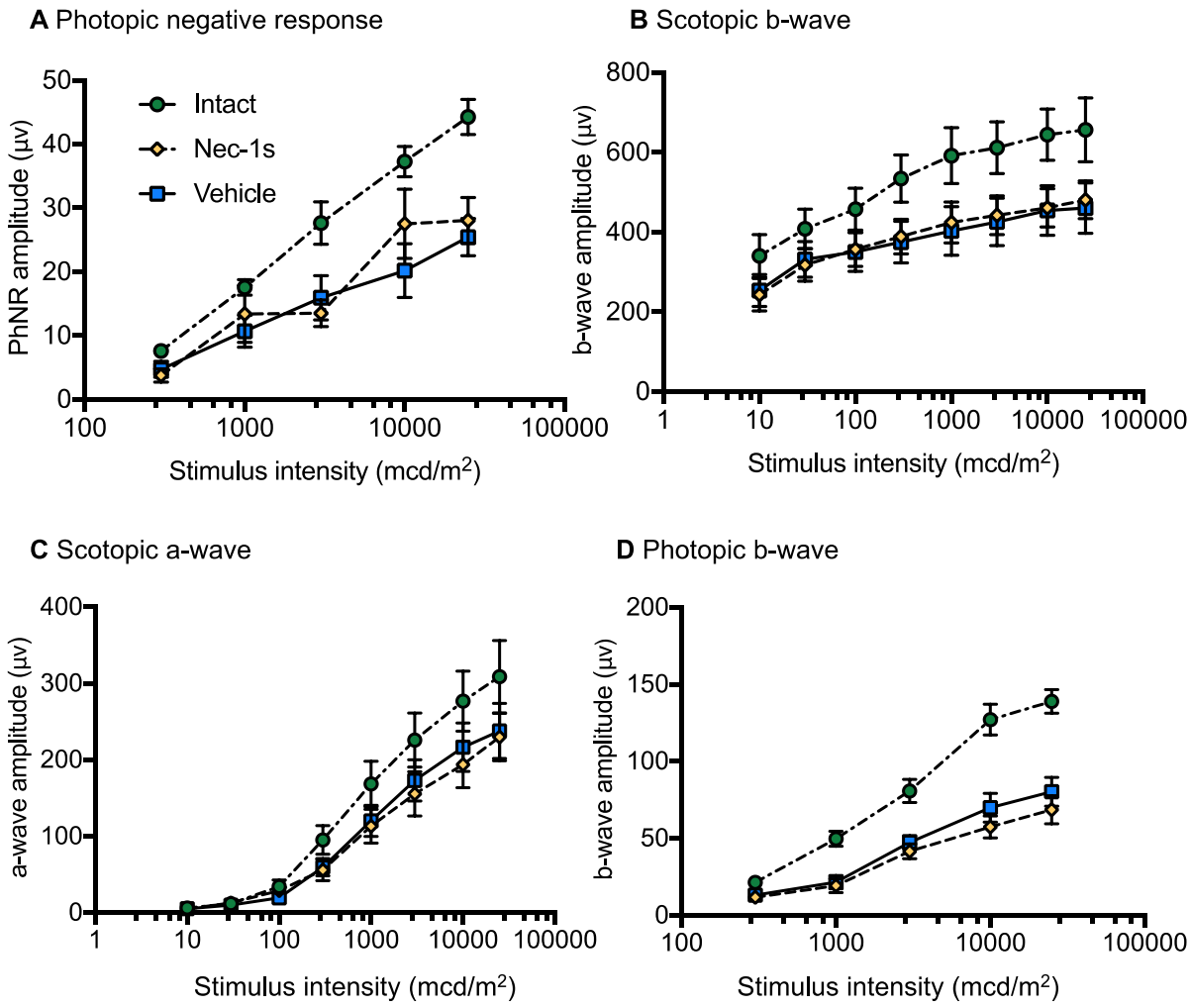


**Figure 4.6. There were no differences in ERG amplitudes in Nec-1s treated eyes compared to vehicle treated eyes after blunt ocular injury . A)** PhNR amplitudes were reduced after blunt ocular injury and PhNR amplitudes were not increased by Nec-1s treatment compared to vehicle control. **B)** Scotopic b-wave; **C)** scotopic a-wave and; **D)** photopic b-wave amplitudes were reduced after blunt ocular injury and there was no improvement with Nec-1s treatment compared to vehicle control. Error bars represent mean ± SEM. n=8 per group (intact = 8 animals, n=8 bilateral blunt injured with unilateral Nec-1s intravitreal injection and contralateral vehicle intravitreal injection)

## 4.4. Discussion

### 4.4.1. Necroptotic RGC death is likely to occur at the centre of the impact site

MLKL protein expression was higher following blunt ocular injury compared with intact retina and RIPK1 expression also tended to be higher. RIPK3 expression localised to $BRN3A^+$ RGCs, although there were no significant changes in protein expression up to 48 hours after injury using immunofluorescent staining and western blotting, suggesting protein levels of RIPK3 are not altered by injury. MLKL immunostaining localised to the OPL, RGCs, the INL and ONL cells 48 hours after blunt injury - specifically at the centre of the impact site - suggesting that multiple retinal cell types may have upregulated MLKL expression and activated necroptotic signalling pathways. Photoreceptors activate necroptotic pathways alongside previously investigated cell death mechanisms such as caspase-9-dependent apoptosis after injury (Blanch et al., 2014). Necroptotic photoreceptor death has been previously investigated in models of ocular injury, including *in vivo* models of retinal detachment and age-related macular degeneration (Murakami et al., 2011, Murakami et al., 2014, Murakami et al., 2012), indicating that necroptosis could possibly also drive photoreceptor degeneration after blunt ocular injury.

The phosphorylation of MLKL at Ser345 is catalysed by RIPK1 and promotes MLKL translocation and accumulation at the plasma membrane, here, MLKL induces membrane permeabilisation and cell lysis (Weinlich et al., 2017, Rodriguez et al., 2016), although the association of RIPK3 and MLKL in the necrosome is not dependent on Ser345 phosphorylation (Rodriguez et al., 2016). In this chapter, I have shown MLKL expression is upregulated 48 hours after injury and that full-length MLKL has a

cytoplasmic distribution in the ONL and OPL, INL and GCL. Immunofluorescent staining in the OPL suggests that MLKL might be present in the connections between the photoreceptors and INL cells and that it may be located in axons or dendrites rather than cell bodies. Further investigation is required to determine if MLKL is upregulated in the ON, as well as other axonal connections in the retina. In the PNS, MLKL is expressed in Schwann cells and its phosphorylation at serine 441 promotes myelin sheath breakdown and some functional axonal regeneration (Ying et al., 2018). MLKL could have a similar effect in the CNS in oligodendrocytes or in neuronal cells and could provide a new avenue for research into ON axonal regeneration. In the developing brain, necroptotic proteins mediate oligodendrocyte death and induce injury of cerebral white matter (Qu et al., 2017). This observation might translate to therapies targeted at necroptotic proteins to preserve myelin structure in the ON after TON, including models of ONC, blunt and blast injury.

For necroptotic signalling to be activated and induce cell death, apoptotic caspase-8 must be inhibited either through endogenous or pharmacological inhibitors or remain uncleaved. This allows for the formation of complex IIb and the association of RIPK1, RIPK3 and MLKL (Gizycka and Chorostowska-Wynimko, 2015). Blanch et al., showed that caspase-8 remained uncleaved up to 48 hours after blunt ocular injury and there was no retinal caspase-8 immunostaining (Blanch et al., 2014). Caspase-capture experiments using b-VAD-fmk confirmed there was no caspase-8 activation since no cleaved caspase-8 was isolated, indicating that caspase-8-independent cell death signalling drives retinal cell death after blunt ocular injury (Blanch et al., 2014).

### 4.4.2. Necroptotic gene expression changes did not correlate with protein changes

The absence of changes in *ripk1* and *mlkl* gene expression suggest that changes in mRNA expression may have occurred earlier than 48 hours or that mRNA levels are not altered and post-translational modifications and protein complexes are occurring. After blunt ocular injury, *ripk3* mRNA expression decreases, suggesting that there may be a negative feedback loop reducing mRNA levels. Alternatively, only certain gene isoforms may have changed in mRNA expression. Using Primer-BLAST (Ye et al., 2012), it was predicted that the RIPK1 primer sequences would target *ripk1* and X1-X7 transcripts, all *ripk3* transcripts and *mlkl* transcripts X1-X3 and X5-X9. The primer sequences designed should be efficient at detecting most gene transcripts, but not all gene transcripts. In future experiments, I would use pre-optimised TaqMan primers which are specific for the DNA sequence and detect fluorescence at the specific cDNA sequence. SYBR green, which was used in this study, emits a fluorescent signal when bound to all dsDNA, irrespective of the sequence. Another explanation for the lack of correlation between protein and mRNA expression could be the experimental design. Instead of using retinal tissue from separate animals for injured and control groups, I could perform unilateral blunt injury and use the contralateral eye as a control. This takes into account and normalises any gene expression changes between animals and allows for the assessment of differences between experimental groups.

### 4.4.3. Nec-1s preserves the number of βIIIT$^{+}$ RGCs compared to vehicle, in primary retinal cultures *in vitro*

A dose response curve was produced using a range of Nec-1s concentrations between 1x10$^{-4}$ to 1x10$^{-8}$ µg/µl in rat primary retinal cultures *in vitro*. RGC survival was assessed by counting the number of βIIIT$^{+}$ RGCs. Following ON injury, RGCs die within 5 days and there is >90% RGC loss at 14 dpi (Berkelaar et al., 1994). RGCs begin to degenerate in retinal cultures due to severing of the ON and disrupted RGC axonal connections. Previous studies have used the same timeframe for retinal cultures and shown effective results from a variety of treatments (Morgan-Warren et al., 2016, Mead et al., 2013). An alternative to primary retinal cultures would be to use an RGC cell-line, such as RGC-5 cells, although, RGC-5 cells do not have normal RGC characteristics and the cell-type is still unknown (Al-Ubaidi, 2014, Krishnamoorthy et al., 2013). Primary retinal cultures allow for many concentrations of a compound to be tested *in vitro* to test for their efficacy. However, primary retinal cultures consist of a mixed retinal cell population and elicit no immune response, such as infiltrating macrophages or neutrophils. As necroptosis can be linked to inflammation and the immune response (Conos et al., 2017, Silke et al., 2015, Pasparakis and Vandenabeele, 2015), this might not be representative of what is occurring *in vivo* in our animal studies. *In vitro* primary retinal cell cultures provide an indication of whether cell death pathways are occurring in injured RGCs, but don't provide information or take into account drug clearance and metabolism. In the eye there are multiple clearance, metabolism and drainage systems which will rapidly reduce the amount of drug which is in contact with the retina.

There was a significant neuroprotective effect from Nec-1s treatment compared to vehicle control, suggesting that necroptotic signalling mediates the death of a proportion of RGCs. At low doses of Nec-1s (1 x $10^{-8}$ µg/µl) there was significant improvement in RGCs numbers, which is likely driving the overall significant improvement, with a ~1.5-fold increase in βIIIT$^{+}$ RGC numbers compared to vehicle control, but at higher doses (1 x$10^{-4}$ µg/µl) there was insignificant RGC neuroprotection. This indicates that lower concentrations of Nec-1s may be more effective *in vitro*.

*In vitro* experiments were used to test the efficiency of Nec-1s treatment in protecting injured RGCs. When translated for *in vivo* experiments, a greater concentration of Nec-1s compound was required due to *in vivo* mechanisms of drug elimination and degradation. Removal of drug can occur by metabolism and outflow via the aqueous humour through the anterior route (available for all types of compounds) or through the posterior route by endothelial and epithelial blood-ocular barriers (depending on compound permeabilisation) (Del Amo et al., 2017). I intravitreally injected a 3.6 mM solution of Nec-1s into rat eyes (reconstituted in 10% DMSO and 0.9% methyl-β-cyclodextrin) and repeated this at 7 dpi and collected tissue at 14 dpi. Similar concentrations of compound and DMSO were used in previous studies using Nec-1. For example, Huang et al. used a 1 mM concentration of Nec-1 in 30% DMSO and PBS, and Rosenbaum et al. used a concentration of 4 mM of Nec-1 in DMSO (undisclosed concentration) (Rosenbaum et al., 2010, Huang et al., 2018). However, the Nec-1s used in my studies has a higher affinity and specificity than Nec-1 and is >1000 fold more selective for RIPK1 than other kinases (Linkermann and Green, 2014,

Takahashi et al., 2012). But, a 1000-fold higher selectivity does not mean that Nec-1s is 1000-fold more potent at inhibiting necroptosis than Nec-1. A lower concentration of Nec-1s could have been used and a range of doses should have been tested *in vivo* to determine that most effective dose.

A high concentration of DMSO was used as Nec-1s was insoluble in lower concentrations of DMSO and precipitated into solution. DMSO can be neurotoxic to RGCs at high concentrations, with retinal apoptosis occurring with 5 µl intravitreal injections of 1-8% concentrations of DMSO *in vivo*. *In vitro,* concentrations with >10% DMSO induce apoptosis and plasma membrane pore formation (Galvao et al., 2014, Notman et al., 2006). In this study, I reconstituted Nec-1s in 10% DMSO and 0.9% methyl-β-cyclodextrin to aid with retinal permeabilisation and solubility. Despite DMSO causing RGC death, I have shown consistent retinal pathology across studies, including our siCASP2 study (siRNA was reconstituted in sterile PBS) and in previous studies by Blanch et al. (Blanch et al., 2012b, Blanch et al., 2014, Thomas CN, 2018).

### 4.4.4. *In vivo* Nec-1s protects RGCs, likely at the centre of the impact site, in the blunt ocular injury model

Our rat blunt ocular injury model induces retinal cell death in a focal area, causing ONL disruption, photoreceptor death and RGC degeneration (Thomas CN, 2018, Blanch et al., 2014, Blanch et al., 2012b). I previously showed that caspase-2 likely drives RGC death 600 µm from the impact site centre and that siCASP2-mediated caspase-2 knockdown protects a proportion of $BRN3A^+$ RGCs and preserves some RGC function (measured by PhNR amplitudes) (Thomas CN, 2018). I previously assumed that the

reduction in RGCs at the centre of the impact site was mediated by uncontrolled necrosis, caused by the physical impact of the blunt force projectile. In this chapter, I demonstrate that a proportion of RGCs may degenerate by necroptotic signalling pathways. This is evidenced by elevated proteins involved in the necroptotic pathway, including a significantly higher expression of MLKL at the impact site and a tendency towards increased RIPK1 expression. Intravitreal injections of Nec-1s significantly preserved the number of $BRN3A^+$ and $RBPMS^+$ RGCs across the retina compared to vehicle. Nec-1s treatment did not preserve the number of RGCs to levels found in intact retina, suggesting that the degeneration of some RGCs occurs through uncontrolled 'explosive' necrosis due to the impact or alternative cell death signalling pathways. In line with my findings, RGCs are also protected by the inhibition of necroptosis in other models of RGC death, including glaucoma models (Do et al., 2017) and in a retinal ischemia-reperfusion injury model (Rosenbaum et al., 2010).

RGCs were quantified by counting $BRN3A^+$ (RGC-specific transcription factor with nuclear immunostaining) and $RBPMS^+$ (cytoplasmic marker) immunostained cells in the GCL (Mead et al., 2014, Mead and Tomarev, 2016). BRN3A only stains a subset of RGCs and its expression can be reduced after RGC injury through phagocytic clearance by microglia (Nadal-Nicolas et al., 2009, Sanchez-Migallon et al., 2011, Sanchez-Migallon et al., 2016) suggesting that BRN3A might not be the most reliable RGC marker. RBPMS immunofluorescently stains a greater proportion of RGC subpopulations (Kwong et al., 2011, Rodriguez et al., 2014a), but further research needs to be performed to confirm the use of RBPMS as a reliable RGC marker (Mead and Tomarev, 2016). I have demonstrated significant RGC neuroprotection using both

BRN3A and RBPMS markers after Nec-1s treatment following blunt ocular injury. Nec-1s might be a potential therapeutic to prevent RGC death and prevent visual loss in patients with indirect TON.

### 4.4.5. Nec-1s treatment had no effect on ONL thickness after blunt ocular injury

Photoreceptor cell bodies populate the ONL; therefore, ONL thickness can be used to assess photoreceptor survival (Blanch et al., 2012b, Blanch et al., 2014). Previous studies have shown necroptosis occurs in photoreceptors. For example, in the rd10 mouse retinitis pigmentosa model, inhibition of RIPK1 using Nec-1 or *ripk3* knockout preserved cone photoreceptors and function (Murakami et al., 2012). Photoreceptor necroptosis also occurs in a model of age-related macular degeneration (Murakami et al., 2014) and a model of retinal detachment (Murakami et al., 2011). In the blunt ocular injury model, intrinsic apoptotic pathway member caspase-9 mediates degeneration of some photoreceptors in the far periphery of the impact site and caspase-9 inhibition using a dominant negative mutant protein provides a small, but significant, preservation of ONL thickness compared to vehicle, and some improvement in ERG amplitudes (Blanch et al., 2014). Despite the immunolocalisation of MLKL to the ONL and OPL, treatment with Nec-1s did not provide any preservation of ONL thickness compared to vehicle. This could be due to 1) necroptosis not occurring in photoreceptors; 2) necroptosis inhibition promoted activation of another cell death signalling pathway; or 3) an ONL thickness preservation occurring at a later time point after treatment.

### 4.4.6. Nec-1s did not provide any protection of retinal function

Scotopic (dark-adapted) and photopic (light-adapted) ERG amplitudes were measured to assess retinal function. The PhNR is a common measure of RGC function; it is reduced in experimental and human glaucoma (Viswanathan et al., 1999) and correlates with reduced RGCs in ONT (Li et al., 2005). Treatment with Nec-1s had no effect on scotopic or phototopic a- or b- wave amplitudes and did not affect PhNR amplitudes, suggesting that retinal function was not improved by Nec-1s treatment. The lack of functional restitution suggests that structurally protected RGCs are non-functional, although the focal nature of the retinal injury and the specific neuroprotection of RGCs at the centre of the impact site, may mean that too few RGC are protected to be detectable in ERGs. To determine region-specific changes in retinal function, I could perform multifocal ERG (mfERG). This technique simultaneously assesses electrophysiological retinal function at multiple locations (Lalonde et al., 2006, Holder, 2004, Azarmina, 2013, Stiefelmeyer et al., 2004). This is further discussed in my general discussion (Section 7.1.3).

### 4.4.7. Further experiments

The results of my investigations suggest that necroptosis may be occurring at the impact site; however, further experiments are required to provide stronger evidence. For example, performing co-immunoprecipitation experiments of RIPK1 and RIPK3 to determine if they are associated in complex IIb (Vandenabeele et al., 2010) and the use of a positive necroptosis control. Necroptosis can be activated through the addition of TNF-α and the inhibition of caspases using pharmacological inhibitor z-VAD.

In my *in vivo* Nec-1s study, a more appropriate control would be to intravitreally inject Nec-1s and vehicle treatments into intact controls to account for injury caused by intravitreal injections and effects of treatments. Also, I would perform a dose response experiment *in vivo*, to determine the lowest dose of Nec-1s which inhibits necroptosis markers and has an effect on RGCs. I would also confirm that necroptosis has been inhibited in my Nec-1s treated groups, for example, through immunofluorescent staining for RIPK1, RIPK3 and MLKL, co-immunoprecipitation for RIPK1-RIPK3 complexes and western blotting for phosphorylated MLKL at Ser 345 (a late stage marker in necroptosis signalling). To extend the project further, these experiments could be performed in knockout mice or rats which have had necroptosis pathway members knocked down (for example, using siRNA against *ripk1*, *ripk3* or *mlkl*).

### 4.4.8. Conclusion

In this chapter, I have demonstrated that RGC death occurs in a region-specific manner after blunt ocular injury, with necroptotic-dependent mechanisms likely driving a reduction in RGC numbers at the centre of the impact site. The inhibition of necroptosis using pharmacological inhibitor, Nec-1s, preserved the number of $RBPMS^+$ and $BRN3A^+$ RGCs compared to vehicle, suggesting that Nec-1s might protect a proportion of RGCs, but, as there was no increase in ERG amplitudes, Nec-1s did not provide any corresponding improvement in retinal function. I have previously shown that caspase-2-dependent RGC death occurred peripheral to the impact site, which, collectively with this chapter, suggest that multiple cell death signalling pathways can occur in parallel, possibly amongst multiple cell types, in a single injury model. Nec-1s might be a potential therapeutic for treatment to prevent RGC death in blunt ocular injury.

# Chapter 5 Caspase-2 mediates retinal degeneration in a mouse ocular repeated primary blast injury model

## 5.1. Rationale

After an explosive blast, individuals can be exposed to multifactorial injuries, including the primary blast overpressure wave and blunt ocular injury. In Chapter 3 and 4, I demonstrated that caspase-2-dependent apoptosis and necroptosis are likely to occur in RGCs in a site-specific manner after blunt ocular injury. In this chapter, I have used a mouse rPBI model to explore whether caspase-2 mediates RGC death and alterations in ON axonal morphology. I hypothesised that knockdown of caspase-2 using siCASP2 would provide RGC neuroprotection and prevent ON axonal degeneration.

## 5.2. Experimental design

12-week old C57 Bl6 male mice were exposed to unilateral rPBI, as described in Section 2.1.2. Briefly, the left eye of mice was exposed to 2 blasts of 15 psi, about 1 second apart and repeated on 3 consecutive days (Bernardo-Colon et al., 2018, Vest et al., 2019). The right eyes that were indirectly affected by the blasts (Bricker-Anthony and Rex, 2015), were also assessed in some analyses and are highlighted in Figure 5.1 and in the results.

To assess the effects of gliosis and infiltrating inflammatory cells, unilateral rPBI was performed, tissue collected at 3 dpi and immunofluorescently stained for GFAP and ED1. ONs were also resin-embedded and stained for PPD and toluidine blue to assess axonal morphology and degenerative profiles (see Section 2.6) at 2, 7, 14 and 28 dpi compared to sham. Intact and degenerating axons and the axon density were quantified.

### 5.2.1. Caspase-2 cleavage and siCASP2-mediated knockdown

Retinal tissue was collected at 7 and 14 dpi and western blotting performed for full-length and cleaved caspase-2 (see Section 2.7) (Figure 5.1A). Caspase-2 was knocked down by bilateral intravitreal injection of 2 µl of 1 µg/µl siCASP2 and in another group of mice, 2 µl of 1 µg/µl of siEGFP was bilaterally injected as control. Intravitreal injections were performed at two time points after the rPBI injury, which are described below. The sequences of siCASP2 and siEGFP are described in Section 2.1.3.1.

### 5.2.2. Outcome measurements from *in vivo* studies

Analyses were performed to assess structural and functional effects of rPBI and siCASP2 treatment. *In vivo* OCT retinal imaging (see Section 2.2.1) and ERG and VEP recordings (see Section 2.2.2) were performed at baseline and at the endpoint of each study. ON axonal pathology was also assessed through counting axons with intact and degenerative profiles on resin-embedded semi-thin sections. The far proximal portion of the ON, closest to the eye, was resin embedded and stained with PPD and toluidine blue to visualise axonal myelin morphology (method described in Section 2.6). Both left and right ONs were embedded, which will be highlighted in the results section. The remaining ON section were processed as longitudinal cryosections and immunofluorescently stained for GFAP and ED1 (see Section 2.3).

### 5.2.3. Delayed siCASP2 *in vivo* study

In a delayed treatment arm, siCASP2 and siEGFP were injected intravitreally into both eyes, ~5 hours after the first blast which was followed by two further blast waves as

part of the rPBI protocol (Figure 6.1B). Injections were repeated every 7 days and animals culled and perfused at 28 dpi. This study is referred to as the “delayed siCASP2” study (Figure 5.1B). *In vivo* analysis was performed, as described above, and ONs processed for axonal quantification and immunofluorescent staining. Retinae were processed as retinal whole mounts and $RBPMS^+$ RGCs quantified (see Section 2.4.3.2).

### 5.2.4. Pre-blast siCASP2 *in vivo* study

A further *in vivo* study was performed, where siCASP2 and siEGFP were injected intravitreally into both eyes 48 hours before the rPBI and these injections were repeated every 7 days until animals were culled and perfused at 14 dpi. This study is referred to as the “pre-blast siCASP2” study (Figure 5.1B). To confirm lack of lens or retinal damage caused by the injections, additional OCT imaging was performed surrounding the intravitreal injections and rPBI as described in Figure 5.1C. Perfused eyes were processed for cryosectioning and immunofluorescent staining. To assess RGC numbers, $RBPMS^+$ RGCs were quantified on retinal cryosections in line with the ONH (see Section 2.4.3 and Section 2.4.2).

**A** *In vivo* protein studies

**i)** Timeline

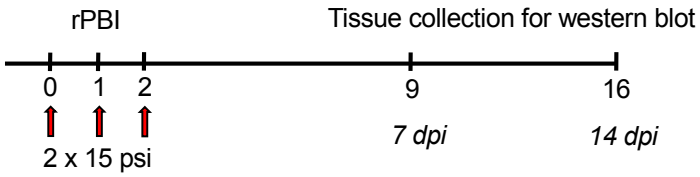


**ii)** Experimental groups, group sizes and measured endpoints

| Time point | n (mice) | Measured endpoints |
|---|---|---|
| 7 dpi | Western blot: 3 retinae per group (unilateral rPBI and sham) | Caspase-2 expression and cleavage in left direct blast eyes |
| 14 dpi | Western blot: 5 retinae per group (unilateral rPBI and sham) | Caspase-2 expression and cleavage in left direct blast eyes |

Cc

**B** *In vivo* "delayed siCASP2" study

**i)** Timeline

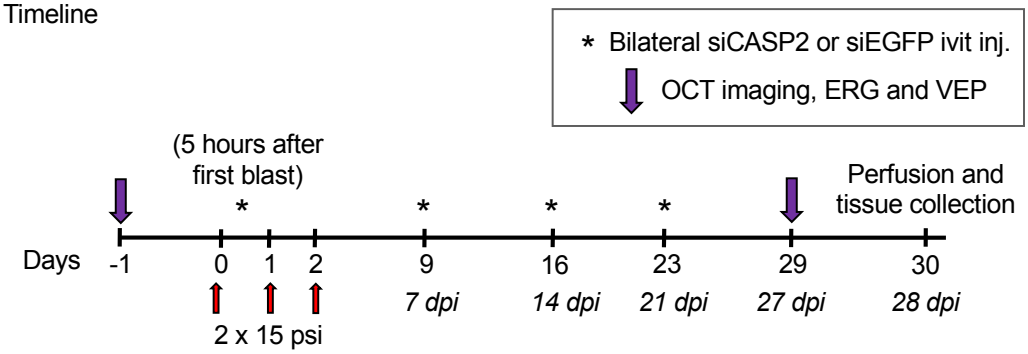


**ii)** Experimental groups, group sizes

| *Groups* | *n (mice)* | *Injury and treatment* |
|---|---|---|
| Sham | 10 | Blast overpressure wave blocked |
| rPBI + no ivit | 10 | 3 x 2 x 15 psi + no ivit injections |
| rPBI + siEGFP | 10 | 3 x 2 x 15 psi + bilateral siEGFP ivit injections |
| rPBI + siCASP2 | 10 | 3 x 2 x 15 psi + bilateral siCASP2 ivit injections |

**iii)** Measured endpoints and eyes analysed

| *Measured endpoints* | *Eyes analysed* |
|---|---|
| OCT imaging | Both eyes |
| Total retinal and GCC thickness | Left direct blast eye |
| Percentage of eyes with vitreal hyper reflective dots | Both eyes |
| ERG and VEP amplitudes | Left direct blast eye |
| $RBPMS^+$ RGC counts on retinal wholemounts | Left direct blast eye |
| ED1 and GFAP IF staining on ON sections | Left direct blast eye |
| Axonal counts in ONs | Left direct blast eye |

Continued…

**C** *In vivo* "pre-blast siCASP2" study

**i)** Timeline

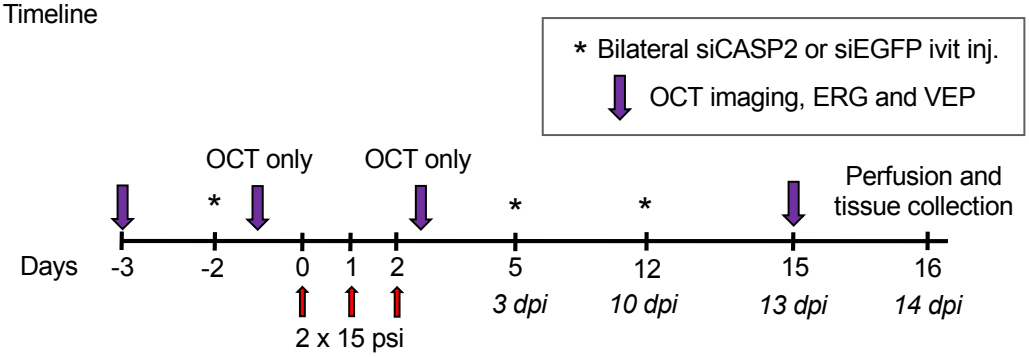


**ii)** Experimental groups and group sizes

| *Groups* | *n (mice)* | *Injury and treatment* |
|---|---|---|
| Sham | 5 | Blast overpressure wave was blocked. Left eyes received no ivit injections. Right eyes had ivit injections of sterile PBS. |
| rPBI + no ivit | 5 | 3 x 2 x 15 psi + no ivit injections |
| rPBI + siEGFP | 5 | 3 x 2 x 15 psi + bilateral siEGFP ivit injections |
| rPBI + siCASP2 | 5 | 3 x 2 x 15 psi + bilateral siCASP2 ivit injections |

**iii)** Measured endpoints and eyes analysed

| *Measured endpoints* | *Eyes analysed* |
|---|---|
| OCT imaging | Both eyes |
| Total retinal and GCC thickness | Left direct blast eye |
| Percentage of eyes with vitreal hyper reflective dots | Both eyes |
| ERG and VEP amplitudes | Left direct blast eye, and right sham eye (ivit injection of sterile PBS) |
| $RBPMS^+$ RGC counts on retinal cryosections | Left direct blast eye |
| ED1 IF staining on ON sections | Left direct blast eye |
| Axonal counts in ONs | Left direct blast eye, and right sham eye (ivit injection of sterile PBS) |

Continued…

**Figure 5.1. Experimental design. A)** Retinal tissue was collected at 7 and 14 dpi and processed for western blotting. **B)** *In vivo "*delayed siCASP2" study. siCASP2 or siEGFP as control were injected intravitreally ~5 hours after the first blast of the rPBI protocol and repeat injections performed every 7 days until perfusion and tissue collection at 28 dpi. OCT imaging, ERG and VEP were performed at baseline (-1d) and endpoint (28 dpi). **C)** *In vivo "*pre-blast siCASP2" study. siCASP2 or siEGFP were injected intravitreally 48 hours before the rPBI and repeated injections performed every 7 days until perfusion and tissue collection at 14 dpi.

## 5.3. Results

### 5.3.1. Three days post injury, infiltrating ED1$^+$ cells were observed but no changes in GFAP$^+$ process morphology or staining intensity

There were few ED1$^+$ macrophages in sham retinae. The number of ED1$^+$ cells was higher in the OPL of eyes that underwent rPBI 3 dpi (Figure 5.2A). There were few reactive glial processes throughout the retina in sham and rPBI treated eyes at 3 dpi, suggesting that retinal glia activation may occur at a later time point (Figure 5.2B).

### 5.3.2. Caspase-2 cleavage increases 7 days after blast injury

Retinal protein was collected 7 and 14 dpi and caspase-2 fragments assessed by western blotting (

Figure **5.3**A). Caspase-2 cleavage fragments were present 7 dpi with sizes of 55 kDa (full-length caspase-2), 35 kDa (intermediate fragment) and 15 kDa (cleaved caspase-2). The 35 kDa and 15 kDa caspase-2 fragments might be increased slightly at 7 dpi, but further experiments and semi-quantitative analysis needs to be performed. There were no 15 kDa cleaved caspase-2 fragments 14 dpi, suggesting that caspase-2 cleavage may peak earlier following rPBI. However, no real conclusions can be drawn from this data, until further experiments are performed.

**A)** Retinal ED1⁺ immunostaining at 3 dpi

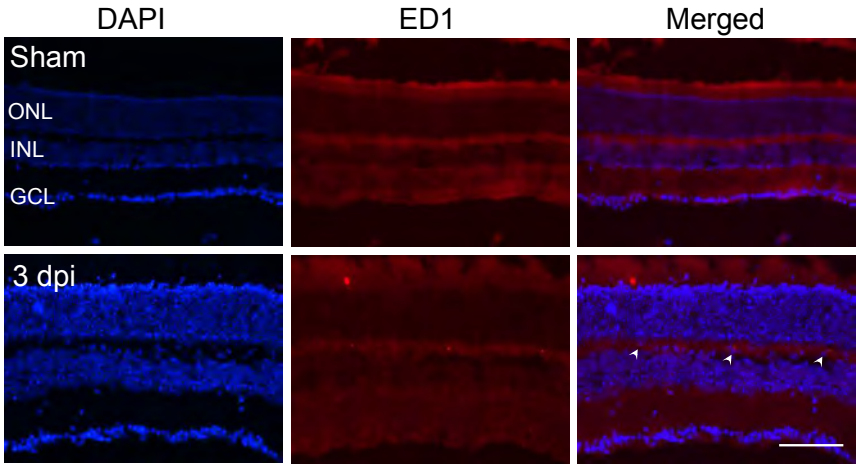


**B)** Retinal GFAP immunostaining at 3 dpi

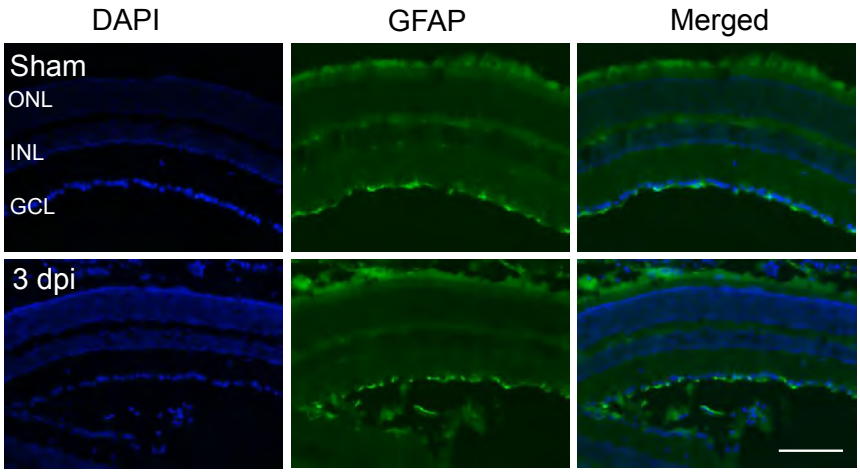


**Figure 3. A)** Retinal ED1⁺ immunostaining at 3 dpi, showing few ED1⁺ cells in the outer plexiform layer (n=4). **B)** Glial fibrillary acidic protein (GFAP) immunostaining at 3 dpi showing no changes in glial reactivity (n=4). Scale bar represents 100µm.

**A)** Caspase-2 western blotting

**i)** 7 dpi

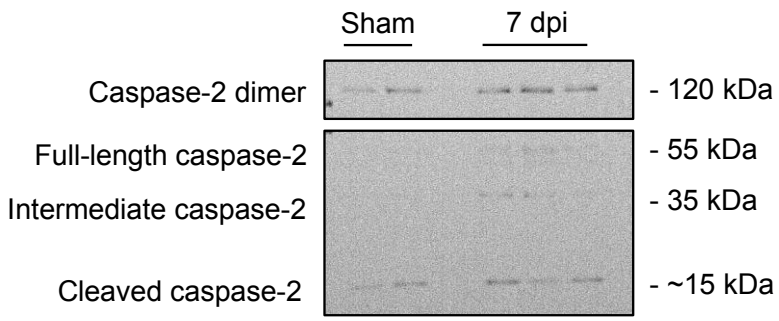


**ii)** 14 dpi

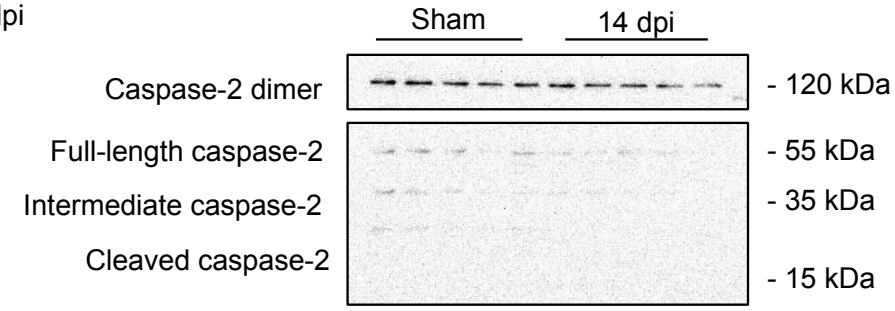


**B)** Retinal caspase-2 immunostaining

**Figure 5.** Caspase-2 cleavage shown through western blotting at 2, 7 and 14 dpi. **i)** Cleaved caspase-2 increases at 7 dpi (n=3 per group). **ii)** 14 dpi (n=5 per group). β-actin as loading control. Error bars represent mean ± SEM.

### 5.3.3. Delayed injection with siCASP2 had no effect on retinal thickness but caused some hyper reflective dots in the vitreous

siCASP2 was intravitreally injected ~5 hours after the first blast, followed by two further blasts on consecutive days (delayed siCASP2 study). OCT imaging was performed at baseline and at the 28 dpi endpoint. Retinal and GCC thickness were measured and the percentage of eyes with hyper reflective dots in the vitreous were quantified.

There was more hyper reflective dots in the vitreous following siEGFP and siCASP2 intravitreal injections after blast injury, which were absent in sham treated animals and after rPBI that was not treated with intravitreal injections, indicating that this was pathology specific to intravitreal injection (Figure 5.4A and Figure 5.4C). The percentage of eyes with hyper reflective dots in the vitreous were quantified and displayed as a percentage of total eyes in that group (Figure 5.4C). Animals received bilateral intravitreal injections: the left eye was directly blasted while the contralateral right eyes received indirect blast and mild blunt injuries. There was no eyes which displayed hyper reflective vitreal dots in left sham-treated eyes or rPBI treated eyes that did not have intravitreal injections in either eye, indicating that the blast wave alone does not cause these appearances. However, 80% of left retinae receiving rPBI and siEGFP injections had hyper-reflective vitreous dots compared to only 30% of right contralateral eyes. This same result was also demonstrated in the siCASP2 treated group, as 70% of directly blasted left eyes showed hyper reflective vitreous dots and only 30% of right eyes. Despite changes in hyper reflective dots in the vitreous, there were no changes in total retinal or GCC thickness at 28 dpi (ANOVA $p=0.121$ and $p=0.101$, respectively) (Figure 5.4B).

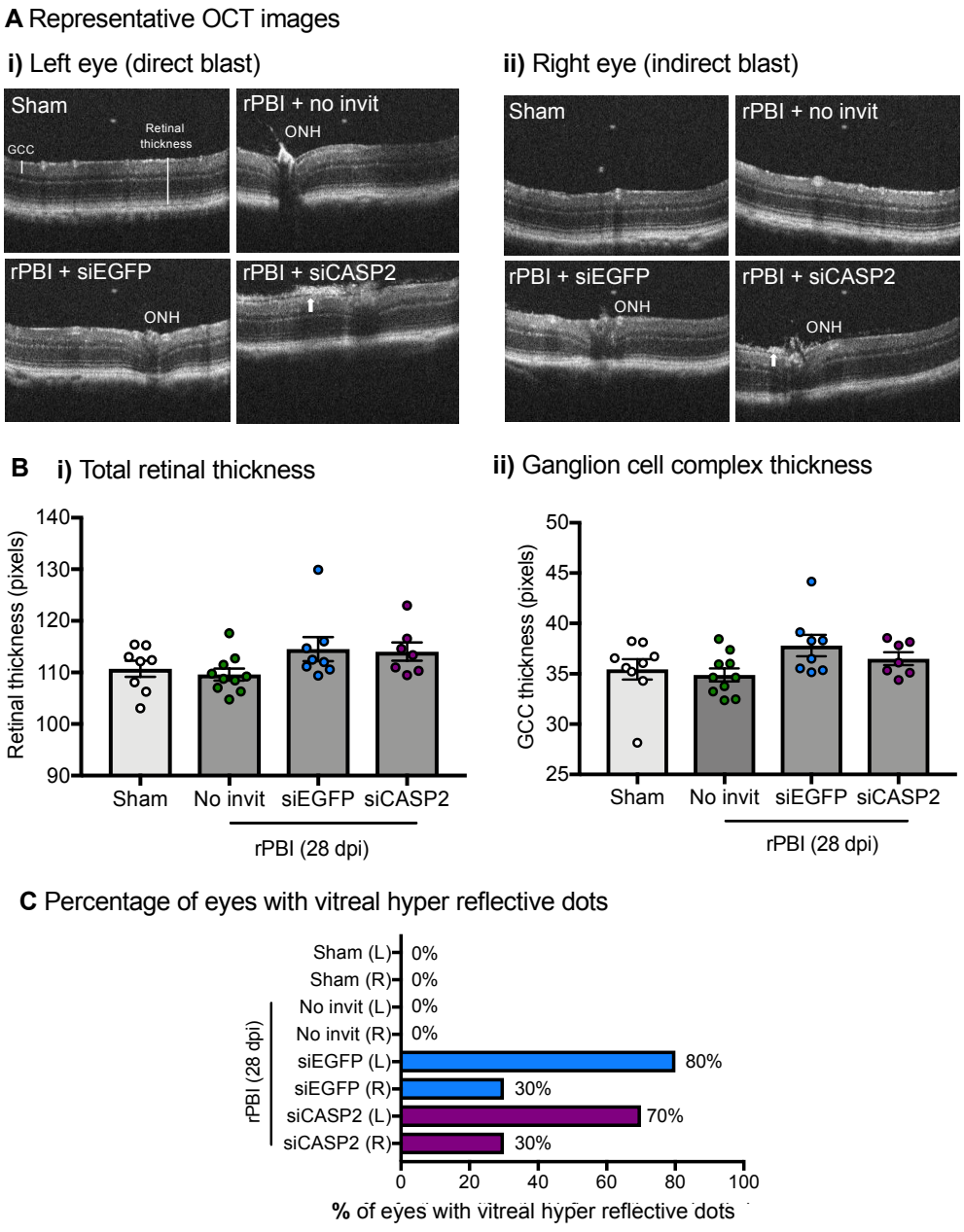


**Figure 14.** OCT imaging after rPBI and delayed siCASP2 intravitreal injection. **A)** Representative OCT images in sham and after rPBI with no intravitreal injections or siEGFP and siCASP2 injections at 28 dpi. **i)** Left (direct blast) and **ii)** right (indirect blast) retinae are shown. **B)** There are no differences in **i)** retinal or **ii)** ganglion cell complex thickness between sham, rPBI or after siCASP2 and siEGFP intravitreal injections at 28 dpi. Error bars represent ± SEM.

Fi … al
A) … eft
inj … es
(di …

in **i)** total retinal and **ii)** GCC thickness between all groups at 28 dpi (ANOVA p=0.121, p=0.101, respectively). **C)** Percentage of eyes with hyper reflective dots in the vitreous in direct blast and contralateral eyes are shown. Error bars represent mean ± SEM.

### 5.3.4. The number of RBPMS$^+$ RGCs were not affected by rPBI and delayed siCASP2 treatment

RBPMS$^+$ RGCs were quantified in the middle portion of retinal whole mounts (Figure 5.5). There were no differences in the number of RBPMS$^+$ RGCs in the middle portion of retinal whole mounts in rPBI treated eyes 28 dpi compared to sham eyes, or in eyes exposed to rPBI and treated with siEGFP or siCASP2 intravitreal injections (ANOVA p=0.505). This suggests that the number of RBPMS$^+$ RGCs were not reduced in experimental groups compared to sham within 28 days or that a reduction in RGC number after injury was focal and I failed to detect it using this method of quantification. For example, there were 406.4 ± 58.85 RBPMS$^+$ cells per mm$^2$ in sham treated eyes, 440.2 ± 50.59 RBPMS$^+$ cells per mm$^2$ after rPBI with no intravitreal injections, 467.10 ± 31.41 RBPMS$^+$ cells per mm$^2$ after rPBI with siEGFP injections and 394.4 ± 23.54 RBPMS$^+$ cells per mm$^2$ after rPBI with siCASP2 injections at 28 dpi.

### 5.3.5. Delayed siCASP2 treatment did not preserve retinal function compared to siEGFP treated eyes

Retinal function was assessed using ERG and VEP recordings. There were no differences in ERG a-wave (ANOVA p=161), b-wave (ANOVA p=0.452), VEP N1 (ANOVA p=0.197) and P1 (ANOVA p=0.544) amplitudes between sham treated eyes and rPBI treated eyes with or without intravitreal injections of siCASP2 and siEGFP (Figure 5.6).This experiment may have been underpowered to detect any significant changes due to the subtle differences caused by rPBI and the baseline amplitudes were lower than expected, likely due to technical problems.

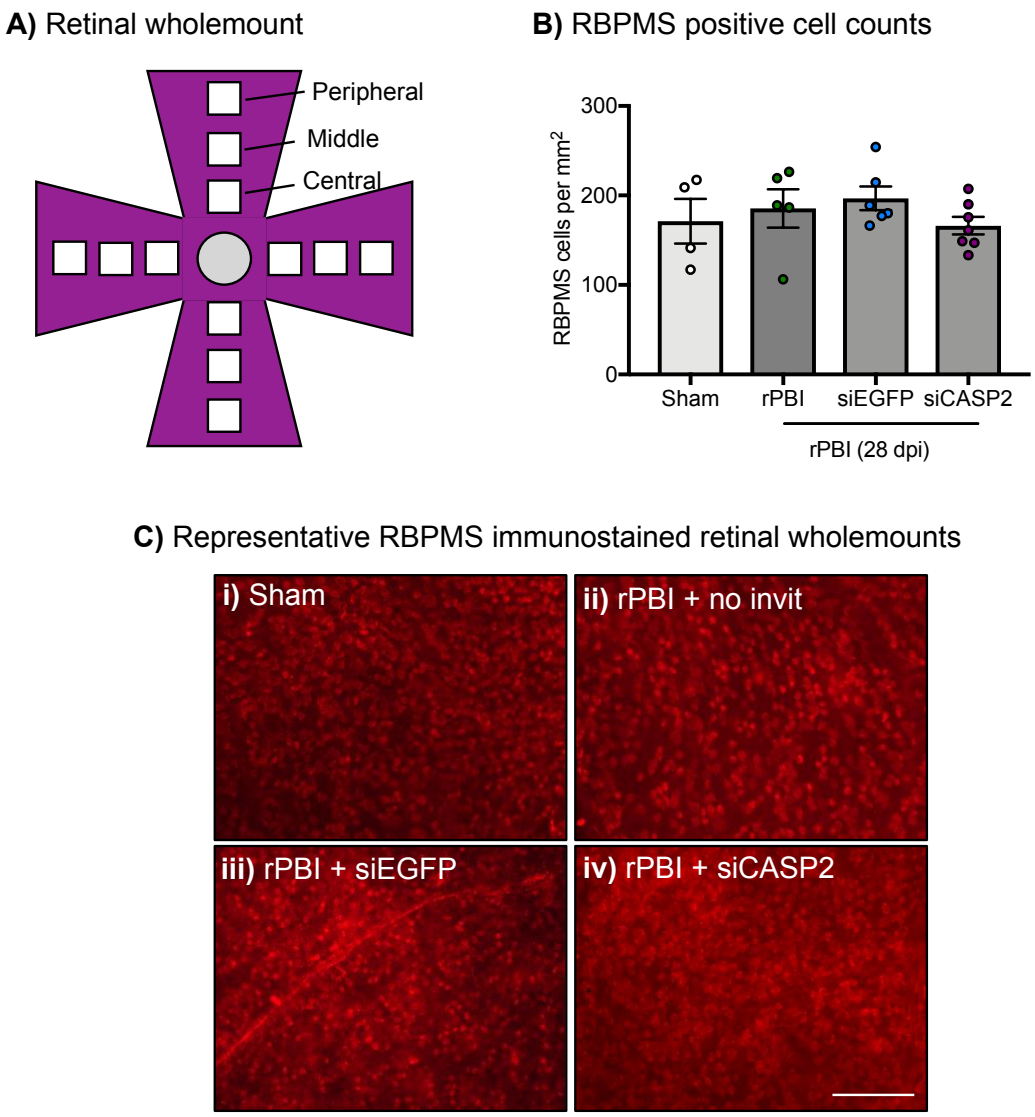


**Figure 18.** Retinal ganglion cell (RGC) counts on retinal wholemounts after delayed siCASP2 intravitreal injections. **A)** RBPMS$^{+}$ RGC were counted in the middle portion of the retinal wholemount leaves. **B)** There are changes in RBPMS$^{+}$ cells in retinal wholemounts in rPBI at 28 dpi with no intravitreal injections (no invit) compared to sham and no differences after intravitreal injections of siEGFP or siCASP2 (ANOVA $p>0.05$). **C)** Representative RBPMS images from the middle portion of the retina in sham and after rPBI with no invitreal injections, siEGFP or siCASP2 injections. Error bars represent mean ± SEM. Scale bar represents 100µm.

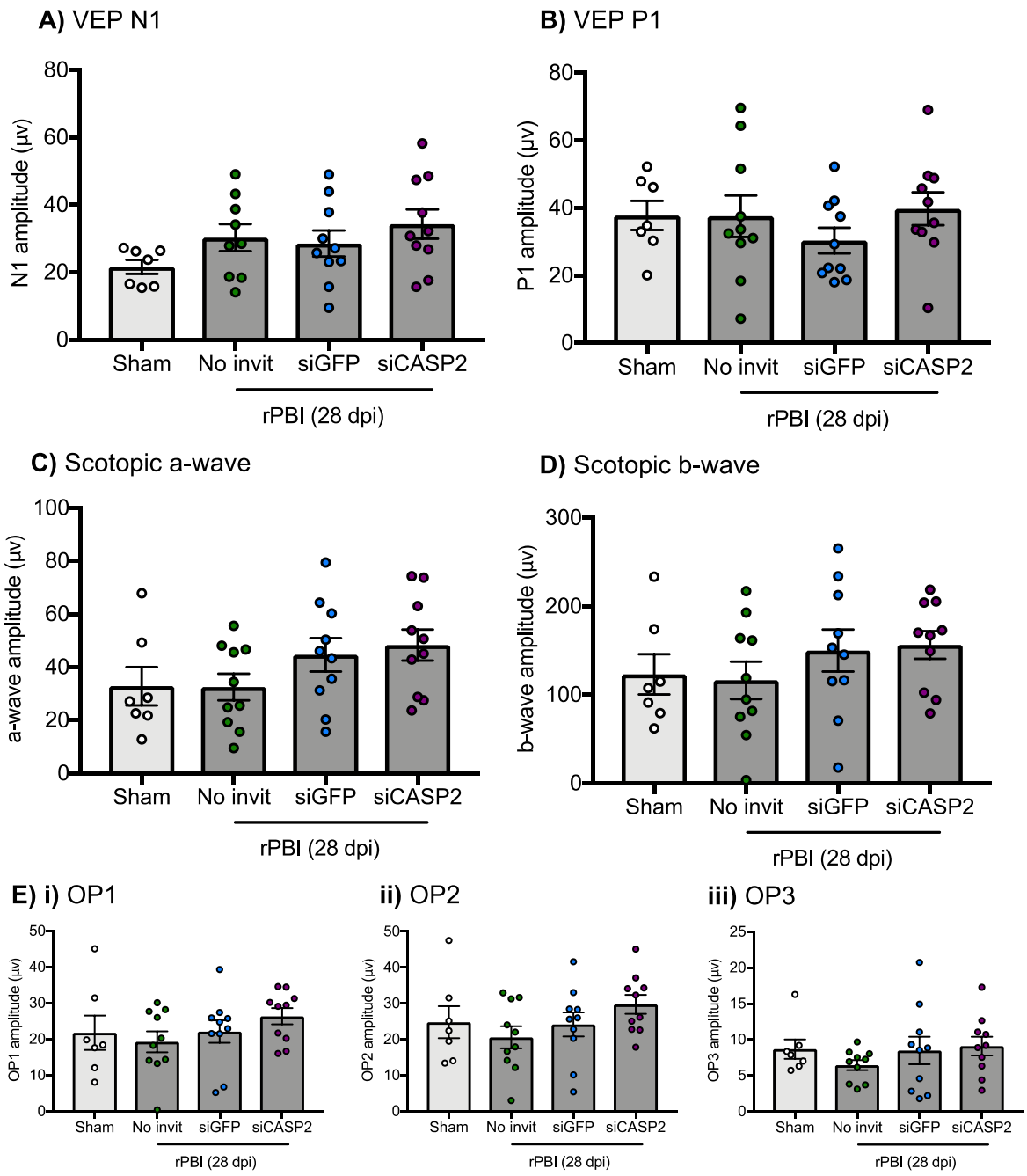


**Figure 5.6. In the delayed siCASP2 study, there were no differences in retinal function after siCASP2 injections at 28 dpi compared with controls.** There were no significant differences in amplitudes of **A)** VEP N1; **B)** VEP P1; **C)** ERG scotopic a-wave **D)** ERG scotopic b-wave, or **E)** oscillatory potential responses (OP). n=10 per group. Error bars represent mean ± SEM.

### 5.3.6. The number of ON axons with degenerative profiles increased up to 28 dpi

Semi-thin resin embedded ON sections were stained with PPD, which stains myelin surrounding ON axons. Intact axons and degenerative profiles were quantified. There were no changes in the total number of intact axons in the ON at 2, 7, 14 or 28 dpi (ANOVA $p=0.133$) (Figure 5.7Ai). However, there was a significant decrease in ON axon density 7 dpi compared to sham (ANOVA $p<0.05$, post-hoc Tukey with multiple comparisons $p=0.0238$) (Figure 5.7C). The lack of change in the number of intact axons but reduction in axon density could suggest ON oedema and hyper gliosis were present. The total number of degenerating axons in the ON increased up to 28 dpi (Figure 5.7Aii; ANOVA $p<0.001$) with an upward trend at 2 dpi and significant elevation at 7, 14 and 28 dpi compared to sham (post-hoc Tukey's multiple comparisons 7 dpi $p<0.001$, 14 dpi $p<0.0001$, 28 dpi $p<0.001$). This elevation in degenerating axons highlights ON pathology at early time points after rPBI.

In addition to ON axons, the ON also has glia which provide structural support through myelination and metabolic support. Glial processes become elongated following rPBI, indicating glial activation and hyper gliosis (Figure 5.7B). ON resin semi-thin sections were also stained with toluidine blue which stains acidic components such as nucleic acids and therefore cells (glia and inflammatory) can be identified. Following rPBI, there were increased numbers of toluidine blue stained cells in the ON, suggesting cellular infiltration. ED1 immunostaining in longitudinal ON sections identified an increase in infiltrating macrophages after rPBI, suggesting that toluidine blue stained cells may correlate with increased ED1 immunostaining. ED1 immunostaining is expanded further in Section 5.3.13.

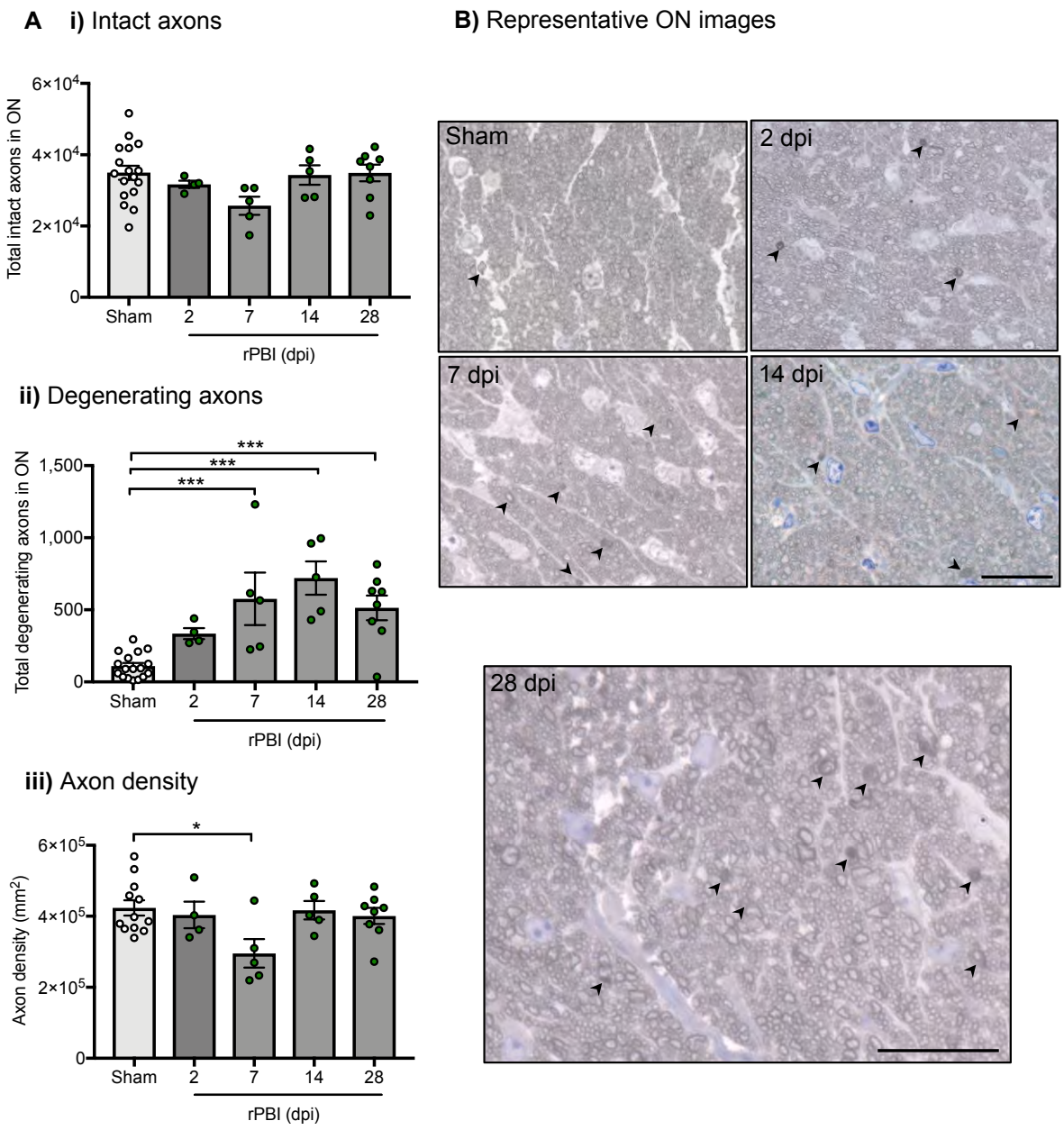


**C)** Mean values for ON axonal counts after rPBI

**Figure 2. A)** ON axon counts in PPD-stained far proximal ON semi-thin sections at 2, 7, 14 and 28 dpi. **i)** Intact axons are not significantly changed up to 28 dpi. **ii)** Degenerating axons increase up to 28 dpi with significant increases at 7, 14 and 28 dpi (ANOVA $p<0.0001$, post-hoc Tukey's multiple comparisons t-tests between sham and rPBI at 7 dpi $p<0.001$, 14 dpi $p<0.0001$, 28 dpi $p<0.001$). **iii)** Axon density decreases between sham and 7 dpi (ANOVA $p<0.05$; post-hoc t-test $p<0.05$) but not at any other timepoint. **B)** Representative PPD and toluidine blue stained semi thin ON sections showing degenerating axons (arrow head) and glial reactivity (*)

Mean ± SEM

**Figure 5.7. ON axon counts in PPD-stained far proximal ON semi-thin sections at 2, 7, 14 and 28 dpi in the rPBI model. A) i)** The number of intact axons were not significantly different up to 28 dpi (ANOVA $p=0.133$). **ii)** The number of degenerating axons increased up to 28 dpi with significant elevation at 7, 14 and 28 dpi compared to sham treated eyes (ANOVA $p<0.0001$, post-hoc Tukey's multiple comparisons between sham and rPBI at 7 dpi $p<0.001$, 14 dpi $p<0.0001$, 28 dpi $p<0.001$). **iii)** Axon density decreased between sham and at 7 dpi (ANOVA $p<0.05$; post-hoc Tukey $p<0.05$) but not at any other time point, suggesting a transient decrease due to oedema and hyper gliosis. **B)** Representative PPD and toluidine blue stained semi thin ON sections showing axons with degenerative profiles (arrow heads) in sham and 2, 7, 14 and 28 dpi. Scale bar represents 20 μm. **C)** Mean values for ON axonal counts after rPBI ± SEM.

### 5.3.7. The delayed siCASP2 protocol caused ON pathology

PPD-stained resin embedded semi-thin ON sections were used to assess the number of intact and degenerating ON axons after rPBI with and without siCASP2 and siEGFP injections (Figure 5.8). The mean values were calculated as total number of axons in the whole ON and the axon density was calculated, these values are displayed in Figure 5.8C. There were no significant differences in mean number of intact axons between sham treated eyes and rPBI treated eyes at 28 dpi with no intravitreal injections or after siCASP2 and siEGFP injections (ANOVA $p=0.156$). But, there was a significant difference in the total number of degenerating ON axons in sham and rPBI treated eyes (no invit, siEGFP and siCASP2) at 28 dpi (ANOVA $p<0.05$). This number was significantly higher after rPBI with no intravitreal injections compared to sham-treated ONs (post-hoc Tukey test $p<0.05$). There was also an increase in the number of degenerating axons after siCASP2 injection (post-hoc Tukey test $p<0.05$) compared with sham, although there were no differences between siCASP2-treated eyes compared to siEGFP-treated eyes, suggesting that siCASP2 did not preserve or increase the number of degenerating ON axons compared with control treated eyes. There was a difference in axonal density between experimental groups (ANOVA $p<0.05$) with a significant reduction in axon density in siCASP2 treated eyes compared to siEGFP treated eyes (post-hoc Tukey $p<0.05$).

There was increased glial reactivity after rPBI which was also present in siEGFP and siCASP2 treated experimental groups. However, GFAP immunostaining on longitudinal ON cryosections showed no obvious differences between groups, but changes might have been too subtle to detect on cryosections (Figure 5.9B). There

was also more infiltrating toluidine blue-stained cells after rPBI, which could be inflammatory cells.

**A i)** Degenerating axons

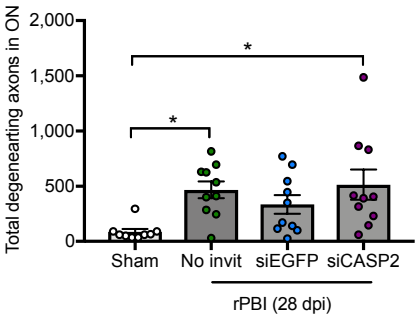


**ii)** Intact axons

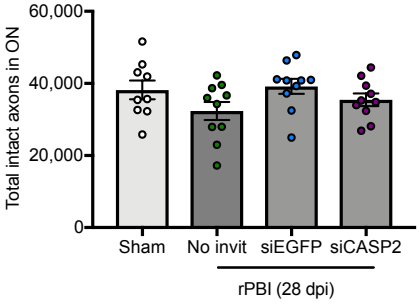


**iii)** Axon density

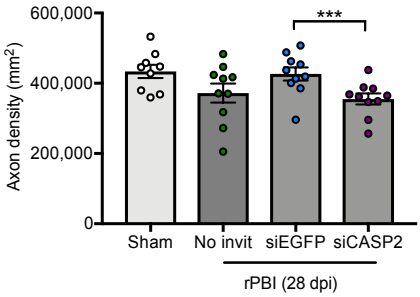


**B)** Representative PPD-stained ON semi-thin images

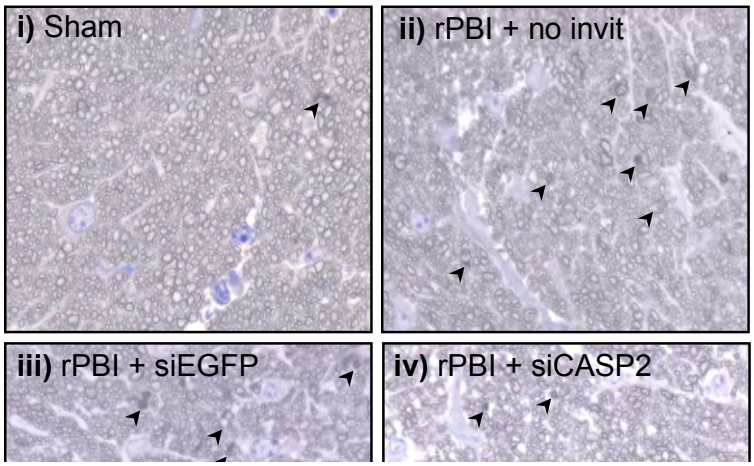


**C)** Mean axon counts for delayed siCASP2 group

| | *Total degenerating axons in ON* | *Total intact axons in ON* | *Axon density (axons per mm²)* |
|---|---|---|---|
| *Sham* | 86.7 ± 26.9 | 38193 ± 2639 | 433727 ± 18997 |
| *rPBI* | 467.0 ± 75.3 | 32351 ± 2541 | 372148 ± 26911 |
| *siEGFP* | 335.5 ± 84.34 | 39190 ± 2082 | 426567 ± 18893 |
| *siCASP2* | 514.0 ± 136.0 | 35451 ± 1770 | 355354 ± 15784 |

Mean ± SEM

Delayed siCASP2 optic nerve counts

| | *Total degenerating axons in ON* | *Total intact axons in ON* | *Axon density (axons per mm²)* |
|---|---|---|---|

**Figure 5.8. rPBI groups displayed increased numbers of ON axons with degenerative profiles compared to sham groups, but axon density was decreased in siCASP2-treated eyes compared to siEGFP treated eyes. A) i)** There was an increase in degenerating ON axons in all rPBI groups compared to sham (ANOVA $p<0.05$), with an increase in rPBI with no intravitreal injections compared to sham (post hoc Tukey with multiple comparisons $p<0.05$) which remained high after siEGFP and siCASP2 injections. **ii)** There were no differences in intact ON axon counts between any groups (ANOVA $p=0.156$). **iii)** But, there was a significant difference in axon density between experimental groups (ANOVA $p<0.05$), with a significant decrease in the rPBI and siCASP2 injection group compared to the rPBI and siEGFP injected group (post-hoc Tukey $p<0.05$). **B)** Representative PPD and toluidine blue stained semi-thin ON sections (degenerating axons; arrowheads). Scale bar represents 20 µm. **C)** Mean values of axon counts ± SEM. n=10 per group. Error bars represent mean ± SEM.

### 5.3.8. An increased number of ED1$^+$ macrophages infiltrate the ON after rPBI

ED1$^+$ macrophages increased in number in the ON after rPBI although this did not reach statistical significance, with 2.09 ± 0.68 ED1$^+$ cells per mm$^2$ detected in sham treated eyes compared to 10.11 ± 3.69 ED1$^+$ cells per mm$^2$ in rPBI treated eyes which received no intravitreal injections (ANOVA p=0.23) (Figure 5.9A). There was also a tendency in rPBI treated eyes to have higher numbers of ED1$^+$ cells after siEGFP and siCASP2 injections compared with those that were not treated with injections. However, this did not reach statistical significance (21.79 ± 13.21 ED1$^+$ cells per mm$^2$ in siEGFP treated eyes and 28.73 ± 12.21 ED1$^+$ cells per mm$^2$ in siCASP2 treated eyes). GFAP immunostaining displayed no changes between groups. However, PPD-staining was performed on thin cross sections whereas GFAP immunostaining was performed on thicker longitudinal sections, so GFAP immunostaining may not have detected subtle changes.

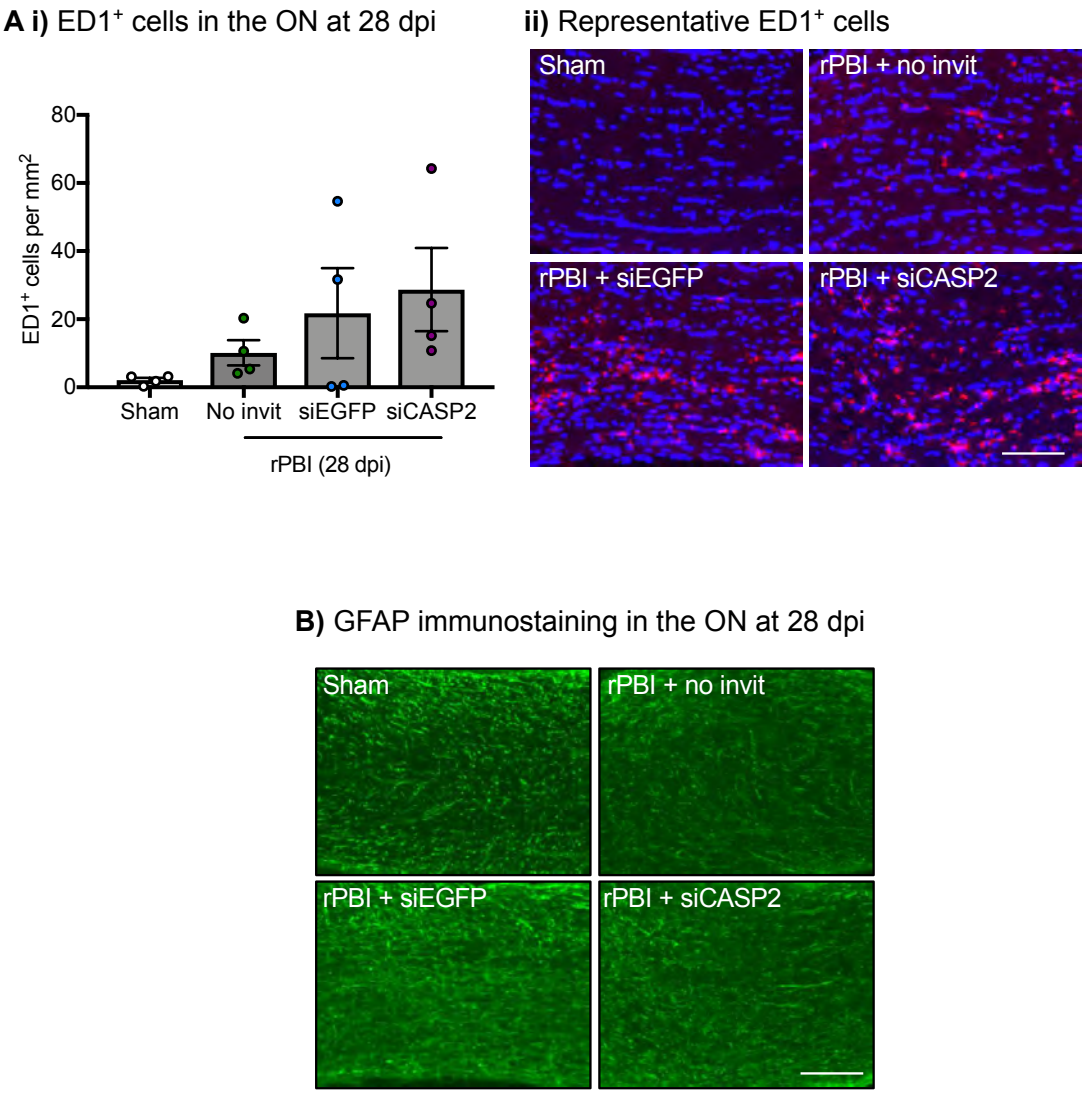


**Figure 17. A) i)** ED1$^+$ cells increase in the ON at 28 dpi after rPBI with no intravitreal injections and with siEGFP and siCASP2 injections (ANOVA p>0.05 with post-hoc t-test with multiple comparisons p____). **B)** GFAP immunostaining in the ON at 28 dpi, there are no differences in glial reactivity after rPBI or with siEGFP and siCASP2 injections. Error bars represent ± SEM. Scale bar represents 100µm.

Due to the results of OCT imaging, indicating possible vitreal inflammation in rPBI treatment groups (hyper-reflective vitreous dots), I performed an additional study in which siCASP2 was injected prior to the blast injury with an endpoint of 14 dpi. This injection time is not clinically practical, but, the study provides an indication of whether siCASP2 treatment has a neuroprotective or axon-protective effect and I predicted I would see fewer vitreal hyper reflective dots if the intravitreal injections were not performed in close proximity with the blast injury.

### 5.3.9. Pre-blast siCASP2 injections have no effect on retinal thickness or the number of vitreal hyper reflective dots in OCT images.

siCASP2 or siEGFP were bilaterally injected 48 hours pre-blast injury and tissue collected at 14 dpi. OCT imaging was performed throughout the experiment to determine the effect of intravitreal injections on vitreal and retinal imaging, total retinal and GCC thickness and the number of hyper-reflective vitreal dots. There were few vitreal opacities detected in eyes treated with rPBI alone at 14 dpi or with siEGFP or siCASP2 intravitreal injections (Figure 5.10A and Figure 5.10D), but 2 out of 5 sham treated right eyes that were injected with sterile PBS had vitreal opacities.. There were no left eyes (both injected and not injected) showing any inflammation. There were no statistically significant changes in retinal or GCC thickness between any groups at 14 dpi (ANOVA retinal thickness $p=0.7667$ and GCC thickness $p=0.1016$) (Figure 5.10C). For example, the mean retinal thickness in sham treated eyes was 113.2 ± 0.71 pixels compared to 111.6 ± 1.86 pixels in rPBI treated eyes without intravitreal injections, and similar thicknesses were observed after rPBI with siEGFP injection (114.5 ± 2.33 pixels) and siCASP2 injection (114.0 ± 1.77 pixels). Mean GCC thickness measurements in sham treated eyes (35.44 ± 1.01 pixels), rPBI treated eyes with no

intravitreal injections (34.89 ± 0.65), and rPBI treated eyes with siEGFP injections (37.8 ± 1.06) or siCASP2 injections (36.5 ± 0.63) also showed no differences.

**A** OCT experimental design

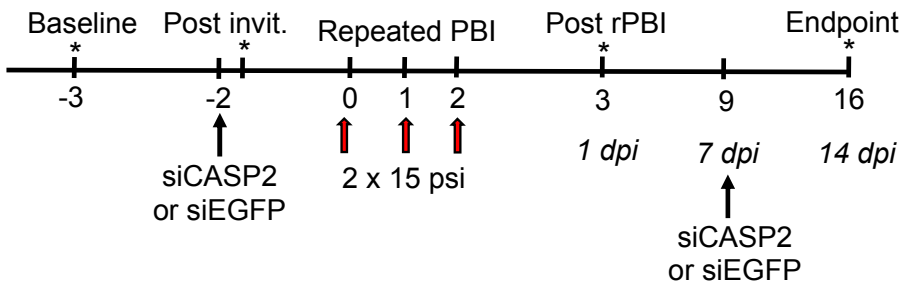


**B** OCT representative images

**i)** Left eye (direct blast)

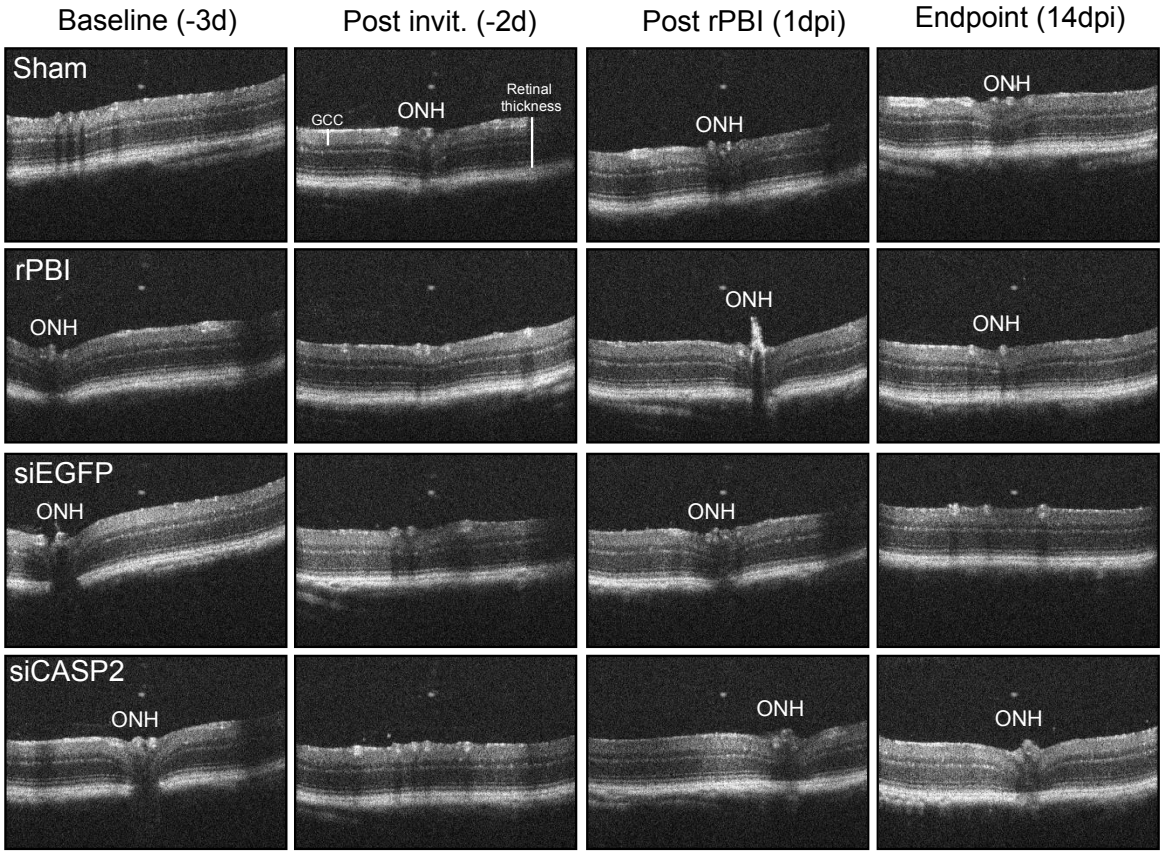

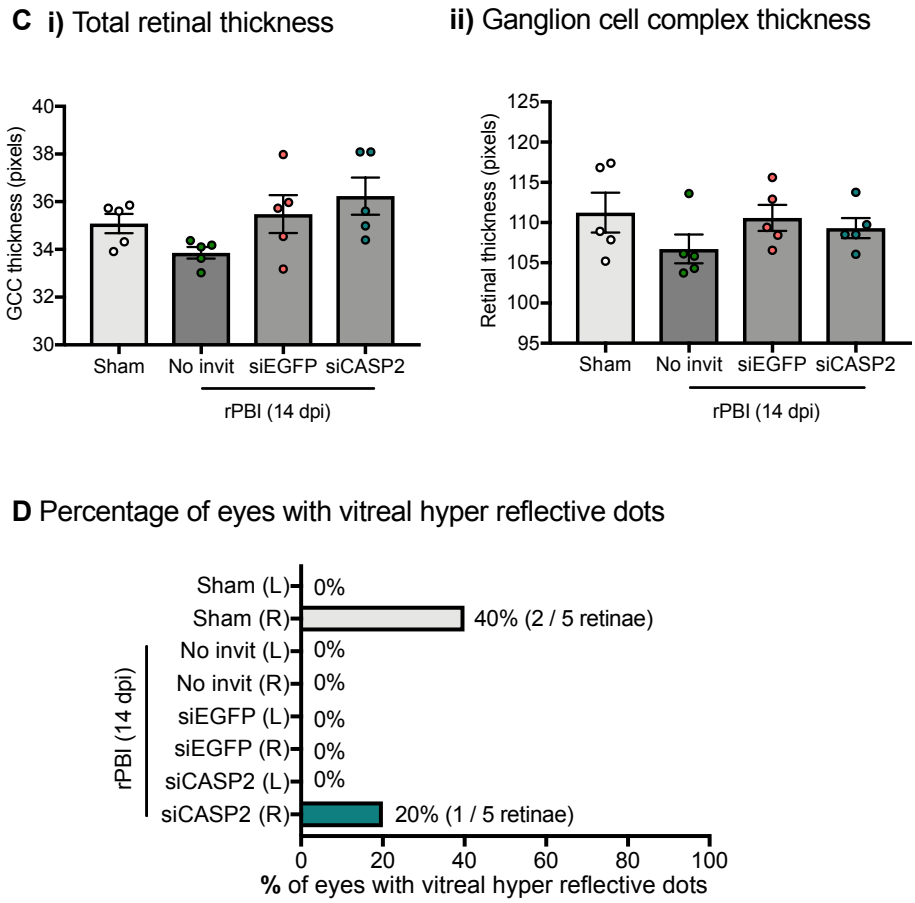


**Figure 6.** Optical coherence tomography (OCT) imaging**. A)** Experimental design of OCT timepoints. **B)** Representative OCT images at the optic nerve head showing no gross structural changes between sham and rPBI or after vehicle or Nec-1s intravitreal injections at 14 dpi. **C) i)** There is a significant decrease in total retinal thickness at 14 dpi after rPBI with no intravitreal injections (stats) **ii)** but no differences in ganglion cell complex thickness. There is no effect after siEGFP or siCASP2 injections on total retinal or ganglion cell complex thickness. Error bars represent mean ± SEM.

### 5.3.10. There were no changes in the number of RBPMS$^+$ RGC after pre-blast siCASP2 injections

The number of RBPMS$^+$ RGCs were counted in retinal cryosections from the central (closest to the ONH), middle and peripheral portion of the retina (Figure 5.11). There were no statistically significant differences between any groups in the peripheral (ANOVA with Bonferroni correction for multiple comparisons [correction factor of 3], p=1.65), middle (ANOVA p=0.1965) or central (ANOVA p=0.21) retinal sections, suggesting that RGCs do not degenerate after rPBI alone or when intravitreal injections are given before rPBI. The mean values for sham, rPBI with no intravitreal injections and rPBI with siEGFP and siCASP2 injection groups are displayed in Figure 5.11C.

### 5.3.11. Pre-blast siCASP2 treatment did not affect ERG and VEP amplitudes

ERG and VEP were recorded to measure retinal function. There were no significant effects on VEP N1 amplitudes (ANOVA p=0.637) and P1 amplitudes (ANOVA p=0.656) (Figure 5.12A-B). There were also no effects on ERG amplitudes measured for scotopic a-waves (ANOVA p=0.585) or b-waves (ANOVA p=0.862) after rPBI alone at 14 dpi or after rPBI with intravitreal injections of siCASP2 or siEGFP (Figure 5.12C-E). There was also no effect on oscillatory potential responses. Baseline values include all mice (n=20) and experimental groups have n=5 mice each.

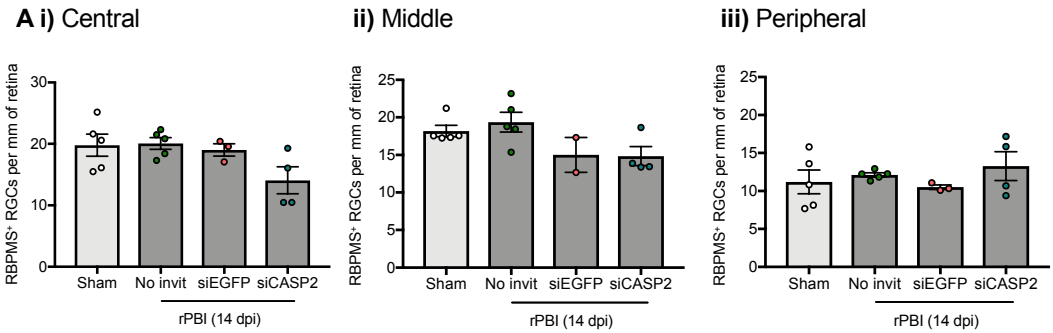


**B)** Representative RBPMS images

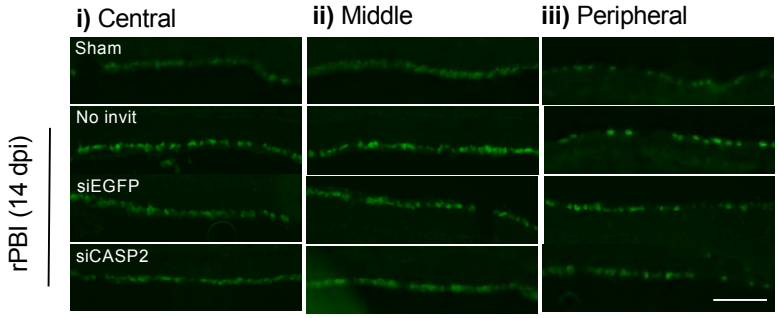


**C)** Mean RBPMS+ RGC counts

| | RBPMS+ RGCs per mm of retina (mean ± SEM) | | |
|---|---|---|---|
| Treatment | Central | Middle | Peripheral |
| Sham | 19.79 ± 1.80 | 18.19 ± 0.76 | 11.2 ± 1.56 |
| rPBI + no invit | 20.07 ± 0.95 | 19.36 ± 1.31 | 12.11 ± 0.26 |
| rPBI + siEGFP | 19.01 ± 1.01 | 15.00 ± 2.32 | 10.5 ± 0.30 |
| rPBI + siCASP2 | 14.07 ± 2.18 | 14.84 ± 1.27 | 13.27 ± 1.91 |
| ANOVA (with Holms Bonferroni correction) | p=0.21 | p=0.131 | p=0.55 |

**Fi** **after**
**pr** ted in
thı etina.
Th ıps in
pe sons,
p=0.55), middle (ANOVA p=0.131) or central (ANOVA p=0.21) sections. B) Representative images of RBPMS+ RGCs. C) Mean number of RBPMS+ RGCs per mm of retina. Scale bar represents 100 µm. Error bars represent mean ± SEM. n=5 animals per group.

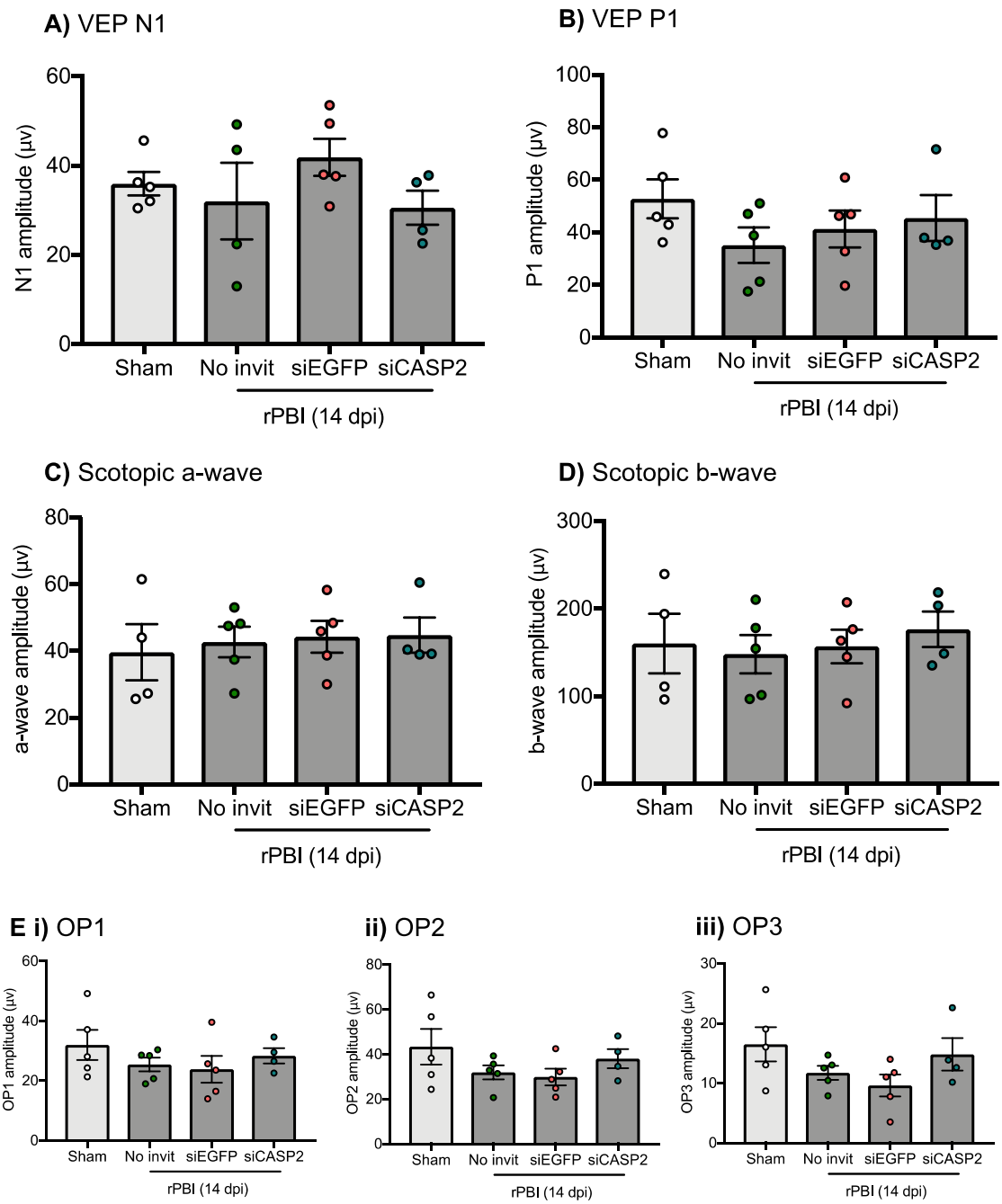


**Figure 5.12. Pre-blast siCASP2 injections did not induce any changes in ERG amplitudes at 14 dpi.** There were no significant effects between shams or after rPBI treated eyes with either no intravitreal injections or injections of siEGFP or siCASP2 in **A)** VEP N1; **B)** VEP P1; **C)** scotopic a-wave or **D)** scotopic b-wave ERG amplitudes or **E) (i-iii)** oscillatory potential (OP) amplitudes. Error bars represent mean ± SEM. n=5 animals per group.

### 5.3.12. Pre-blast siCASP2 injections reduced the number of degenerating ON axons compared to siEGFP treated eyes.

PPD-stained resin semi-thin ON sections were used to assess the number of intact and degenerating ON axons after rPBI and following rPBI in combination with intravitreal injections of siCASP2 or siEGFP (n=5 mice per group) (Figure 5.13). The mean values for the number of intact and degenerating axons in the ON were calculated as well as axon density displayed as the number of axons per $mm^2$. There were no significant differences in the number of intact axons between sham and rPBI treated eyes with no intravitreal injections at 14 dpi (ANOVA $p=0.214$) (35469 ± 677.1 axons in sham compared to 34301 ± 2737 axons in rPBI treated eyes) or following rPBI with siCASP2 or siEGFP intravitreal injections (34019 ± 2104 axons in rPBI with siCASP2 injections compared to 29610 ± 1875 axons in rPBI with siEGFP injections). However, there was a significant elevation in the total number of degenerating ON axons in rPBI treated eyes with no intravitreal injections compared to sham at 14 dpi, with 130 ± 26.6 axons in sham compared to 720 ± 116.2 axons in rPBI treated eyes (ANOVA $p<0.0001$, post hoc Tukey with multiple comparisons $p<0.0001$). Following rPBI with injections of siCASP2 or siEGFP, there was a decrease in the number of degenerating ON axons, suggesting a possible axon-protective effect of intravitreal injections. However, there was a further decline in the number of degenerating ON axons in siCASP2 treated eyes compared to siEGFP treated eyes (166 ± 22.1 axons in siCASP2 treated compared to 80 ± 18.23 axons in siEGFP treated eyes), suggesting a greater neuroprotective effect of siCASP2 (post-hoc Tukey $p<0.05$). There were significant differences in ON axonal density across groups (ANOVA $p<0.05$), with a lower axon density in rPBI treated eyes with siCASP2 injection compared to sham

(post hoc Tukey with multiple comparisons $p<0.05$). For example, there were 429321 ± 21949; 416979 ± 25809; 385309 ± 6855 and 367916 ± 12521 axons per $mm^2$ in sham, rPBI with no intravitreal injections, and rPBI with siEGFP and rPBI with siCASP2 injections, respectively. ON axon quantification suggested there was additional ON neuroprotection with siCASP2 treatment compared to siEGFP. However, there was also a lower ON axon density, in rPBI treated eyes with siCASP2 injections suggesting the presence of gliosis or ON oedema.

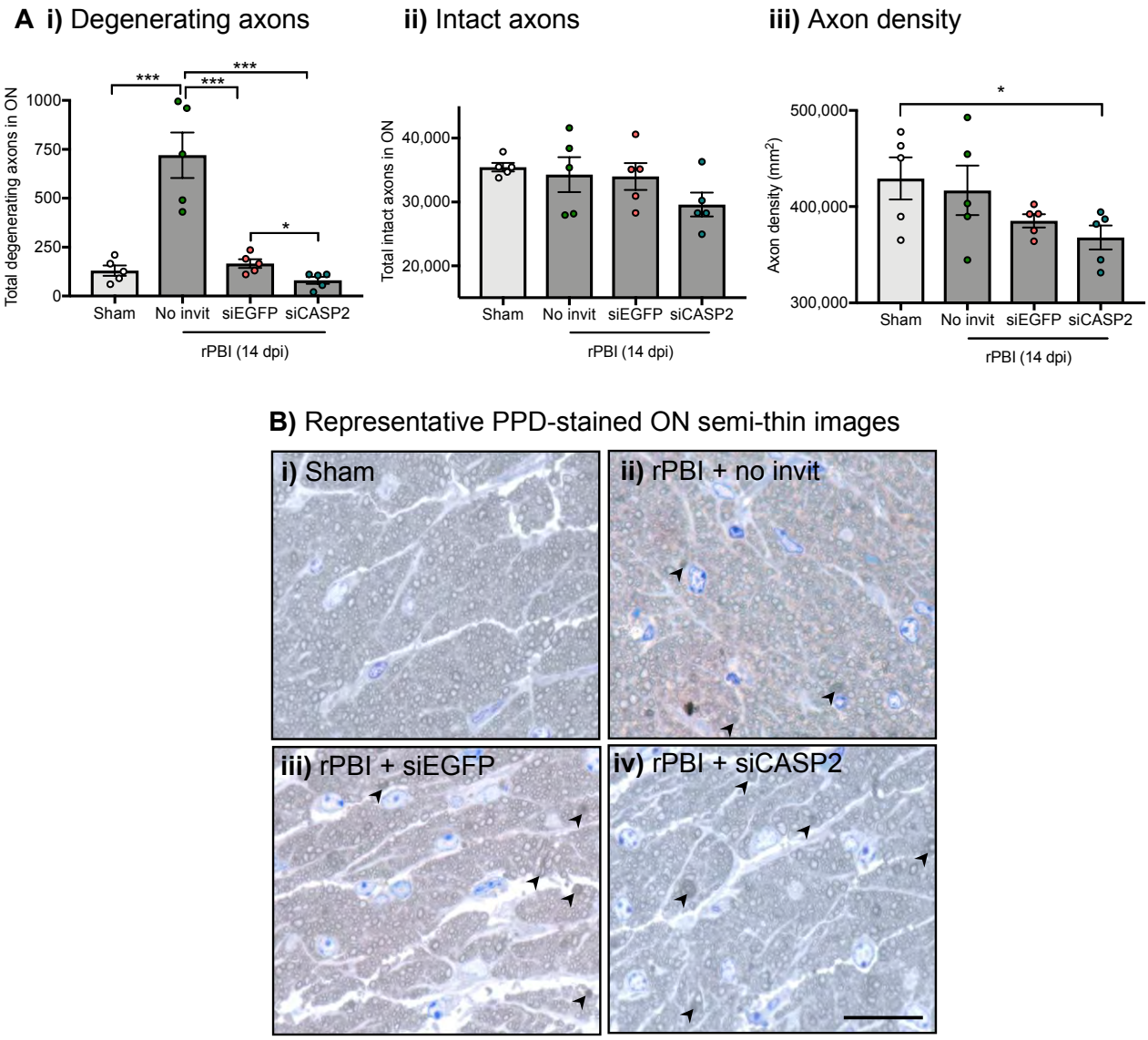


**Figure 9.** Axonal counts in PPD stained far proximal ON semi-thin sections at 2 weeks after pre-blast siCASP2 intravitreal injection **A) i)** There are increased degenerating axons in the whole ON after rPBI with no intravitreal injections compared to sham (_____). There are decreased degenerating axons after rPBI with siEGFP and siCASP2 intravitreal injections (post-hoc t-test _____) and a further decline in degenerating axons after siCASP2 compared to siEGFP intravitreal injection. **(ii-iii)** There are no differences in intact axons or axon density. **B)** Representative PPD and toluidine blue stained resin ON semi-thin sections with degenerating axons (arrowheads). Error bars represent ± SEM.

**Figure 5.13. ON axonal counts in PPD stained far proximal ON semi-thin sections in the pre-blast siCASP2 study at 14 dpi. A) i)** There were increased number of degenerating axons in the ON after rPBI with no intravitreal injections compared to sham (ANOVA $p<0.0001$, post hoc Tukey $p<0.001$) and fewer degenerating axons following rPBI with siEGFP and siCASP2 injections (post-hoc Tukey $p<0.001$ for both), with a further reduction in the number of degenerating axons treated with siCASP2 compared to siEGFP injections, indicating an additive ON neuroprotective effect of siCASP2 (post hoc Tukey $p<0.05$). **ii)** There were no differences in the number of intact ON axons (ANOVA $p=0.214$), **iii)** but there was a difference in axon density across groups (ANOVA $p<0.05$) with a decrease in the siCASP2 treated group compared to sham (post hoc Tukey with multiple comparisons $p<0.05$). **B)** Representative PPD and toluidine blue stained resin ON semi-thin sections with degenerating axons (arrowheads). Scale bars represent 20 μm. Error bars represent mean ± SEM. n=5 animals per group.

### 5.3.13. Infiltrating ED1$^+$ macrophages were detected in the ON at 14 dpi

In semi-thin ON sections, there were more toluidine blue stained cells in all groups at 14 dpi, indicating there was cell infiltration after rPBI (Figure 5.13B). Longitudinal ON sections were immunostained for ED1 (Figure 5.14) and demonstrated an increasing trend in the number of ED1$^+$ cells in rPBI treated eyes with no intravitreal injections (8.40 ± 2.20 ED1$^+$ cells per mm$^2$) compared to sham (0.75 ± 0.17 ED1$^+$ cells per mm$^2$) but did not reach statistical significance (ANOVA p=0.075). ED1$^+$ cell numbers remained high following rPBI with intravitreal injections of siEGFP (12.96 ± 3.82 ED1$^+$ cells per mm$^2$) and siCASP2 (9.77 ± 3.37 ED1$^+$ cells per mm$^2$).

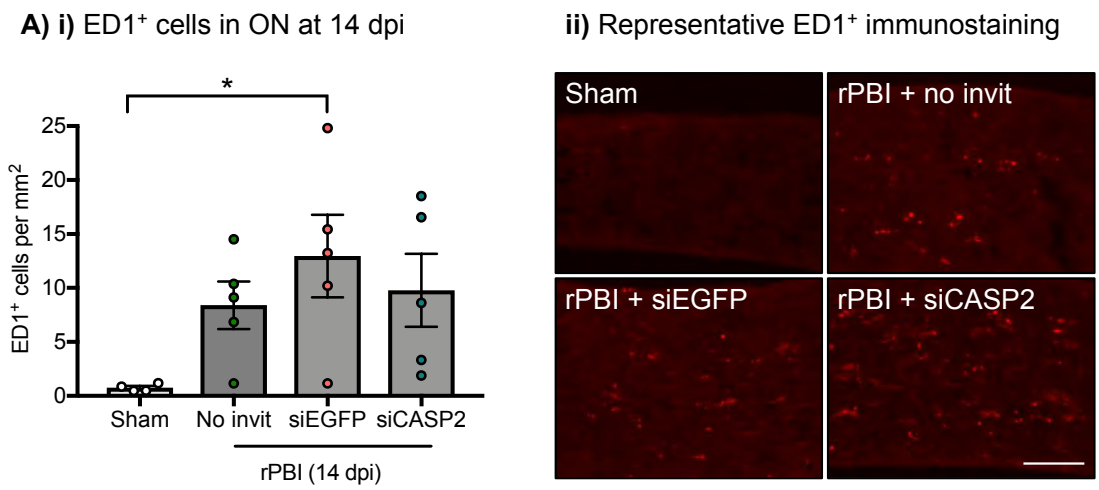


**Figure 11. A)** ED1⁺ cells in the ON at 14 dpi. **i)** There is an increase after rPBI with no intravitreal injections and with siEGFP and siCASP2 injections (ANOVA post hoc t-test with multiple comparisons _____). **ii)** Representative ED1⁺ cell immunostaining in the ON at 14 dpi. Scale bar represents 100μm.

### 5.3.14. There was a small hole in the sclera, which did not heal, caused by delayed intravitreal siCASP2 treatment injections but not after pre-blast siCASP2 treatment.

In the delayed siCASP2 study, I observed that a small hole in the sclera was formed by the needle used for injections that did not heal sufficiently before the second and third blast waves produced more inflammation and trauma mimicking an open globe injury caused by a penetrating object. This was not observed after pre-blast siCASP2 injections in the pre-blast siCASP2 study.

### 5.3.15. Characterisation of the effects of intravitreal injection in sham eyes

To test the effects of intravitreal injections without rPBI, 2 µl of sterile PBS was injected into the right eyes of sham treated mice, with the left eyes receiving no intravitreal injections. Sham treated mice in the pre-blast siCASP2 study received intravitreal injections in the right eye, at 2 days before blast at 5 dpi and 12 dpi and culled at 14 dpi (experimental design in Figure 5.1C). Intact and degenerating ON axons and axon density were quantified (Figure 5.15A). There were no differences in total number of degenerating axons (130 ± 26.06 in sham compared to 266 ± 83.48 in PBS injected; unpaired student t-test p=0.159) or axon density (429321 ± 21949 in sham compared to 459931 ± 22047 in PBS injected; student t-test p=0.354). However, there was a significant decrease in the number of intact axons in sham treated eyes compared to PBS injected eyes (35469 ± 677.1 compared to 41288 ± 1739; unpaired students t-test p=0.0143), suggesting that there were fewer intact axons in the ON of sham treated mice which have had the blast blocked compared to the contralateral eye receiving intravitreal injections.

ERG scotopic a-wave and b-wave amplitudes and N1 and P1 VEP amplitudes were also analysed (Figure 5.15B).There were no differences in the amplitudes of N1 (35.94 μV ± 2.64 compared to 40.34 μV ± 2.68; t-test p=0.276), P1 (52.8 μV ± 7.45 compared to 49.03 μV ± 7.14; t-test p=0.725), scotopic a-waves (39.62 μV ± 8.39 compared to 45.35 μV ± 8.94; t-test p=0.662) and scotopic b-waves (160.4 μV ± 34.0 compared to 188.6 μV ± 30.0; t-test p=0.552) between groups.

A summary of the results found in the pre-blast siCASP2 study and delayed siCASP2 study are shown in Table 5.1.

**A)** ON axonal quantification

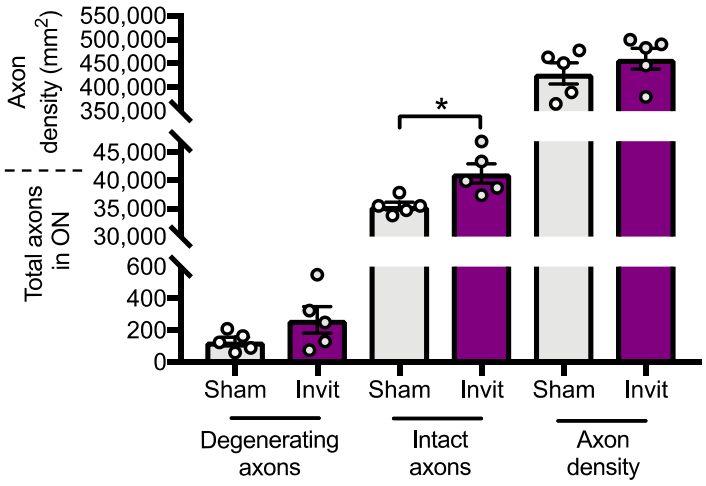


**B)** ERG and VEP amplitudes

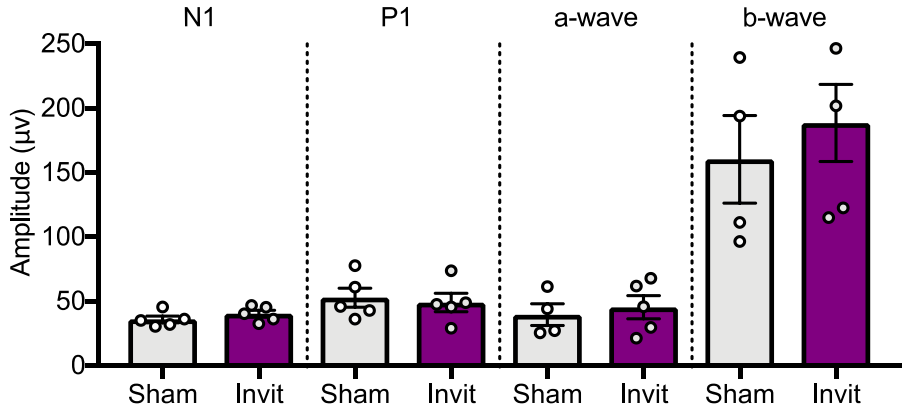


**Figure 5.15. Intravitreal injections of sterile PBS into the right eye of sham treated eyes did not affect the number of degenerating axons or axon density, but was associated with a greater number of intact axons, and there were no changes in ERG and VEP amplitude.** Left sham treated eyes received no intravitreal injections and right (contralateral) eyes received sterile PBS injections. **A)** There were no changes in the number of degenerating ON axons or axon density after sterile PBS intravitreal injections. However, there was a significant increase in the number of intact ON axons after sterile PBS injections compared to non-injected sham treated eyes (unpaired t-test p=0.0143). **B)** There were no differences in ERG or VEP amplitudes in sham treated eyes or the contralateral eyes receiving intravitreal PBS injections, indicating that intravitreal injections did not cause changes in retinal function. n=5 animals per group. Error bars represents mean ± SEM.

| Endpoint | "Delayed siCASP2" study at 28 dpi | "Pre-blast siCASP2" study at 14 dpi |
|---|---|---|
| Vitreal inflammation on OCT imaging | Lots of vitreal inflammation in left directly blasted eyes and less in contralateral eyes. | Minimal vitreal inflammation |
| Total retinal and GCC thickness | No effect with rPBI +/- siCASP2 / siEGFP | No effect with rPBI +/- siCASP2 / siEGFP |
| RGC count | No reduction in number of $RBPMS^+$ RGCs with rPBI +/- siCASP2 / siEGFP on retinal whole mounts | No reduction in number of $RBPMS^+$ RGCs rPBI +/- siCASP2 / siEGFP on retinal cryosections |
| Retinal function | No effect on VEP or ERG amplitudes with rPBI +/- siCASP2 / siEGFP | No effect on VEP or ERG amplitudes with rPBI +/- siCASP2 / siEGFP |
| Degenerating ON axons | Increased number after rPBI which remains high after siEGFP or siCASP2 | Increased number after rPBI but reduces after siCASP2 or siEGFP. Further decrease after siCASP2 compared to siEGFP |
| Intact ON axons | No effect with rPBI +/- siCASP2 / siEGFP | No effect with rPBI +/- siCASP2 / siEGFP |
| Axon density | No effect from rPBI but a decrease after siCASP2 compared to siEGFP | No effect from rPBI but a decrease after siCASP2 compared to sham |
| $ED1^+$ cells in ON | No statistically significant differences in $ED1^+$ cell numbers. | Increased number of $ED1^+$ cells in the ON and significant increase in counts in sham compared with siEGFP treatment |

**Table 5.1. Summary of findings with "delayed siCASP2" and "pre-blast siCASP2" studies.**

## 5.4. Discussion

### 5.4.1. ED1$^+$ macrophages infiltrate the OPL at early time points after rPBI

ED1 stains circulating monocytes (e.g. macrophages) and resident monocytes (e.g. microglia). Macrophage infiltration can be advantageous after injury because macrophages phagocytose debris and allow for tissue repair (Stoll et al., 1989). Furthermore, oncomodulin$^+$ macrophages can promote RGC survival and axonal regeneration (Yin et al., 2006, Yin et al., 2009). ED1$^+$ cells were present in the OPL 3 days after rPBI, which suggests that there could be degeneration of photoreceptors or INL cells at early time points after blast injury, and macrophages have been recruited to the site of injury to clear debris. However, macrophages can be damaging if inflammation persists beyond tissue resolution and repair (Duffield, 2003).

### 5.4.2. Caspase-2 is cleaved and localised to RGC after blast injury

Caspase-2 mediates neuronal death in neurodegenerative disease, including Alzheimer's disease (Zhao et al., 2016, Troy et al., 2000) and after traumatic ocular injuries, including direct TON, as in the ONC model (Vigneswara et al., 2014, Vigneswara and Ahmed, 2016, Vigneswara et al., 2012) and indirect TON, as in the blunt ocular trauma model (Thomas CN, 2018). In this study, I detected a possible increase in 35kDa and 15kDa cleaved caspase-2 fragments 7 days after rPBI, suggesting that caspase-2 is cleaved and activated at this time point after blast injury. But, further investigation and quantification is required; therefore, no real conclusions can be drawn from this data, until further experiments are performed.

### 5.4.3. The timing of siCASP2 intravitreal injections have varied effects

Intravitreal injections of siCASP2 can be used to knockdown *casp2* mRNA and subsequent protein expression (see section 1.7.7.3 for more details on siCASP2-mediated knockdown). siCASP2 was intravitreally injected at two different time points surrounding the blast injury which had varied effects. In the original study, I performed bilateral siCASP2 injections 5 hours after the first blast followed by two further blasts (delayed siCASP2 study); however, at the end of the study, at 28 dpi, there were hyper-reflective dots in the vitreal cavity in the OCT imaging of eyes receiving siCASP2 injections and blast injuries, which may have been infiltrating macrophages (Kokona et al., 2017), and fewer in the contralateral eyes which received indirect blast injuries and equivalent siCASP2 treatment. Another experiment was set up to determine if giving injections before the blast injury caused the same effect. I performed intravitreal injections 48 hours before all three blasts of the rPBI (pre-blast siCASP2 study) and assessed outcomes at 2 weeks.

Treatment with a therapeutic intravitreal injection after a blast injury might be possible in real-life situations; for example, a victim could be injured by an explosive blast wave and receive treatment after the initial blast injury when symptoms appear. A prophylactic siCASP2 intravitreal injection would not be practical or well received. However, in experimental paradigms it does provide us with information on the mechanistic effects of caspase-2 knockdown without the complications of inflammation and pathology caused by blast injuries and intraocular injections in close proximity.

The effects on ocular pathology of these two time points of intravitreal injections are further discussed.

### 5.4.4. RGCs did not degenerate 28 dpi and siCASP2 injections had no effect

RGCs were counted by two methods, depending on the process of tissue collection. Both methods are commonly used RGC quantification techniques (Mead et al., 2014, Mead and Tomarev, 2016). At both 14 and 28 dpi, in pre-siCASP2 and delayed treatment groups, there were no changes in $RBPMS^+$ RGC numbers detected in either retinal cryosections or in the middle portion of the retina in whole mounts, suggesting that in my study, RGCs do not degenerate up to 1 month after rPBI. Alternatively, there could be reduced RGC numbers in focal pockets of the retina, which is consistent with previous studies showing $TUNEL^+$ staining after single 26 psi blast exposure (Bricker-Anthony et al., 2014b). This might not have been detected using our quantification methods. Other studies of blast wave exposure have shown a reduction in RGCs at much later time points, with GCC thinning at 4 months post exposure (Dutca et al., 2014, Mohan et al., 2013), suggesting that RGC death could be progressive after injury and later time points should be investigated.

### 5.4.5. There were no changes in retinal thickness after rPBI in the pre-blast or delayed siCASP2 studies

To assess retinal layer thickness and ocular inflammation, *in vivo* retinal OCT imaging was performed. The GCC thickness measurement consists of the RNFL, IPL and the GCL. A reduced GCC thickness partly correlates with RGC degeneration (Cennamo et al., 2013, Kanamori et al., 2012), as the RNFL consists of RGC axons, although,

RGC loss does not always correlate with RNFL thinning (Mead and Tomarev, 2016). In the ONC model, the degree of RGC loss is under-estimated by measuring the RNFL thickness; for example, at 7 dpi the RNFL is 40% thinner when ~50% of RGCs are lost (Mead et al., 2013, Berkelaar et al., 1994). At 4 months post injury, there is 70% RNFL thinning when 98% of RGC are lost (Rovere et al., 2015). In contrast, in ocular hypertension models, RNFL measurements provide an overestimation of RGC loss (Chen et al., 2015, Mead et al., 2016). These studies suggest that RNFL measurements may be useful for indicating retinal changes but cannot be accurately used to assess RGC loss. In additional to RGC axons, the RNFL also contains blood vessels, astrocytes, displaced amacrine cells and macrophages; therefore, activated gliosis may cause increased RNFL thickness after injury. In a repeated blast injury model using acoustic blast induction, there was increased retinal thickness, which correlates with reactive gliosis and persisted up to 8 months (Allen et al., 2018). In my study, there were no changes in retinal thickness at 14 or 28 dpi and siCASP2 or siEGFP injections had no effect.

### 5.4.6. There was no vitreal inflammation after rPBI or after pre-blast siCASP2 injections but delayed siCASP2 injections did cause vitreal inflammation

Hyper reflective dots in the vitreal cavity in OCT images can indicate infiltrating inflammatory cells, including macrophages, and breakdown of the blood retinal barrier secondary to inflammation (Kokona et al., 2017). It is likely that these hyper reflective dots are inflammatory cells, rather than the contents of the intravitreal injection, as there were no hyper reflective dots present in the OCT images immediately after intravitreal injections in the pre-blast siCASP2 study (Figure 6.10). There were no

vitreal hyper reflective dots at 14 or 28 dpi in animals receiving rPBI without intravitreal injections, suggesting that there was not likely to be vitreal inflammation induced by the overpressure blast alone, at least at the time points analysed. The majority of left eyes that were directly blasted and injected with siEGFP or siCASP2 did have increased vitreal hyper reflective dots on OCT images compared with the contralateral eye receiving indirect blast and mild blunt injuries, suggesting that the combination of intravitreal injection and direct rPBI may cause additive vitreal inflammation.

In the delayed siCASP2 study, I observed that a small hole in the sclera formed by the needle from injections that did not heal sufficiently before the second and third blast waves. This is likely to have led to more inflammation and trauma mimicking an open globe injury caused by a penetrating object. This was not observed with pre-blast siCASP2 injections in the pre-blast siCASP2 study. In both experiments, I moved the intravitreal injection site to prevent a persistent hole in the sclera. I cannot provide a sufficient explanation for this hole, but perhaps a blast overpressure wave after the injection heightened inflammation and prevented healing.

ED1 immunostaining can be performed to confirm the presence of circulating or resident macrophages (microglia) in the retina. The tissue derived from the delayed siCASP2 study was collected for retinal whole mounts and could not be stained for this purpose. In Chapter 6, I describe eyes which received either vehicle (10% DMSO, 0.9% methyl-β-cyclodextrin in PBS) or Nec-1s intravitreal injections at equivalent time points to the siCASP2 delayed study, that showed an increase in $ED1^+$ cells in the retina after vehicle injections, which correlated with the presence of vitreal hyper

reflective dots on OCT images, suggesting that more macrophages infiltrate the retina following rPBI in combination with intravitreal injection after the first blast. This observation has important implications for treatment plans and intravitreal injections must be administered with caution in close proximity to the time points of injury.

### 5.4.7. rPBI causes greater pathology than a single blast

My study used a unilateral rPBI model, in which the left eye is directly exposed to a blast overpressure wave (Bernardo-Colon et al., 2018, Vest et al., 2019), but the right eye also receives some blunt trauma (Bricker-Anthony and Rex, 2015). A pressure transducer recorded the blast pressure at 14-17 psi before and immediately after blast induction. In sham treated animals, the blast wave was blocked by reinforced cardboard and the pressure was recorded at ~2 psi, suggesting that the cardboard successfully blocked the majority of the blast pressure wave.

Previous studies have investigated a single overpressure blast wave on head and ocular pathology and demonstrated progressive and delayed retinal and ON injuries (Dutca et al., 2014, Allen et al., 2018, Bricker-Anthony et al., 2014b, Hines-Beard et al., 2012, Mohan et al., 2013, Petras et al., 1997). However, during an explosive blast, the overpressure wave can propagate off solid surfaces such as buildings and objects (Blanch and Scott, 2008), thus impacting the individual multiple times in quick succession, in addition to or instead of a single high-pressure wave (Rex et al., 2015). Furthermore, blast overpressure waves can be produced from the barrel of machine guns, which are likely to impact multiple times in quick succession.

In a mouse modified paintball model, multiple low overpressure blast waves of 15 psi in quick succession caused greater ON axonal degeneration than a single high-pressure blast wave of 26 psi (Vest et al., 2019). This result was replicated using a compressed air shock tube by Choi et al., who performed a single blast wave or repeated blasts daily over 5 consecutive days with a blast overpressure wave measuring 70kPa (~10 psi) (Choi et al., 2015). The authors demonstrated more activated caspase-3 immunostaining in the ON after rPBI than a single blast, suggesting greater optic neuropathy with multiple compared to single blast exposure. The detection of $ED1^+$ cells in the ON after all types of blast injuries suggests that infiltrating macrophages clear debris in all scenarios (Stoll et al., 1989, Choi et al., 2015). Repeated overpressure waves performed in quick succession may directly impact the ON causing contraction with inefficient time to fully recover before the second blast wave impact. ON contraction could be visualised in real-time by performing the rPBI injury inside a magnetic resonance imaging (MRI) scanner.

### 5.4.8. ON axons with degenerative profiles increase up to 1 month after rPBI

Axons degenerate through unravelling their myelin sheath or through axonal compaction (Saggu et al., 2010). After repeated blast injury, the appearances of the ON axons did not distinguish between a disorder of myelin or axonal degeneration, and therefore, I have referred to axons with a degenerative profile ("degenerating axons"). I showed that after rPBI there were more degenerating ON axons, which tended to be higher 2 days after the injury and significantly higher 7, 14 and 28 dpi. Early ON axonal injury suggests that rPBI may directly injure the ON, rather than the ON degenerating secondary to ocular pathology due to downstream inflammation or

due to RGC death. I also demonstrated that ON axons are degenerating up to 28 days after injury, implying that ON injury is progressive in this model. Other studies have demonstrated prolonged, progressive RGC degeneration and a reduced GCC thickness at 4 months (Dutca et al., 2014) and reduced GCL cellularity at 10 months after unilateral 20 psi PBI using a blast chamber (Mohan et al., 2013), although these studies did not examine the effects on ON pathology. There was no effect on the number of intact ON axons in my experiments up to 28 dpi; however, due to the progressive nature of the injury, if I extended the study to 4, 8 and 12 months then I may have observed more axons with degenerative profiles, resulting in fewer intact axons at these time points. There was a transient reduction in axon density at 7 dpi, which may have been due to elevated gliosis or oedema, resulting in fewer ON axons per $mm^2$. I did not collect longitudinal ON sections to stain for glial markers at 2 or 7 dpi.

### 5.4.9. Pre-blast siCASP2 injections reduced ON pathology, but there was greater ON degeneration after delayed siCASP2 treatment

Pre-blast siCASP2 injections provided some ON neuroprotection at 14 dpi, since less ON axons had a degenerative profile compared to siEGFP treated eyes. There was also a reduction in axon density in siCASP2 treated eyes compared to sham, potentially due to the presence of more reactive glia or ON oedema in siCASP2 treated animals. siCASP2 and siEGFP injections were both associated with less degenerating ON axons compared to rPBI treated eyes without injections, suggesting that intravitreal injections pre-rPBI or siRNA per se cause some neuroprotection. There was a further reduction in the number of degenerating axons in siCASP2 treated eyes compared to

siEGFP treated eyes suggesting that siCASP2 has a greater axon protective effect compared to control siRNA.

Delayed siCASP2 injections did not provide any ON axon protection at 28 dpi and there were more degenerating axons in rPBI treated mice receiving no intravitreal injections or siCASP2 injections than mice treated with siEGFP injections which did not reach statistical significance. After pre-blast intravitreal injections, there were fewer degenerating axons in both siEGFP and siCASP2 treated groups compared to the rPBI treated group without injections, whereas with delayed injections, the number of degenerating axons where as high as rPBI alone. Furthermore, there was a significantly lower axon density with siCASP2 treatment compared to siEGFP treatment, suggesting that there may be more reactive gliosis or ON oedema and therefore less axons per $mm^2$ of ON. However, I have only analysed one time point so this requires further investigation.

Lens damage is a possible side-effect of intravitreal injections, which can cause neuroprotection through factors derived from activated retinal glia (Fischer et al., 2000, Lorber et al., 2005, Lorber et al., 2008, Cao et al., 1997). Traumatic cataracts can be formed through lens damage, but I did not detect cataracts in any eyes, as demonstrated by clear fundoscopy and OCT imaging. To my knowledge, no other studies have treated rPBI by intravitreal injections, but another study delivered a novel beta-adrenergic receptor agonist topically (in eye drops) which reduced expression of inflammatory and apoptotic markers. This study did not directly assess retinal cell death or ON degeneration (Jiang et al., 2013). The authors did not define the

mechanism for the compound to reach the retina; therefore, it is presumed that the cornea was permeable to the compound which reached a sufficient concentration to have a therapeutic effect at the retina.

As a control for intravitreal injections, the right eye of sham treated mice in the pre-blast siCASP2 study were injected with 2 µl of sterile PBS to determine the effects of intravitreal injections without rPBI. There were no changes in the number of degenerating axons or axon density, suggesting that intravitreal injections do not cause myelin alterations or gliosis (increased gliosis results in decreased axon density per $mm^2$). However, there were fewer intact ON axons in sham treated left eyes which were exposed to a blocked blast wave, compared to contralateral right eyes which received sterile PBS injections. This could suggest that there is trauma to the ON even when the blast wave is blocked.

In previous studies, successful knockdown of *caspase-2* mRNA has been demonstrated *in vivo*. However, I have not specifically shown that caspase-2 is knocked down in this model. In future experiments, extra mice should be collected, and RT-qPCR performed for *caspase-2* mRNA to ensure successful knockdown.

### 5.4.10. There were more ED1$^+$ cells in the ON after rPBI and after pre-blast and delayed siCASP2 injections

There was a greater number of ED1$^+$ cells, which are likely infiltrating macrophages in the ON following rPBI. This was observed in groups receiving no intravitreal injections and in both pre-blast and delayed siCASP2 groups. There were ED1$^+$ cells were

observed at 28 dpi compared to 14 dpi. This elevation in the number of $ED1^+$ cells was associated with an increased number of toluidine blue positive cells in resin-embedded ONs. This suggests that inflammatory macrophages were infiltrating into the ON after injury to clear degenerating myelin debris from degenerating axons (Stoll et al., 1989). Furthermore, macrophages can promote ON axonal regeneration after injury (Cui et al., 2009), suggesting they may have a positive effect.

### 5.4.11. siEGFP might have some non-specific effects

siEGFP is commonly used as a control siRNA, but it can have non-specific effects (Tschuch et al., 2008, Thakur et al., 2012). For example, siRNA can induce unintended knockdown through binding to sequences with similar homology (Thakur et al., 2012). Further, dsRNA molecules can induce activation of the immune response through Toll-like Receptor activation (TLR), cytokine production, interferon release and subsequent non-specific gene expression alterations (Kleinman et al., 2008, Forsbach et al., 2008). The siEGFP from Quark Pharmaceuticals used in this study has previously been shown to have minimal off-target effects and does not activate an immune response (Ahmed et al., 2011), although, further tests could be performed to confirm this using our *in vivo* models. An alternative to using siEGFP is to use a scrambled siRNA based upon the target sequence, which should not bind to anything above background levels. Furthermore, to be sure that the siRNA is not acting on any other pathways and thus providing its effect through knocking down a non-specific signalling pathway, multiple siRNA sequences for the same gene could be used and compared.

## 5.5. Conclusion

This chapter indicates that caspase-2 might be cleaved and activated in a mouse model of repeated blast injury, however further investigation is still required. I have demonstrated that siCASP2 has variable impact depending on the timing of the intravitreal injections and that vitreal inflammation is potentially exacerbated if the injections are delivered too close to the time of injury. For example, pre-blast siCASP2 injections (2 days before blast) did not cause any vitreal inflammation in either eye on OCT images, whereas delayed siCASP2 injections (5 hours after blast) caused vitreal inflammation in left eyes that were directly blasted and some inflammation to a lesser extent in the contralateral eyes. Interestingly, pre-blast siCASP2 treatment reduced the number of degenerating axons compared to control siEGFP, suggesting a potential axon protective effect. The number of $RBPMS^+$ RGCs was not different between sham and rPBI groups up to 1 month post injury, suggesting that ON degeneration may precede RGC death. The observation of increased numbers of degenerating axons in the ON, increased numbers of $ED1^+$ cells in the ON but no evidence of $RBPMS^+$ RGC death after rPBI suggests that the injury directly affects the ON rather than secondary to retinal injury, and that rPBI may induce direct TON. More research is required to determine whether siCASP2 is a potential therapeutic for blast induced ocular trauma.

# Chapter 6 Necroptosis in the retina in an ocular repeated primary blast injury mouse model

## 6.1. Rationale

In blunt ocular injury, I found that necroptosis occurred in a site-specific manner and promoted the death of a proportion of RGCs. Furthermore, necroptosis is implicated in PBI, since RIPK1 and RIPK3 immunostaining is elevated at 3 days dpi following a single 26 psi blast wave delivered directly to the eye in C57 Bl6 mice (Bricker-Anthony et al., 2014a). RIPK1 expression is increased in the ONL, INL and Müller glia, whilst RIPK3 expression is elevated in the ONL, INL, IPL and GCL. At 28 dpi, RIPK1 expression remains elevated in the ONL and INL and RIPK3 expression is elevated in the IPL (Bricker-Anthony et al., 2014a). In this study, other necroptotic markers, such as MLKL phosphorylation, or the effects of a necroptotic inhibitor were not investigated. In this chapter, I investigate necroptosis in an rPBI mouse model and use Nec-1s to inhibit necroptosis to determine the effects on retinal and ON pathology.

## 6.2. Experimental design

This chapter investigates whether necroptosis occurs in RGC during degeneration and whether this induces ON axonal pathology in a mouse rPBI model (see Section 2.1.2).

### 6.2.1. Assessment of necroptotic markers

Unilateral repeated blast injury was performed as described previously; briefly, 2 blasts of 15 psi were performed in quick succession and this was repeated over 3 consecutive days (Bernardo-Colon et al., 2018, Vest et al., 2019). Retinal tissue was collected 7 and 14 dpi and western blotting performed for necroptotic markers RIPK1, RIPK3 and MLKL (full-length and phosphorylated at Ser345) (Figure 6.1A) (see Section 2.7).

### 6.2.2. *In vivo* necroptosis inhibition study

Necroptosis was inhibited by bilateral intravitreal injections of Nec-1s (2 µl of 3.6 mM in 10% DMSO, 0.9% methyl-β-cyclodextrin in PBS) 5 hours after the first blast followed by two further blast waves (Figure 6.1B). The left eyes were directly exposed to the blast wave, although the right eyes were also analysed for some experiments for comparison. These will be highlighted in the results section. *In vivo* structural and functional assessments were performed, including bilateral OCT imaging (see Section 2.2.1) and functional ERG and VEP recordings (see Section 2.2.2). All analyses were performed at baseline and at the 28 dpi endpoint. Mice were culled at 28 dpi and eyes processed for cryosectioning and immunofluorescent staining. $RBPMS^{+}$ RGCs were quantified in the central, middle and peripheral portions of the retina (see Section 2.3 and Section 2.4.3). Sections of far proximal ONs were processed as resin-embedded semi-thin sections and the number of intact and degenerating ON axons were quantified (see Section 2.6). The remaining ON length was processed as longitudinal cryosections for immunofluorescent staining analysis.

**A** *In vivo* protein studies

**i)** Timeline

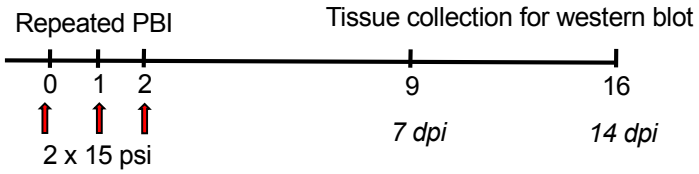


**ii)** Experimental groups, group sizes and measured endpoints

| Time point | n (mice) | Measured endpoints |
|---|---|---|
| 7 dpi | Western blot: 3 retinae per group (unilateral rPBI and sham) | RIPK3 and MLKL protein expression in left direct blast eyes |
| 14 dpi | Western blot: 5 retinae per group (unilateral rPBI and sham) | MLKL-P protein expression in left direct blast eyes |

Cc

**B** *In vivo* Necrostatin-1s study

**i)** Timeline

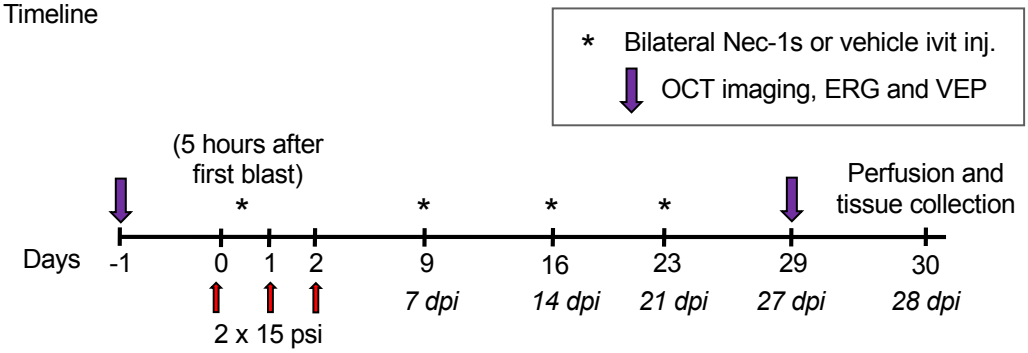


**ii)** Experimental groups, group sizes

| *Groups* | *n (mice)* | *Injury and treatment* |
|---|---|---|
| Sham | 10 | Blast overpressure wave blocked |
| rPBI + no ivit | 10 | 3 x 2 x 15 psi + no ivit injections |
| rPBI + vehicle | 10 | 3 x 2 x 15 psi + bilateral vehicle ivit injections |
| rPBI + Nec-1s | 10 | 3 x 2 x 15 psi + bilateral Nec-1s ivit injections |

**iii)** Measured endpoints and eyes analysed

| *Measured endpoints* | *Eyes analysed* |
|---|---|
| OCT imaging | Both eyes |
| Total retinal and GCC thickness | Left direct blast eye |
| Percentage of eyes with vitreal hyper reflective dots | Both eyes |
| ERG and VEP amplitudes | Left direct blast eye |
| $RBPMS^+$ RGC counts on retinal cryosections | Left direct blast eye |
| ED1 and GFAP IF staining on retinal and ON sections | Left direct blast eye |
| Axonal counts in ONs | Left direct blast eye |

**Fi** as
co 1s
st rst
blast of the rPBI followed by two further blasts, and then every 7 dpi until perfusion and tissue collection at 28 dpi. At baseline and endpoint, OCT imaging, ERG and VEP were performed.

## 6.3. Results

### 6.3.1. RIPK3 and MLKL protein expression is no different after rPBI

Western blotting was performed on whole retinal lysates 7 and 14 dpi for RIPK3 and MLKL and phosphorylated MLKL (Ser345) at 14 dpi (Figure 6.2). The results showed there were no differences between sham and rPBI groups, although further repeats and lab work is required.

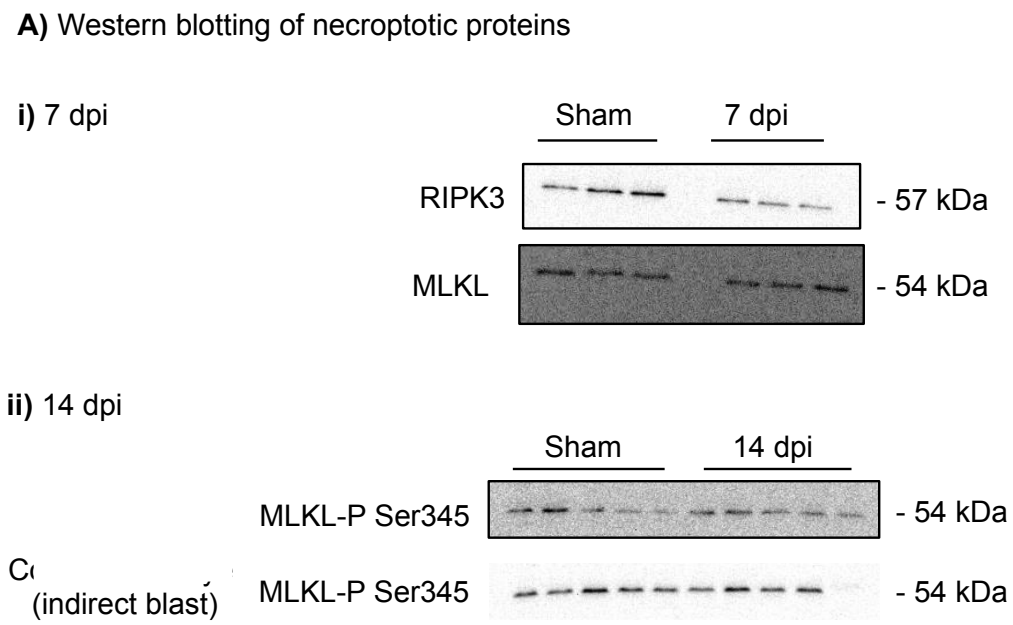


**Figure 2. Necroptotic proteins are upregulated after repeated primary blast ocular trauma.** Mice received unilateral repeated PBI to the left eye and retinae were collected after 48 hours, 7 days and 2 weeks. Sham and injured samples were collected at each time point. RIPK1, RIPK3, MLKL, phosphorylated MLKL and caspase 8 protein expression was analysed

### 6.3.2. There was a reduction in the number of RBPMS$^+$ RGCs after Nec-1s and vehicle intravitreal injections compared to rPBI alone, although Nec-1s treated eyes had more RBPMS$^+$ RGCs compared to vehicle-treated eyes in the middle portion of the retina.

RBPMS immunostaining was performed an retinal sections taken 28 dpi and RBPMS$^+$ cells counted in the central (closest to ONH), middle and peripheral retina in sham and rPBI treated groups (with no intravitreal injections: vehicle or Nec-1s) (Figure 6.3). There was no reduction in the number of RGCs 28 days after rPBI without intravitreal injections (Figure 6.3A). For example, in the peripheral retina there were 12.43 ± 0.98 RBPMS$^+$ RGCs in sham treated eyes compared to 12.66 ± 1.38 RBPMS$^+$ cells in rPBI treated eyes, in the middle retina portion there were 15.32 ± 0.47 RBPMS$^+$ RGCs in sham treated eyes compared to 14.59 ± 0.71 RBPMS$^+$ RGCs in rPBI treated eyes and in the central retina, there were 16.98 ± 2.61 RBPMS$^+$ RGCs in sham treated eyes compared to 18.45 ± 1.32 RBPMS$^+$ RGCs in rPBI. However, rPBI in combination with intravitreal injections caused a reduction in the number of RBPMS$^+$ RGCs both in vehicle and Nec-1s injected eyes. There were significant differences across all groups in the central, middle and peripheral portion of the retina (ANOVA $p<0.05$). In the middle and peripheral retina, there was a significant decrease in the number of RBPMS$^+$ RGCs after rPBI with vehicle injection (post hoc Tukey with multiple corrections $p<0.05$) compared with rPBI with no intravitreal injection (post hoc Tukey with multiple corrections middle portion $p<0.01$, peripheral portion $p<0.05$). In the middle portion of the retina, there was significant protection of RBPMS$^+$ RGCs after rPBI with Nec-1s injection compared to rPBI with vehicle injection, since 13.08 ± 0.81 RBPMS$^+$ RGCs were counted compared to 10.29 ± 0.37 RBPMS$^+$ cells per 1000 μm

of retina in Nec-1s treated eyes compared with vehicle. There were no differences between rPBI groups treated with vehicle or Nec-1s injections in the central or peripheral retinal portions, suggesting that Nec-1s has a protective effect only in the middle portion of the retina. Representative RBPMS immunofluorescent staining is displayed in Figure 6.3B.

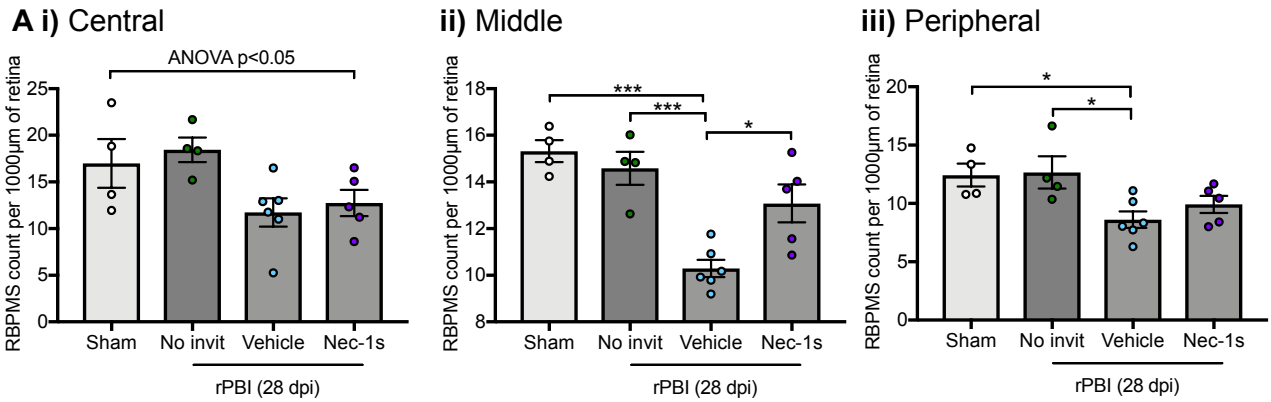


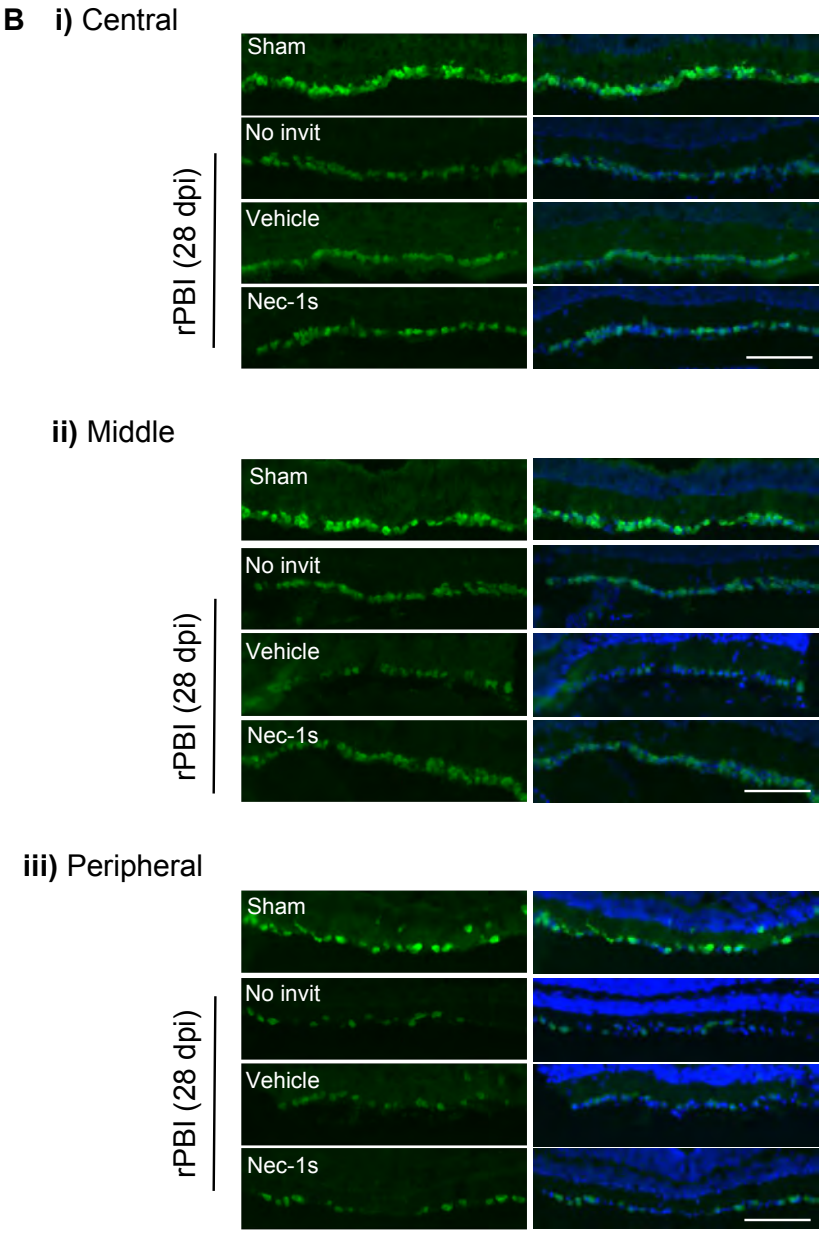


Figure legend on next page …

**Figure 6.3. The number of RBPMS$^+$ RGCs were reduced after intraocular injections in combination with rPBI, but was increased in the middle portion of the retina after Nec-1s treatment compared to vehicle control. A)** The number of RBPMS$^+$ RGCs were counted in three regions of left directly blasted eyes, in the central (close to the ONH), middle and peripheral retina. **i)** In the central retina, there was a significant difference in RBPMS$^+$ cells across all groups (ANOVA $p<0.05$). **ii)** In the middle portion of the retina, there was no reduction in RGCs after rPBI with no intravitreal injections, but there was a significant reduction after rPBI with vehicle injection (post hoc Tukey $p<0.01$) compared with Nec-1s injection (post hoc Tukey $p<0.05$). **iii)** In the peripheral retina there was no reduction in the number of RBPMS+ RGCs after rPBI with vehicle injection compared to sham and rPBI treated eyes with no intravitreal injections (ANOVA $p>0.05$). **B)** Representative RBPMS images from the central, middle and peripheral retina from sham and rPBI treated groups (no intravitreal injections, vehicle and Nec-1s). Scale bar represents 100 µm. n=4 for sham and rPBI, n=6 for vehicle and n=5 for Nec-1s. Error bars represent mean ± SEM.

### 6.3.3. There were no changes in retinal thickness after rPBI

OCT imaging was performed at baseline and 28 dpi in sham and rPBI treated eyes with either no intravitreal injections or bilateral vehicle or Nec-1s injections (Figure 6.4A). Total retinal thickness (ANOVA p=0.085) and GCC thickness (ANOVA 0.929) were not changed in any groups.

### 6.3.4. Vitreal hyper reflective dots were observed in eyes following rPBI treated with intravitreal injections

There was no gross structural retinal pathology or vitreal inflammation in the rPBI treated group without intravitreal injections compared to the sham treated group, suggesting that the rPBI alone does not cause significant retinal degeneration or ocular inflammation. After rPBI with bilateral intravitreal injections with Nec-1s or vehicle, there were hyper reflective dots detected in the vitreous in left eyes that were directly blasted but minimal numbers in right eyes that were indirectly blasted (Figure 6.4C). In 80% of left eyes in both the vehicle and Nec-1s treated groups there was vitreal hyper reflective dots and fewer contralateral eyes that were indirectly blasted had hyper reflective dots. There was hyper reflective dots in the vitreous of 40% of vehicle treated and 10% of Nec-1s treated, suggesting inflammation is caused by rPBI in combination with injections (Figure 6.4A).

### 6.3.5. There were more ED1$^+$ cells in the retina after rPBI, although fewer in Nec-1s treated eyes

ED1 immunostaining was performed for the presence of infiltrating macrophages in the retina. There were few ED1$^+$ cells in sham and rPBI treated eyes with no intravitreal

injections in the retina at 28 dpi. However, there were more ED1$^+$ cells after rPBI and vehicle injections. In contrast, few ED1$^+$ cells were detected in rPBI treated eyes with Nec-1s injection at 28 dpi, suggesting that there may have been more macrophages at an earlier time point or less inflammation compared to other groups (Figure 6.5A). Furthermore, retinal GFAP immunostaining was increased after rPBI with vehicle injection but not in other groups, suggesting there were activated astrocytes at 28 dpi caused by the vehicle (Figure 6.5B). Together, this data might suggest that intravitreal injection causes greater retinal pathology after blast injury, and that Nec-1s may provide some neuroprotection or anti-inflammatory effects.

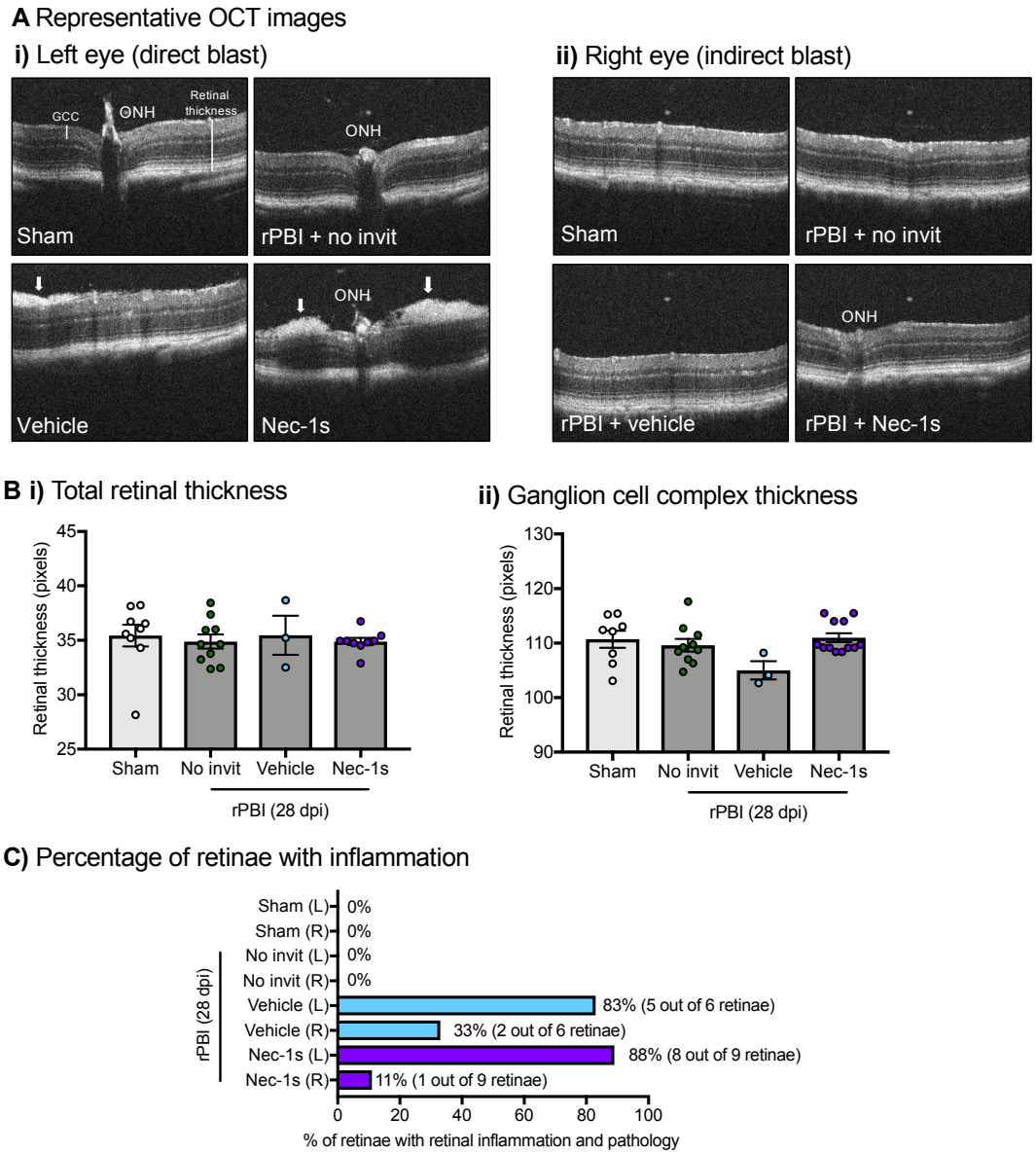


**Figure 4 Optical coherence tomography (OCT) imaging. A)** Representative OCT images at the optic nerve head showing no gross structural changes between sham and rPBI or after vehicle or Nec-1s intravitreal injections. There are some denser areas on the surface of the retina. **B)** OCT imaging at the optic nerve head showed no changes in total retinal thickness or ganglion cell complex thickness. **C)** Intravitreal injections of Nec-1s and vehicle caused increased inflammation in the left eye (direct blast) but not the right eye (indirect blast), suggesting penetrating injury in combination with repeated PBI causes additive inflammation. Error bars represent mean ± SEM.

**Fi** **nd**
**ve** **an**
**in** **to**
**rP** **ral**
ch **ve**
de **eal**
inj **ss**

or **ii)** GCC thickness across all groups (ANOVA p=0.0.085, p=0.929). **C)** Percentage of eyes displaying vitreal hyper reflective dots. Error bars represent mean ± SEM.

**A)** Retinal ED1⁺ immunostaining at 28 dpi

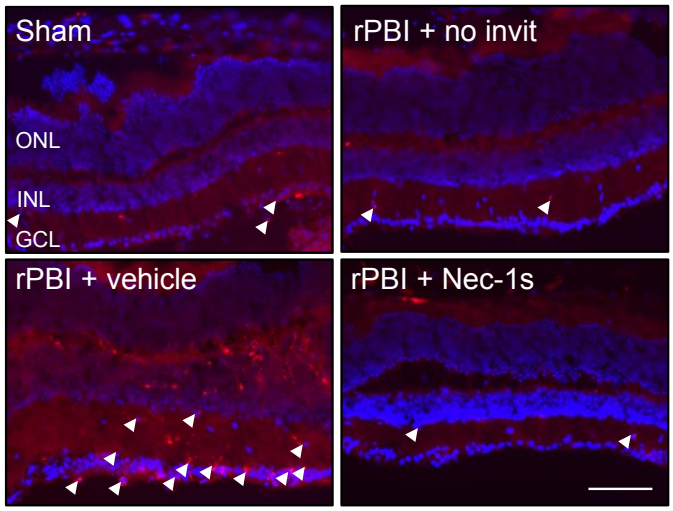


**B)** Retinal GFAP immunostaining at 28 dpi

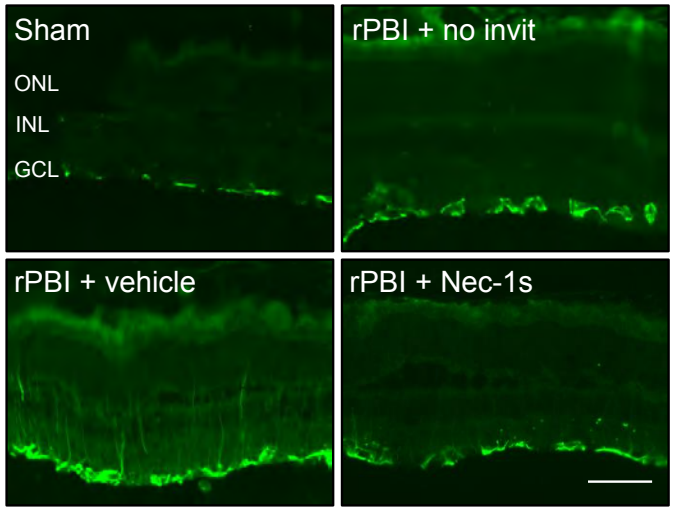


**Figure 5**

Scale bar represents 100um

### 6.3.6. There were no changes in ERG or VEP amplitudes after Nec-1s treatment

Scotopic ERGs and VEPs were performed to assess retinal and ON functional activity (Figure 6.6). There was a borderline significant difference in P1 (ANOVA p=0.051) and N1 (ANOVA p=0.054) amplitudes but no significant differences in a-wave (ANOVA p=0.265) or b-wave (ANOVA p=0.301) amplitudes at 28 dpi between groups (Figure 6.6).

### 6.3.7. There was no effect on the number of ON axons after Nec-1s treatment

Semi-thin proximal ON cross-sections were stained with PPD and toluidine blue to quantify intact and degenerating ON axons, gliosis and infiltrating cells (Figure 6.7). There were no significant differences 28 dpi in the total number of intact axons in the ON between sham and rPBI treated groups with no intravitreal injections (38193 ± 2639 axons in sham compared to 32351 ± 2542 axons in rPBI treated groups) or following rPBI with vehicle or Nec-1s injections (31624 ± 2334 axons in vehicle compared to 31943 ± 1463 axons in Nec-1s treated groups) (ANOVA p=0.173) (Figure 6.7Aii). There were more degenerating ON axons in the rPBI treated eyes with no intravitreal injections compared to the sham treated group, since 86.67 ± 26.87 degenerating axons in the ON were counted in sham compared to 467 ± 75.3 after rPBI with no intravitreal injections (Figure 6.7Ai; ANOVA p<0.001; post hoc Tukey with multiple comparisons p<0.001). However, there were no differences between rPBI treated eyes with vehicle or Nec-1s injections, since 275 ± 42.33 intact axons in the ON were counted in vehicle treated eyes compared to 307.5 ± 91.53 Nec-1s treated eyes, indicating that Nec-1s has no protective effect on ON pathology 28 dpi. There were no differences in axonal density between any groups (Figure 6.7Aiii; ANOVA

p=0.151): 4337272 ± 18997 axons in sham, 372148 ± 26911 axons in rPBI with no intravitreal injections, 392061 ± 12375 axons in rPBI with vehicle injection and 387159 ± 9762 axons in rPBI with Nec-1s injection. Representative PPD and toluidine blue stained ON sections are displayed in Figure 6.7B.

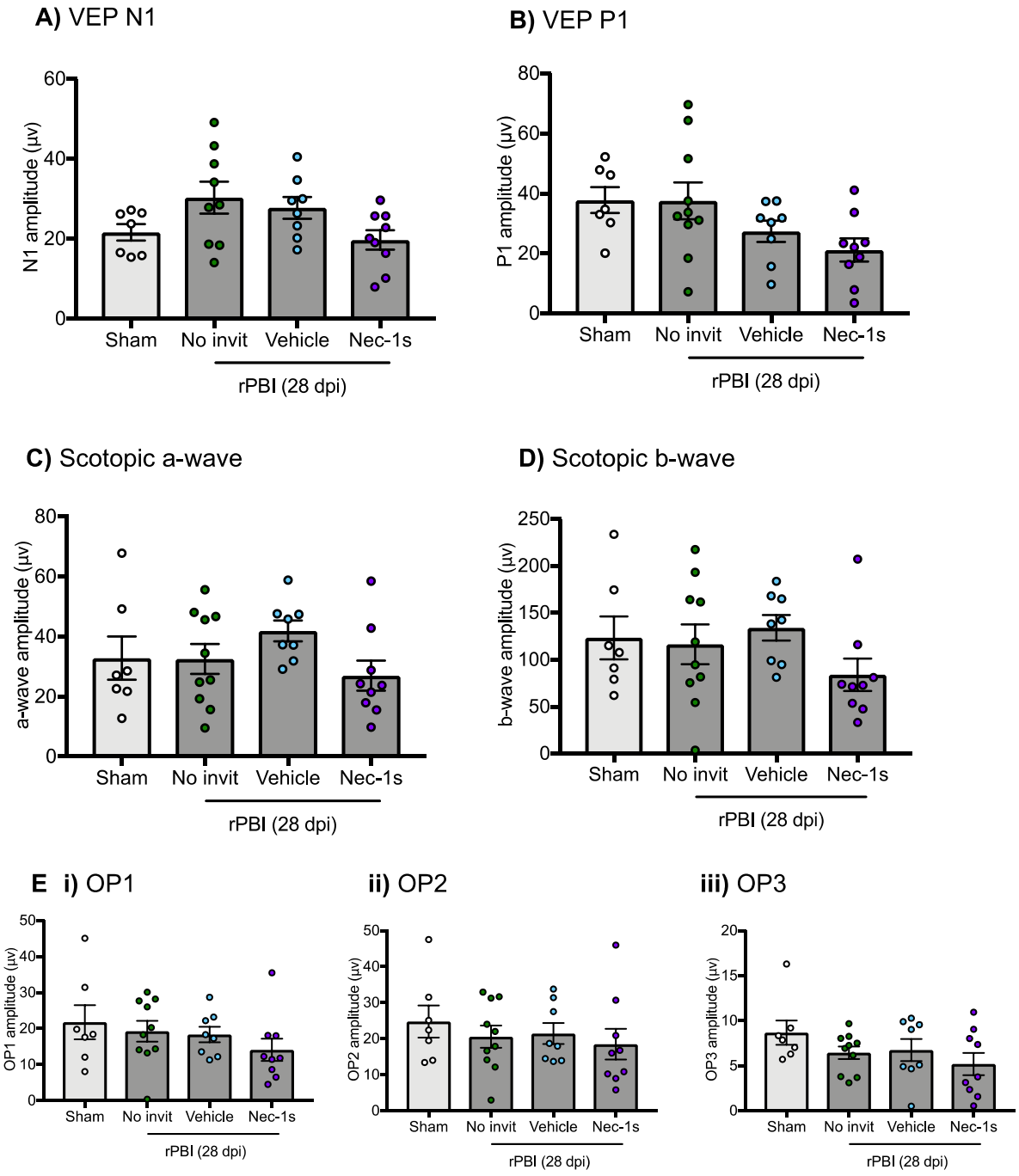


**Figure 6.6. There were no changes in ERG or VEP amplitudes after Nec-1s treatment. (A-B)** There were no significant differences in VEP N1 (ANOVA p=0.054) and P1 (ANOVA p=0.051) amplitudes between groups. **(C-E)** There were also no differences in ERG scotopic a-wave (ANOVA p=0.266), b-wave (ANOVA p=0.301) and OPs amplitudes between sham and rPBI treated eyes with no intravitreal injections, vehicle or Nec-1s injections. Error bars represent mean ± SEM. n=10 animals per group.

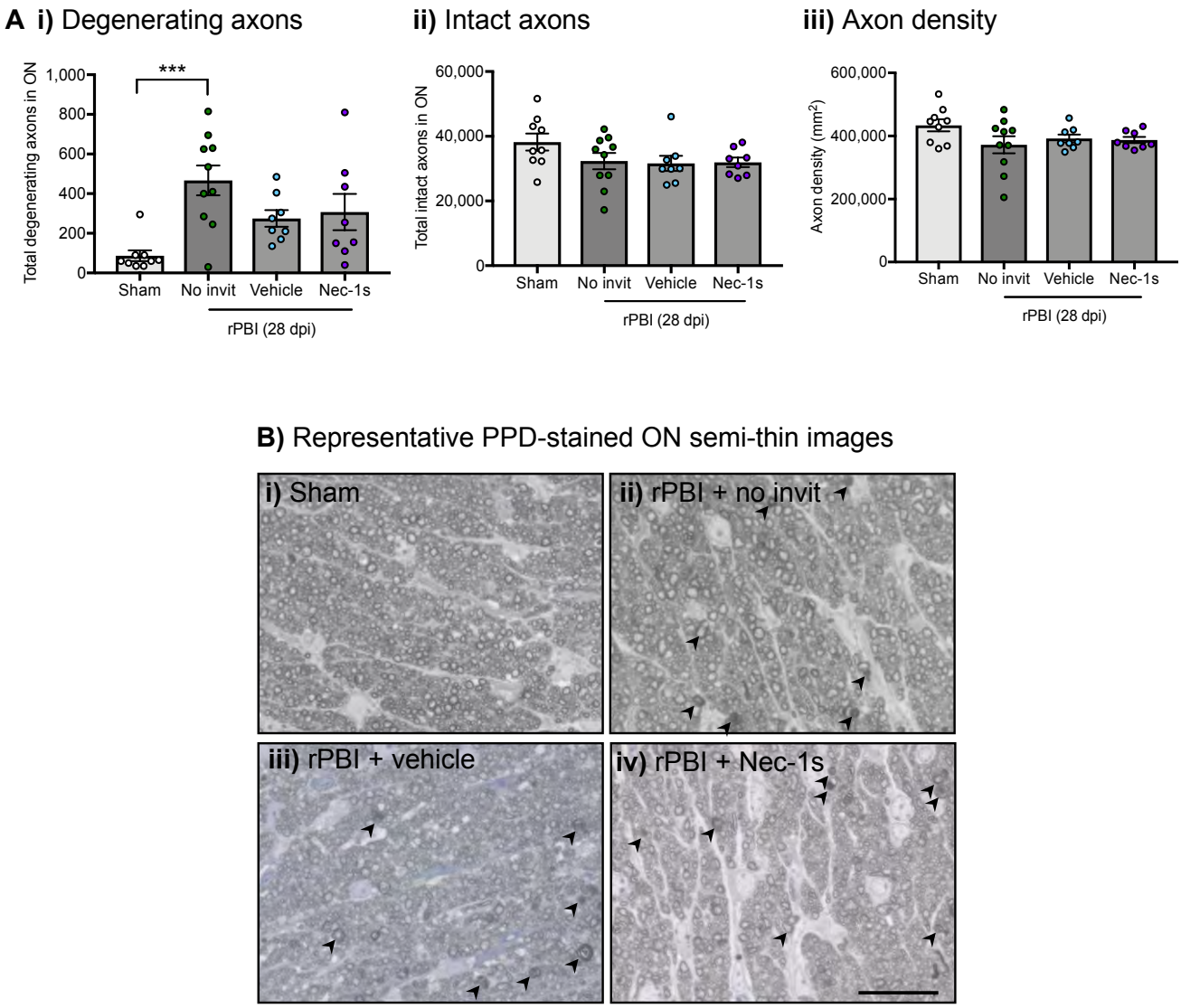


**Figure 7. The effects of Nec-1s on optic nerve axons and glia. A)** Total number of intact and degenerating axons were counted in the ON between sham and repeated PBI and after intravitreal injections of vehicle and Nec-1s. **i)** After rPBI degenerating axons in the ON increased (ANOVA p_____) but was not significantly changed after Nec-1s or vehicle administration. **ii-iii)** Intact axons and axon density were not affected at 1 month after rPBI or by vehicle or Nec-1s administration. Delayed administration of Nec-1s or vehicle. There is no change in healthy axons after rPBI. B. There are increased degenerating axons after rPBI compared to sham. There are less degenerating axons in siCASP2 treated eyes compared to siGFP eyes. C. There is no difference in axon density across all groups.

### 6.3.8. There was an increased number of ED1$^+$ cells in the ON after rPBI and Nec-1s treatment.

ED1$^+$ immunostaining was performed in longitudinal ON sections and quantified. The number of ED1$^+$ cells increased in the ON after rPBI since 4.81 ± 0.68 ED1$^+$ cells per mm$^2$ were detected in sham treated eyes compared to 49.79 ± 7.18 ED1$^+$ cells per mm$^2$ in rPBI treated eyes with no intravitreal injections (ANOVA $p<0.01$, post hoc Tukey with multiple corrections $p<0.05$) and were also elevated after rPBI with intravitreal injections of vehicle (49.26 ± 8.70 ED1$^+$ cells per mm$^2$; post hoc Tukey $p<0.01$) and Nec-1s (40.03 ± 9.59 ED1$^+$ cells per mm$^2$, post hoc Tukey $p<0.05$) (Figure 6.8). This data suggests that ED1$^+$ macrophages infiltrate the ON after rPBI and intravitreal injections of Nec-1s and vehicle.

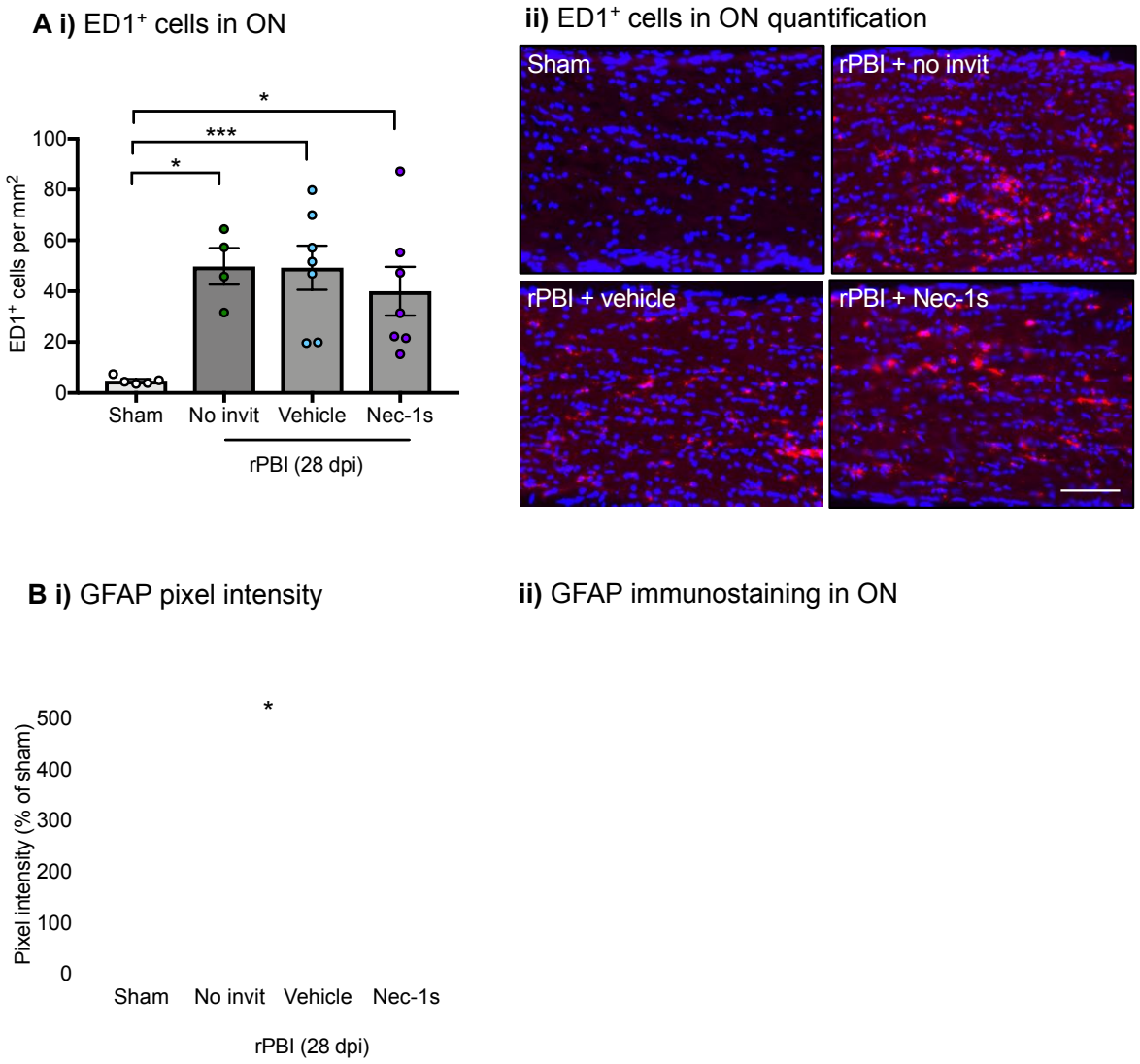


**Figure 8. The effects of Nec-1s on optic nerve axons and glia. A)** Total number of intact and degenerating axons were counted in the ON between sham and repeated PBI and after intravitreal injections of vehicle and Nec-1s. **i)** After rPBI degenerating axons in the ON increased (ANOVA p_____) but was not significantly changed after Nec-1s or vehicle administration. **ii-iii)** Intact axons and axon density were not affected at 1 month after rPBI or by vehicle or Nec-1s administration. Delayed administration of Nec-1s or vehicle. There is no change in healthy axons after rPBI. B. There are increased degenerating axons after rPBI compared to sham. There are less degenerating axons in siCASP2 treated eyes compared to siGFP eyes. C. There is no difference in axon density across all groups.

## 6.4. Discussion

### 6.4.1. RIPK1, RIPK3 and MLKL expression changes after blast injury.

There were no changes in the expression of necroptotic markers, RIPK3 and MLKL, 7 dpi or phosphorylated MLKL (Ser 345) 14 dpi. Necroptosis might not be occurring after rPBI alone. I did not observe a reduction in $RBPMS^+$ RGCs 28 dpi, which suggests that RGCs might not be degenerating early after rPBI and therefore cell death signalling pathways might not become activated until later time points after secondary injury. Further investigation is required into the effects of rPBI in combination with intravitreal injections in close proximity, which could mimic a controlled penetrating injury, to determine whether necroptotic markers are elevated and activated in this experimental situation. In Chapter 4, I showed that the expression of necroptotic markers was elevated after blunt ocular injury. Although further investigation is required, primary blast wave exposure alone might not induce necroptotic cell death, but in combination with a blunt impact injury (or penetrating injury from the intravitreal injections) might cause necroptotic pathway activation. The time constraints of this project meant that western blots for all necroptotic markers were not performed. Further research into the expression of RIPK1, RIPK3, MLKL, phosphorylated MLKL and caspase-8 needs to be performed at more time points after blast injury to confirm whether necroptosis is occurring or not.

### 6.4.2. Nec-1s may provide some RGC neuroprotection in the middle portion of the retina after rPBI.

In this study, $RBPMS^+$ RGCs were counted in retinal cryosections. This is a valid method to quantify RGCs in models of ONC and ocular hypertension (Mead et al.,

2014, Hill et al., 2015, Mead and Tomarev, 2016). There was no reduction in the number of $RBPMS^+$ RGCs after rPBI alone at 28 dpi, suggesting that 1) a low-overpressure blast wave is not sufficient without other associated injuries to cause RGC death; 2) RGCs degenerate at a later time point; or 3) that the method of counting RGCs missed focal pockets of RGC loss. Previous studies have shown TUNEL staining (which labels DNA breaks and cell death) after a single blast exposure in focal areas of the retina (Bricker-Anthony et al., 2014b). Other studies have shown delayed and progressive RGC degeneration 4 and 10 months following PBI (Dutca et al., 2014, Mohan et al., 2013), indicating that later time points need to be investigated in the rPBI model.

The significant reduction in RGCs after rPBI in combination with intravitreal injections - which are consistent with similar findings described in Chapter 5 after siRNA injections - could replicate the effect of a penetrating ocular injury in close proximity to the primary blast wave; for example, a combination of primary and secondary explosive blast injury (Scott, 2011), and therefore, mimics an open globe injury, inducing inflammation and subsequent RGC degeneration. Alternatively, RGC degeneration could have been caused by the high DMSO concentration that Nec-1s was reconstituted in. Previous studies have shown that concentrations >1% DMSO cause caspase-3 independent RGC death *in vivo* (Galvao et al., 2014) and concentrations >10% DMSO cause apoptosis through plasma membrane permeabilisation *in vitro* (Notman et al., 2006). However, other studies have used similar DMSO concentrations *in vivo* (Huang et al., 2018, Rosenbaum et al., 2010) and I did not observe excess RGC loss after blunt ocular injury and injections with the same composition of Nec-1s which

I described in Chapter 4, or in eyes injected with control siRNA (siEGFP) which I described in Chapter 3 (Thomas CN, 2018), suggesting that this was not the likely cause of additive RGC loss.

### 6.4.3. Vitreal inflammation may occur in rPBI in combination with intravitreal injections

OCT imaging was performed to assess retinal layer thickness, gross retinal pathology and vitreal inflammation. I observed hyper reflective vitreal dots in eyes exposed to rPBI and injected with either Nec-1s or vehicle, but did not see any hyper reflective dots in eyes exposed to rPBI without any intravitreal injections. The hyper reflective vitreous dots seen on OCT images were similar to those described in other studies which found that they correlated with the number of mononuclear cells detected in histological sections, suggestive of macrophages (Kokona et al., 2017). In addition, I saw minimal inflammation in the contralateral right eyes which received indirect blast wave exposure and potential mild blunt injuries from the side of the casing, and received equivalent intravitreal injections, suggesting that the combination of intravitreal injection and repeated low-overpressure blast waves caused increased vitreal inflammation.

### 6.4.4. Changes in retinal thickness after blast injury

In the military, blast wave exposure is associated with delayed visual deficits (Capo-Aponte et al., 2015); however, this could be due, in part, to injury of the visual cortex and brain. In rats exposed to a single acoustic blast overpressure wave of ~80 psi generated using a shock-tube device, retinal thickness increased in eyes directly

exposed to the blast compared to sham treated eyes and there was an increase in retinal GFAP immunostaining, suggesting that reactive gliosis may have caused the increase in retinal thickness up to 8-months post blast (Allen et al., 2018). In my study, I only investigated 1-month post blast injury, and did not detect any change in retinal thickness. In addition, a blast shock tube may provide a wider spread of blast-waves, whereas my model induced direct ocular injury.

### 6.4.5. Microglial GFAP$^+$ processes in the retina are activated by rPBI combined with intravitreal injections

The number of microglial GFAP$^+$ processes spanning the retina increased after rPBI and vehicle intravitreal injections but not after Nec-1s treatment or rPBI alone, compared to sham mice. This implies that the injury alone does not cause reactive gliosis, but may have been activated by vehicle injection and prevented by the anti-inflammatory effects of Nec-1s. GFAP was not quantified in this study. I could have performed further experiments to semi-quantify GFAP protein levels using western blotting, or immunofluorescently stained for GFAP on retinal whole mounts.

### 6.4.6. Inflammatory macrophages infiltrate the retina and ON after rPBI

After injury, inflammatory cells can infiltrate tissue and clear debris. One month after rPBI, I detected few ED1$^+$ cells in the retina, suggesting that rPBI causes minimal injury alone. However, rPBI in combination with vehicle injection induced multiple macrophages to infiltrate the retina, specifically in the GCL and IPL, which may have been there to clear degenerating RGCs or induce inflammation. There were fewer macrophages detected after rPBI and Nec-1s injection, indicating that either an

inflammatory infiltrate occurred at a different time point or that there was less inflammation and therefore fewer macrophages.

Macrophages infiltrated into the ON 28 dpi in all rPBI treated groups (no intravitreal injections, vehicle and Nec-1s injections). Macrophages are stimulated by ON axonal degeneration and the need for them to clear degenerating myelin debris (Stoll et al., 1989). Additionally, rPBI may be directly injuring the ON, ON axonal degeneration and causing the infiltration of inflammatory cells which precedes retinal inflammation and RGC death.

### 6.4.7. There were no functional differences between rPBI eyes treated with or without intravitreal injections

The ERG and VEP amplitudes I recorded were much lower compared to other studies, but were consistent between animals, suggesting that there may have been issues with the experimental set up which meant that I did not have sufficient sensitivity to detect differences between groups and that these recordings should be excluded. In future studies, the scotopic threshold response (STR) could be recorded as a measure of RGC function (Saszik et al., 2002), and multifocal ERG (mfERG) can be used to detect retinal function in specific areas of the retina (Bui and Fortune, 2004, Lalonde et al., 2006, Holder, 2004), which could be beneficial if there are focal pockets of retinal cell death in the PBI model (Bricker-Anthony et al., 2014b).

### 6.4.8. The number of degenerating ON axons increase after rPBI and were elevated despite treatment with intravitreal injections

PPD-stained resin embedded ON semi-thin sections were used to assess the number of degenerating and intact ON axons following rPBI and necroptosis inhibition. At 28 dpi, there were increased number of degenerating axons, but no reduction in RGCs at this time point, indicating that rPBI may be injuring the ON directly. The number of intact axons were slightly reduced across all rPBI treated groups (with no intravitreal injections, vehicle or Nec-1s), which did not reach statistical significance. Axonal degeneration after rPBI may be delayed and progressive and so there may be a reduction that could be detected at later time points.

## 6.5. Chapter summary

Western blotting for necroptotic proteins requires more investigation, although I have indicated that RIPK3 and MLKL protein expression did not change 7 dpi and the phosphorylation of MLKL at Ser 345 was not altered 14 dpi, suggesting that necroptosis might not be upregulated after rPBI. The number of $RBPMS^+$ RGCs was not different between sham and rPBI-treated eyes, suggesting that RGCs do not degenerate after rPBI at 28 dpi. There was a significant reduction in the number of $RBPMS^+$ RGCs after rPBI combined with intravitreal injections of Nec-1s or vehicle, suggesting there are additive effects from penetrating injuries on rPBI injuries leading to RGC death. Inhibition of necroptosis using Nec-1s might provide some RGC protection in the middle portion of the retina, as there were more $RBPMS^+$ RGCs in Nec-1s treated eyes compared to vehicle treated eyes in this region, suggesting RGC injury may be focal and necroptosis may be mediating RGC-death in these focal areas. There were also vitreal hyper reflective dots on OCT images, which could indicate

vitreal inflammation in directly blasted eyes that received intravitreal injections of Nec-1s or vehicle. Vitreal inflammation was minimal in contralateral eyes that also received equivalent intravitreal injections, but were indirectly injured, illustrating that the combination of rPBI and intravitreal injections caused additive injury. $ED1^+$ cells, which may have been infiltrating macrophages, were present in the ON in all blast injured groups, associated with increased numbers of degenerating ON axons after injury, suggesting that they may have been there to clear myelin debris or induce inflammation. Treatment with Nec-1s injections had no protective effect on ON pathology.

### 6.6. Conclusion

Collectively, my results indicate that the timing of intravitreal injections around a primary blast-wave injury is important and if treatment is given intraocularly within 5 hours after the injury, this can cause additive effects. Treatment with Nec-1s may provide some RGC neuroprotection when primary blast injuries and penetrating blunt injuries occur in close proximity or when there is an open globe injury or other insult causing neurodegeneration. This work requires further investigation, including analysis of the expression of necroptosis proteins after blast injury and intraocular injections.

# Chapter 7 General Discussion

In this thesis, I aimed to investigate the mechanisms which drive RGC death in rodent models of indirect and direct TON, and to test therapeutic agents in these models. I used two rodent models which replicated specific stages of explosive blast injury. The first was a mouse model which exposed the eye to a repeated primary blast wave and was known to induce ON degeneration, but the effects on RGCs were previously unknown (Bernardo-Colon et al., 2018, Vest et al., 2019). The second model was a rat model of a closed globe blunt injury and modelled secondary blast injury (Blanch et al., 2012b). It was known from previous studies that in the rat model, there are features of commotio retinae including photoreceptor degeneration, and a decreased number of cells in the GCL, which implies RGC or displaced amacrine cell death (Blanch et al., 2012b), but there was no knowledge of the effects of the injury on RGC function or RGC numbers using specific RGC markers. My research in this thesis adds to this previous work and provides further indications of the likely mechanisms which mediate RGC death.

## 7.1. Comparison between the effects of primary blast and secondary blunt ocular injuries on RGC death and ON degeneration

A summary of my findings using the primary blast and secondary blunt ocular injury models on RGC and ON pathologies, caspase-2 and necroptosis signalling pathways, is summarised in Table 7.3, Table 7.2 and Table 7.3.

| *Finding* | *Blunt injury finding* | *Blast injury finding* | *Implications* | *Further investigation* |
|---|---|---|---|---|
| Inflammatory response | $ED1^+$ cells are present in the retina 3 dpi. Later time points were not assessed. | $ED1^+$ cells are present in the retina 28 dpi and also present in the ON at 14 and 28 dpi. *In vivo* OCT imaging displays no vitreal hyper reflective dots at 14 or 28 dpi with blast wave exposure alone. | $ED1^+$ cells can be protective and can clear debris or can be detrimental if the inflammation becomes persistent and chronic. | 1. Assess and quantify $ED1^+$ cells in blunt injured ON.<br>2. Label $ED1^+$ cells for oncomodulin and assess CNTF levels.<br>3. ED1 stains microglia and macrophages, so perform double-labelling experiments to confirm cell type.<br>4. Assess hyper reflective dots in OCT images *in vivo* in blunt injured animals. |
| ON pathology | N/A | There are more ON axons with degenerative profiles 7 dpi and 28 dpi. | The ON is the main connection from the eye to the brain and if these axons degenerate this can lead to visual loss. | 1. Perform immunolabelling experiments on PPD-stained resin embedded ON in blunt injured ONs at 2, 7, 14 and 28 dpi.<br>2. Extend the rPBI study to longer than 28 dpi.<br>3. Perform electron microscopy to see whether the axons degenerate, or it is just myelin unravelling. |
| RGC pathology | There is a reduction in the number of $BRN3A^+$ and $RBPMS^+$ RGCs at the centre of the impact site, in blunt injured eyes treated with vehicle compared to intact animals. | There are no changes in the number of $RBPMS^+$ RGCs on retinal sections or retinal whole mounts up to 28 dpi, compared to sham-treated eyes. | The number of RGCs decrease after blunt ocular injury, with greatest reduction at the centre of the impact site. But, RGCs do not degenerate up to 1 month after PBI, suggesting RGC death might be delayed or progressive and follow ON pathology. | 1. *In vivo* RGC imaging of apoptosis such as DARC (Yap et al., 2018, Cordeiro et al., 2004, Cordeiro et al., 2017) , or measure Fluorogold labelled RGCs or perform experiments in Thy 1.1 reporter mice to see if there are pockets of cell death in blunt injury.<br>2. Assess later time points for both blunt and blast injury models |

| | | | | |
|---|---|---|---|---|
| Electrophysiological function | Photopic and scotopic a and b wave amplitudes, and PhNR amplitudes are all reduced after blunt injury compared to intact eyes. | There are no changes in ERG or VEP amplitudes. | Blunt ocular injury causes reduced function of photoreceptors, INL cells and RGCs at 2 weeks. Blast injury does not cause any changes in retinal or ON function at 28 dpi in my experiments. | 1. Assess mfERG responses after blunt and blast injuries to determine specific area of retinal ERG dysfunction.<br>2. Perform visual acuity tests. |

**Table 7.1 Summary of findings, implications and suggestion for future investigation using the blunt and blast injury models**

| *Finding* | *Blunt injury finding* | *Blast injury finding* | *Implications* | *Further investigation* |
|---|---|---|---|---|
| Caspase-2 expression | There was increased *caspase-2* mRNA and cleaved 12 kDa caspase-2 protein fragments at 48 hours after blunt injury. Caspase-2 was immuno-localised to BRN3A$^+$ RGCs and INL cells. | Evidence suggestive of increased cleaved caspase-2 7 dpi, but further investigation is required. | After blunt ocular injury, cleaved caspase-2 is increased and is localised to RGC and INL cells, indicating caspase-2 activation, but, further investigation is required to determine caspase-2 expression after blast injury. | 1. Investigate the upstream mechanisms of caspase-2 activation.<br>2. Investigate the downstream mechanisms of caspase-2-dependent RGC death in blunt ocular injury<br>3. Determine if caspase-2 and necroptosis are linked.<br>4. Use another siRNA against caspase-2 and a scrambled siRNA control to confirm that there are no off-target effects<br>5. Assess off-target effects in these models |
| Inflammatory response | N/A | There were vitreal hyper reflective dots in OCT imaging after delayed siCASP2 injections but not after pre-blast siCASP2 treatment or rPBI alone. There were ED1$^+$ cells in the ON in all blast injured groups but not in sham-treated eyes. | Vitreal inflammation occurs due to intravitreal injections in combinations with rPBI, but not exposure to the blast wave alone. ED1$^+$ cells could be infiltrating macrophages or activated microglia and are increased in all blast injured groups. | 1. Quantify ED1$^+$ macrophages in blunt injured ON<br>2. Quantify ED1$^+$ macrophages in blunt and blast eyes treated with siCASP2.<br>3. Label oncomodulin$^+$ macrophages and assess CNTF levels<br>4. ED1 stains microglia and macrophages, so perform double-labelling experiments to confirm cell type<br>5. Assess hyper reflective dots in OCT *in vivo* images in blunt injured animals. |
| ON pathology | N/A | There were increased numbers of degenerating axons in the ON of rPBI | The timing of siCASP2 intravitreal injections is important in determining the | 1. Assess the effects of caspase-2 injections at different time points after blunt injury. |

| | | | | |
|---|---|---|---|---|
| | | eyes, and fewer in siCASP2 treated eyes if siCASP2 was injected before the blast. | outcome of ON pathology. If the injections are given at the same time as the blast there is no effect, but if siCASP2 and siEGFP are given prophylactically then there are reduced numbers of degenerating ON axons compared to rPBI with no injections. siCASP2 treatment leads to fewer degenerating axons compared to siEGFP treatment, indicating siCASP2 might have some ON axon protective effect. Intravitreal injections at the same time as blast injury will not be clinically translatable and further investigation is required to determine whether giving the intravitreal injection 2 – 7 days after injury will be beneficial. | 2. Assess therapeutic window of delivery.<br>3. Extend blast injured studies to later time points.<br>4. Use a different siRNA, such as a scrambled siRNA to confirm that siEGFP isn't having off-target effects in these models.<br>5. Perform EM to determine whether myelin or axonal degeneration is occurring |
| RGC pathology | Treatment with siCASP2 protects BRN3A$^+$ RGCs in the peripheral region of the impact site (600 µm), but not at the centre, compared to siEGFP controls. | There are no differences in the number of RBPMS$^+$ RGCs in retinal cryosections in eyes treated with siCASP2 pre-blast at 14 dpi, or the number of RBPMS$^+$ RGCs on retinal whole mounts at 28 dpi, compared to siEGFP controls. | siCASP2 may prevent RGC death in a specific area in the blunt injury model if injected at time of injury, suggesting this could be beneficial in clinical translation. After blast injury, RBPMS$^+$ RGCs did not decrease in numbers compared to sham-treated eyes at 28 dpi, indicating that RGCs do not degenerate at | 1. Perform *in vivo* imaging of RGCs in blunt injured eyes to confirm effect of focal impact and in rPBI eyes to determine if there are focal pockets of RGC death in the same animals.<br>2. Perform quantification of RBPMS$^+$ RGCs in retinal whole mounts on blunt injured eyes to confirm focal nature of injury |

| | | | | |
|---|---|---|---|---|
| | | | this time point. Therefore no effect of siCASP2 treatment was seen. | |
| Electrophysiological function | siCASP2 treatment preserves PhNR amplitudes compared to siEGFP treatment, but there is no effect on photopic or scotopic a -wave or b-wave amplitudes. | There are no changes in ERG or VEP amplitudes. | In blunt ocular injury, siCASP2 is likely to restore some functional activity of RGCs, but not other retinal cells. The impact on electrophysiological function from rPBI needs further investigation. | 1. Perform mfERG after blunt and blast injuries to determine function of specific areas of retina<br>2. Perform visual acuity tests |

**Table 7.2 Summary of findings, implications and further investigation of caspase-2 expression in blunt and blast ocular injuries**

| *Finding* | *Blunt injury finding* | *Blast injury finding* | *Implications* | *Further investigation* |
|---|---|---|---|---|
| RIPK1, RIPK3 and MLKL expression | There are no changes in *ripk1* and *mlkl* mRNA levels but a decrease in *ripk3* mRNA at 48 hours after blunt injury is detected. MLKL protein expression is higher 5 hours after injury and remains elevated until 48 hours. MLKL expression increases at the focal impact site in OPL, ONL, INL and GCL cells at 48 hours. | Expression of necroptotic markers is still under investigation | Necroptosis is likely to be occurring at the centre of the blunt impact site, but the expression of necroptotic pathway members after blast injury requires further investigation. | 1. Re-do RT-qPCR experiments with pre-optimised and specific TaqMan primers and perform unilateral injury and treat contralateral eye as control to account for inter animal genetic variability.<br>2. Complete western blots for RIPK1, RIPK3 , MLKl and P-MLKL in rPBI studies<br>3. Determine if RIPK1 and RIPK3 are co-localised through co-immunoprecipitation or confocal imaging<br>4. Determine if MLKL translocates to the plasma membrane by confocal microscopy. |
| Inflammatory response | N/A | There are vitreal hyper reflective dots in OCT imaging after Nec-1s and vehicle injections but not after rPBI alone or in sham-treated eyes. There are $ED1^+$ cells in the ON in all blast injured groups but not in sham. | Vitreal inflammation occurs due to injections in combination with rPBI, but not exposure to the blast wave alone. $ED1^+$ cells could be infiltrating macrophages or activated microglia and increase in all blast injured groups. | 1. Quantify $ED1^+$ macrophages in blunt injured ON<br>2. ED1 stains microglia and macrophages, so perform double labelling experiments to confirm cell type<br>3. Assess hyper reflective dots in OCT images *in vivo* in blunt injured animals. |
| ON pathology | N/A | There are more axons with degenerative profiles after rPBI at 28 dpi, and they are not affected by Nec-1s and | After rPBI there are degenerating ON axons, but these aren't reduced by Nec-1s treatment. | 1. Extend blast injury studies to later time points. |

| | | | | |
|---|---|---|---|---|
| | | vehicle injections. There are no differences in the number of intact axons or axon density across groups. | | 2. Perform EM to determine whether myelin or axonal degeneration is occurring |
| RGC pathology | The number of RBPMS$^+$ and RBPMS$^+$ RGCs is greater in Nec-1s treated eyes compared to vehicle treated eyes at the centre of the impact site. | There is a reduction in the number of RBPMS$^+$ RGCs after Nec-1s and vehicle intravitreal injections compared to rPBI alone, although Nec-1s treated eyes have more RBPMS$^+$ RGCs compared to vehicle in the middle portion of the retina. | Inhibition of necroptosis using Nec-1s might provide some RGC neuroprotection at the centre of the focal blunt injured impact site. After rPBI, intravitreal injections - irrespective of the compound - reduced the number of RBPMS$^+$ RGCs, suggesting that this caused additive pathology. The higher RGC number in the middle portion of the retinae in Nec-1s treated eyes compared to vehicle, might suggest some neuroprotective effect, although this requires further investigation | 1. Assess the effects on RBPMS$^+$ RGC of siCASP2 and Nec-1s injections after blunt ocular injury to see if there are additive neuroprotective effects.<br>2. Perform *in vivo* imaging of RGCs in blunt injured eyes to confirm focal nature of impact site effects and in rPBI eyes to determine if there are focal pockets of RGC death in the same animals. |
| Electrophysiological function | There is no improvement in photopic or scotopic a-wave or b-wave amplitudes or PhNR amplitudes after Nec-1s treatment compared to vehicle treatment. | There are no changes in ERG or VEP amplitudes. | Nec-1s treatment did not provide functional RGC protection compared to vehicle, indicating that RGCs may be surviving but are not functional, or that the effects are too subtle to be detected. | 1. Perform mfERG after blunt and blast injury to determine function of specific areas of retina |

**Table 7.3 Summary of findings, implications and further investigation of necroptosis in blunt and blast ocular injuries**

### 7.1.1. Cell death mechanisms

The mechanisms that initiate ocular pathology and cell death signalling pathways in the blunt injured eyes compared to repeated blast exposed eyes may be due to differences in injury induction. For instance, blunt injury causes a physical impact to the sclera covering the retina, which is likely to cause mass necrotic death and release of ATP from these cells, triggering death of surrounding cells (Mikolajewicz et al., 2018, Zheng et al., 1991). Alternatively, the primary blast wave might cause sheering of ON axons and blood vessels causing direct damage to the ON, rather than a physical impact to the cells in the eye (Bridges, 2006).

Cell death mechanisms are often interlinked and the downregulation of one signalling pathway member can induce another cell death signalling pathway to become activated. It has recently been proposed that caspase-2 negatively regulates necroptosis, and downregulation of caspase-2 using shRNA or the CRISPR/Casp9 system enhances phosphorylation of RIPK1 and MLKL, indicators of the activation of necroptosis (Zamaraev et al., 2018). Interestingly, after blunt ocular injury, downregulation of caspase-2 did improve RGC survival in the region peripheral to the impact site, but the number of RGCs preserved could have been under represented if the suppression of caspase-2 expression was causing activation of necroptosis in some RGCs. More experiments to determine whether necroptosis is affected by siCASP2 in our models would help provide more insight. Further, a combination of caspase-2 and necroptosis inhibition might provide additive improvement of RGC survival and functional restoration of vision. Apoptotic and necroptotic death can occur simultaneously in the same cell type (Lin et al., 2016) , so potentially, siCASP2 could be enhancing necroptotic death at the centre of the impact site, where Nec-1s

improved RGC numbers, through disinhibition of necroptosis (by preventing caspase-2 negatively regulating necroptosis).

I have not investigated photoreceptor death in the rPBI model. Mammadova et al., found there was degeneration of photoreceptors causing reduced ONL thickness after a single blast exposure of 43.5 psi repeated over 3 consecutive days (Mammadova et al., 2017). This could be due to the high-pressure causing blast wind as well as a blast wave, potentially causing some low-level blunt injury. Interestingly, in a low level primary blast injury rodent brain model which used TNT in an open space, there were prominent $TUNEL^+$ oligodendrocytes and astrocytes in the white matter as early as 1 day after a blast of 7.1 psi but low caspase-3 immunofluorescent staining, suggesting the mechanisms of damage were non-apoptotic (Pun et al., 2011). The authors identified genes which were upregulated after mild blast exposure; genes related to tissue repair were upregulated at 4 and 7 days after blast exposure (Pun et al., 2011), suggesting that there were attempts to repair brain injury induced by low blast wave exposure.

A recent study by Bernardo-Colon et al., has demonstrated in the same mouse rPBI model as my studies, that caspase-1-dependent pyroptotic death, indicating increased caspase-1 cleavage, at 28 dpi (Bernardo-Colon et al., 2018). A high vitamin C or E diet prevented caspase-1 cleavage and downstream pyroptosis, as well as restitution of ON degenerative profiles and electrophysiological retinal function (Bernardo-Colon et al., 2018). Interestingly, necroptosis has been shown to act upstream of the NLRP3 inflammasome and pyroptosis. In necroptosis, MLKL is phosphorylated and translocates to the cell membrane, causing pore formation, $K^+$ efflux and cell death

(Conos et al., 2017, Gutierrez et al., 2017, Kang et al., 2014). A decrease in intracellular $K^+$ can activate the NLRP3 inflammasome, leading to caspase-1 cleavage and activation, downstream interleukin maturation and pyroptotic death. RIPK3 can also activate the NLRP3 inflammasome in the absence of MLKL (Lawlor et al., 2015). A recent study demonstrated that different cell death pathways can occur in the same model in different cell types (Viringipurampeer et al., 2016). The authors investigated photoreceptor cell death in the P23H rhodopsin model of retinal degeneration. They showed that necroptotic proteins are upregulated in rods and treatment with Nec-1 improves rod photoreceptor survival, whereas, NLRP3, caspase-1 and mature IL-1β and IL-18 are upregulated in cone photoreceptors and cone survival is improved in an *Nlrp3*-deficient mouse (Viringipurampeer et al., 2016).

### 7.1.2. Inflammation in blunt versus blast injury

Inflammation can be advantageous but also detrimental if it becomes uncontrolled. $ED1^+$ cells could be infiltrating macrophages or activated resident microglia. The number of retinal $ED1^+$ cells were higher after injury compared to sham at 3 dpi, suggesting that macrophages may be infiltrating the retina and phagocytosing cell debris. PBI does not cause a physical injury or pathogen invasion; therefore, PBI can be classed as causing sterile inflammation. Bernardo et al., have proven sterile inflammation and activation of the inflammasome pathway occurs in the same rPBI model as my experiments; however, the authors did not investigate inflammatory cell infiltration (Bernardo-Colon et al., 2018). Sterile inflammation occurs after ischaemic stroke, where the infiltrating macrophages remove DAMPS and promote recovery, as well as releasing neurotrophic factors to promote neural repair (Nakamura and

Shichita, 2019). Sterile inflammation may be beneficial in rPBI and help promote tissue repair and recovery.

Retinal macrophages also infiltrate at early time points after blunt ocular injury, demonstrating that there is inflammation occurring within days of injury in both injury models. Inflammatory macrophages clear debris (Stoll et al., 1989) and can promote ON axonal regeneration after injury (Cui et al., 2009, Yin et al., 2009). My results are consistent with previous work by Blanch et al., who showed there were ED1$^+$ macrophages in the INL and ONL 2 days after blunt ocular injury, which clear debris from degenerating photoreceptor outer segments (Blanch et al., 2012b).

At later time points, for example 1 month later, there were few macrophages in the retina after rPBI untreated with intravitreal injections, but increased levels after vehicle injections and intermediate levels in Nec-1s treated eyes. This result was similar to the results of *in vivo* OCT imaging, which showed more hyper reflective dots in the vitreous of eyes exposed to rPBI and intravitreal injections, but fewer in contralateral eyes exposed indirectly to the blast wave but which also received intravitreal injections. This implies that the combination of blast wave exposure and intravitreal injections is causing increased inflammation and inflammatory cell infiltration which persists for up to 1 month. This persistent inflammation might not be advantageous and may be causing further damage. In the ON, there were infiltrating ED1$^+$ macrophages in eyes exposed to rPBI, with similar levels after intravitreal injections, at 28 dpi. This suggests that there is persistent inflammation in the ON, but, as this observation is associated with increased axons with degenerative profiles and

unravelling myelin, the infiltrating macrophages are most likely phagocytosing and clearing debris.

Cell death pathways can also be induced in inflammatory cells to help resolve inflammation or promote neuroprotection. Microglia can induce neuronal loss when activated in traumatic, ischemic and neurodegenerative disease. Fricker et al., showed that neurons can be protected using a pharmacological caspase inhibitor, as this promotes necroptosis specifically within inflamed microglia (Fricker et al., 2013). In another study, inhibition of necroptosis using Nec-1 resolved inflammation through inducing caspase-dependent apoptosis in neutrophils (Jie et al., 2016).

### 7.1.3. Retinal and visual function

Recordings of electroretinograms were performed in both blunt and blast injured animals. The ERG results in the blunt injury model replicated results from previous publications, demonstrating that there is a reduction in ERG amplitudes at 2 weeks after blunt ocular injury (Blanch et al., 2014, Blanch et al., 2012b). However, previous studies from our laboratory had not analysed the PhNR response, which reflects RGC function (Wilsey et al., 2017, Li et al., 2005, Porciatti, 2015). In this thesis, I demonstrated there was a reduction in PhNR amplitudes in blunt injured animals treated with siRNA control injections compared to sham-treated eyes. siCASP2 injections were associated with higher PhNR amplitudes which suggests that knockdown of caspase-2 may improve the function of RGCs. There were no alterations in upstream ERG responses representing photoreceptor and inner nuclear cell electrical activity, suggesting that this increase in PhNR amplitudes is specific to RGCs. However, there were no changes in retinal function after blunt injury followed

by Nec-1s treatment compared to vehicle control, even though there were more surviving RBPMS$^+$ RGCs at the centre of the impact site after blunt injury in Nec-1s treated eyes compared to vehicle treated eyes, indicating that there is likely some prevention of RGC death by Nec-1s treatment which is not enough to translate to detectable functional recovery. Alternatively, Nec-1s may promote an increase in RBPMS$^+$ immunofluorescent staining within RGCs or RGCs remain present but non-functional before they are phagocytosed and cleared.

The ERG and VEP amplitudes in rPBI experiments were lower than expected for sham-treated mice compared to experiments performed previously in the same laboratory. For instance, my recordings of sham-treated mice detected N1 responses approximately 20 μV in amplitude, whereas previous experiments recorded N1 amplitudes of 40μV (Bernardo-Colon et al., 2018). Mice were dark-adapted overnight and anaesthetised using ketamine. Under project license regulations, mice could only be anaesthetised with ketamine once per week, and since light exposure during recordings reverses the effects of dark-adaptation, each mouse could only be tested at one opportunity.

To confirm the reduction of RGC function after blunt ocular injury and to assess the localisation of the injury, I could perform multifocal ERG (mfERG) which simultaneously assesses electrophysiological retinal function at multiple locations (Lalonde et al., 2006, Holder, 2004, Azarmina, 2013, Stiefelmeyer et al., 2004). This would allow assessment of the specific localisation of the blunt injury, and whether function of the whole retina is affected or focal areas. I could also assess RGC function by measuring the scotopic threshold response (pSTR) or pattern ERG (PERG). PERG

measures the electrical responses similar to flash ERGs, but the stimulus is a flickering from a contrast-reversing checkerboard rather than a flash of light (Porciatti, 2015). The electrophysiological responses are RGC-dependent and the recordings from PERGs are more sensitive to RGC degeneration than pSTR measurement in ERG recordings. Following ONC injury, RGCs begin to structurally degenerate at 7 dpi shown by a decrease in RGC numbers (Berkelaar et al., 1994), which is replicated by the absence of a PERG response. Alternatively, the pSTR response displays an under representation of RGC degeneration, with only a 50% decrease in pSTR amplitude after ONC (Liu et al., 2014).

VEPs measure post-retinal visual pathway responses and are a more invasive measure since they require the implantation of electrodes into the visual cortex. An injury to any part of the visual pathway will result in a reduction in VEP responses, which includes injury to the ON (Ridder and Nusinowitz, 2006). The amplitude and latency can be measured from the VEP: latency correlates with the speed of conduction and can be used to assess the degree of myelination since longer latencies correlate with demyelination; amplitude correlates with axonal loss (You et al., 2011).

### 7.1.4. Assessment of RGC survival

Throughout this thesis, I quantified RGC numbers using different methods and markers, which developed and evolved throughout the project. Initially, in the blunt injury model, I counted RGCs using β-IIII-tubulin (results not shown in thesis) and BRN3A$^+$ immunofluorescent staining and quantified the number of cells in the GCL which were positively labelled. However, I found that the quantification of β-III-tubulin positive cells was subjective, because β-III-tubulin stains overlapping cell membranes

and the GCL is in immediate proximity to the RNFL containing RGC axons, which were also immunolabelled. BRN3A is a nuclear transcription factor and was easier to quantify positively labelled cells due to its nuclear location, but, studies have shown that BRN3A expression is affected by injury (Nadal-Nicolas et al., 2009). For later studies, I introduced RBPMS as an RGC marker and although it requires more research to assess its reliability, it does not appear to undergo changes in expression after injury, it stains a greater proportion of the RGC population than BRN3A, and it is easy to quantify positively labelled cells, thus making it the best immunofluorescent RGC marker for research on ocular injury models (Kwong et al., 2011, Rodriguez et al., 2014b, Kwong et al., 2010).

Immunofluorescence and protein expression can be altered after injury. BRN3A expression is altered after ocular injury and this can provide an underestimation of the number of $BRN3A^+$ RGCs that have degenerated (Nadal-Nicolas et al., 2009). However, to date, RBPMS has not shown these effects and measurements with RBPMS are consistent with the gold standard Fluorogold quantitative measure of RGC numbers (Kwong et al., 2011, Kwong et al., 2010). As my results show similar results for both $BRN3A^+$ and $RBPMS^+$ RGC counts in my studies, I am confident my results for this study are representative of surviving RGCs.

It must be highlighted that the increased number of surviving RGCs which were positively labelled by specific RGC markers in my studies, indicate, but do not confirm that these treatments are promoting RGC survival. An alternative method would be to perform *in vivo* imaging of RGCs and assess the same cell population in the same animal over time. One of the ways that this can be achieved is by using a confocal

scanning laser ophthalmoscope to image fluorescent cells expressing Annexin-5 on the outside of the phospholipid membrane, which is a feature of cellular apoptosis (Yap et al., 2018, Cordeiro et al., 2004, Maass et al., 2007). This method is called DARC technology and has successfully been used in multiple animal studies of neuroprotection, as well as in patients with glaucoma (Cordeiro et al., 2017). However, not all retinal cells degenerate through apoptosis. RGCs can also be imaged in vivo using viral vectors (Smith and Chauhan, 2018) or through adaptive optics scanning light ophthalmoscopy, which doesn't require any invasive injections (Rossi et al., 2017). I found that there was variation in the location where there were increased numbers of RGCs compared to controls after siCASP2 and Nec-1s treatments, implying that caspase-2-dependent apoptotic RGC death is likely to occur in the peripheral region to the impact site and necroptotic death may occur at the centre of the impact site. Further investigation using *in vivo* RGC imaging techniques alongside treatments, would provide a better understanding of these injuries.

### 7.1.5. ON degeneration

In the ON, axons are wrapped in a myelin sheath which allows for fast conduction of electrical signals from the eye to the brain. If the myelin sheath is damaged, the signal can be delayed or distorted. I assessed ON axonal morphology in the far proximal section of the ON (closest to the eye) using resin embedded semi-thin cross sections stained with PPD and toluidine blue to stain the myelin and cells, respectively. After rPBI, there were increases in the number of axons with a degenerative profile as early as 7 days, which persisted until 28 dpi. The ON injury at this early time point suggests that the ON itself is being damaged directly by the overpressure blast wave, rather

than secondary to retinal injury and RGC degeneration. The primary blast wave causes axonal shearing and rupture of cortical vessels (Bridges, 2006).

Vest et al., showed that blast exposure in quick succession causes significant ON axonal degeneration (Vest et al., 2019). For example, 3 blasts separated by 0.5 seconds caused 15% axonal degeneration at 2 weeks after injury, but, if this interval was increased to 10 minutes, there was no significant injury compared to sham (Vest et al., 2019). Furthermore, exposure to 15 psi once per day over 6 consecutive days only caused 3% axonal degeneration (Vest et al., 2019), suggesting that the impact of multiple blasts in quick succession caused more ocular pathology and may be representative of closed-space explosions where the blast overpressure wave will impact multiple times within seconds. An explanation is that the ON is bending and compacting and there is not enough time between the 0.5 second interval for the ON axons to recover, whereas with longer time intervals the ON axons recover, and therefore, there is not as much damage observed. In a future experiment, I could perform the rPBI inside an MRI scanner and observe the effects on the visual system in real-time, including the movement of the ON. But, current MRI sequences might be too slow to detect any changes.

It is not possible to distinguish whether the myelin surrounding axons is damaged or the actual axon itself is degenerating from their appearance in thin sections. Instead, I could image the axons using electron microscopy to look for axonal compaction and degeneration.

## 7.2. Choice of animal models

Most of the models of blunt ocular injury, which are summarised in Table 1.2 were not considered for use in this study. The rat blunt ocular injury model I used for my research was developed at University of Birmingham by Lt Col Richard Blanch (Blanch et al., 2012b), and consistently produces a reproducible retinal impact site with ONL thinning, which is a feature of commotio retinae and reflects what is seen in humans with closed globe injuries (Islam et al., 2016). The other models of blunt ocular injury used larger species, such as pigs, rabbits, cats and owl monkeys (Hart and Blight, 1979, Blight and Hart, 1977, Gregor and Ryan, 1982b, Bunt-Milam et al., 1986, Cox, 1980, Sipperley et al., 1978); whereas, our model uses rats which are easier to house and cheaper. The other animal models mainly aim the impacting object at the cornea, rather than the sclera overlying the retina. This is discussed further later in the discussion.

The primary blast injury model which I used in my studies specifically exposes the left eye of mice to a primary blast wave induced by a modified paintball gun (Bricker-Anthony et al., 2014b, Hines-Beard et al., 2012), whilst the right eye receives a milder blunt injury from impact against the side of the placement tube (Bricker-Anthony and Rex, 2015). The model was updated in the last few years, from a single blast of 26 psi to repeat exposure to low level overpressure waves of 15 psi (Bernardo-Colon et al., 2018, Vest et al., 2019). Exposure to an overpressure wave of 26 psi caused minimal retinal and ON pathology and there was a high incidence of mortality (Bricker-Anthony et al., 2016). This finding is consistent with TBI studies, where PBI was induced by a compressed gas shock tube, causing moderate TBI with a blast exposure of between 22-32 psi and lethality above 42 psi (Mishra et al., 2016).

Many studies have previously focused on a single blast wave exposure of >20 psi (Allen et al., 2018, Bricker-Anthony et al., 2016, Bricker-Anthony et al., 2014b, Bricker-Anthony and Rex, 2015, DeMar et al., 2016, Dutca et al., 2014, Jiang et al., 2013, Koliatsos et al., 2011, Reiner et al., 2014, Zou et al., 2013b, Hines-Beard et al., 2012). Repeated exposure to 15 psi in quick succession models a closed-space explosion which could be experienced by military personnel during combat or victims of terrorist attacks. In this scenario, the blast wave does not dissipate and propagates off surfaces, resulting in multiple impacts in quick succession (Ning and Zhou, 2015). Exposure to multiple low-level blasts can also affect military instructors of breacher training (Capo-Aponte et al., 2015). I wanted to investigate the effects of repeated low-overpressure blast wave exposure, rather than a single high-pressure blast. I also wanted to examine the effects of primary blast wave exposure specifically to the eye, rather than to the head and body. Therefore, I decided to use the modified paintball gun model in Dr Tonia Rex's lab, where only the eye is exposed and the head and body are covered with PVC.

### 7.3. Do the models replicate direct or indirect TON?

Direct TON can occur from penetrating injury, violent rotational injury which causes avulsion from the globe or crush due to fragments of bone following an impact (Thanos et al., 2012, Steinsapir and Goldberg, 2011). The ONC model causes direct TON and is commonly used to investigate RGC degeneration and regeneration and can be used to test therapeutics. Indirect TON is more common and is caused by injury distant to the ON, such as blunt impact to the eye, which can be caused by debris or shrapnel carried in an explosive blast wind or impact from a sports ball. At the start of the project,

I thought that both the rPBI and blunt injury models were replicating indirect TON, where the ON is not directly impacted or damaged but degenerates due to secondary injury. I still believe that blunt ocular injury causes indirect TON, because the direct physical impact to the eye is to the underlying retina; however, ON degeneration has not been investigated in this model, and therefore it cannot be concluded whether it is causing optic neuropathy. In my studies, I have shown that myelin is unravelling from degenerating axons as early as 7 days after rPBI and persists until the latest time point I measured at 28 dpi. However, I have shown that there was no reduction in RGC count up to 28 dpi, but I cannot discount the fact that RGCs may have been degenerating or dysfunctional later on. In this model, unravelling of myelin from the ON axons precedes RGC death, and thus, this result suggests that PBI may be directly impacting the ON and primarily causing ON axonal degeneration. This data implies that PBI might be a model of direct TON.

In a rodent blunt ocular injury model, there is focal retinal injury with photoreceptor and RGC death, caused by projection of a low weight plastic pellet impacting the inferior sclera (Thomas CN, 2018, Blanch et al., 2014, Blanch et al., 2012b). I focused on the retinal injury and did not directly research ON pathology. Therefore, I did not determine whether ON injury precedes ocular injury; however, this could be investigated in future experiments. For example, I could produce PPD-stained resin embedded semi-thin ON cross-sections at different time points after blunt ocular injury and quantify the number of ON axons with a degenerative profile and myelin structure.

### 7.4. Comparisons with human studies

My results demonstrate a reduction in both $RBPMS^+$ and $BRN3A^+$ RGC counts 2 weeks after injury and there is also a functional decrease in PhNR amplitudes,

implying that RGCs have reduced numbers and functional activity after injury. In human studies of blunt ocular injury, the GCC and RNFL, which are measures of RGC axons and indirectly RGC survival, are reduced 2 weeks after injury (Cennamo et al., 2013). Furthermore, commotio retinae occurs in approximately 17% of closed globe injuries, and is characterised by photoreceptor degeneration (Islam et al., 2016), and in our blunt ocular injury model there is reduced ONL thickness 2 weeks after injury, which is representative of the human disease. My results are representative of what occurs in human injured eyes to both RGCs and photoreceptors, and therefore, is a good model to test therapeutics which could be clinically translated.

Soldiers who are deployed to train at breacher schools can be exposed to blast waves of approximately 6 psi on average up to 15 times per day and display reduced corneal endothelial cell density and visual field sensitivity but display no significant retinal or optic nerve pathology (Capo-Aponte et al., 2015). Blast exposure within closed-spaces can reach much higher pressures and multiple impacts within a short timeframe, due to the lack of dissipation of the blast wave and deflection off structures. I have shown significant ON injury after rPBI but no ON pathology was demonstrated in military breachers. This difference may be because they are exposed to multiple blasts with large interblast intervals. It is still likely that ON pathology will occur after exposure to multiple blast overpressure waves impacting the ON in quick succession (Vest et al., 2019), which is likely to occur during a closed-space explosion rather than an open-space explosion. It is difficult to study the effects of primary blast wave exposure in humans without the confounding effects of secondary, tertiary and quaternary injuries.

## 7.5. Study limitations

### 7.5.1. Species variations between models

One of the limitations of this research was the variation in animal species used throughout the study. In blunt injury experiments, female Lister-hooded rats were used, and in rPBI experiments, male C57 Bl6 mice were used. These were the species that were well-characterised for these models from previous studies, and I wanted to primarily investigate the effects of neuroprotective compounds rather than alter components of the models.

### 7.5.2. Technical limitations of the *in vivo* models

The blunt ocular injury rat model was developed by Lt Col Richard Blanch (Blanch et al., 2012b), and involves propelling a small plastic pellet to impact the inferior sclera and thus produce a reproducible retinal injury. However, in a real-life situation the cornea is probably more likely to be impacted or an eye injury produced through a closed eye lid. For the purposes of producing an *in vivo* rodent model, which produces reproducible impact and injury to the retina, impacting the inferior sclera is sufficient. For future experiments, I could create a model which impacts the cornea directly or through a closed eye-lid and compare the outcomes of ocular injury, as well as testing therapeutics.

The rPBI mouse model also has some limitations. The primary blast wave is produced from a modified paintball gun and is in close proximity with the eye. The blast wave is blocked from the rest of the head and body using PVC covering. However, PBI will not exclusively effect the eye in a real-life scenarios.

### 7.5.3. Controls

In the blunt ocular injury experiments, intact rats which did not receive an injury were used as uninjured controls. I also used vehicle controls which received the blunt injury but received intravitreal injections of the vehicle. In the rPBI study, I used sham treated mice that were exposed to the same procedure as rPBI exposed mice (anaesthetics, placed inside blast tubing etc.), except the overpressure blast wave was blocked using reinforced cardboard. A pressure transducer measured the blast to be >2 psi for sham treated mice and between 14-18 psi for blast injured mice. This means that there were still very low levels of the blast overpressure wave that were not blocked by the reinforced cardboard. To investigate whether ON pathology is occurring in sham treated animals, intact animals that were not exposed to any blocked blast wave should also be included. In other PBI studies, the sham mice are not exposed to the blast wave (Dutca et al., 2014, DeMar et al., 2016). I have included vehicle controls in my rPBI and blunt injury experiments, but I could have also included intact and sham-treated mice receiving intravitreal injections of treatments to determine whether the injections themselves (without the injury) had an effect.

#### 7.5.3.1. Eyes used for genetic studies

mRNA expression was measured in retina exposed to blunt ocular injury. However, I exposed animals to bilateral blunt ocular injuries and then used both eyes. If I was to perform the experiments again, I would have designed the experiment so that a single animal is exposed to a unilateral blunt injury and the contralateral eye is used as an intact control. This takes into account the variability in gene expression between animals of mixed genetic background.

### 7.5.4. Timing of intravitreal injections

I performed intravitreal injections immediately after the blunt ocular injury and repeated injections at 7 dpi, but the injections did not affect ocular pathology. In studies using the rPBI model, I found that the timing of my intravitreal injections surrounding the blast-wave was important, and in some cases, was detrimental.

In Chapter 5, I injected siCASP2 and siEGFP at two different times surrounding the rPBI. I was concerned about performing an intravitreal injection into an injured eye as, anecdotally, this can cause additive trauma and inflammation. However, I also wanted to inject the animals at a time that was clinically relevant. In my first experiment using the rPBI model, I performed intravitreal injections at 5 hours after the first blast followed by two further blasts on the following two consecutive days. However, at the 28-dpi endpoint, there were hyper reflective dots in the vitreal cavity. This could be suggestive of inflammatory cell infiltration and vitreal inflammation (Kokona et al., 2017). These hyper reflective dots were not present in the sham or rPBI treated groups which received no injections, suggesting that the injections themselves were causing more pathology. I then performed an additional study giving injections 48 hours pre-blast and performed OCT imaging at baseline, after the intravitreal injections, after the rPBI and 14 dpi. Due to time constraints and access to a limited quantity of mice, I only had 5 mice per group and could only perform the extra study with siCASP2 and siEGFP. I did not detect any vitreal hyper reflective dots or retinal structural abnormalities at any of the OCT imaging time points. This suggests that the intravitreal injections themselves did not cause vitreal hyper reflective dots and also that the dots were not present due to the compound that was injected. These studies imply that the timing of injections was important.

Vitreal inflammation in uveitis has been quantified by automated algorithms combined with OCT for use in human clinics, and this could be applied to my future studies to provide a quantitative measure of vitreal inflammation in rodents (Denniston et al., 2017, Montesano et al., 2018).

Intravitreal injections of compounds were repeated every 7 days, which is comparable to previous studies from our group, who injected siCASP2 every 8 days after ONC (Ahmed et al., 2011, Vigneswara and Ahmed, 2016, Vigneswara et al., 2014). Performing intravitreal injections weekly is not translatable to clinical practice due to the discomfort and inconvenience to patients and burden on the healthcare service. Therefore, there is a requirement for further research into the efficacy of siCASP2 at different time points after injury, for example, immediately following the injury, within a few hours and a few weeks afterwards. Further investigation is also required to determine whether reducing the frequency of injections provides as effective RGC neuroprotection.

### 7.5.5. Alternative methods of drug delivery

Intravitreal injections are used in the clinic to deliver therapeutics into the vitreous, which have an effect at back of the eye, for example, in the retina, choroid, RPE. But, intravitreal injections can be uncomfortable for patients, costly to provide by the healthcare service and can have side effects, such as infectious endophthalmitis (Falavarjani and Nguyen, 2013). I observed additive pathology when intravitreal injections were combined with rPBI, suggesting that this mechanism of delivery may not be translatable to humans. There are many emerging alternative mechanisms of

drug delivery which could overcome these issues. For example, the therapeutic compound could be applied as an eye drop and delivered topically. However, there are issues with drug delivery to the posterior portion of the eye, including biological barriers (such as the cornea), drug metabolism and elimination (Gower et al., 2016). Nanocarriers such as cell penetrating peptides (CPP) can be used to coat the compound and increase its permeability through biological barriers (Pescina et al., 2018) and to promote cellular internalisation (Bechara and Sagan, 2013). CPPs have been used to promote the drug penetration of anti-VEGF drugs, ranibizumab and bevacizumab, through the anterior segment to reduce choroidal neovascularisation in an age-related macular degeneration mouse model (de Cogan et al., 2017) and to deliver human acidic fibroblast growth factor after retinal ischemia-refusion injuries (Wang et al., 2010). CPP can be combined with siRNA, due to the negative charge of the RNA and positive charge of the CPP it forms electrostatic interactions (Beloor et al., 2015). Topical administration of siCASP2 with CPP complexes may be useful for future investigation to develop an eye drop that is less invasive but has the same therapeutic effect.

Another method of drug delivery is to administer the compounds systemically. For example, by subcutaneous injections or by mouth. There needs to be appropriate controls to ensure the compound is successfully reaching the target tissue and that there are no side-effects. Viringipurampeer et al., demonstrated that Nec-1s could be delivered through subcutaneous injections and rescue ONL thinning in a P23H rhodopsin model of retinal degeneration (Viringipurampeer et al., 2016), suggesting that the subcutaneous route could deliver compounds to the retina and provide RGC neuroprotection in my models of TON. In a rPBI mouse model, a diet with high levels

of vitamin C or E or a ketogenic diet have been shown to reduce inflammasome-induced mechanisms of retinal degeneration and ON pathology (Bernardo-Colon et al., 2018).

### 7.6. Future experiments

In this project, I have made a contribution to the ocular trauma field, particularly to retinal and ON pathologies caused by explosive blast devices. There are multiple future experiments that I would like to perform, given more time and unlimited funds. Firstly, the variation in animal models used to study explosive blast injuries tend to be limited to one aspect of the injury, for example, focusing exclusively on the primary blast wave in the eye and not accounting for other effects of the blast explosion. I'd like to perform primary blast wave exposure and secondary blunt impact injuries in combination, specifically to the eye, to determine whether the pathologies are comparable to primary or secondary injuries alone. Secondly, the modified paintball gun rPBI model only impacts the eye and does not account for injury to the head and visual centres. Also, other models have not investigated ON axonal structure and myelination or investigated the effects of caspase-2 and necroptosis. Therefore, I would like to repeat my experiments and outcomes using other PBI models, in particular a blast cannon (DeMar et al., 2016, Dutca et al., 2014) and the shock tube by Goldstein et al., where the mouse is not constrained and its head is allowed to move to allow for acceleration-declaration forces, which are likely to be present in real-life scenarios (Goldstein et al., 2012).

Furthermore, I would like to test a less invasive method of delivering therapeutics. It would have to be clinically relevant and appropriate for the current treatment of ocular

injury during combat or after traumatic events such as terrorist attacks. In particular, the drug would need to be easily applied, as victims often have multifactorial life-threatening injuries which need emergency attention. The therapeutics could be combined into an eye drop with an agent to improve the ocular permeability and potentially developed to be targeted to a specific cell type via its receptor (Vhora et al., 2014). Moreover, military ophthalmologists are not currently deployed to sites of conflict, therefore, soldiers with ocular injuries are flown to UK hospitals (including QE hospital in Birmingham) and treated by surgical teams. I need to investigate the therapeutic window for treatments, as if the treatment has an effect only within a couple of hours after injury, then the therapeutics may not be viable if delayed until the patient reaches hospital. An ideal treatment would be to place the therapeutic inside a gel or as an eye drop which provides slow release over the time between the injuries and when the eye can be treated, providing patients with the best chance of retaining their eye sight.

### 7.7. Translation of *in vivo* animal studies to human clinical trials

To ensure efficacy and safety, there are multiple steps to translate therapeutics from preclinical studies to being used to treat patients in the clinic (Umscheid et al., 2011). To test the safety and toxicity on a small group of healthy individuals, an initial proof of concept phase I clinical trial is performed. Next, phase II clinical trials test the safety and efficacy of the therapeutic in a larger group of subjects, which will include patients with the disease. Phase III clinical trials test the clinical effectiveness of the compound and compare the new therapeutic to the standard or commonly used drug to ensure that it has better efficacy in treating the disease and will be an improvement on the current standard of care. Finally, phase IV clinical trials are used to monitor the long-

term effectiveness and safety in the general population and is performed when the drug is on the market.

siCASP2 has completed phase I/IIa clinical trials for NAION and is in phase II trials for acute primary angle closure glaucoma (protocols QRK007 NCT01064505 and QRK208 NCT01965106) and is ongoing phase II / III trials for NAION with Quark Pharmaceuticals Inc. As the safety and toxicity effects have been tested in humans and efficacy tested in patients this is promising for the translation of this therapeutic for other ocular disease.

### 7.8. Other implications of our studies

In addition to providing information about retinal injuries after PBI and blunt impact ocular trauma, the findings of this thesis might also provide insight into pathologies that might occur in other scenarios. For example, neuronal death in TBI induced by explosive blasts (primary blast wave and also blunt impact), sports injuries such as an impact by a sports ball or during a tackle on a rugby pitch. Further, mild blunt impact to the eye or head may occur during a road traffic accident or during a fall.

### 7.9. Summary

In summary, I have investigated retinal and ON pathology and tested neuroprotective agents in models of primary and secondary explosive blast injury. In the blunt ocular injury model, there is focal retinal injury and RGC death. Necroptosis inhibition with Nec-1s provided some protection at the centre of the injury site whilst caspase-2 knockdown with siCASP2 provided protection in the immediate periphery and provided some improved RGC function. In a model of rPBI, there was early ON pathology at 7

days after injury, which persisted until 28 days, but this was not associated with RGC death up to 1-month post injury. Intravitreal injections after the first blast exacerbated RGC death and increased vitreal inflammation, mimicking the effect of a penetrating injury. Nec-1s treatment provided some RGC protection in the middle portion of the retina, suggesting that necroptosis occurs after rPBI combined with penetrating injuries, but perhaps not after rPBI alone. In the rPBI model, pre-blast injections of siCASP2 reduced the number of degenerating ON axons 14 dpi but had no effect on the number of RGCs. Delayed siCASP2 injections were detrimental and caused greater ON axonal pathology.

### 7.10. Conclusion

Caspase-2-dependent and necroptotic RGC death is likely to occur after blunt ocular injury and inhibition of caspase-2 and necroptotic pathways provides a degree of both structural and functional protection in animal studies; however, the roles of caspase-2 and necroptosis in blast injury remain unclear and require more investigation. My studies of rPBI have highlighted the importance of the timing of intravitreal injections around the time of injury, as this led to exacerbated RGC death and inflammation if given in quick succession. Taken collectively, this thesis provides some new information on the mechanisms of cell death in ocular injuries caused by primary blast wave exposure or blunt impact and the translation of possible therapeutics targeting caspase-2 and necroptotic pathways could help preserve vision in victims injured in terrorist attacks or our military personnel.

## References

ADAMS, J. M. & CORY, S. 1998. The Bcl-2 protein family: arbiters of cell survival. *Science (New York, N Y ),* 281**,** 1322-6.

ADAMS, J. M. & CORY, S. 2002. Apoptosomes: engines for caspase activation. *Current opinion in cell biology,* 14**,** 715-20.

AGUDO, M., PEREZ-MARIN, M. C., LONNGREN, U., SOBRADO, P., CONESA, A., CANOVAS, I., SALINAS-NAVARRO, M., MIRALLES-IMPERIAL, J., HALLBOOK, F. & VIDAL-SANZ, M. 2008. Time course profiling of the retinal transcriptome after optic nerve transection and optic nerve crush. *Mol Vis,* 14**,** 1050-63.

AGUDO, M., PEREZ-MARIN, M. C., SOBRADO-CALVO, P., LONNGREN, U., SALINAS-NAVARRO, M., CANOVAS, I., NADAL-NICOLAS, F. M., MIRALLES-IMPERIAL, J., HALLBOOK, F. & VIDAL-SANZ, M. 2009. Immediate Upregulation of Proteins Belonging to Different Branches of the Apoptotic Cascade in the Retina after Optic Nerve Transection and Optic Nerve Crush. *Investigative Ophthalmology & Visual Science,* 50**,** 424-431.

AHMED, Z., KALINSKI, H., BERRY, M., ALMASIEH, M., ASHUSH, H., SLAGER, N., BRAFMAN, A., SPIVAK, I., PRASAD, N., METT, I., SHALOM, E., ALPERT, E., DI POLO, A., FEINSTEIN, E. & LOGAN, A. 2011. Ocular neuroprotection by siRNA targeting caspase-2. *Cell death & disease,* 2**,** e173.

AL-UBAIDI, M. R. 2014. RGC-5: are they really 661W? The saga continues. *Exp Eye Res,* 119**,** 115.

ALLAM, R., LAWLOR, K. E., YU, E. C. W., MILDENHALL, A. L., MOUJALLED, D. M., LEWIS, R. S., KE, F., MASON, K. D., WHITE, M. J., STACEY, K. J., STRASSER, A., O'REILLY, L. A., ALEXANDER, W., KILE, B. T., VAUX, D. L. & VINCE, J. E. 2014. Mitochondrial apoptosis is dispensable for NLRP3 inflammasome activation but non-apoptotic caspase-8 is required for inflammasome priming. *Embo Reports,* 15**,** 982-990.

ALLEN, R., MOTZ, C. T., FEOLA, A., CHESLER, K., HAIDER, R., RAMACHANDRA RAO, S., SKELTON, L., FLIESLER, S. & PARDUE, M. T. 2018. Long-term functional and structural consequences of primary blast overpressure to the eye. *J Neurotrauma*.

ANDO, K., PARSONS, M. J., SHAH, R. B., CHARENDOFF, C. I., PARIS, S. L., LIU, P. H., FASSIO, S. R., ROHRMAN, B. A., THOMPSON, R., OBERST, A., SIDI, S. & BOUCHIER-HAYES, L. 2017. NPM1 directs PIDDosome-dependent caspase-2 activation in the nucleolus. *J Cell Biol*.

AZARMINA, M. 2013. Full-Field versus Multifocal Electroretinography. *J Ophthalmic Vis Res,* 8**,** 191-2.

BAHR, M. 2000. Live or let die - retinal ganglion cell death and survival during development and in the lesioned adult CNS. *Trends in Neurosciences,* 23**,** 483-490.

BALIGA, B. C., COLUSSI, P. A., READ, S. H., DIAS, M. M., JANS, D. A. & KUMAR, S. 2003. Role of prodomain in importin-mediated nuclear localization and activation of caspase-2. *J Biol Chem,* 278**,** 4899-905.

BECHARA, C. & SAGAN, S. 2013. Cell-penetrating peptides: 20 years later, where do we stand? *FEBS Lett,* 587**,** 1693-702.

BELOOR, J., ZELLER, S., CHOI, C. S., LEE, S. K. & KUMAR, P. 2015. Cationic cell-penetrating peptides as vehicles for siRNA delivery. *Ther Deliv,* 6**,** 491-507.

BEN SIMON, G. J., HOVDA, D. A., HARRIS, N. G., GOMEZ-PINILLA, F. & GOLDBERG, R. A. 2006. Traumatic brain injury induced neuroprotection of retinal ganglion cells to optic nerve crush. *J Neurotrauma,* 23**,** 1072-82.

BERGER, A. B., SEXTON, K. B. & BOGYO, M. 2006. Commonly used caspase inhibitors designed based on substrate specificity profiles lack selectivity. *Cell Res,* 16**,** 961-3.

BERGERON, L., PEREZ, G. I., MACDONALD, G., SHI, L., SUN, Y., JURISICOVA, A., VARMUZA, S., LATHAM, K. E., FLAWS, J. A., SALTER, J. C., HARA, H., MOSKOWITZ, M. A., LI, E., GREENBERG, A., TILLY, J. L. & YUAN, J. 1998. Defects in regulation of apoptosis in caspase-2-deficient mice. *Genes Dev,* 12**,** 1304-14.

BERKELAAR, M., CLARKE, D. B., WANG, Y. C., BRAY, G. M. & AGUAYO, A. J. 1994. Axotomy results in delayed death and apoptosis of retinal ganglion cells in adult rats. *The Journal of neuroscience : the official journal of the Society for Neuroscience,* 14**,** 4368-74.

BERNARDO-COLON, A., VEST, V., CLARK, A., COOPER, M. L., CALKINS, D. J., HARRISON, F. E. & REX, T. S. 2018. Antioxidants prevent inflammation and preserve the optic projection and visual function in experimental neurotrauma. *Cell Death Dis,* 9**,** 1097.

BERRY, M., AHMED, Z., LORBER, B., DOUGLAS, M. & LOGAN, A. 2008. Regeneration of axons in the visual system. *Restor Neurol Neurosci,* 26**,** 147-74.

BERRY, M., CARLILE, J. & HUNTER, A. 1996. Peripheral nerve explants grafted into the vitreous body of the eye promote the regeneration of retinal ganglion cell axons severed in the optic nerve. *Journal of neurocytology,* 25**,** 147-70.

BERRY, M., CARLILE, J., HUNTER, A., TSANG, W., ROSENSTIEL, P., ROSUSTREL, P. & SIEVERS, J. 1999. Optic nerve regeneration after intravitreal peripheral nerve implants: trajectories of axons regrowing through the optic chiasm into the optic tracts. *Journal of neurocytology,* 28**,** 721-41.

BIANCHI, M. E. 2007. DAMPs, PAMPs and alarmins: all we need to know about danger. *J Leukoc Biol,* 81**,** 1-5.

BLANCH, R. J., AHMED, Z., BERRY, M., SCOTT, R. A. H. & LOGAN, A. 2012a. Animal models of retinal injury. *Investigative ophthalmology & visual science,* 53**,** 2913-20.

BLANCH, R. J., AHMED, Z., SIK, A., SNEAD, D. R. J., GOOD, P. A., O'NEILL, J., BERRY, M., SCOTT, R. A. H. & LOGAN, A. 2012b. Neuroretinal cell death in a murine model of closed globe injury: pathological and functional characterization. *Investigative ophthalmology & visual science,* 53**,** 7220-6.

BLANCH, R. J., AHMED, Z., THOMPSON, A. R., AKPAN, N., SNEAD, D. R. J., BERRY, M., TROY, C. M., SCOTT, R. A. H. & LOGAN, A. 2014. Caspase-9 mediates photoreceptor death after blunt ocular trauma. *Investigative ophthalmology & visual science,* 55**,** 6350-7.

BLANCH, R. J., BINDRA, M. S., JACKS, A. S. & SCOTT, R. A. H. 2011. Ophthalmic injuries in British Armed Forces in Iraq and Afghanistan. *Eye (London, England),* 25**,** 218-23.

BLANCH, R. J., GOOD, P. A., SHAH, P., BISHOP, J. R. B., LOGAN, A. & SCOTT, R. A. H. 2013. Visual outcomes after blunt ocular trauma. *Ophthalmology,* 120**,** 1588-91.

BLANCH, R. J. & SCOTT, R. A. H. 2008. Primary blast injury of the eye. *Journal of the Royal Army Medical Corps,* 154**,** 76.

BLIGHT, R. & HART, J. C. 1977. Structural changes in the outer retinal layers following blunt mechanical non-perforating trauma to the globe: an experimental study. *Br J Ophthalmol,* 61**,** 573-87.

BOUCHIER-HAYES, L. & GREEN, D. R. 2012. Caspase-2: the orphan caspase. *Cell Death Differ,* 19**,** 51-7.

BRACKEN, M. B., SHEPARD, M. J., COLLINS, W. F., HOLFORD, T. R., YOUNG, W., BASKIN, D. S., EISENBERG, H. M., FLAMM, E., LEO-SUMMERS, L., MAROON, J. & ET AL. 1990. A randomized, controlled trial of

methylprednisolone or naloxone in the treatment of acute spinal-cord injury. Results of the Second National Acute Spinal Cord Injury Study. *N Engl J Med,* 322**,** 1405-11.

BRICKER-ANTHONY, C., HINES-BEARD, J., D'SURNEY, L. & REX, T. S. 2014a. Exacerbation of blast-induced ocular trauma by an immune response. *Journal of neuroinflammation,* 11**,** 192.

BRICKER-ANTHONY, C., HINES-BEARD, J. & REX, T. S. 2014b. Molecular changes and vision loss in a mouse model of closed-globe blast trauma. *Investigative ophthalmology & visual science,* 55**,** 4853-62.

BRICKER-ANTHONY, C., HINES-BEARD, J. & REX, T. S. 2016. Eye-Directed Overpressure Airwave-Induced Trauma Causes Lasting Damage to the Anterior and Posterior Globe: A Model for Testing Cell-Based Therapies. *J Ocul Pharmacol Ther,* 32**,** 286-95.

BRICKER-ANTHONY, C. & REX, T. S. 2015. Neurodegeneration and Vision Loss after Mild Blunt Trauma in the C57Bl/6 and DBA/2J Mouse. *PLoS One,* 10**,** e0131921.

BRIDGES, E. J. 2006. Blast injuries: from triage to critical care. *Crit Care Nurs Clin North Am,* 18**,** 333-48.

BROZ, P. & DIXIT, V. M. 2016. Inflammasomes: mechanism of assembly, regulation and signalling. *Nat Rev Immunol,* 16**,** 407-20.

BUI, B. V. & FORTUNE, B. 2004. Ganglion cell contributions to the rat full-field electroretinogram. *J Physiol,* 555**,** 153-73.

BUNT-MILAM, A. H., BLACK, R. A. & BENSINGER, R. E. 1986. Breakdown of the outer blood-retinal barrier in experimental commotio retinae. *Exp Eye Res,* 43**,** 397-412.

CALLUS, B. A. & VAUX, D. L. 2007. Caspase inhibitors: viral, cellular and chemical. *Cell Death Differ,* 14**,** 73-8.

CAO, W., WEN, R., LI, F., LAVAIL, M. M. & STEINBERG, R. H. 1997. Mechanical injury increases bFGF and CNTF mRNA expression in the mouse retina. *Exp Eye Res,* 65**,** 241-8.

CAO, Y., LI, X., SHI, P., WANG, L. X. & SUI, Z. G. 2014. Effects of L-carnitine on high glucose-induced oxidative stress in retinal ganglion cells. *Pharmacology,* 94**,** 123-30.

CAPO-APONTE, J. E., JUREK, G. M., WALSH, D. V., TEMME, L. A., AHROON, W. A. & RIGGS, D. W. 2015. Effects of repetitive low-level blast exposure on visual system and ocular structures. *J Rehabil Res Dev,* 52**,** 273-90.

CASERTA, T. M., SMITH, A. N., GULTICE, A. D., REEDY, M. A. & BROWN, T. L. 2003. Q-VD-OPh, a broad spectrum caspase inhibitor with potent antiapoptotic properties. *Apoptosis,* 8**,** 345-52.

CECCONI, F., ALVAREZ-BOLADO, G., MEYER, B. I., ROTH, K. A. & GRUSS, P. 1998. Apaf1 (CED-4 homolog) regulates programmed cell death in mammalian development. *Cell,* 94**,** 727-37.

CELLERINO, A., BAHR, M. & ISENMANN, S. 2000. Apoptosis in the developing visual system. *Cell Tissue Res,* 301**,** 53-69.

CENNAMO, G., FORTE, R., REIBALDI, M., MAGLI, A., DE CRECCHIO, G. & CENNAMO, G. 2013. Evaluation of retinal nerve fiber layer and ganglion cell complex thickness after ocular blunt trauma. *Eye,* 27**,** 1382-1387.

CERNAK, I., WANG, Z., JIANG, J., BIAN, X. & SAVIC, J. 2001. Ultrastructural and functional characteristics of blast injury-induced neurotrauma. *J Trauma,* 50**,** 695-706.

CHAMPION, H. R., HOLCOMB, J. B. & YOUNG, L. A. 2009. Injuries from explosions: physics, biophysics, pathology, and required research focus. *J Trauma,* 66**,** 1468-77; discussion 1477.

CHAUDHARY, P., AHMED, F., QUEBADA, P. & SHARMA, S. C. 1999a. Caspase inhibitors block the retinal ganglion cell death following optic nerve transection. *Brain research Molecular brain research,* 67**,** 36-45.

CHAUDHARY, P., AHMED, F., QUEBADA, P. & SHARMA, S. C. 1999b. Caspase inhibitors block the retinal ganglion cell death following optic nerve transection. *Molecular Brain Research,* 67**,** 36-45.

CHAUVIER, D., ANKRI, S., CHARRIAUT-MARLANGUE, C., CASIMIR, R. & JACOTOT, E. 2007. Broad-spectrum caspase inhibitors: from myth to reality? *Cell Death Differ,* 14**,** 387-91.

CHEN, G. Y. & NUNEZ, G. 2010. Sterile inflammation: sensing and reacting to damage. *Nat Rev Immunol,* 10**,** 826-37.

CHEN, H., ZHAO, Y., LIU, M., FENG, L., PUYANG, Z., YI, J., LIANG, P., ZHANG, H. F., CANG, J., TROY, J. B. & LIU, X. 2015. Progressive degeneration of retinal and superior collicular functions in mice with sustained ocular hypertension. *Invest Ophthalmol Vis Sci,* 56**,** 1971-84.

CHEUNG, Z. H., CHAN, Y.-M., SIU, F. K. W., YIP, H. K., WU, W., LEUNG, M. C. P. & SO, K.-F. 2004a. Regulation of caspase activation in axotomized retinal ganglion cells. *Molecular and cellular neurosciences,* 25**,** 383-93.

CHEUNG, Z. H., CHAN, Y. M., SIU, F. K., YIP, H. K., WU, W., LEUNG, M. C. & SO, K. F. 2004b. Regulation of caspase activation in axotomized retinal ganglion cells. *Mol Cell Neurosci,* 25**,** 383-93.

CHINNAIYAN, A. M., O'ROURKE, K., TEWARI, M. & DIXIT, V. M. 1995. FADD, a novel death domain-containing protein, interacts with the death domain of Fas and initiates apoptosis. *Cell,* 81**,** 505-12.

CHINNERY, H. R., MCMENAMIN, P. G. & DANDO, S. J. 2017. Macrophage physiology in the eye. *Pflugers Arch,* 469**,** 501-515.

CHO, R. I., BAKKEN, H. E., REYNOLDS, M. E., SCHLIFKA, B. A. & POWERS, D. B. 2009a. Concomitant cranial and ocular combat injuries during Operation Iraqi Freedom. *J Trauma,* 67**,** 516-20; discussion 519-20.

CHO, Y., CHALLA, S., MOQUIN, D., GENGA, R., RAY, T. D., GUILDFORD, M. & CHAN, F. K. M. 2009b. Phosphorylation-Driven Assembly of the RIP1-RIP3 Complex Regulates Programmed Necrosis and Virus-Induced Inflammation. *Cell,* 137**,** 1112-1123.

CHOI, J. H., GREENE, W. A., JOHNSON, A. J., CHAVKO, M., CLELAND, J. M., MCCARRON, R. M. & WANG, H. C. 2015. Pathophysiology of blast-induced ocular trauma in rats after repeated exposure to low-level blast overpressure. *Clin Experiment Ophthalmol,* 43**,** 239-46.

CHOUDHURY, S., LIU, Y., CLARK, A. F. & PANG, I. H. 2015. Caspase-7: a critical mediator of optic nerve injury-induced retinal ganglion cell death. *Mol Neurodegener,* 10**,** 40.

COCKERHAM, G. C., RICE, T. A., HEWES, E. H., COCKERHAM, K. P., LEMKE, S., WANG, G., LIN, R. C., GLYNN-MILLEY, C. & ZUMHAGEN, L. 2011. Closed-Eye Ocular Injuries in the Iraq and Afghanistan Wars. *New England Journal of Medicine,* 364**,** 2172-2173.

COLUSSI, P. A., HARVEY, N. L. & KUMAR, S. 1998. Prodomain-dependent nuclear localization of the caspase-2 (Nedd2) precursor. A novel function for a caspase prodomain. *J Biol Chem,* 273**,** 24535-42.

CONNOLLY, P. F., JAGER, R. & FEARNHEAD, H. O. 2014. New roles for old enzymes: killer caspases as the engine of cell behavior changes. *Front Physiol,* 5**,** 149.

CONOS, S. A., CHEN, K. W., DE NARDO, D., HARA, H., WHITEHEAD, L., NUNEZ, G., MASTERS, S. L., MURPHY, J. M., SCHRODER, K., VAUX, D. L., LAWLOR, K. E., LINDQVIST, L. M. & VINCE, J. E. 2017. Active MLKL triggers the NLRP3 inflammasome in a cell-intrinsic manner. *Proc Natl Acad Sci U S A,* 114**,** E961-E969.

CORDEIRO, M. F., GUO, L., LUONG, V., HARDING, G., WANG, W., JONES, H. E., MOSS, S. E., SILLITO, A. M. & FITZKE, F. W. 2004. Real-time imaging of single nerve cell apoptosis in retinal neurodegeneration. *Proc Natl Acad Sci U S A,* 101**,** 13352-6.

CORDEIRO, M. F., NORMANDO, E. M., CARDOSO, M. J., MIODRAGOVIC, S., JEYLANI, S., DAVIS, B. M., GUO, L., OURSELIN, S., A'HERN, R. & BLOOM, P. A. 2017. Real-time imaging of single neuronal cell apoptosis in patients with glaucoma. *Brain,* 140**,** 1757-1767.

COUGNOUX, A., CLUZEAU, C., MITRA, S., LI, R., WILLIAMS, I., BURKERT, K., XU, X., WASSIF, C. A., ZHENG, W. & PORTER, F. D. 2016. Necroptosis in Niemann-Pick disease, type C1: a potential therapeutic target. *Cell Death Dis,* 7**,** e2147.

COX, M. S. 1980. Retinal breaks caused by blunt nonperforating trauma at the point of impact. *Trans Am Ophthalmol Soc,* 78**,** 414-66.

CUI, Q. & HARVEY, A. R. 2000. CNTF promotes the regrowth of retinal ganglion cell axons into murine peripheral nerve grafts. *Neuroreport,* 11**,** 3999-4002.

CUI, Q., LU, Q., SO, K. F. & YIP, H. K. 1999. CNTF, not other trophic factors, promotes axonal regeneration of axotomized retinal ganglion cells in adult hamsters. *Invest Ophthalmol Vis Sci,* 40**,** 760-6.

CUI, Q., YIN, Y. & BENOWITZ, L. I. 2009. The role of macrophages in optic nerve regeneration. *Neuroscience,* 158**,** 1039-48.

CULLEN, S. P. & MARTIN, S. J. 2009. Caspase activation pathways: some recent progress. *Cell Death Differ,* 16**,** 935-8.

CULLIS, I. G. 2001. Blast waves and how they interact with structures. *J R Army Med Corps,* 147**,** 16-26.

CZABOTAR, P. E., LESSENE, G., STRASSER, A. & ADAMS, J. M. 2014. Control of apoptosis by the BCL-2 protein family: implications for physiology and therapy. *Nature reviews Molecular cell biology,* 15**,** 49-63.

DAMOISEAUX, J. G., DOPP, E. A., CALAME, W., CHAO, D., MACPHERSON, G. G. & DIJKSTRA, C. D. 1994. Rat macrophage lysosomal membrane antigen recognized by monoclonal antibody ED1. *Immunology,* 83**,** 140-7.

DAVIS, T., INGS, A., NATIONAL INSTITUTE OF, H. & CARE, E. 2015. Head injury: triage, assessment, investigation and early management of head injury in children, young people and adults (NICE guideline CG 176). *Arch Dis Child Educ Pract Ed,* 100**,** 97-100.

DE COGAN, F., HILL, L. J., LYNCH, A., MORGAN-WARREN, P. J., LECHNER, J., BERWICK, M. R., PEACOCK, A. F. A., CHEN, M., SCOTT, R. A. H., XU, H. & LOGAN, A. 2017. Topical Delivery of Anti-VEGF Drugs to the Ocular Posterior Segment Using Cell-Penetrating Peptides. *Invest Ophthalmol Vis Sci,* 58**,** 2578-2590.

DECLERCQ, W., VANDEN BERGHE, T. & VANDENABEELE, P. 2009. RIP Kinases at the Crossroads of Cell Death and Survival. *Cell,* 138**,** 229-232.

DEGTEREV, A., HITOMI, J., GERMSCHEID, M., CH'EN, I. L., KORKINA, O., TENG, X., ABBOTT, D., CUNY, G. D., YUAN, C., WAGNER, G., HEDRICK, S. M., GERBER, S. A., LUGOVSKOY, A. & YUAN, J. 2008. Identification of RIP1 kinase as a specific cellular target of necrostatins. *Nature Chemical Biology,* 4**,** 313-321.

DEGTEREV, A., HUANG, Z., BOYCE, M., LI, Y., JAGTAP, P., MIZUSHIMA, N., CUNY, G. D., MITCHISON, T. J., MOSKOWITZ, M. A. & YUAN, J. 2005. Chemical inhibitor of nonapoptotic cell death with therapeutic potential for ischemic brain injury. *Nat Chem Biol,* 1**,** 112-9.

DEL AMO, E. M., RIMPELA, A. K., HEIKKINEN, E., KARI, O. K., RAMSAY, E., LAJUNEN, T., SCHMITT, M., PELKONEN, L., BHATTACHARYA, M., RICHARDSON, D., SUBRIZI, A., TURUNEN, T., REINISALO, M., ITKONEN, J., TOROPAINEN, E., CASTELEIJN, M., KIDRON, H., ANTOPOLSKY, M., VELLONEN, K. S., RUPONEN, M. & URTTI, A. 2017. Pharmacokinetic aspects of retinal drug delivery. *Prog Retin Eye Res,* 57**,** 134-185.

DEMAR, J., SHARROW, K., HILL, M., BERMAN, J., OLIVER, T. & LONG, J. 2016. Effects of Primary Blast Overpressure on Retina and Optic Tract in Rats. *Front Neurol,* 7**,** 59.

DEMPSEY, P. W., VAIDYA, S. A. & CHENG, G. 2003. The art of war: Innate and adaptive immune responses. *Cell Mol Life Sci,* 60**,** 2604-21.

DENNISTON, A. K., KEANE, P. A. & SRIVASTAVA, S. K. 2017. Biomarkers and Surrogate Endpoints in Uveitis: The Impact of Quantitative Imaging. *Invest Ophthalmol Vis Sci,* 58**,** BIO131-BIO140.

DEVERAUX, Q. L., TAKAHASHI, R., SALVESEN, G. S. & REED, J. C. 1997. X-linked IAP is a direct inhibitor of cell-death proteases. *Nature,* 388**,** 300-304.

DEWALT, G. J. & ELDRED, W. D. 2017. Visual system pathology in humans and animal models of blast injury. *J Comp Neurol,* 525**,** 2955-2967.

DIEM, R., HOBOM, M., MAIER, K., WEISSERT, R., STORCH, M. K., MEYER, R. & BAHR, M. 2003. Methylprednisolone increases neuronal apoptosis during autoimmune CNS inflammation by inhibition of an endogenous neuroprotective pathway. *J Neurosci,* 23**,** 6993-7000.

DO, Y. J., SUL, J. W., JANG, K. H., KANG, N. S., KIM, Y. H., KIM, Y. G. & KIM, E. 2017. A novel RIPK1 inhibitor that prevents retinal degeneration in a rat glaucoma model. *Exp Cell Res,* 359**,** 30-38.

DORSTYN, L., PUCCINI, J., WILSON, C. H., SHALINI, S., NICOLA, M., MOORE, S. & KUMAR, S. 2012. Caspase-2 deficiency promotes aberrant DNA-damage response and genetic instability. *Cell Death Differ,* 19**,** 1288-98.

DOUGHERTY, A. L., MACGREGOR, A. J., HAN, P. P., HELTEMES, K. J. & GALARNEAU, M. R. 2011. Visual dysfunction following blast-related traumatic brain injury from the battlefield. *Brain Inj,* 25**,** 8-13.

DROIN, N., BICHAT, F., REBE, C., WOTAWA, A., SORDET, O., HAMMANN, A., BERTRAND, R. & SOLARY, E. 2001. Involvement of caspase-2 long isoform in Fas-mediated cell death of human leukemic cells. *Blood,* 97**,** 1835-44.

DUAN, H. & DIXIT, V. M. 1997. RAIDD is a new 'death' adaptor molecule. *Nature,* 385**,** 86-9.

DUFFIELD, J. S. 2003. The inflammatory macrophage: a story of Jekyll and Hyde. *Clin Sci (Lond),* 104**,** 27-38.

DUTCA, L. M., STASHEFF, S. F., HEDBERG-BUENZ, A., RUDD, D. S., BATRA, N., BLODI, F. R., YOREK, M. S., YIN, T., SHANKAR, M., HERLEIN, J. A., NAIDOO, J., MORLOCK, L., WILLIAMS, N., KARDON, R. H., ANDERSON, M. G., PIEPER, A. A. & HARPER, M. M. 2014. Early Detection of Subclinical Visual Damage After Blast-Mediated TBI Enables Prevention of Chronic Visual Deficit by Treatment With P7C3-S243. *Investigative Ophthalmology & Visual Science,* 55**,** 8330-8341.

DVORIANTCHIKOVA, G., DEGTEREV, A. & IVANOV, D. 2014. Retinal ganglion cell (RGC) programmed necrosis contributes to ischemia-reperfusion-induced retinal damage. *Experimental Eye Research,* 123**,** 1-7.

EDWARDS, P., ARANGO, M., BALICA, L., COTTINGHAM, R., EL-SAYED, H., FARRELL, B., FERNANDES, J., GOGICHAISVILI, T., GOLDEN, N., HARTZENBERG, B., HUSAIN, M., ULLOA, M. I., JERBI, Z., KHAMIS, H., KOMOLAFE, E., LALOE, V., LOMAS, G., LUDWIG, S., MAZAIRAC, G., MUNOZ SANCHEZ MDE, L., NASI, L., OLLDASHI, F., PLUNKETT, P., ROBERTS, I., SANDERCOCK, P., SHAKUR, H., SOLER, C., STOCKER, R., SVOBODA, P., TRENKLER, S., VENKATARAMANA, N. K., WASSERBERG, J., YATES, D., YUTTHAKASEMSUNT, S. & COLLABORATORS, C. T. 2005. Final results of MRC CRASH, a randomised placebo-controlled trial of intravenous corticosteroid in adults with head injury-outcomes at 6 months. *Lancet,* 365**,** 1957-9.

EKERT, P. G., SILKE, J. & VAUX, D. L. 1999. Caspase inhibitors. *Cell Death Differ,* 6**,** 1081-6.

ELMORE, S. 2007. Apoptosis: a review of programmed cell death. *Toxicol Pathol,* 35**,** 495-516.

FALAVARJANI, K. G. & NGUYEN, Q. D. 2013. Adverse events and complications associated with intravitreal injection of anti-VEGF agents: a review of literature. *Eye (Lond),* 27**,** 787-94.

FAN, T.-J., HAN, L.-H., CONG, R.-S. & LIANG, J. 2005. Caspase family proteases and apoptosis. *Acta biochimica et biophysica Sinica,* 37**,** 719-27.

FAUSTER, A., REBSAMEN, M., HUBER, K. V., BIGENZAHN, J. W., STUKALOV, A., LARDEAU, C. H., SCORZONI, S., BRUCKNER, M., GRIDLING, M., PARAPATICS, K., COLINGE, J., BENNETT, K. L., KUBICEK, S., KRAUTWALD, S., LINKERMANN, A. & SUPERTI-FURGA, G. 2015. A cellular screen identifies ponatinib and pazopanib as inhibitors of necroptosis. *Cell Death Dis,* 6**,** e1767.

FELTHAM, R., VINCE, J. E. & LAWLOR, K. E. 2017. Caspase-8: not so silently deadly. *Clin Transl Immunology,* 6**,** e124.

FEOKTISTOVA, M., GESERICK, P., PANAYOTOVA-DIMITROVA, D. & LEVERKUS, M. 2012. Pick your poison: the Ripoptosome, a cell death platform regulating apoptosis and necroptosis. *Cell Cycle,* 11**,** 460-7.

FESTJENS, N., VANDEN BERGHE, T., CORNELIS, S. & VANDENABEELE, P. 2007. RIP1, a kinase on the crossroads of a cell's decision to live or die. *Cell Death and Differentiation,* 14**,** 400-410.

FISCHER, D., HEIDUSCHKA, P. & THANOS, S. 2001. Lens-injury-stimulated axonal regeneration throughout the optic pathway of adult rats. *Exp Neurol,* 172**,** 257-72.

FISCHER, D. & LEIBINGER, M. 2012. Promoting optic nerve regeneration. *Prog Retin Eye Res,* 31**,** 688-701.

FISCHER, D., PAVLIDIS, M. & THANOS, S. 2000. Cataractogenic lens injury prevents traumatic ganglion cell death and promotes axonal regeneration both in vivo and in culture. *Investigative Ophthalmology & Visual Science,* 41**,** 3943-3954.

FLEMING, B. D. & MOSSER, D. M. 2011. Regulatory macrophages: setting the threshold for therapy. *Eur J Immunol,* 41**,** 2498-502.

FORSBACH, A., NEMORIN, J. G., MONTINO, C., MULLER, C., SAMULOWITZ, U., VICARI, A. P., JURK, M., MUTWIRI, G. K., KRIEG, A. M., LIPFORD, G. B. & VOLLMER, J. 2008. Identification of RNA sequence motifs stimulating sequence-specific TLR8-dependent immune responses. *J Immunol,* 180**,** 3729-38.

FORSBERG, J., ZHIVOTOVSKY, B. & OLSSON, M. 2017. Caspase-2: an orphan enzyme out of the shadows. *Oncogene,* 36**,** 5441-5444.

FRANCHI, L., EIGENBROD, T., MUNOZ-PLANILLO, R. & NUNEZ, G. 2009. The inflammasome: a caspase-1-activation platform that regulates immune responses and disease pathogenesis. *Nat Immunol,* 10**,** 241-7.

FRICKER, M., VILALTA, A., TOLKOVSKY, A. M. & BROWN, G. C. 2013. Caspase inhibitors protect neurons by enabling selective necroptosis of inflamed microglia. *J Biol Chem,* 288**,** 9145-52.

GAIDT, M. M., EBERT, T. S., CHAUHAN, D., SCHMIDT, T., SCHMID-BURGK, J. L., RAPINO, F., ROBERTSON, A. A., COOPER, M. A., GRAF, T. & HORNUNG, V. 2016. Human Monocytes Engage an Alternative Inflammasome Pathway. *Immunity,* 44**,** 833-46.

GALLUZZI, L., VITALE, I., AARONSON, S. A., ABRAMS, J. M., ADAM, D., AGOSTINIS, P., ALNEMRI, E. S., ALTUCCI, L., AMELIO, I., ANDREWS, D. W., ANNICCHIARICO-PETRUZZELLI, M., ANTONOV, A. V., ARAMA, E., BAEHRECKE, E. H., BARLEV, N. A., BAZAN, N. G., BERNASSOLA, F., BERTRAND, M. J. M., BIANCHI, K., BLAGOSKLONNY, M. V., BLOMGREN, K., BORNER, C., BOYA, P., BRENNER, C., CAMPANELLA, M., CANDI, E., CARMONA-GUTIERREZ, D., CECCONI, F., CHAN, F. K., CHANDEL, N. S., CHENG, E. H., CHIPUK, J. E., CIDLOWSKI, J. A., CIECHANOVER, A., COHEN, G. M., CONRAD, M., CUBILLOS-RUIZ, J. R., CZABOTAR, P. E., D'ANGIOLELLA, V., DAWSON, T. M., DAWSON, V. L., DE LAURENZI, V., DE MARIA, R., DEBATIN, K. M., DEBERARDINIS, R. J., DESHMUKH, M., DI DANIELE, N., DI VIRGILIO, F., DIXIT, V. M., DIXON, S. J., DUCKETT, C. S., DYNLACHT, B. D., EL-DEIRY, W. S., ELROD, J. W., FIMIA, G. M., FULDA, S., GARCIA-SAEZ, A. J., GARG, A. D., GARRIDO, C., GAVATHIOTIS, E., GOLSTEIN, P., GOTTLIEB, E., GREEN, D. R., GREENE, L. A., GRONEMEYER, H., GROSS, A., HAJNOCZKY, G., HARDWICK, J. M., HARRIS, I. S., HENGARTNER, M. O., HETZ, C., ICHIJO, H., JAATTELA, M., JOSEPH, B., JOST, P. J., JUIN, P. P., KAISER, W. J., KARIN, M., KAUFMANN, T., KEPP, O., KIMCHI, A., KITSIS, R. N., KLIONSKY, D. J., KNIGHT, R. A., KUMAR, S., LEE, S. W., LEMASTERS, J. J., LEVINE, B., LINKERMANN, A., LIPTON, S. A., LOCKSHIN, R. A., LOPEZ-OTIN, C., LOWE, S. W., LUEDDE, T., LUGLI, E., MACFARLANE, M., MADEO, F., MALEWICZ, M., MALORNI, W., MANIC, G., et al. 2018. Molecular mechanisms of cell death: recommendations of the Nomenclature Committee on Cell Death 2018. *Cell Death Differ,* 25**,** 486-541.

GALVAO, J., DAVIS, B., TILLEY, M., NORMANDO, E., DUCHEN, M. R. & CORDEIRO, M. F. 2014. Unexpected low-dose toxicity of the universal solvent DMSO. *FASEB J,* 28**,** 1317-30.

GARCIA-VALENZUELA, E., GORCZYCA, W., DARZYNKIEWICZ, Z. & SHARMA, S. C. 1994. Apoptosis in adult retinal ganglion cells after axotomy. *J Neurobiol,* 25**,** 431-8.

GIZYCKA, A. & CHOROSTOWSKA-WYNIMKO, J. 2015. Programmed necrosis and necroptosis - molecular mechanisms. *Postepy Hig Med Dosw (Online),* 69**,** 1353-63.

GOH, S. H. 2009. Bomb blast mass casualty incidents: initial triage and management of injuries. *Singapore Med J,* 50**,** 101-6.

GOLAN, R., SOFFER, D., GIVON, A., ISRAEL TRAUMA, G. & PELEG, K. 2014. The ins and outs of terrorist bus explosions: injury profiles of on-board explosions versus explosions occurring adjacent to a bus. *Injury,* 45**,** 39-43.

GOLDSTEIN, L. E., FISHER, A. M., TAGGE, C. A., ZHANG, X. L., VELISEK, L., SULLIVAN, J. A., UPRETI, C., KRACHT, J. M., ERICSSON, M., WOJNAROWICZ, M. W., GOLETIANI, C. J., MAGLAKELIDZE, G. M., CASEY, N., MONCASTER, J. A., MINAEVA, O., MOIR, R. D., NOWINSKI, C. J., STERN, R. A., CANTU, R. C., GEILING, J., BLUSZTAJN, J. K., WOLOZIN, B. L., IKEZU, T., STEIN, T. D., BUDSON, A. E., KOWALL, N. W., CHARGIN, D., SHARON, A., SAMAN, S., HALL, G. F., MOSS, W. C., CLEVELAND, R. O., TANZI, R. E., STANTON, P. K. & MCKEE, A. C. 2012. Chronic traumatic encephalopathy in blast-exposed military veterans and a blast neurotrauma mouse model. *Sci Transl Med,* 4**,** 134ra60.

GOLDSTEIN, L. E., MCKEE, A. C. & STANTON, P. K. 2014. Considerations for animal models of blast-related traumatic brain injury and chronic traumatic encephalopathy. *Alzheimers Res Ther,* 6**,** 64.

GOODRICH, G. L., FLYG, H. M., KIRBY, J. E., CHANG, C. Y. & MARTINSEN, G. L. 2013. Mechanisms of TBI and Visual Consequences in Military and Veteran Populations. *Optometry and Vision Science,* 90**,** 105-112.

GOWER, N. J. D., BARRY, R. J., EDMUNDS, M. R., TITCOMB, L. C. & DENNISTON, A. K. 2016. Drug discovery in ophthalmology: past success, present challenges, and future opportunities. *BMC Ophthalmol,* 16**,** 11.

GRATCHEV, A., GUILLOT, P., HAKIY, N., POLITZ, O., ORFANOS, C. E., SCHLEDZEWSKI, K. & GOERDT, S. 2001. Alternatively activated macrophages differentially express fibronectin and its splice variants and the extracellular matrix protein betaIG-H3. *Scand J Immunol,* 53**,** 386-92.

GREENBAUM, D., COLANGELO, C., WILLIAMS, K. & GERSTEIN, M. 2003. Comparing protein abundance and mRNA expression levels on a genomic scale. *Genome Biol,* 4**,** 117.

GREGOR, Z. & RYAN, S. J. 1982a. Blood-retinal barrier after blunt trauma to the eye. *Graefes Arch Clin Exp Ophthalmol,* 219**,** 205-8.

GREGOR, Z. & RYAN, S. J. 1982b. Combined posterior contusion and penetrating injury in the pig eye. I. A natural history study. *Br J Ophthalmol,* 66**,** 793-8.

GROSSKREUTZ, C. L., HANNINEN, V. A., PANTCHEVA, M. B., HUANG, W., POULIN, N. R. & DOBBERFUHL, A. P. 2005. FK506 blocks activation of the intrinsic caspase cascade after optic nerve crush. *Exp Eye Res,* 80**,** 681-6.

GULEY, N. H., ROGERS, J. T., DEL MAR, N. A., DENG, Y., ISLAM, R. M., D'SURNEY, L., FERRELL, J., DENG, B., HINES-BEARD, J., BU, W., REN, H., ELBERGER, A. J., MARCHETTA, J. G., REX, T. S., HONIG, M. G. & REINER, A. 2016. A Novel Closed-Head Model of Mild Traumatic Brain Injury Using Focal Primary Overpressure Blast to the Cranium in Mice. *J Neurotrauma,* 33**,** 403-22.

GUO, Y., SRINIVASULA, S. M., DRUILHE, A., FERNANDES-ALNEMRI, T. & ALNEMRI, E. S. 2002. Caspase-2 induces apoptosis by releasing proapoptotic proteins from mitochondria. *J Biol Chem,* 277**,** 13430-7.

GUTIERREZ, K. D., DAVIS, M. A., DANIELS, B. P., OLSEN, T. M., RALLI-JAIN, P., TAIT, S. W., GALE, M., JR. & OBERST, A. 2017. MLKL Activation Triggers NLRP3-Mediated Processing and Release of IL-1beta Independently of Gasdermin-D. *J Immunol,* 198**,** 2156-2164.

GUZMAN-ARANGUEZ, A., LOMA, P. & PINTOR, J. 2013. Small-interfering RNAs (siRNAs) as a promising tool for ocular therapy. *Br J Pharmacol,* 170**,** 730-47.

GYRD-HANSEN, M. & MEIER, P. 2010. IAPs: from caspase inhibitors to modulators of NF-kappaB, inflammation and cancer. *Nat Rev Cancer,* 10**,** 561-74.

HAINES, D. E. & MIHAILOFF, G. A. 2018. *Fundamental neuroscience for basic and clinical applications,* Philadelphia, PA, Elsevier.

HAMAR, P., SONG, E., KOKENY, G., CHEN, A., OUYANG, N. & LIEBERMAN, J. 2004. Small interfering RNA targeting Fas protects mice against renal ischemia-reperfusion injury. *Proc Natl Acad Sci U S A,* 101**,** 14883-8.

HARRIS, P. A., BERGER, S. B., JEONG, J. U., NAGILLA, R., BANDYOPADHYAY, D., CAMPOBASSO, N., CAPRIOTTI, C. A., COX, J. A., DARE, L., DONG, X., EIDAM, P. M., FINGER, J. N., HOFFMAN, S. J., KANG, J., KASPARCOVA, V., KING, B. W., LEHR, R., LAN, Y., LEISTER, L. K., LICH, J. D., MACDONALD, T. T., MILLER, N. A., OUELLETTE, M. T., PAO, C. S., RAHMAN, A., REILLY, M. A., RENDINA, A. R., RIVERA, E. J., SCHAEFFER, M. C., SEHON, C. A., SINGHAUS, R. R., SUN, H. H., SWIFT, B. A., TOTORITIS, R. D., VOSSENKAMPER, A., WARD, P., WISNOSKI, D. D., ZHANG, D., MARQUIS, R. W., GOUGH, P. J. & BERTIN, J. 2017. Discovery of a First-in-Class Receptor Interacting Protein 1 (RIP1) Kinase Specific Clinical Candidate (GSK2982772) for the Treatment of Inflammatory Diseases. *J Med Chem,* 60**,** 1247-1261.

HARRIS, P. A., KING, B. W., BANDYOPADHYAY, D., BERGER, S. B., CAMPOBASSO, N., CAPRIOTTI, C. A., COX, J. A., DARE, L., DONG, X., FINGER, J. N., GRADY, L. C., HOFFMAN, S. J., JEONG, J. U., KANG, J., KASPARCOVA, V., LAKDAWALA, A. S., LEHR, R., MCNULTY, D. E., NAGILLA, R., OUELLETTE, M. T., PAO, C. S., RENDINA, A. R., SCHAEFFER, M. C., SUMMERFIELD, J. D., SWIFT, B. A., TOTORITIS, R. D., WARD, P., ZHANG, A., ZHANG, D., MARQUIS, R. W., BERTIN, J. & GOUGH, P. J. 2016. DNA-Encoded Library Screening Identifies Benzo[b][1,4]oxazepin-4-ones as Highly Potent and Monoselective Receptor Interacting Protein 1 Kinase Inhibitors. *J Med Chem,* 59**,** 2163-78.

HART, J. C. & BLIGHT, R. 1979. Early changes in peripheral retina following concussive ocular injuries: an experimental study. *J R Soc Med,* 72**,** 180-4.

HE, M. H., CHEUNG, Z. H., YU, E. H., TAY, D. K. & SO, K. F. 2004. Cytochrome c release and caspase-3 activation in retinal ganglion cells following different distance of axotomy of the optic nerve in adult hamsters. *Neurochem Res,* 29**,** 2153-61.

HE, W. T., WAN, H., HU, L., CHEN, P., WANG, X., HUANG, Z., YANG, Z. H., ZHONG, C. Q. & HAN, J. 2015. Gasdermin D is an executor of pyroptosis and required for interleukin-1beta secretion. *Cell Res,* 25**,** 1285-98.

HENRY, C. M. & MARTIN, S. J. 2017. Caspase-8 Acts in a Non-enzymatic Role as a Scaffold for Assembly of a Pro-inflammatory "FADDosome" Complex upon TRAIL Stimulation. *Mol Cell,* 65**,** 715-729 e5.

HERNANDEZ, C., GARCIA-RAMIREZ, M., CORRALIZA, L., FERNANDEZ-CARNEADO, J., FARRERA-SINFREU, J., PONSATI, B., GONZALEZ-RODRIGUEZ, A., VALVERDE, A. M. & SIMO, R. 2013. Topical administration of somatostatin prevents retinal neurodegeneration in experimental diabetes. *Diabetes,* 62**,** 2569-78.

HILL, L. J., MEAD, B., BLANCH, R. J., AHMED, Z., DE COGAN, F., MORGAN-WARREN, P. J., MOHAMED, S., LEADBEATER, W., SCOTT, R. A., BERRY, M. & LOGAN, A. 2015. Decorin Reduces Intraocular Pressure and Retinal Ganglion Cell Loss in Rodents Through Fibrolysis of the Scarred Trabecular Meshwork. *Invest Ophthalmol Vis Sci,* 56**,** 3743-57.

HINES-BEARD, J., MARCHETTA, J., GORDON, S., CHAUM, E., GEISERT, E. E. & REX, T. S. 2012. A mouse model of ocular blast injury that induces closed globe anterior and posterior pole damage. *Experimental eye research,* 99**,** 63-70.

HO, L. H., READ, S. H., DORSTYN, L., LAMBRUSCO, L. & KUMAR, S. 2008. Caspase-2 is required for cell death induced by cytoskeletal disruption. *Oncogene,* 27**,** 3393-404.

HO, L. H., TAYLOR, R., DORSTYN, L., CAKOUROS, D., BOUILLET, P. & KUMAR, S. 2009. A tumor suppressor function for caspase-2. *Proc Natl Acad Sci U S A,* 106**,** 5336-41.

HOLDER, G. E. 2004. Electrophysiological assessment of optic nerve disease. *Eye (Lond),* 18**,** 1133-43.

HORROCKS, C. L. 2001. Blast injuries: biophysics, pathophysiology and management principles. *J R Army Med Corps,* 147**,** 28-40.

HOUSDEN, S. 2012. Blast injury: a case study. *Int Emerg Nurs,* 20**,** 173-8.

HU, S. & YANG, X. 2003. Cellular inhibitor of apoptosis 1 and 2 are ubiquitin ligases for the apoptosis inducer Smac/DIABLO. *J Biol Chem,* 278**,** 10055-60.

HU, Y., PARK, K. K., YANG, L., WEI, X., YANG, Q., CHO, K. S., THIELEN, P., LEE, A. H., CARTONI, R., GLIMCHER, L. H., CHEN, D. F. & HE, Z. 2012. Differential effects of unfolded protein response pathways on axon injury-induced death of retinal ganglion cells. *Neuron,* 73**,** 445-52.

HUANG, Z., ZHOU, T., SUN, X., ZHENG, Y., CHENG, B., LI, M., LIU, X. & HE, C. 2018. Necroptosis in microglia contributes to neuroinflammation and retinal degeneration through TLR4 activation. *Cell Death Differ,* 25**,** 180-189.

HUSAIN, S., ABDUL, Y. & CROSSON, C. E. 2012. Preservation of retina ganglion cell function by morphine in a chronic ocular-hypertensive rat model. *Invest Ophthalmol Vis Sci,* 53**,** 4289-98.

INOMATA, Y., NAKAMURA, H., TANITO, M., TERATANI, A., KAWAJI, T., KONDO, N., YODOI, J. & TANIHARA, H. 2006. Thioredoxin inhibits NMDA-induced neurotoxicity in the rat retina. *J Neurochem,* 98**,** 372-85.

ISLAM, Q. U., ISHAQ, M., YAQUB, A. & SAEED, M. K. 2016. Functional and anatomical outcome in closed globe combat ocular injuries. *J Pak Med Assoc,* 66**,** 1582-1586.

ITO, Y., OFENGEIM, D., NAJAFOV, A., DAS, S., SABERI, S., LI, Y., HITOMI, J., ZHU, H., CHEN, H., MAYO, L., GENG, J., AMIN, P., DEWITT, J. P., MOOKHTIAR, A. K., FLOREZ, M., OUCHIDA, A. T., FAN, J. B., PASPARAKIS, M., KELLIHER, M. A., RAVITS, J. & YUAN, J. 2016. RIPK1 mediates axonal degeneration by promoting inflammation and necroptosis in ALS. *Science,* 353**,** 603-8.

JACKSON, A. L. & LINSLEY, P. S. 2010. Recognizing and avoiding siRNA off-target effects for target identification and therapeutic application. *Nat Rev Drug Discov,* 9**,** 57-67.

JHA, P., BANDA, H., TYTARENKO, R., BORA, P. S. & BORA, N. S. 2011. Complement mediated apoptosis leads to the loss of retinal ganglion cells in animal model of glaucoma. *Mol Immunol,* 48**,** 2151-8.

JIANG, Y., PAGADALA, J., MILLER, D. D. & STEINLE, J. J. 2014. Insulin-like growth factor-1 binding protein 3 (IGFBP-3) promotes recovery from trauma-induced

expression of inflammatory and apoptotic factors in retina. *Cytokine,* 70**,** 115-9.

JIANG, Y. D., LIU, L., PAGADALA, J., MILLER, D. D. & STEINLE, J. J. 2013. Compound 49b protects against blast-induced retinal injury. *Journal of Neuroinflammation,* 10.

JIE, H., HE, Y., HUANG, X., ZHOU, Q., HAN, Y., LI, X., BAI, Y. & SUN, E. 2016. Necrostatin-1 enhances the resolution of inflammation by specifically inducing neutrophil apoptosis. *Oncotarget,* 7**,** 19367-81.

JIMENEZ FERNANDEZ, D. & LAMKANFI, M. 2015. Inflammatory caspases: key regulators of inflammation and cell death. *Biological chemistry,* 396**,** 193-203.

JOHN R. HECKENLIVELY, G. B. A. 2006. *Principles and Practice of Clinical Electrophysiology of Vision*, MIT Press.

JONES, K., CHOI, J. H., SPONSEL, W. E., GRAY, W., GROTH, S. L., GLICKMAN, R. D., LUND, B. J. & REILLY, M. A. 2016. Low-Level Primary Blast Causes Acute Ocular Trauma in Rabbits. *J Neurotrauma,* 33**,** 1194-201.

JONES, N. P., HAYWARD, J. M., KHAW, P. T., CLAOUE, C. M. & ELKINGTON, A. R. 1986. Function of an ophthalmic "accident and emergency" department: results of a six month survey. *Br Med J (Clin Res Ed),* 292**,** 188-90.

KANAMORI, A., NAKAMURA, M., YAMADA, Y. & NEGI, A. 2012. Longitudinal study of retinal nerve fiber layer thickness and ganglion cell complex in traumatic optic neuropathy. *Arch Ophthalmol,* 130**,** 1067-9.

KANG, T. B., YANG, S. H., TOTH, B., KOVALENKO, A. & WALLACH, D. 2014. Activation of the NLRP3 inflammasome by proteins that signal for necroptosis. *Methods Enzymol,* 545**,** 67-81.

KAPUR, G. B., HUTSON, H. R., DAVIS, M. A. & RICE, P. L. 2005. The United States twenty-year experience with bombing incidents: implications for terrorism preparedness and medical response. *J Trauma,* 59**,** 1436-44.

KAYAGAKI, N., STOWE, I. B., LEE, B. L., O'ROURKE, K., ANDERSON, K., WARMING, S., CUELLAR, T., HALEY, B., ROOSE-GIRMA, M., PHUNG, Q. T., LIU, P. S., LILL, J. R., LI, H., WU, J., KUMMERFELD, S., ZHANG, J., LEE, W. P., SNIPAS, S. J., SALVESEN, G. S., MORRIS, L. X., FITZGERALD, L., ZHANG, Y., BERTRAM, E. M., GOODNOW, C. C. & DIXIT, V. M. 2015. Caspase-11 cleaves gasdermin D for non-canonical inflammasome signalling. *Nature,* 526**,** 666-71.

KERMER, P., ANKERHOLD, R., KLOCKER, N., KRAJEWSKI, S., REED, J. C. & BAHR, M. 2000a. Caspase-9: involvement in secondary death of axotomized rat retinal ganglion cells in vivo. *Brain research Molecular brain research,* 85**,** 144-50.

KERMER, P., ANKERHOLD, R., KLÖCKER, N., KRAJEWSKI, S., REED, J. C. & BÄHR, M. 2000b. Caspase-9: Involvement in secondary death of axotomized rat retinal ganglion cells in vivo. *Molecular Brain Research,* 85**,** 144-150.

KERMER, P., KLOCKER, N. & BAHR, M. 1999a. Long-term effect of inhibition of ced 3-like caspases on the survival of axotomized retinal ganglion cells in vivo. *Experimental neurology,* 158**,** 202-5.

KERMER, P., KLÖCKER, N. & BÄHR, M. 1999b. Long-Term Effect of Inhibition of ced 3-Like Caspases on the Survival of Axotomized Retinal Ganglion Cells in Vivo. *Experimental Neurology,* 158**,** 202-205.

KERMER, P., KLOCKER, N., LABES, M., THOMSEN, S., SRINIVASAN, A. & BAHR, M. 1999c. Activation of caspase-3 in axotomized rat retinal ganglion cells in vivo. *FEBS letters,* 453**,** 361-4.

KIEL, J. & CHEN, S. 2001. Contusion injuries and their ocular effects. *Clin Exp Optom,* 84**,** 19-25.

KIM, C. R., KIM, J. H., PARK, H. L. & PARK, C. K. 2017. Ischemia Reperfusion Injury Triggers TNFalpha Induced-Necroptosis in Rat Retina. *Curr Eye Res,* 42**,** 771-779.

KIM, I. R., MURAKAMI, K., CHEN, N. J., SAIBIL, S. D., MATYSIAK-ZABLOCKI, E., ELFORD, A. R., BONNARD, M., BENCHIMOL, S., JURISICOVA, A., YEH, W. C. & OHASHI, P. S. 2009. DNA damage- and stress-induced apoptosis occurs independently of PIDD. *Apoptosis,* 14**,** 1039-1049.

KIM, S. Y., SHIM, M. S., KIM, K. Y., WEINREB, R. N., WHEELER, L. A. & JU, W. K. 2014. Inhibition of cyclophilin D by cyclosporin A promotes retinal ganglion cell survival by preventing mitochondrial alteration in ischemic injury. *Cell Death Dis,* 5**,** e1105.

KISCHKEL, F. C., HELLBARDT, S., BEHRMANN, I., GERMER, M., PAWLITA, M., KRAMMER, P. H. & PETER, M. E. 1995. Cytotoxicity-Dependent Apo-1 (Fas/Cd95)-Associated Proteins Form a Death-Inducing Signaling Complex (Disc) with the Receptor. *Embo Journal,* 14**,** 5579-5588.

KLEINMAN, M. E., YAMADA, K., TAKEDA, A., CHANDRASEKARAN, V., NOZAKI, M., BAFFI, J. Z., ALBUQUERQUE, R. J., YAMASAKI, S., ITAYA, M., PAN, Y., APPUKUTTAN, B., GIBBS, D., YANG, Z., KARIKO, K., AMBATI, B. K., WILGUS, T. A., DIPIETRO, L. A., SAKURAI, E., ZHANG, K., SMITH, J. R., TAYLOR, E. W. & AMBATI, J. 2008. Sequence- and target-independent angiogenesis suppression by siRNA via TLR3. *Nature,* 452**,** 591-7.

KLUGER, Y. 2003. Bomb explosions in acts of terrorism--detonation, wound ballistics, triage and medical concerns. *Isr Med Assoc J,* 5**,** 235-40.

KOCH, J. C., TONGES, L., BARSKI, E., MICHEL, U., BAHR, M. & LINGOR, P. 2014. ROCK2 is a major regulator of axonal degeneration, neuronal death and axonal regeneration in the CNS. *Cell Death & Disease,* 5.

KOCSIS, J. D. & TESSLER, A. 2009. Pathology of blast-related brain injury. *J Rehabil Res Dev,* 46**,** 667-72.

KOEBERLE, P. D., WANG, Y. & SCHLICHTER, L. C. 2010. Kv1.1 and Kv1.3 channels contribute to the degeneration of retinal ganglion cells after optic nerve transection in vivo. *Cell Death Differ,* 17**,** 134-44.

KOKONA, D., HANER, N. U., EBNETER, A. & ZINKERNAGEL, M. S. 2017. Imaging of macrophage dynamics with optical coherence tomography in anterior ischemic optic neuropathy. *Exp Eye Res,* 154**,** 159-167.

KOLIATSOS, V. E., CERNAK, I., XU, L., SONG, Y., SAVONENKO, A., CRAIN, B. J., EBERHART, C. G., FRANGAKIS, C. E., MELNIKOVA, T., KIM, H. & LEE, D. 2011. A mouse model of blast injury to brain: initial pathological, neuropathological, and behavioral characterization. *J Neuropathol Exp Neurol,* 70**,** 399-416.

KOU, P. M. & BABENSEE, J. E. 2011. Macrophage and dendritic cell phenotypic diversity in the context of biomaterials. *J Biomed Mater Res A,* 96**,** 239-60.

KRISHNAMOORTHY, R. R., CLARK, A. F., DAUDT, D., VISHWANATHA, J. K. & YORIO, T. 2013. A forensic path to RGC-5 cell line identification: lessons learned. *Invest Ophthalmol Vis Sci,* 54**,** 5712-9.

KROEMER, G. & BLOMGREN, K. 2007. Mitochondrial cell death control in familial Parkinson disease. *PLoS Biol,* 5**,** e206.

KROEMER, G., GALLUZZI, L. & BRENNER, C. 2007. Mitochondrial membrane permeabilization in cell death. *Physiological reviews,* 87**,** 99-163.

KRUMSCHNABEL, G., SOHM, B., BOCK, F., MANZL, C. & VILLUNGER, A. 2009. The enigma of caspase-2: the laymen's view. *Cell Death and Differentiation,* 16**,** 195-207.

KUIDA, K., HAYDAR, T. F., KUAN, C. Y., GU, Y., TAYA, C., KARASUYAMA, H., SU, M. S., RAKIC, P. & FLAVELL, R. A. 1998. Reduced apoptosis and cytochrome c-mediated caspase activation in mice lacking caspase 9. *Cell,* 94**,** 325-37.

KUIDA, K., ZHENG, T. S., NA, S., KUAN, C., YANG, D., KARASUYAMA, H., RAKIC, P. & FLAVELL, R. A. 1996. Decreased apoptosis in the brain and premature lethality in CPP32-deficient mice. *Nature,* 384**,** 368-72.

KUMAR, S. 2007. Caspase function in programmed cell death. *Cell Death and Differentiation,* 14**,** 32-43.

KURIMOTO, T., YIN, Y., HABBOUB, G., GILBERT, H. Y., LI, Y., NAKAO, S., HAFEZI-MOGHADAM, A. & BENOWITZ, L. I. 2013. Neutrophils express oncomodulin and promote optic nerve regeneration. *J Neurosci,* 33**,** 14816-24.

KUROKAWA, T., KATAI, N., KUROIWA, S., SHIBUKI, H., KURIMOTO, Y. & YOSHIMURA, N. 1999a. BDNF suppresses expression of caspase-2 but not of c-Jun in rat retinal ganglion cells after ischemia-reperfusion injury. *Investigative Ophthalmology & Visual Science,* 40**,** S481-S481.

KUROKAWA, T., KATAI, N., SHIBUKI, H., KUROIWA, S., KURIMOTO, Y., NAKAYAMA, C. & YOSHIMURA, N. 1999b. BDNF diminishes caspase-2 but not c-Jun immunoreactivity of neurons in retinal ganglion cell layer after transient ischemia. *Invest Ophthalmol Vis Sci,* 40**,** 3006-11.

KUWANA, T., SMITH, J. J., MUZIO, M., DIXIT, V., NEWMEYER, D. D. & KORNBLUTH, S. 1998. Apoptosis induction by caspase-8 is amplified through

the mitochondrial release of cytochrome c. *Journal of Biological Chemistry,* 273**,** 16589-16594.

KWONG, J. M., CAPRIOLI, J. & PIRI, N. 2010. RNA binding protein with multiple splicing: a new marker for retinal ganglion cells. *Invest Ophthalmol Vis Sci,* 51**,** 1052-8.

KWONG, J. M. & LAM, T. T. 2000. N -methyl- D -aspartate (NMDA) induced apoptosis in adult rabbit retinas. *Exp Eye Res,* 71**,** 437-44.

KWONG, J. M. K., QUAN, A., KYUNG, H., PIRI, N. & CAPRIOLI, J. 2011. Quantitative Analysis of Retinal Ganglion Cell Survival with Rbpms Immunolabeling in Animal Models of Optic Neuropathies. *Investigative Ophthalmology & Visual Science,* 52**,** 9694-9702.

LALONDE, M. R., CHAUHAN, B. C. & TREMBLAY, F. 2006. Retinal ganglion cell activity from the multifocal electroretinogram in pig: optic nerve section, anaesthesia and intravitreal tetrodotoxin. *J Physiol,* 570**,** 325-38.

LAMKANFI, M., D'HONDT, K., VANDE WALLE, L., VAN GURP, M., DENECKER, G., DEMEULEMEESTER, J., KALAI, M., DECLERCQ, W., SAELENS, X. & VANDENABEELE, P. 2005. A novel caspase-2 complex containing TRAF2 and RIP1. *J Biol Chem,* 280**,** 6923-32.

LASSUS, P., OPITZ-ARAYA, X. & LAZEBNIK, Y. 2002. Requirement for caspase-2 in stress-induced apoptosis before mitochondrial permeabilization. *Science,* 297**,** 1352-4.

LAVRIK, I. N., GOLKS, A., BAUMANN, S. & KRAMMER, P. H. 2006. Caspase-2 is activated at the CD95 death-inducing signaling complex in the course of CD95-induced apoptosis. *Blood,* 108**,** 559-65.

LAVRIK, I. N., GOLKS, A. & KRAMMER, P. H. 2005. Caspases: pharmacological manipulation of cell death. *J Clin Invest,* 115**,** 2665-72.

LAWLOR, K. E., KHAN, N., MILDENHALL, A., GERLIC, M., CROKER, B. A., D'CRUZ, A. A., HALL, C., KAUR SPALL, S., ANDERTON, H., MASTERS, S. L., RASHIDI, M., WICKS, I. P., ALEXANDER, W. S., MITSUUCHI, Y., BENETATOS, C. A., CONDON, S. M., WONG, W. W., SILKE, J., VAUX, D. L. & VINCE, J. E. 2015. RIPK3 promotes cell death and NLRP3 inflammasome activation in the absence of MLKL. *Nat Commun,* 6**,** 6282.

LEAVER, S. G., CUI, Q., PLANT, G. W., ARULPRAGASAM, A., HISHEH, S., VERHAAGEN, J. & HARVEY, A. R. 2006. AAV-mediated expression of CNTF promotes long-term survival and regeneration of adult rat retinal ganglion cells. *Gene Ther,* 13**,** 1328-41.

LEE, V., FORD, R. L., XING, W., BUNCE, C. & FOOT, B. 2010. Surveillance of traumatic optic neuropathy in the UK. *Eye (Lond),* 24**,** 240-50.

LEIBOVICI, D., GOFRIT, O. N., STEIN, M., SHAPIRA, S. C., NOGA, Y., HERUTI, R. J. & SHEMER, J. 1996. Blast injuries: bus versus open-air bombings--a comparative study of injuries in survivors of open-air versus confined-space explosions. *J Trauma,* 41**,** 1030-5.

LEMKE, S., COCKERHAM, G. C., GLYNN-MILLEY, C. & COCKERHAM, K. P. 2013. Visual Quality of Life in Veterans With Blast-Induced Traumatic Brain Injury. *Jama Ophthalmology,* 131**,** 1602-1609.

LEON, S., YIN, Y. Q., NGUYEN, J., IRWIN, N. & BENOWITZ, L. I. 2000. Lens injury stimulates axon regeneration in the mature rat optic nerve. *Journal of Neuroscience,* 20**,** 4615-4626.

LEVIN, L. A., BECK, R. W., JOSEPH, M. P., SEIFF, S. & KRAKER, R. 1999. The treatment of traumatic optic neuropathy: the International Optic Nerve Trauma Study. *Ophthalmology,* 106**,** 1268-77.

LEVKOVITCH-VERBIN, H., DARDIK, R., VANDER, S. & MELAMED, S. 2010. Mechanism of retinal ganglion cells death in secondary degeneration of the optic nerve. *Exp Eye Res,* 91**,** 127-34.

LEVKOVITCH-VERBIN, H., WASERZOOG, Y., VANDER, S., MAKAROVSKY, D. & ILIA, P. 2014a. Minocycline mechanism of neuroprotection involves the Bcl-2 gene family in optic nerve transection. *Int J Neurosci,* 124**,** 755-61.

LEVKOVITCH-VERBIN, H., WASERZOOG, Y., VANDER, S., MAKAROVSKY, D. & PIVEN, I. 2014b. Minocycline upregulates pro-survival genes and downregulates pro-apoptotic genes in experimental glaucoma. *Graefes Archive for Clinical and Experimental Ophthalmology,* 252**,** 761-772.

LI, B., BARNES, G. E. & HOLT, W. F. 2005. The decline of the photopic negative response (PhNR) in the rat after optic nerve transection. *Doc Ophthalmol,* 111**,** 23-31.

LI, P., NIJHAWAN, D., BUDIHARDJO, I., SRINIVASULA, S. M., AHMAD, M., ALNEMRI, E. S. & WANG, X. 1997. Cytochrome c and dATP-dependent formation of Apaf-1/caspase-9 complex initiates an apoptotic protease cascade. *Cell,* 91**,** 479-89.

LI, Y., QIAN, L. & YUAN, J. 2017. Small molecule probes for cellular death machines. *Curr Opin Chem Biol,* 39**,** 74-82.

LIDSTER, K., JACKSON, S. J., AHMED, Z., MUNRO, P., COFFEY, P., GIOVANNONI, G., BAKER, M. D. & BAKER, D. 2013. Neuroprotection in a novel mouse model of multiple sclerosis. *PLoS One,* 8**,** e79188.

LIN, C. Y., CHANG, T. W., HSIEH, W. H., HUNG, M. C., LIN, I. H., LAI, S. C. & TZENG, Y. J. 2016. Simultaneous induction of apoptosis and necroptosis by Tanshinone IIA in human hepatocellular carcinoma HepG2 cells. *Cell Death Discov,* 2**,** 16065.

LIN, Y., DEVIN, A., RODRIGUEZ, Y. & LIU, Z. G. 1999. Cleavage of the death domain kinase RIP by Caspase-8 prompts TNF-induced apoptosis. *Genes & Development,* 13**,** 2514-2526.

LIN, Y., MA, W. & BENCHIMOL, S. 2000. Pidd, a new death-domain-containing protein, is induced by p53 and promotes apoptosis. *Nature genetics,* 26**,** 122-7.

LING, C., SANDOR, M., SURESH, M. & FABRY, Z. 2006. Traumatic injury and the presence of antigen differentially contribute to T-cell recruitment in the CNS. *J Neurosci,* 26**,** 731-41.

LINGOR, P., TONGES, L., PIEPER, N., BERMEL, C., BARSKI, E., PLANCHAMP, V. & BAHR, M. 2008. ROCK inhibition and CNTF interact on intrinsic signalling pathways and differentially regulate survival and regeneration in retinal ganglion cells. *Brain,* 131**,** 250-63.

LINKERMANN, A. & GREEN, D. R. 2014. Necroptosis. *N Engl J Med,* 370**,** 455-65.

LIU, H. X., SUN, H. & LIU, C. Y. 2011. Interference of the Apoptotic Signaling Pathway in RGC Stress Response by SP600125 in Moderate Ocular Hypertensive Rats. *Chinese Journal of Physiology,* 54**,** 124-132.

LIU, Y., FAN, C., ZHANG, Y., YU, X., WU, X., ZHANG, X., ZHAO, Q., ZHANG, H., XIE, Q., LI, M., LI, X., DING, Q., YING, H., LI, D. & ZHANG, H. 2017. RIP1 kinase activity-dependent roles in embryonic development of Fadd-deficient mice. *Cell Death Differ,* 24**,** 1459-1469.

LIU, Y., MCDOWELL, C. M., ZHANG, Z., TEBOW, H. E., WORDINGER, R. J. & CLARK, A. F. 2014. Monitoring retinal morphologic and functional changes in mice following optic nerve crush. *Invest Ophthalmol Vis Sci,* 55**,** 3766-74.

LIU, Y., YAN, H., CHEN, S. & SABEL, B. A. 2015a. Caspase-3 inhibitor Z-DEVD-FMK enhances retinal ganglion cell survival and vision restoration after rabbit traumatic optic nerve injury. *Restor Neurol Neurosci,* 33**,** 205-20.

LIU, Y., YAN, H., CHEN, S. & SABEL, B. A. 2015b. Caspase-3 inhibitor Z-DEVD-FMK enhances retinal ganglion cell survival and vision restoration after rabbit traumatic optic nerve injury. *Restorative neurology and neuroscience,* 33**,** 205-20.

LOPEZ-CRUZAN, M., SHARMA, R., TIWARI, M., KARBACH, S., HOLSTEIN, D., MARTIN, C. R., LECHLEITER, J. D. & HERMAN, B. 2016. Caspase-2 resides in the mitochondria and mediates apoptosis directly from the mitochondrial compartment. *Cell Death Discov,* 2.

LORBER, B., BERRY, M. & LOGAN, A. 2005. Lens injury stimulates adult mouse retinal ganglion cell axon regeneration via both macrophage- and lens-derived factors. *Eur J Neurosci,* 21**,** 2029-34.

LORBER, B., BERRY, M. & LOGAN, A. 2008. Different factors promote axonal regeneration of adult rat retinal ganglion cells after lens injury and intravitreal peripheral nerve grafting. *J Neurosci Res,* 86**,** 894-903.

LYSKO MEGHAN, D. O. P., MAGHARIOUS MARK, KOEBERLE PAULO 2012. The role of Receptor Interacting Proteins in Retinal Ganglion Cell apoptosis following axotomy. *Investigative Ophthalmology and Visual Science,* 53**,** 3483.

MAASS, A., VON LEITHNER, P. L., LUONG, V., GUO, L., SALT, T. E., FITZKE, F. W. & CORDEIRO, M. F. 2007. Assessment of rat and mouse RGC apoptosis imaging in vivo with different scanning laser ophthalmoscopes. *Curr Eye Res,* 32**,** 851-61.

MACFARLANE, M., MERRISON, W., BRATTON, S. B. & COHEN, G. M. 2002. Proteasome-mediated degradation of Smac during apoptosis: XIAP promotes Smac ubiquitination in vitro. *J Biol Chem,* 277**,** 36611-6.

MACMICKING, J., XIE, Q. W. & NATHAN, C. 1997. Nitric oxide and macrophage function. *Annu Rev Immunol,* 15**,** 323-50.

MAMMADOVA, N., GHAISAS, S., ZENITSKY, G., SAKAGUCHI, D. S., KANTHASAMY, A. G., GREENLEE, J. J. & WEST GREENLEE, M. H. 2017. Lasting Retinal Injury in a Mouse Model of Blast-Induced Trauma. *Am J Pathol,* 187**,** 1459-1472.

MANSOUR-ROBAEY, S., CLARKE, D. B., WANG, Y. C., BRAY, G. M. & AGUAYO, A. J. 1994. Effects of ocular injury and administration of brain-derived neurotrophic factor on survival and regrowth of axotomized retinal ganglion cells. *Proc Natl Acad Sci U S A,* 91**,** 1632-6.

MANTOVANI, A., SICA, A., SOZZANI, S., ALLAVENA, P., VECCHI, A. & LOCATI, M. 2004. The chemokine system in diverse forms of macrophage activation and polarization. *Trends Immunol,* 25**,** 677-86.

MANZL, C., KRUMSCHNABEL, G., BOCK, F., SOHM, B., LABI, V., BAUMGARTNER, F., LOGETTE, E., TSCHOPP, J. & VILLUNGER, A. 2009. Caspase-2 activation in the absence of PIDDosome formation. *J Cell Biol,* 185**,** 291-303.

MARSDEN, V. S., EKERT, P. G., VAN DELFT, M., VAUX, D. L., ADAMS, J. M. & STRASSER, A. 2004. Bcl-2-regulated apoptosis and cytochrome c release can occur independently of both caspase-2 and caspase-9. *J Cell Biol,* 165**,** 775-80.

MATZINGER, P. 1994. Tolerance, danger, and the extended family. *Annu Rev Immunol,* 12**,** 991-1045.

MCSTAY, G. P., SALVESEN, G. S. & GREEN, D. R. 2008. Overlapping cleavage motif selectivity of caspases: implications for analysis of apoptotic pathways. *Cell Death Differ,* 15**,** 322-31.

MEAD, B., HILL, L. J., BLANCH, R. J., WARD, K., LOGAN, A., BERRY, M., LEADBEATER, W. & SCHEVEN, B. A. 2016. Mesenchymal stromal cell-

mediated neuroprotection and functional preservation of retinal ganglion cells in a rodent model of glaucoma. *Cytotherapy,* 18**,** 487-96.

MEAD, B., LOGAN, A., BERRY, M., LEADBEATER, W. & SCHEVEN, B. A. 2013. Intravitreally transplanted dental pulp stem cells promote neuroprotection and axon regeneration of retinal ganglion cells after optic nerve injury. *Invest Ophthalmol Vis Sci,* 54**,** 7544-56.

MEAD, B., THOMPSON, A., SCHEVEN, B. A., LOGAN, A., BERRY, M. & LEADBEATER, W. 2014. Comparative evaluation of methods for estimating retinal ganglion cell loss in retinal sections and wholemounts. *PLoS One,* 9**,** e110612.

MEAD, B. & TOMAREV, S. 2016. Evaluating retinal ganglion cell loss and dysfunction. *Exp Eye Res,* 151**,** 96-106.

MENU, P. & VINCE, J. E. 2011. The NLRP3 inflammasome in health and disease: the good, the bad and the ugly. *Clin Exp Immunol,* 166**,** 1-15.

MEYER, C. H., RODRIGUES, E. B. & MENNEL, S. 2003. Acute commotio retinae determined by cross-sectional optical coherence tomography. *Eur J Ophthalmol,* 13**,** 816-8.

MICHEAU, O. & TSCHOPP, J. 2003. Induction of TNF receptor I-mediated apoptosis via two sequential signaling complexes. *Cell,* 114**,** 181-90.

MIKOLAJEWICZ, N., MOHAMMED, A., MORRIS, M. & KOMAROVA, S. V. 2018. Mechanically stimulated ATP release from mammalian cells: systematic review and meta-analysis. *J Cell Sci,* 131.

MISHRA, V., SKOTAK, M., SCHUETZ, H., HELLER, A., HAORAH, J. & CHANDRA, N. 2016. Primary blast causes mild, moderate, severe and lethal TBI with increasing blast overpressures: Experimental rat injury model. *Sci Rep,* 6**,** 26992.

MO, J. S., ANDERSON, M. G., GREGORY, M., SMITH, R. S., SAVINOVA, O. V., SERREZE, D. V., KSANDER, B. R., STREILEIN, J. W. & JOHN, S. W. 2003. By altering ocular immune privilege, bone marrow-derived cells pathogenically contribute to DBA/2J pigmentary glaucoma. *J Exp Med,* 197**,** 1335-44.

MOHAN, K., KECOVA, H., HERNANDEZ-MERINO, E., KARDON, R. H. & HARPER, M. M. 2013. Retinal ganglion cell damage in an experimental rodent model of blast-mediated traumatic brain injury. *Invest Ophthalmol Vis Sci,* 54**,** 3440-50.

MONNIER, P. P., D'ONOFRIO, P. M., MAGHARIOUS, M., HOLLANDER, A. C., TASSEW, N., SZYDLOWSKA, K., TYMIANSKI, M. & KOEBERLE, P. D. 2011. Involvement of caspase-6 and caspase-8 in neuronal apoptosis and the regenerative failure of injured retinal ganglion cells. *The Journal of neuroscience : the official journal of the Society for Neuroscience,* 31**,** 10494-505.

MONTESANO, G., WAY, C. M., OMETTO, G., IBRAHIM, H., JONES, P. R., CARMICHAEL, R., LIU, X., ASLAM, T., KEANE, P. A., CRABB, D. P. & DENNISTON, A. K. 2018. Optimizing OCT acquisition parameters for assessments of vitreous haze for application in uveitis. *Sci Rep,* 8**,** 1648.

MOQUIN, D. M., MCQUADE, T. & CHAN, F. K. M. 2013. CYLD Deubiquitinates RIP1 in the TNF alpha-Induced Necrosome to Facilitate Kinase Activation and Programmed Necrosis. *Plos One,* 8.

MORGAN-WARREN, P. J., BERRY, M., AHMED, Z., SCOTT, R. A. & LOGAN, A. 2013. Exploiting mTOR signaling: a novel translatable treatment strategy for traumatic optic neuropathy? *Invest Ophthalmol Vis Sci,* 54**,** 6903-16.

MORGAN-WARREN, P. J., O'NEILL, J., DE COGAN, F., SPIVAK, I., ASHUSH, H., KALINSKI, H., AHMED, Z., BERRY, M., FEINSTEIN, E., SCOTT, R. A. & LOGAN, A. 2016. siRNA-Mediated Knockdown of the mTOR Inhibitor RTP801 Promotes Retinal Ganglion Cell Survival and Axon Elongation by Direct and Indirect Mechanisms. *Invest Ophthalmol Vis Sci,* 57**,** 429-43.

MOSSER, D. M. 2003. The many faces of macrophage activation. *J Leukoc Biol,* 73**,** 209-12.

MOSSER, D. M. & EDWARDS, J. P. 2008. Exploring the full spectrum of macrophage activation. *Nat Rev Immunol,* 8**,** 958-69.

MULLER, A., HAUK, T. G. & FISCHER, D. 2007. Astrocyte-derived CNTF switches mature RGCs to a regenerative state following inflammatory stimulation. *Brain,* 130**,** 3308-20.

MUNOZ-PLANILLO, R., KUFFA, P., MARTINEZ-COLON, G., SMITH, B. L., RAJENDIRAN, T. M. & NUNEZ, G. 2013. K(+) efflux is the common trigger of NLRP3 inflammasome activation by bacterial toxins and particulate matter. *Immunity,* 38**,** 1142-53.

MURAKAMI, Y., MATSUMOTO, H., ROH, M., GIANI, A., KATAOKA, K., MORIZANE, Y., KAYAMA, M., THANOS, A., NAKATAKE, S., NOTOMI, S., HISATOMI, T., IKEDA, Y., ISHIBASHI, T., CONNOR, K. M., MILLER, J. W. & VAVVAS, D. G. 2014. Programmed necrosis, not apoptosis, is a key mediator of cell loss and DAMP-mediated inflammation in dsRNA-induced retinal degeneration. *Cell Death Differ,* 21**,** 270-7.

MURAKAMI, Y., MATSUMOTO, H., ROH, M., SUZUKI, J., HISATOMI, T., IKEDA, Y., MILLER, J. W. & VAVVAS, D. G. 2012. Receptor interacting protein kinase mediates necrotic cone but not rod cell death in a mouse model of inherited degeneration. *Proc Natl Acad Sci U S A,* 109**,** 14598-603.

MURAKAMI, Y., MILLER, J. W. & VAVVAS, D. G. 2011. RIP Kinase-Mediated Necrosis as an Alternative Mechanism of Photoreceptor Death. *Oncotarget,* 2**,** 497-509.

MURRAY, C. K., REYNOLDS, J. C., SCHROEDER, J. M., HARRISON, M. B., EVANS, O. M. & HOSPENTHAL, D. R. 2005. Spectrum of care provided at an

echelon II medical unit during Operation Iraqi Freedom. *Military Medicine,* 170**,** 516-520.

MUZIO, M. 1998. Signalling by proteolysis: death receptors induce apoptosis. *International Journal of Clinical & Laboratory Research,* 28**,** 141-147.

NADAL-NICOLAS, F. M., GALINDO-ROMERO, C., VALIENTE-SORIANO, F. J., BARBERA-CREMADES, M., DETORRE-MINGUELA, C., SALINAS-NAVARRO, M., PELEGRIN, P. & AGUDO-BARRIUSO, M. 2016. Involvement of P2X7 receptor in neuronal degeneration triggered by traumatic injury. *Sci Rep,* 6**,** 38499.

NADAL-NICOLAS, F. M., JIMENEZ-LOPEZ, M., SOBRADO-CALVO, P., NIETO-LOPEZ, L., CANOVAS-MARTINEZ, I., SALINAS-NAVARRO, M., VIDAL-SANZ, M. & AGUDO, M. 2009. Brn3a as a Marker of Retinal Ganglion Cells: Qualitative and Quantitative Time Course Studies in Naive and Optic Nerve-Injured Retinas. *Investigative Ophthalmology & Visual Science,* 50**,** 3860-3868.

NAJJAR, M., SUEBSUWONG, C., RAY, S. S., THAPA, R. J., MAKI, J. L., NOGUSA, S., SHAH, S., SALEH, D., GOUGH, P. J., BERTIN, J., YUAN, J., BALACHANDRAN, S., CUNY, G. D. & DEGTEREV, A. 2015. Structure guided design of potent and selective ponatinib-based hybrid inhibitors for RIPK1. *Cell Rep,* 10**,** 1850-60.

NAKAMURA, K. & SHICHITA, T. 2019. Cellular and molecular mechanisms of sterile inflammation in ischemic stroke. *J Biochem*.

NAU, H. E., GERHARD, L., FOERSTER, M., NAHSER, H. C., REINHARDT, V. & JOKA, T. 1987. Optic-Nerve Trauma - Clinical, Electrophysiological and Histological Remarks. *Acta Neurochirurgica,* 89**,** 16-27.

NAYAK, D., ROTH, T. L. & MCGAVERN, D. B. 2014. Microglia development and function. *Annu Rev Immunol,* 32**,** 367-402.

NGUYEN, H. X., O'BARR, T. J. & ANDERSON, A. J. 2007. Polymorphonuclear leukocytes promote neurotoxicity through release of matrix metalloproteinases, reactive oxygen species, and TNF-alpha. *J Neurochem,* 102**,** 900-12.

NICHOLSON, D. W. 1999. Caspase structure, proteolytic substrates, and function during apoptotic cell death. *Cell Death Differ,* 6**,** 1028-42.

NICHOLSON, D. W. & THORNBERRY, N. A. 1997. Caspases: killer proteases. *Trends Biochem Sci,* 22**,** 299-306.

NICKELLS, R. W. 2010. Variations in the rheostat model of apoptosis: what studies of retinal ganglion cell death tell us about the functions of the Bcl2 family proteins. *Exp Eye Res,* 91**,** 2-8.

NING, Y. L. & ZHOU, Y. G. 2015. Shock tubes and blast injury modeling. *Chin J Traumatol,* 18**,** 187-93.

NOTMAN, R., NORO, M., O'MALLEY, B. & ANWAR, J. 2006. Molecular basis for dimethylsulfoxide (DMSO) action on lipid membranes. *J Am Chem Soc,* 128**,** 13982-3.

O'BYRNE, K. J. & RICHARD, D. J. 2017. Nucleolar caspase-2: Protecting us from DNA damage. *J Cell Biol,* 216**,** 1521-1523.

O'REILLY, L. A., EKERT, P., HARVEY, N., MARSDEN, V., CULLEN, L., VAUX, D. L., HACKER, G., MAGNUSSON, C., PAKUSCH, M., CECCONI, F., KUIDA, K., STRASSER, A., HUANG, D. C. & KUMAR, S. 2002. Caspase-2 is not required for thymocyte or neuronal apoptosis even though cleavage of caspase-2 is dependent on both Apaf-1 and caspase-9. *Cell Death Differ,* 9**,** 832-41.

OFENGEIM, D. & YUAN, J. 2013. Regulation of RIP1 kinase signalling at the crossroads of inflammation and cell death. *Nat Rev Mol Cell Biol,* 14**,** 727-36.

OLSSON, M., FORSBERG, J. & ZHIVOTOVSKY, B. 2015. Caspase-2: the reinvented enzyme. *Oncogene,* 34**,** 1877-82.

OLSSON, M., VAKIFAHMETOGLU, H., ABRUZZO, P. M., HOGSTRAND, K., GRANDIEN, A. & ZHIVOTOVSKY, B. 2009. DISC-mediated activation of caspase-2 in DNA damage-induced apoptosis. *Oncogene,* 28**,** 1949-59.

PARK, K. K., LIU, K., HU, Y., SMITH, P. D., WANG, C., CAI, B., XU, B., CONNOLLY, L., KRAMVIS, I., SAHIN, M. & HE, Z. 2008. Promoting axon regeneration in the adult CNS by modulation of the PTEN/mTOR pathway. *Science,* 322**,** 963-6.

PARRISH, A. B., FREEL, C. D. & KORNBLUTH, S. 2013. Cellular mechanisms controlling caspase activation and function. *Cold Spring Harb Perspect Biol,* 5.

PASPARAKIS, M. & VANDENABEELE, P. 2015. Necroptosis and its role in inflammation. *Nature,* 517**,** 311-20.

PATIL, K. & SHARMA, S. C. 2004. Broad spectrum caspase inhibitor rescues retinal ganglion cells after ischemia. *Neuroreport,* 15**,** 981-4.

PEREIRA, N. A. & SONG, Z. 2008. Some commonly used caspase substrates and inhibitors lack the specificity required to monitor individual caspase activity. *Biochem Biophys Res Commun,* 377**,** 873-7.

PERNET, V. & DI POLO, A. 2006. Synergistic action of brain-derived neurotrophic factor and lens injury promotes retinal ganglion cell survival, but leads to optic nerve dystrophy in vivo. *Brain,* 129**,** 1014-26.

PESCINA, S., OSTACOLO, C., GOMEZ-MONTERREY, I. M., SALA, M., BERTAMINO, A., SONVICO, F., PADULA, C., SANTI, P., BIANCHERA, A. & NICOLI, S. 2018. Cell penetrating peptides in ocular drug delivery: State of the art. *J Control Release,* 284**,** 84-102.

PETRAS, J. M., BAUMAN, R. A. & ELSAYED, N. M. 1997. Visual system degeneration induced by blast overpressure. *Toxicology,* 121**,** 41-49.

PIERAMICI, D. J., STERNBERG, P., JR., AABERG, T. M., SR., BRIDGES, W. Z., JR., CAPONE, A., JR., CARDILLO, J. A., DE JUAN, E., JR., KUHN, F., MEREDITH, T. A., MIELER, W. F., OLSEN, T. W., RUBSAMEN, P. & STOUT, T. 1997. A system for classifying mechanical injuries of the eye (globe). The Ocular Trauma Classification Group. *Am J Ophthalmol,* 123**,** 820-31.

POLITI, K. & PRZEDBORSKI, S. 2016. Axonal Degeneration: RIPK1 Multitasking in ALS. *Curr Biol,* 26**,** R932-R934.

POLYKRATIS, A., HERMANCE, N., ZELIC, M., RODERICK, J., KIM, C., VAN, T. M., LEE, T. H., CHAN, F. K. M., PASPARAKIS, M. & KELLIHER, M. A. 2014. Cutting edge: RIPK1 Kinase inactive mice are viable and protected from TNF-induced necroptosis in vivo. *J Immunol,* 193**,** 1539-1543.

PORCIATTI, V. 2015. Electrophysiological assessment of retinal ganglion cell function. *Exp Eye Res,* 141**,** 164-70.

POZUETA, J., LEFORT, R., RIBE, E. M., TROY, C. M., ARANCIO, O. & SHELANSKI, M. 2013. Caspase-2 is required for dendritic spine and behavioural alterations in J20 APP transgenic mice. *Nat Commun,* 4**,** 1939.

PUN, P. B., KAN, E. M., SALIM, A., LI, Z., NG, K. C., MOOCHHALA, S. M., LING, E. A., TAN, M. H. & LU, J. 2011. Low level primary blast injury in rodent brain. *Front Neurol,* 2**,** 19.

PUYANG, Z., FENG, L., CHEN, H., LIANG, P., TROY, J. B. & LIU, X. 2016. Retinal Ganglion Cell Loss is Delayed Following Optic Nerve Crush in NLRP3 Knockout Mice. *Sci Rep,* 6**,** 20998.

QINLI, Z., MEIQING, L., XIA, J., LI, X., WEILI, G., XIULIANG, J., JUNWEI, J., HAILAN, Y., CE, Z. & QIAO, N. 2013. Necrostatin-1 inhibits the degeneration

of neural cells induced by aluminum exposure. *Restor Neurol Neurosci,* 31**,** 543-55.

QU, Y., TANG, J., WANG, H., LI, S., ZHAO, F., ZHANG, L., RICHARD LU, Q. & MU, D. 2017. RIPK3 interactions with MLKL and CaMKII mediate oligodendrocytes death in the developing brain. *Cell Death Dis,* 8**,** e2629.

RABACCHI, S. A., BONFANTI, L., LIU, X. H. & MAFFEI, L. 1994. Apoptotic Cell-Death Induced by Optic-Nerve Lesion in the Neonatal Rat. *Journal of Neuroscience,* 14**,** 5292-5301.

RE, D. B., LE VERCHE, V., YU, C., AMOROSO, M. W., POLITI, K. A., PHANI, S., IKIZ, B., HOFFMANN, L., KOOLEN, M., NAGATA, T., PAPADIMITRIOU, D., NAGY, P., MITSUMOTO, H., KARIYA, S., WICHTERLE, H., HENDERSON, C. E. & PRZEDBORSKI, S. 2014. Necroptosis drives motor neuron death in models of both sporadic and familial ALS. *Neuron,* 81**,** 1001-1008.

REINER, A., HELDT, S. A., PRESLEY, C. S., GULEY, N. H., ELBERGER, A. J., DENG, Y., D'SURNEY, L., ROGERS, J. T., FERRELL, J., BU, W., DEL MAR, N., HONIG, M. G., GURLEY, S. N. & MOORE, B. M., 2ND 2014. Motor, visual and emotional deficits in mice after closed-head mild traumatic brain injury are alleviated by the novel CB2 inverse agonist SMM-189. *Int J Mol Sci,* 16**,** 758-87.

REX, T. S. 2014. Delayed vision loss and therapeutic intervention after blast injury. *Invest Ophthalmol Vis Sci,* 55**,** 8342.

REX, T. S., REILLY, M. A. & SPONSEL, W. E. 2015. Elucidating the effects of primary blast on the eye. *Clin Exp Ophthalmol,* 43**,** 197-9.

RIDDER, W. H., 3RD & NUSINOWITZ, S. 2006. The visual evoked potential in the mouse--origins and response characteristics. *Vision Res,* 46**,** 902-13.

RITENOUR, A. E. & BASKIN, T. W. 2008. Primary blast injury: Update on diagnosis and treatment. *Critical Care Medicine,* 36**,** S311-S317.

RODRIGUEZ, A. R., DE SEVILLA MULLER, L. P. & BRECHA, N. C. 2014a. The RNA binding protein RBPMS is a selective marker of ganglion cells in the mammalian retina. *J Comp Neurol,* 522**,** 1411-43.

RODRIGUEZ, A. R., MULLER, L. P. D. & BRECHA, N. C. 2014b. The RNA binding protein RBPMS is a selective marker of ganglion cells in the mammalian retina. *Journal of Comparative Neurology,* 522**,** 1411-1443.

RODRIGUEZ, D. A., WEINLICH, R., BROWN, S., GUY, C., FITZGERALD, P., DILLON, C. P., OBERST, A., QUARATO, G., LOW, J., CRIPPS, J. G., CHEN, T. & GREEN, D. R. 2016. Characterization of RIPK3-mediated phosphorylation of the activation loop of MLKL during necroptosis. *Cell Death Differ,* 23**,** 76-88.

ROSENBAUM, D. M., DEGTEREV, A., DAVID, J., ROSENBAUM, P. S., ROTH, S., GROTTA, J. C., CUNY, G. D., YUAN, J. & SAVITZ, S. I. 2010. Necroptosis, a novel form of caspase-independent cell death, contributes to neuronal damage in a retinal ischemia-reperfusion injury model. *J Neurosci Res,* 88**,** 1569-76.

ROSSI, E. A., GRANGER, C. E., SHARMA, R., YANG, Q., SAITO, K., SCHWARZ, C., WALTERS, S., NOZATO, K., ZHANG, J., KAWAKAMI, T., FISCHER, W., LATCHNEY, L. R., HUNTER, J. J., CHUNG, M. M. & WILLIAMS, D. R. 2017. Imaging individual neurons in the retinal ganglion cell layer of the living eye. *Proc Natl Acad Sci U S A,* 114**,** 586-591.

ROVERE, G., NADAL-NICOLAS, F. M., AGUDO-BARRIUSO, M., SOBRADO-CALVO, P., NIETO-LOPEZ, L., NUCCI, C., VILLEGAS-PEREZ, M. P. & VIDAL-SANZ, M. 2015. Comparison of Retinal Nerve Fiber Layer Thinning and Retinal Ganglion Cell Loss After Optic Nerve Transection in Adult Albino Rats. *Invest Ophthalmol Vis Sci,* 56**,** 4487-98.

ROZMAN-PUNGERCAR, J., KOPITAR-JERALA, N., BOGYO, M., TURK, D., VASILJEVA, O., STEFE, I., VANDENABEELE, P., BROMME, D., PUIZDAR,

V., FONOVIC, M., TRSTENJAK-PREBANDA, M., DOLENC, I., TURK, V. & TURK, B. 2003. Inhibition of papain-like cysteine proteases and legumain by caspase-specific inhibitors: when reaction mechanism is more important than specificity. *Cell Death Differ,* 10**,** 881-8.

RYAN, C. A. & SALVESEN, G. S. 2003. Caspases and neuronal development. *Biological chemistry,* 384**,** 855-61.

SAGGU, S. K., CHOTALIYA, H. P., BLUMBERGS, P. C. & CASSON, R. J. 2010. Wallerian-like axonal degeneration in the optic nerve after excitotoxic retinal insult: an ultrastructural study. *BMC Neurosci,* 11**,** 97.

SANCHEZ-MIGALLON, M. C., NADAL-NICOLAS, F. M., JIMENEZ-LOPEZ, M., SOBRADO-CALVO, P., VIDAL-SANZ, M. & AGUDO-BARRIUSO, M. 2011. Brain derived neurotrophic factor maintains Brn3a expression in axotomized rat retinal ganglion cells. *Exp Eye Res,* 92**,** 260-7.

SANCHEZ-MIGALLON, M. C., VALIENTE-SORIANO, F. J., NADAL-NICOLAS, F. M., VIDAL-SANZ, M. & AGUDO-BARRIUSO, M. 2016. Apoptotic Retinal Ganglion Cell Death After Optic Nerve Transection or Crush in Mice: Delayed RGC Loss With BDNF or a Caspase 3 Inhibitor. *Invest Ophthalmol Vis Sci,* 57**,** 81-93.

SANDVIG, A., BERRY, M., BARRETT, L. B., BUTT, A. & LOGAN, A. 2004. Myelin-, reactive glia-, and scar-derived CNS axon growth inhibitors: expression, receptor signaling, and correlation with axon regeneration. *Glia,* 46**,** 225-51.

SARKIES, N. 2004. Traumatic optic neuropathy. *Eye (Lond),* 18**,** 1122-5.

SASZIK, S. M., ROBSON, J. G. & FRISHMAN, L. J. 2002. The scotopic threshold response of the dark-adapted electroretinogram of the mouse. *J Physiol,* 543**,** 899-916.

SATTLER, M. B., MERKLER, D., MAIER, K., STADELMANN, C., EHRENREICH, H., BAHR, M. & DIEM, R. 2004. Neuroprotective effects and intracellular

signaling pathways of erythropoietin in a rat model of multiple sclerosis. *Cell Death Differ,* 11 Suppl 2**,** S181-92.

SCHOLZ, M., CINATL, J., SCHADEL-HOPFNER, M. & WINDOLF, J. 2007. Neutrophils and the blood-brain barrier dysfunction after trauma. *Med Res Rev,* 27**,** 401-16.

SCHOTTE, P., DECLERCQ, W., VAN HUFFEL, S., VANDENABEELE, P. & BEYAERT, R. 1999. Non-specific effects of methyl ketone peptide inhibitors of caspases. *FEBS Lett,* 442**,** 117-21.

SCHROETER, M. & JANDER, S. 2005. T-cell cytokines in injury-induced neural damage and repair. *Neuromolecular Med,* 7**,** 183-95.

SCHUETTAUF, F., STEIN, T., CHORAGIEWICZ, T. J., REJDAK, R., BOLZ, S., ZURAKOWSKI, D., VARDE, M. A., LATIES, A. M. & THALER, S. 2011. Caspase inhibitors protect against NMDA-mediated retinal ganglion cell death. *Clin Experiment Ophthalmol,* 39**,** 545-54.

SCOTT, F. L., DENAULT, J. B., RIEDL, S. J., SHIN, H., RENATUS, M. & SALVESEN, G. S. 2005. XIAP inhibits caspase-3 and -7 using two binding sites: evolutionarily conserved mechanism of IAPs. *EMBO J,* 24**,** 645-55.

SCOTT, R. 2011. The injured eye. *Philosophical Transactions of the Royal Society B-Biological Sciences,* 366**,** 251-260.

SCOTT, R. A. H., BLANCH, R. J. & MORGAN-WARREN, P. J. 2015. Aspects of ocular war injuries. *Trauma-England,* 17**,** 83-92.

SHABANZADEH, A. P., D'ONOFRIO, P. M., MONNIER, P. P. & KOEBERLE, P. D. 2015. Targeting caspase-6 and caspase-8 to promote neuronal survival following ischemic stroke. *Cell Death Dis,* 6**,** e1967.

SHAN, B., PAN, H., NAJAFOV, A. & YUAN, J. 2018. Necroptosis in development and diseases. *Genes Dev,* 32**,** 327-340.

SHELAH, M., WEINBERGER, D. & OFRI, R. 2007. Acute blindness in a dog caused by an explosive blast. *Vet Ophthalmol,* 10**,** 196-8.

SHEN, H., LIU, C., ZHANG, D., YAO, X., ZHANG, K., LI, H. & CHEN, G. 2017. Role for RIP1 in mediating necroptosis in experimental intracerebral hemorrhage model both in vivo and in vitro. *Cell Death Dis,* 8**,** e2641.

SHERWOOD, D., SPONSEL, W. E., LUND, B. J., GRAY, W., WATSON, R., GROTH, S. L., THOE, K., GLICKMAN, R. D. & REILLY, M. A. 2014. Anatomical manifestations of primary blast ocular trauma observed in a postmortem porcine model. *Invest Ophthalmol Vis Sci,* 55**,** 1124-32.

SHI, C. & PAMER, E. G. 2011. Monocyte recruitment during infection and inflammation. *Nat Rev Immunol,* 11**,** 762-74.

SHI, J., ZHAO, Y., WANG, K., SHI, X., WANG, Y., HUANG, H., ZHUANG, Y., CAI, T., WANG, F. & SHAO, F. 2015. Cleavage of GSDMD by inflammatory caspases determines pyroptotic cell death. *Nature,* 526**,** 660-5.

SIDI, S., SANDA, T., KENNEDY, R. D., HAGEN, A. T., JETTE, C. A., HOFFMANS, R., PASCUAL, J., IMAMURA, S., KISHI, S., AMATRUDA, J. F., KANKI, J. P., GREEN, D. R., D'ANDREA, A. A. & LOOK, A. T. 2008. Chk1 suppresses a caspase-2 apoptotic response to DNA damage that bypasses p53, Bcl-2, and caspase-3. *Cell,* 133**,** 864-877.

SILKE, J., RICKARD, J. A. & GERLIC, M. 2015. The diverse role of RIP kinases in necroptosis and inflammation. *Nature Immunology,* 16**,** 689-697.

SIPPERLEY, J. O., QUIGLEY, H. A. & GASS, D. M. 1978. Traumatic retinopathy in primates. The explanation of commotio retinae. *Arch Ophthalmol,* 96**,** 2267-73.

SMITH, C. A. & CHAUHAN, B. C. 2018. In vivo imaging of adeno-associated viral vector labelled retinal ganglion cells. *Sci Rep,* 8**,** 1490.

SOLANO, E. C., KORNBRUST, D. J., BEAUDRY, A., FOY, J. W., SCHNEIDER, D. J. & THOMPSON, J. D. 2014. Toxicological and pharmacokinetic properties of QPI-1007, a chemically modified synthetic siRNA targeting caspase 2 mRNA, following intravitreal injection. *Nucleic Acid Ther,* 24**,** 258-66.

SONG, E., OUYANG, N., HORBELT, M., ANTUS, B., WANG, M. & EXTON, M. S. 2000. Influence of alternatively and classically activated macrophages on fibrogenic activities of human fibroblasts. *Cell Immunol,* 204**,** 19-28.

SPANDIDOS, A., WANG, X., WANG, H. & SEED, B. 2010. PrimerBank: a resource of human and mouse PCR primer pairs for gene expression detection and quantification. *Nucleic Acids Res,* 38**,** D792-9.

STEIN, M. 2005. Urban bombing: a trauma surgeon's perspective. *Scand J Surg,* 94**,** 286-92.

STEINSAPIR, K. D. & GOLDBERG, R. A. 1994. Traumatic optic neuropathy. *Surv Ophthalmol,* 38**,** 487-518.

STEINSAPIR, K. D. & GOLDBERG, R. A. 2011. Traumatic optic neuropathy: an evolving understanding. *Am J Ophthalmol,* 151**,** 928-933 e2.

STEINSAPIR, K. D., GOLDBERG, R. A., SINHA, S. & HOVDA, D. A. 2000. Methylprednisolone exacerbates axonal loss following optic nerve trauma in rats. *Restor Neurol Neurosci,* 17**,** 157-163.

STIEFELMEYER, S., NEUBAUER, A. S., BERNINGER, T., ARDEN, G. B. & RUDOLPH, G. 2004. The multifocal pattern electroretinogram in glaucoma. *Vision Res,* 44**,** 103-12.

STOCKLEY, P. & HOBSON, L. 2016. Paternal care and litter size coevolution in mammals. *Proc Biol Sci,* 283.

STOLL, G., TRAPP, B. D. & GRIFFIN, J. W. 1989. Macrophage function during Wallerian degeneration of rat optic nerve: clearance of degenerating myelin and Ia expression. *J Neurosci,* 9**,** 2327-35.

SUN, C., LI, X. X., HE, X. J., ZHANG, Q. & TAO, Y. 2013. Neuroprotective effect of minocycline in a rat model of branch retinal vein occlusion. *Exp Eye Res,* 113**,** 105-16.

TAGGE, C. A., FISHER, A. M., MINAEVA, O. V., GAUDREAU-BALDERRAMA, A., MONCASTER, J. A., ZHANG, X. L., WOJNAROWICZ, M. W., CASEY, N., LU, H., KOKIKO-COCHRAN, O. N., SAMAN, S., ERICSSON, M., ONOS, K. D., VEKSLER, R., SENATOROV, V. V., JR., KONDO, A., ZHOU, X. Z., MIRY, O., VOSE, L. R., GOPAUL, K. R., UPRETI, C., NOWINSKI, C. J., CANTU, R. C., ALVAREZ, V. E., HILDEBRANDT, A. M., FRANZ, E. S., KONRAD, J., HAMILTON, J. A., HUA, N., TRIPODIS, Y., ANDERSON, A. T., HOWELL, G. R., KAUFER, D., HALL, G. F., LU, K. P., RANSOHOFF, R. M., CLEVELAND, R. O., KOWALL, N. W., STEIN, T. D., LAMB, B. T., HUBER, B. R., MOSS, W. C., FRIEDMAN, A., STANTON, P. K., MCKEE, A. C. & GOLDSTEIN, L. E. 2018. Concussion, microvascular injury, and early tauopathy in young athletes after impact head injury and an impact concussion mouse model. *Brain,* 141**,** 422-458.

TAKAHASHI, N., DUPREZ, L., GROOTJANS, S., CAUWELS, A., NERINCKX, W., DUHADAWAY, J. B., GOOSSENS, V., ROELANDT, R., VAN HAUWERMEIREN, F., LIBERT, C., DECLERCQ, W., CALLEWAERT, N., PRENDERGAST, G. C., DEGTEREV, A., YUAN, J. & VANDENABEELE, P. 2012. Necrostatin-1 analogues: critical issues on the specificity, activity and in vivo use in experimental disease models. *Cell Death Dis,* 3**,** e437.

TALANIAN, R. V., QUINLAN, C., TRAUTZ, S., HACKETT, M. C., MANKOVICH, J. A., BANACH, D., GHAYUR, T., BRADY, K. D. & WONG, W. W. 1997. Substrate specificities of caspase family proteases. *J Biol Chem,* 272**,** 9677-82.

TENEV, T., BIANCHI, K., DARDING, M., BROEMER, M., LANGLAIS, C., WALLBERG, F., ZACHARIOU, A., LOPEZ, J., MACFARLANE, M., CAIN, K. & MEIER, P. 2011. The Ripoptosome, a signaling platform that assembles in response to genotoxic stress and loss of IAPs. *Mol Cell,* 43**,** 432-48.

TENG, X., DEGTEREV, A., JAGTAP, P., XING, X., CHOI, S., DENU, R., YUAN, J. & CUNY, G. D. 2005. Structure-activity relationship study of novel necroptosis inhibitors. *Bioorg Med Chem Lett,* 15**,** 5039-44.

THAKUR, A., FITZPATRICK, S., ZAMAN, A., KUGATHASAN, K., MUIRHEAD, B., HORTELANO, G. & SHEARDOWN, H. 2012. Strategies for ocular siRNA delivery: Potential and limitations of non-viral nanocarriers. *J Biol Eng,* 6**,** 7.

THANOS, S., BOHM, M. R., SCHALLENBERG, M. & OELLERS, P. 2012. Traumatology of the optic nerve and contribution of crystallins to axonal regeneration. *Cell Tissue Res,* 349**,** 49-69.

THOMAS, C. N., BERRY, M., LOGAN, A., BLANCH, R. J. & AHMED, Z. 2017. Caspases in retinal ganglion cell death and axon regeneration. *Cell Death Discov,* 3**,** 17032.

THOMAS CN, T. A., MCCANCE E, BERRY M, LOGAN A, BLANCH RJ, AHMED Z 2018. Caspase-2 mediates site-specific retinal ganglion cell death after blunt ocular injury. *Investigative Ophthalmology & Visual Science,* 59**,** 4453-4462.

THOMAS, R., MCMANUS, J. G., JOHNSON, A., MAYER, P., WADE, C. & HOLCOMB, J. B. 2009. Ocular injury reduction from ocular protection use in current combat operations. *J Trauma,* 66**,** S99-103.

TINEL, A. & TSCHOPP, J. 2004. The PIDDosome, a protein complex implicated in activation of caspase-2 in response to genotoxic stress. *Science,* 304**,** 843-6.

TITZE-DE-ALMEIDA, R., DAVID, C. & TITZE-DE-ALMEIDA, S. S. 2017. The Race of 10 Synthetic RNAi-Based Drugs to the Pharmaceutical Market. *Pharm Res,* 34**,** 1339-1363.

TROY, C. M., RABACCHI, S. A., FRIEDMAN, W. J., FRAPPIER, T. F., BROWN, K. & SHELANSKI, M. L. 2000. Caspase-2 mediates neuronal cell death induced by beta-amyloid. *J Neurosci,* 20**,** 1386-92.

TSCHUCH, C., SCHULZ, A., PSCHERER, A., WERFT, W., BENNER, A., HOTZ-WAGENBLATT, A., BARRIONUEVO, L. S., LICHTER, P. & MERTENS, D. 2008. Off-target effects of siRNA specific for GFP. *BMC Mol Biol,* 9**,** 60.

TU, S., MCSTAY, G. P., BOUCHER, L. M., MAK, T., BEERE, H. M. & GREEN, D. R. 2006. In situ trapping of activated initiator caspases reveals a role for caspase-2 in heat shock-induced apoptosis. *Nature Cell Biology,* 8**,** 72-U24.

TURA, A., SCHUETTAUF, F., MONNIER, P. P., BARTZ-SCHMIDT, K. U. & HENKE-FAHLE, S. 2009. Efficacy of Rho-kinase inhibition in promoting cell survival and reducing reactive gliosis in the rodent retina. *Invest Ophthalmol Vis Sci,* 50**,** 452-61.

UMSCHEID, C. A., MARGOLIS, D. J. & GROSSMAN, C. E. 2011. Key concepts of clinical trials: a narrative review. *Postgrad Med,* 123**,** 194-204.

UPTON, J. P., AUSTGEN, K., NISHINO, M., COAKLEY, K. M., HAGEN, A., HAN, D., PAPA, F. R. & OAKES, S. A. 2008. Caspase-2 cleavage of BID is a critical apoptotic signal downstream of endoplasmic reticulum stress. *Molecular and Cellular Biology,* 28**,** 3943-3951.

VAN LOO, G., VAN GURP, M., DEPUYDT, B., SRINIVASULA, S. M., RODRIGUEZ, I., ALNEMRI, E. S., GEVAERT, K., VANDEKERCKHOVE, J., DECLERCQ, W. & VANDENABEELE, P. 2002. The serine protease Omi/HtrA2 is released from mitochondria during apoptosis. Omi interacts with caspase-inhibitor XIAP and induces enhanced caspase activity. *Cell Death Differ,* 9**,** 20-6.

VANAJA, S. K., RATHINAM, V. A. & FITZGERALD, K. A. 2015. Mechanisms of inflammasome activation: recent advances and novel insights. *Trends Cell Biol,* 25**,** 308-15.

VANDEN BERGHE, T., LINKERMANN, A., JOUAN-LANHOUET, S., WALCZAK, H. & VANDENABEELE, P. 2014. Regulated necrosis: the expanding network of non-apoptotic cell death pathways. *Nat Rev Mol Cell Biol,* 15**,** 135-47.

VANDENABEELE, P., GALLUZZI, L., VANDEN BERGHE, T. & KROEMER, G. 2010. Molecular mechanisms of necroptosis: an ordered cellular explosion. *Nat Rev Mol Cell Biol,* 11**,** 700-14.

VEST, V., BERNARDO-COLON, A., WATKINS, D., KIM, B. & REX, T. S. 2019. Rapid Repeat Exposure to Subthreshold Trauma Causes Synergistic Axonal Damage and Functional Deficits in the Visual Pathway in a Mouse Model. *J Neurotrauma*.

VHORA, I., PATIL, S., BHATT, P., GANDHI, R., BARADIA, D. & MISRA, A. 2014. Receptor-targeted drug delivery: current perspective and challenges. *Ther Deliv,* 5**,** 1007-24.

VIGNESWARA, V. & AHMED, Z. 2016. Long-term neuroprotection of retinal ganglion cells by inhibiting caspase-2. *Cell Death Discovery,* 2**,** 16044.

VIGNESWARA, V. & AHMED, Z. 2019. Pigment epithelium-derived factor mediates retinal ganglion cell neuroprotection by suppression of caspase-2. *Cell Death Dis,* 10**,** 102.

VIGNESWARA, V., AKPAN, N., BERRY, M., LOGAN, A., TROY, C. M. & AHMED, Z. 2014. Combined suppression of CASP2 and CASP6 protects retinal ganglion cells from apoptosis and promotes axon regeneration through CNTF-mediated JAK/STAT signalling. *Brain : a journal of neurology,* 137**,** 1656-75.

VIGNESWARA, V., BERRY, M., LOGAN, A. & AHMED, Z. 2012. Pharmacological inhibition of caspase-2 protects axotomised retinal ganglion cells from apoptosis in adult rats. *PloS one,* 7**,** e53473.

VIGNESWARA, V., BERRY, M., LOGAN, A. & AHMED, Z. 2013. Caspase-2 is upregulated after sciatic nerve transection and its inhibition protects dorsal

root ganglion neurons from apoptosis after serum withdrawal. *PLoS One,* 8**,** e57861.

VILLEGAS-PEREZ, M. P., VIDAL-SANZ, M., RASMINSKY, M., BRAY, G. M. & AGUAYO, A. J. 1993. Rapid and protracted phases of retinal ganglion cell loss follow axotomy in the optic nerve of adult rats. *J Neurobiol,* 24**,** 23-36.

VIRINGIPURAMPEER, I. A., METCALFE, A. L., BASHAR, A. E., SIVAK, O., YANAI, A., MOHAMMADI, Z., MORITZ, O. L., GREGORY-EVANS, C. Y. & GREGORY-EVANS, K. 2016. NLRP3 inflammasome activation drives bystander cone photoreceptor cell death in a P23H rhodopsin model of retinal degeneration. *Hum Mol Genet,* 25**,** 1501-16.

VISWANATHAN, S., FRISHMAN, L. J., ROBSON, J. G., HARWERTH, R. S. & SMITH, E. L., 3RD 1999. The photopic negative response of the macaque electroretinogram: reduction by experimental glaucoma. *Invest Ophthalmol Vis Sci,* 40**,** 1124-36.

VON MASSENHAUSEN, A., TONNUS, W., HIMMERKUS, N., PARMENTIER, S., SALEH, D., RODRIGUEZ, D., OUSINGSAWAT, J., ANG, R. L., WEINBERG, J. M., SANZ, A. B., ORTIZ, A., ZIERLEYN, A., BECKER, J. U., BARATTE, B., DESBAN, N., BACH, S., SCHIESSL, I. M., NOGUSA, S., BALACHANDRAN, S., ANDERS, H. J., TING, A. T., BLEICH, M., DEGTEREV, A., KUNZELMANN, K., BORNSTEIN, S. R., GREEN, D. R., HUGO, C. & LINKERMANN, A. 2018. Phenytoin inhibits necroptosis. *Cell Death Dis,* 9**,** 359.

WAGNER, K. W., ENGELS, I. H. & DEVERAUX, Q. L. 2004. Caspase-2 can function upstream of bid cleavage in the TRAIL apoptosis pathway. *The Journal of biological chemistry,* 279**,** 35047-52.

WAJANT, H. 2002. The Fas signaling pathway: more than a paradigm. *Science,* 296**,** 1635-6.

WANG, H. C., CHOI, J. H., GREENE, W. A., PLAMPER, M. L., CORTEZ, H. E., CHAVKO, M., LI, Y., DALLE LUCCA, J. J. & JOHNSON, A. J. 2014a. Pathophysiology of blast-induced ocular trauma with apoptosis in the retina and optic nerve. *Mil Med,* 179**,** 34-40.

WANG, H. C. H., CHOI, J. H., GREENE, W. A., PLAMPER, M. L., CORTEZ, H. E., CHAVKO, M., LI, Y. S., LUCCA, J. J. D. & JOHNSON, A. J. 2014b. Pathophysiology of Blast-Induced Ocular Trauma With Apoptosis in the Retina and Optic Nerve. *Military Medicine,* 179**,** 34-40.

WANG, Y., LIN, H., LIN, S., QU, J., XIAO, J., HUANG, Y., XIAO, Y., FU, X., YANG, Y. & LI, X. 2010. Cell-penetrating peptide TAT-mediated delivery of acidic FGF to retina and protection against ischemia-reperfusion injury in rats. *J Cell Mol Med,* 14**,** 1998-2005.

WANG, Y., WANG, H., TAO, Y., ZHANG, S., WANG, J. & FENG, X. 2014c. Necroptosis inhibitor necrostatin-1 promotes cell protection and physiological function in traumatic spinal cord injury. *Neuroscience,* 266**,** 91-101.

WANG, Y., ZHANG, H., LIU, Y., LI, P., CAO, Z. & CAO, Y. 2015. Erythropoietin (EPO) protects against high glucose-induced apoptosis in retinal ganglional cells. *Cell Biochem Biophys,* 71**,** 749-55.

WARDEN, D. 2006. Military TBI during the Iraq and Afghanistan wars. *Journal of Head Trauma Rehabilitation,* 21**,** 398-402.

WEICHEL, E. D., COLYER, M. H., LUDLOW, S. E., BOWER, K. S. & EISEMAN, A. S. 2008. Combat Ocular Trauma Visual Outcomes during Operations Iraqi and Enduring Freedom. *Ophthalmology,* 115**,** 2235-2245.

WEINLICH, R., OBERST, A., BEERE, H. M. & GREEN, D. R. 2017. Necroptosis in development, inflammation and disease. *Nat Rev Mol Cell Biol,* 18**,** 127-136.

WEINSTEIN, O., MANDEL, Y., LEVY, J., LIFSHITZ, T., YITZHAK, A. & ABU TAILAKH, M. 2018. Ballistic Eye Protection: Why Are Soldiers Reluctant to Use Them? *Mil Med*.

WEISHAUPT, J. H., DIEM, R., KERMER, P., KRAJEWSKI, S., REED, J. C. & BAHR, M. 2003. Contribution of caspase-8 to apoptosis of axotomized rat retinal ganglion cells in vivo. *Neurobiology of disease,* 13**,** 124-35.

WILSEY, L., GOWRISANKARAN, S., CULL, G., HARDIN, C., BURGOYNE, C. F. & FORTUNE, B. 2017. Comparing three different modes of electroretinography in experimental glaucoma: diagnostic performance and correlation to structure. *Doc Ophthalmol,* 134**,** 111-128.

WOLF, A. J., REYES, C. N., LIANG, W., BECKER, C., SHIMADA, K., WHEELER, M. L., CHO, H. C., POPESCU, N. I., COGGESHALL, K. M., ARDITI, M. & UNDERHILL, D. M. 2016. Hexokinase Is an Innate Immune Receptor for the Detection of Bacterial Peptidoglycan. *Cell,* 166**,** 624-36.

WOLF, S. J., BEBARTA, V. S., BONNETT, C. J., PONS, P. T. & CANTRILL, S. V. 2009. Blast injuries. *Lancet,* 374**,** 405-15.

WONG, T. Y., KLEIN, B. E. K. & KLEIN, R. 2000. The prevalence and 5-year incidence of ocular trauma - The Beaver Dam Eye Study. *Ophthalmology,* 107**,** 2196-2202.

WU, J., HUANG, Z., REN, J., ZHANG, Z., HE, P., LI, Y., MA, J., CHEN, W., ZHANG, Y., ZHOU, X., YANG, Z., WU, S. Q., CHEN, L. & HAN, J. 2013. Mlkl knockout mice demonstrate the indispensable role of Mlkl in necroptosis. *Cell Res,* 23**,** 994-1006.

WU, N., YIN, Z. Q. & WANG, Y. 2008. Traumatic Optic Neuropathy Therapy: an Update of Clinical and Experimental Studies. *Journal of International Medical Research,* 36**,** 883-889.

XIA, Z. & TRIFFITT, J. T. 2006. A review on macrophage responses to biomaterials. *Biomed Mater,* 1**,** R1-9.

YAN, B., LIU, L., HUANG, S., REN, Y., WANG, H., YAO, Z., LI, L., CHEN, S., WANG, X. & ZHANG, Z. 2017. Discovery of a new class of highly potent necroptosis inhibitors targeting the mixed lineage kinase domain-like protein. *Chem Commun (Camb),* 53**,** 3637-3640.

YANG, D., HE, Y., MUNOZ-PLANILLO, R., LIU, Q. & NUNEZ, G. 2015. Caspase-11 Requires the Pannexin-1 Channel and the Purinergic P2X7 Pore to Mediate Pyroptosis and Endotoxic Shock. *Immunity,* 43**,** 923-32.

YANG, S. H., LEE, D. K., SHIN, J., LEE, S., BAEK, S., KIM, J., JUNG, H., HAH, J. M. & KIM, Y. 2017. Nec-1 alleviates cognitive impairment with reduction of Abeta and tau abnormalities in APP/PS1 mice. *EMBO Mol Med,* 9**,** 61-77.

YAP, T. E., DONNA, P., ALMONTE, M. T. & CORDEIRO, M. F. 2018. Real-Time Imaging of Retinal Ganglion Cell Apoptosis. *Cells,* 7.

YE, J., COULOURIS, G., ZARETSKAYA, I., CUTCUTACHE, I., ROZEN, S. & MADDEN, T. L. 2012. Primer-BLAST: a tool to design target-specific primers for polymerase chain reaction. *BMC Bioinformatics,* 13**,** 134.

YEH, D. D. & SCHECTER, W. P. 2012. Primary blast injuries--an updated concise review. *World J Surg,* 36**,** 966-72.

YIN, Y., CUI, Q., GILBERT, H. Y., YANG, Y., YANG, Z., BERLINICKE, C., LI, Z., ZAVERUCHA-DO-VALLE, C., HE, H., PETKOVA, V., ZACK, D. J. & BENOWITZ, L. I. 2009. Oncomodulin links inflammation to optic nerve regeneration. *Proc Natl Acad Sci U S A,* 106**,** 19587-92.

YIN, Y., CUI, Q., LI, Y., IRWIN, N., FISCHER, D., HARVEY, A. R. & BENOWITZ, L. I. 2003. Macrophage-derived factors stimulate optic nerve regeneration. *J Neurosci,* 23**,** 2284-93.

YIN, Y., HENZL, M. T., LORBER, B., NAKAZAWA, T., THOMAS, T. T., JIANG, F., LANGER, R. & BENOWITZ, L. I. 2006. Oncomodulin is a macrophage-derived signal for axon regeneration in retinal ganglion cells. *Nat Neurosci,* 9**,** 843-52.

YING, Z., PAN, C., SHAO, T., LIU, L., LI, L., GUO, D., ZHANG, S., YUAN, T., CAO, R., JIANG, Z., CHEN, S., WANG, F. & WANG, X. 2018. Mixed Lineage Kinase Domain-like Protein MLKL Breaks Down Myelin following Nerve Injury. *Mol Cell,* 72**,** 457-468 e5.

YOSHIDA, H., KONG, Y. Y., YOSHIDA, R., ELIA, A. J., HAKEM, A., HAKEM, R., PENNINGER, J. M. & MAK, T. W. 1998. Apaf1 is required for mitochondrial pathways of apoptosis and brain development. *Cell,* 94**,** 739-50.

YOU, Y., KLISTORNER, A., THIE, J. & GRAHAM, S. L. 2011. Latency delay of visual evoked potential is a real measurement of demyelination in a rat model of optic neuritis. *Invest Ophthalmol Vis Sci,* 52**,** 6911-8.

YOU, Z., SAVITZ, S. I., YANG, J., DEGTEREV, A., YUAN, J., CUNY, G. D., MOSKOWITZ, M. A. & WHALEN, M. J. 2008. Necrostatin-1 reduces histopathology and improves functional outcome after controlled cortical impact in mice. *J Cereb Blood Flow Metab,* 28**,** 1564-73.

YOULE, R. J. & STRASSER, A. 2008. The BCL-2 protein family: opposing activities that mediate cell death. *Nature Reviews Molecular Cell Biology,* 9**,** 47-59.

YUAN, D., XU, Y., HANG, H., LIU, X., CHEN, X., XIE, P., YUAN, S., ZHANG, W., LIN, X. & LIU, Q. 2014. Edaravone protect against retinal damage in streptozotocin-induced diabetic mice. *PLoS One,* 9**,** e99219.

ZAMARAEV, A. V., KOPEINA, G. S., BUCHBINDER, J. H., ZHIVOTOVSKY, B. & LAVRIK, I. N. 2018. Caspase-2 is a negative regulator of necroptosis. *Int J Biochem Cell Biol,* 102**,** 101-108.

ZHANG, D. W., LIN, J. A. & HAN, J. H. 2010. Receptor-interacting protein (RIP) kinase family. *Cellular & Molecular Immunology,* 7**,** 243-249.

ZHANG, D. W., SHAO, J., LIN, J., ZHANG, N., LU, B. J., LIN, S. C., DONG, M. Q. & HAN, J. H. 2009. RIP3, an Energy Metabolism Regulator That Switches TNF-Induced Cell Death from Apoptosis to Necrosis. *Science,* 325**,** 332-336.

ZHANG, S., TANG, M. B., LUO, H. Y., SHI, C. H. & XU, Y. M. 2017. Necroptosis in neurodegenerative diseases: a potential therapeutic target. *Cell Death Dis,* 8**,** e2905.

ZHANG, Z., TONG, N., GONG, Y., QIU, Q., YIN, L., LV, X. & WU, X. 2011. Valproate protects the retina from endoplasmic reticulum stress-induced apoptosis after ischemia-reperfusion injury. *Neurosci Lett,* 504**,** 88-92.

ZHANG, Z. Z., GONG, Y. Y., SHI, Y. H., ZHANG, W., QIN, X. H. & WU, X. W. 2012a. Valproate promotes survival of retinal ganglion cells in a rat model of optic nerve crush. *Neuroscience,* 224**,** 282-93.

ZHANG, Z. Z., QIN, X. H., TONG, N. T., ZHAO, X. F., GONG, Y. Y., SHI, Y. H. & WU, X. W. 2012b. Valproic acid-mediated neuroprotection in retinal ischemia injury via histone deacetylase inhibition and transcriptional activation. *Experimental Eye Research,* 94**,** 98-108.

ZHAO, H., JAFFER, T., EGUCHI, S., WANG, Z., LINKERMANN, A. & MA, D. 2015. Role of necroptosis in the pathogenesis of solid organ injury. *Cell Death Dis,* 6**,** e1975.

ZHAO, X., KOTILINEK, L. A., SMITH, B., HLYNIALUK, C., ZAHS, K., RAMSDEN, M., CLEARY, J. & ASHE, K. H. 2016. Caspase-2 cleavage of tau reversibly impairs memory. *Nat Med,* 22**,** 1268-1276.

ZHENG, L. M., ZYCHLINSKY, A., LIU, C. C., OJCIUS, D. M. & YOUNG, J. D. 1991. Extracellular ATP as a trigger for apoptosis or programmed cell death. *J Cell Biol,* 112**,** 279-88.

ZHOU, W. & YUAN, J. 2014. Necroptosis in health and diseases. *Semin Cell Dev Biol,* 35**,** 14-23.

ZHOU, W., ZHU, X., ZHU, L., CUI, Y. Y., WANG, H., QI, H., REN, Q. S. & CHEN, H. Z. 2008. Neuroprotection of muscarinic receptor agonist pilocarpine against glutamate-induced apoptosis in retinal neurons. *Cell Mol Neurobiol,* 28**,** 263-75.

ZONG, W. X., LINDSTEN, T., ROSS, A. J., MACGREGOR, G. R. & THOMPSON, C. B. 2001. BH3-only proteins that bind pro-survival Bcl-2 family members fail to induce apoptosis in the absence of Bax and Bak. *Genes Dev,* 15**,** 1481-6.

ZOU, Y. Y., KAN, E. M., LU, J., NG, K. C., TAN, M. H., YAO, L. & LING, E. A. 2013a. Primary blast injury-induced lesions in the retina of adult rats. *J Neuroinflammation,* 10**,** 79.

ZOU, Y. Y., KAN, E. M., LU, J., NG, K. C., TAN, M. H., YAO, L. L. & LING, E. A. 2013b. Primary blast injury-induced lesions in the retina of adult rats. *Journal of Neuroinflammation,* 10.

## Appendices

**Appendix 1:** Caspases in retinal ganglion cell death and axon regeneration. Chloe N Thomas, Martin Berry, Ann Logan, Richard J Blanch, Zubair Ahmed. *Cell Death and Discovery* (2017) 3 17032.

**Appendix 2:** Caspase-2 mediates site-specific retinal ganglion cell death after blunt ocular injury. Chloe N Thomas, Adam M Thompson, Eleanor McCance, Martin Berry, Ann Logan, Richard J Blanch, Zubair Ahmed. *Investigative Ophthalmology & Visual Science* (2018) 59 4453-4462.